

2237

JUL 21

N64-26370

Code-1

Cat. 29

NASA Cr.-58136

ICATE

2-2-1

# VON KARMAN CENTER

PRODUCTION PROJECTS DIVISION

ENGINE OPERATING PROBLEMS IN SPACE

FINAL REPORT

VOL. I - THE SPACE ENVIRONMENT

(of 3 volumes)

A Report To

NATIONAL AERONAUTICS AND  
SPACE ADMINISTRATION

Contract No. NAS 7-98

Report No. 2824 / April 1964 / Copy No.

96

OTS PRICE

XEROX \$ 15.00 *ph.*  
MICROFILM \$ \_\_\_\_\_



AEROJET-GENERAL CORPORATION

AZUSA, CALIFORNIA



---

ENGINE OPERATING PROBLEMS IN SPACE

FINAL REPORT

VOL. I - THE SPACE ENVIRONMENT

D. Christensen

A Report To

NATIONAL AERONAUTICS AND SPACE ADMINISTRATION

Report No. 2824

April 1964

---

**AEROJET-GENERAL CORPORATION**  
A SUBSIDIARY OF THE GENERAL TIRE & RUBBER COMPANY

FOREWORD

This report, which summarizes the work performed on NASA Contract NAS7-98, is submitted in partial fulfillment of contract provisions. It was prepared by the Production Projects Division of the Von Karman Center, Azusa, California. The contract was initiated by Dr. Henry Burlage, Chief, Liquid Propulsion Systems, NASA Headquarters, Washington, D.C. The Headquarters Project Manager was Mr. Frank Compitello, and the program was under the technical direction of Mr. Louis Toth of the Jet Propulsion Laboratory, California Institute of Technology, Pasadena, California. The work described herein was performed between 15 February 1962 and 14 March 1964.

This Final Report consists of three volumes:

Volume I: The Space Environment

A comprehensive definition of the space environment as compiled under Task I of the contract.

Volume II: Environmental Effects on Engines and Components

An evaluation of environmental effects on ablative and pyrolytic graphite thrust chambers, gas generators, igniters, actuators, transducers, lubricants, structural materials, and surface finishes; performed under Task 2 of the contract.

Volume III: Improvement of System Reliability

Evaluation and analyses of areas related to system reliability, including:

- self-sealing of meteoroid penetrations (Task 3)
- space maintenance (Task 4)
- improved environmental testing techniques (Task 5)
- operation of ablative chamber with fluorine (Task 6)

Some of the data in this volume have been adapted from material originally prepared for Contract AF04(611)-7441, "Rockets in Space Environment," which was sponsored by the Rocket Propulsion Laboratory, Air Force Systems Command, Edwards, California.

AEROJET-GENERAL CORPORATION

*W. W. Howard*

W. W. Howard, Project Manager  
Space Environment Department

*U. A. Coty*  
U. A. Coty, Manager  
Production Projects Division

ABSTRACT

26370

This volume presents a comprehensive definition of the space environment as it is presently known. For the purposes of this program, this environment consists of the solar system, excluding the earth and its inner atmosphere. Special emphasis is given to data on electromagnetic and particulate radiation, meteoroid flux, and the structure and composition of the planetary atmospheres.

A list of 405 references is included; many of these are annotated.

*author*



CONTENTS

	<u>Page</u>
INTRODUCTION _____	viii
I. THE SOLAR SYSTEM _____	1
A. The Sun _____	4
B. Interplanetary Space _____	9
C. Asteroids _____	12
D. Meteoroids _____	14
E. Comets _____	17
II. PLANETS AND THEIR SATELLITES _____	20
A. Mercury _____	21
B. Venus _____	25
C. The Earth-Moon System _____	32
D. Mars _____	55
E. Jupiter _____	61
F. Saturn _____	65
G. Uranus and Neptune _____	68
H. Pluto _____	69
III. RADIATION AND SPACE DEBRIS HAZARDS _____	71
A. Introductory Comments _____	71
B. Electromagnetic Radiation _____	73
C. Solar Flares _____	77
D. Primary Cosmic Radiation _____	84
E. Meteoroid Environment _____	85
References _____	R-1

CONTENTS (cont.)

	<u>Table</u>
The Planets - Orbital Data _____	1
The Planets - Physical Data _____	2
The Planets - Surface Data _____	3
The Satellites of the Solar System _____	4
The Major Asteroids _____	5
Selected Periodic Comets _____	6
Model Venusian Atmosphere _____	7
Some Lunar Constants _____	8
Van Allen's Estimate of Particle Flux _____	9
Atmospheric Parameters as a Function of Altitude Near Solar Maximum _____	10
Atmospheric Parameters as a Function of Altitude Near Solar Minimum _____	11
Mars Model Atmospheres with 13.0 mb Argon _____	12
Mars Model Atmospheres with no Argon _____	13
Solar Spectral-Irradiance Data - 0.22 to 7.0 $\mu$ _____	14
Characteristics of Extreme Ultraviolet Radiation (300 to 1300 A) _____	15
Characteristics of the Solar Spectrum Below 1300 A _____	16
Composition and Energy Spectrum of Cosmic Rays _____	17
Meteor Streams _____	18
Parameters of Micrometeoroids _____	19
Direct Measurements Obtained with Microphone Systems on the U.S. Satellites and Space Probes _____	20
Direct Measurements Obtained with Microphone Systems on the Soviet Satellites and Space Probes _____	21

CONTENTS (cont.)

	<u>Figure</u>
Orbital Inclinations of the Planets and Selected Asteroids _____	1
Orbits of the Outer Planets _____	2
Orbits of the Inner Planets _____	3
Planetary Satellites _____	4
Solar Temperature Distribution _____	5
Energetic Particles Observed in the Solar System _____	6
Electron Density and Temperature in Space _____	7
Orbits of Asteroids _____	8
Perturbations of a Comet Orbit by a Large Planet _____	9
Time and Velocity Required for Space Missions _____	10
Planetary Temperatures _____	11
Venusian Model Atmosphere _____	12
Thermal Environment of Venus _____	13
Greenhouse Model of the Venusian Atmosphere _____	14
Aeolosphere Model of the Venusian Atmosphere _____	15
Proton Belt (Inner Zone) of the Van Allen Radiation _____	16
Quiet-Day Electron Fluxes as a Function of Distance From the Center of the Earth and Latitude _____	17
Van Allen Radiation-Belt Particle Flux Versus Altitude in the Equatorial Plane _____	18
The Van Allen Belts _____	19
Relationship Between Polar-Coordinate and Magnetic-Shell Reference Systems for a Dipole Field _____	20
Paths Described by Mirror Points of Particles Trapped in the Geomagnetic Field _____	21

CONTENTS (cont.)

	<u>Figure</u>
Location and Altitude of the Integral-Invariant Equator with Repsect to Geographic Coordinates _____	22
Distribution of Protons in the Inner Van Allen Belt _____	23
Proton Spectrum in Inner Van Allen Belt _____	24
Differential Energy Spectra at Four Positions in the Inner Van Allen Belt _____	25
The Integral Energy Spectrum of Solar Particles _____	26
Omnidirectional Electron Flux at 920 Km _____	27
Absolute Differential Energy Spectrum for the Omnidirectional Electron Intensity in the Heart of the Electron Belt _____	28
Heat Balance of the Earth _____	29
Average Insolation Incident on the Earth's Atmosphere _____	30
Average Short-Wave Energy Absorption _____	31
Average Short-Wave Solar Energy Reflected by the Atmosphere and Earth _____	32
Thermal Emission Spectrum of the Earth _____	33
Relative Air Density as Determined by Satellite Measurements _____	34
Concentrations of the Major Atmospheric Constituents _____	35
Distribution of Atomic Hydrogen Out to 60,000 Km from the Earth at the Extremes of the Sunspot Cycle _____	36
Average Daytime Atmospheric Densities at the Extremes of the Sunspot Cycle _____	37
Pressure in the Exosphere _____	38
Electron Concentrations in the Equatorial Plane _____	39
Ion Concentrations in the Transition Region Between the Normal Ionosphere and the Protonosphere _____	40

CONTENTS (cont.)

	<u>Figure</u>
Radiation Energy Field of the Sun _____	41
Radiation Equilibrium Temperatures for a Spherical Blackbody in Space _____	42
Solar Spectral Irradiance Above the Earth's Atmosphere at the Earth's Mean Distance from the Sun _____	43
Extreme Ultraviolet Spectrum _____	44
Bimonthly Distribution of Polar Cap Absorption Events for the Period 1949 to 1960 _____	45
Frequency of Solar-Flare Proton Impingement of the Polar Cap _____	46
Spectra of Particles Arriving at the Earth at Various Times Following a Solar Flare _____	47
Micrometeoroid Flux _____	48
Frequency of Occurrence of Meteors in the Vicinity of Earth _____	49
Altitude - Dependence of Micrometeoroid Flux _____	50
Distribution of Visual Radiants of Sporadic Meteors in the Ecliptic Latitude _____	51
Apparent Meteor Radiants _____	52
Relative Meteor Flux Crossing the Earth's Orbit _____	53
Observed Radiants of Meteoroids Impacting the Earth _____	54
Velocity Distribution of 10,933 Sporadic Meteorites _____	55

## INTRODUCTION

Important elements of the planetary and interplanetary environments are discussed in this volume. Our present knowledge of this environment is so quantitatively incomplete, and concepts and ideas develop or change so rapidly, that a description of this environment cannot be presented simply as a collection of formulas, tables, and graphs. Therefore, the description of the space environment is given in the form of a concise discussion combined with tables and graphs showing the test, or otherwise typical, quantitative information. In this way, the most intelligent use of existing data can be made. Before use is made of any particular figure or table, it is recommended that the entire relevant discussion be read.

## I. THE SOLAR SYSTEM

The solar system and its neighboring stars travel along a spiral arm of the Milky Way galaxy at a velocity of 300 km/sec in the direction of the star Deneb. The sun and its companions travel in approximately circular orbits, completing one revolution about the galaxy in a period of  $2 \times 10^8$  years. Since the solar system is  $5 \times 10^9$  years old, it has made approximately 25 revolutions in its lifetime.

Superimposed on this average stellar motion, the sun is moving 20 km/sec relative to the surrounding stars toward the constellation Hercules. Like most stars, the sun's peculiar motion is much less than the velocity of galactic rotation.

The sun is an average star accompanied by nine planets and many lesser bodies. Since the sun represents 99.2% of the solar system's mass, it dominates the motion of all other objects and occupies a central position in the system. In addition to the sun, the main components are the interplanetary space including gas particles and associated magnetic fields and radiation, the asteroids, meteoroids and comets, and the planets and their satellites.

For convenient reference, various physical and orbital data of the solar system and its components are presented in Tables 1 through 5. Most of this material is from Ehricke\*, with certain modifications, particularly with relation to improved physical data of the planets now available, which is discussed in detail in Section II. The orbital data have been calculated with reference to January 1, 1963, as an arbitrarily selected recent date of interest.

---

\* K. A. Ehricke, Space Flight (I. Environment and Celestial Mechanics), Van Nostrand, New York-London, 1960.

Possessing more than 98% of the entire system's angular momentum, the planets extend the domain more than 6000 solar radii. With the exception of Mercury and Pluto, all the planets move in nearly circular orbits about the sun in a plane very slightly inclined to the sun's equator (Figure 1). Both Mercury and Pluto have relatively large inclinations and eccentricities. This is especially pronounced in the case of Pluto, whose eccentricity permits it to come within the orbit of Neptune while its inclination prevents any possible collision with that planet (see Figure 2).

In trying to draw to scale the distances of the planets from the sun, one finds that the innermost of these bodies are much closer together than their remote counterparts. Indeed, the amount of space between the orbits of the sixth and the seventh planets (Saturn and Uranus) is three times greater than the area occupied by all six inner planets. In 1772, J. E. Bode made an attempt to find a relation which would agree with the known distances of the planets. Taking the earth's distance as unity and using the relation  $0.4 + (0.3 \times 2^n)$ , he came up with values given in the following tabulation:

<u>Planet</u>	<u>True Distance A.U.</u>	<u>Bode's Relation</u>
Mercury	0.4	$0.4 \times (0.3 \times 2^{-1}) = 0.5$
Venus	0.7	$0.4 \times (0.3 \times 2^0) = 0.7$
Earth	1.0	$0.4 \times (0.3 \times 2) = 1.0$
Mars	1.5	$0.4 \times (0.3 \times 2^2) = 1.6$
Asteroids	2.8	$0.4 \times (0.3 \times 2^3) = 2.8$
Jupiter	5.2	$0.4 \times (0.3 \times 2^4) = 5.2$
Saturn	9.5	$0.4 \times (0.3 \times 2^5) = 10.0$
Uranus	19.2	$0.4 \times (0.3 \times 2^6) = 19.6$
Neptune	30.1	$0.4 \times (0.3 \times 2^7) = 38.8$
Pluto	39.5	$0.4 \times (0.3 \times 2^8) = 77.2$

There seems to be no scientific basis for his formula, and although it does not work too well for Neptune and Pluto, it must be remembered that the relation was used before the discovery of Uranus and the minor planets. In fact,



Bode's relation stimulated the search for a planet between Mars and Jupiter after the discovery of Uranus yielded a value close to that predicted by Bode. As a result, the asteroids were discovered.

As seen from the north, almost all motions in the solar system are in the counterclockwise direction (direct motion). Because of the different sidereal period for each planet, they are constantly changing position relative to one another. Figures 2 and 3 show, to scale, their relative positions for January 1, 1963.

All the planets revolve and rotate directly, with the exception of Uranus and probably Venus. Uranus is unusual in that its equator is inclined more than  $90^{\circ}$  to its orbital plane, resulting in a technically retrograde rotation. From recent radar data, Venus is known to have a slow retrograde diurnal motion assuming the axis of rotation is perpendicular to the orbital plane. Whether or not the Venus rotational axis is inclined (making the rotation technically direct) is not yet known because of the thick Venusian atmosphere which obscures the surface.

Though not so opaque as the Venusian clouds, the atmospheres of all the other planets are substantial, again excepting the innermost and outermost planets of the system. Mercury is hot, causing most gases on its surface to boil away, while Pluto's low temperatures freeze out all elements but hydrogen. One other body, Titan (the sixth and largest of Saturn's satellites), possesses a significant atmosphere. In this respect, it is unique among the satellites.

Jupiter, with 12 of the system's 31 satellites, is a solar system in miniature (Figure 4). Varying in size from rocks 8 km in diameter to planetoids as big as Mercury, the satellites revolve about their primaries while following the parent around the sun. As in the case of the planets, most of the satellites revolve directly, except for a few of the outer and less stable bodies. The five satellites of Uranus revolve in the plane of that planet's equator and are technically in retrograde motion due to the unusual inclination of the planet. The rings of Saturn complete the list of features connected with the planets. One of the most beautiful features of the solar system, it is also one of the marvels of nature in that it forms the most perfect plane known to man.

## A. THE SUN

The sun, a typical yellow dwarf star of spectral class G2, is the energy source for essentially all the dynamic processes occurring in the solar system (Reference 1). While the diameter of the sharp observed solar boundary is nearly a million miles ( $1.4 \times 10^6$  km), at the earth-sun distance of 93 million miles the sun subtends an angle of only  $1/2^\circ$ . From the sun, the earth is a tiny disk of only  $17''$  of arc, or less than  $0.005^\circ$ . Consequently, the earth intercepts only an exceedingly small fraction of the sun's radiant energy. It has been estimated (Reference 2) that three days of solar flux provide as much energy as could be derived by burning the entire oil, coal, and wood supplies found on earth.

1. Solar Structure

The ultrahigh temperature and pressures of the sun's interior are estimated to be as much as  $10,000,000^\circ\text{K}$  at 50 million atmospheres (Reference 3), these values declining rapidly away from the center region. It was formerly believed that the central regions of the sun were dominated by convective processes where the hot gases travelled outward from the center to the cooler periphery. Now it is known that the dominant heat-transfer process in the sun's interior is by radiation. The diameter of the inner core is considered to be about  $8 \times 10^6$  km, or a little more than half that of the apparent sun diameter. The temperature and density diminish rapidly from the inner core toward the outside, with radiative transfer still dominating this extended core region. Adjacent to the radiative interior is a convective envelope ranging from 140,000 to 200,000 km in thickness extending to a layer just below the visible surface and containing no more than 2% of the total mass. The estimated temperature gradient (Reference 1) throughout this inner structure is given in Figure 5.

The outer atmospheres of the sun are classified into three main regions: the photosphere, the chromosphere, and the corona, shown in the following short tabulation. The extremes in thermal environment across these regions are shown in Figure 5.

<u>Region</u>	<u>Depth</u>	
Core	4,000,000 km	
Convective Envelope	200,000 km	
Photosphere	600 km	
Chromosphere	10,000 km	} solar "atmosphere"
Corona	60 solar radii	

The distinguishing features of the solar "atmosphere" regions, the photosphere, chromosphere, and corona, are summarized below.

a. Photosphere

The photosphere, or light sphere, is the apparent sun surface, a relatively thin layer (600 km) of highly luminous gas. The gaseous photosphere emits the greater part of the sun's radiant energy at a temperature of  $6,000^{\circ}\text{K}$ , with a pressure of less than one-hundredth that of the earth's atmosphere. The surface of the photosphere is observed to have a mottled appearance, called "granulation," associated with the convective instability and turbulence of the lower layers. These granules, often 1,000 miles across, appear to move upward at speeds of 1 km/sec. Sunspot disturbances, discussed below, are observed in the photosphere region.

b. Chromosphere

The chromosphere, adjacent to the photosphere, is a hazy region 10,000 km thick characterized by irregular, fine, jet-like streaks that shoot upward at velocities of 20 km/sec to heights of 10,000 km. The temperature increases across the chromosphere from  $6,000^{\circ}\text{K}$  in the photosphere to  $10^6\text{K}$  in the corona.

c. Corona

The solar corona, the outermost region of the sun, is a halo of hot, tenuous, ionized gases extending far into the solar system. During an eclipse of the sun by the moon, the solar corona can be observed for as far as 20 solar radii. The eclipse of the Crab nebula shows that the corona extends to 60 solar radii. The corona, made visible by the white light from the photosphere scattered by the corona free electrons, is responsible for the emission of solar X-rays.

## 2. Composition

Various chemical compositions for the interior of the sun have been calculated. Some of the predicted compositions (by weight), based on various solar models, are listed below.

<u>Theorist</u>	<u>Composition</u>		
	<u>Hydrogen</u>	<u>Helium</u>	<u>Heavy Elements</u>
Friedman (Reference 2, 1962)	0.60	0.29	0.11
Kuiper (Reference 1, 1953)	0.76	0.23	0.0075
Epstein, 1951	0.82	0.17	0.01
Keller, 1948	0.67	0.29	0.045
Schwarzschild, 1946	0.47	0.41	0.12
Bethe, 1939	0.35	0.00	0.65

Sixty-seven elements have been identified spectroscopically in the sun, with 15 known elements missing. Certain elements cannot be identified because of present inadequacies of laboratory equipment; these include Hg, I, Br, Xe, Cl, A, Ne, and others. Conversely, a number of solar lines exist which defy identification. Hydrogen and calcium are predominant elements in the chromosphere. Bright clouds of hydrogen and calcium are also a particular feature of the photosphere over regions containing sunspots.

## 3. Solar Magnetic Field

The sun has a dipole magnetic field of the order of a few gauss. At the poles, the field is small, having opposite polarity in the northern and southern hemispheres. Near the surface of the sun at sunspots, the local magnetic intensity is as much as 3,000 gauss and is, therefore, large enough to impart and control the motion of the solar plasma. Further away from the sun in interplanetary space, the situation is reversed with the plasma particles determining the positioning of the magnetic lines of force. The interplanetary magnetic fields are discussed on subsequent pages of this section.

## 4. Solar Rotation

The period of rotation of the sun varies from about 24 to 27 days, depending on the latitude, with the period increasing at the poles. The

rotation is in the same direction as the orbital motion of the planets and with the same axial rotation of all the planets, except Uranus.

#### 5. Flares and Prominences

While the mass, radius, and luminosity of the sun have not changed appreciably over billions of years, the solar surface exhibits a vast number of transient phenomena. The most obvious disturbance is the sunspot, a cool ( $4,500^{\circ}\text{K}$ ) region visible as a dark spot with dimensions of about 10,000 km. The occurrence of sunspots, generally indicative of solar activity, follows a 22-year cycle.

The solar flare that is associated with sunspots and sunspot groups is by far the most important solar activity insofar as interplanetary travel is concerned. A flare is a bright cloud forming above the photosphere and lasting for as long as 30 min. A large flare,  $4 \cdot 10^4$  km, may radiate  $10^{33}$  ergs during a 1,000-sec lifetime. Such flares constitute a serious hazard to interplanetary flight, and are discussed separately in Section III.

Certain specific active regions of the sun often maintain their identity through several solar rotations ( $\sim 27$  days). Careful charting, based on satellite observations, of these activity periods - particularly the flares - is currently in progress.

#### 6. Solar Radiation

The total flux of electromagnetic radiation from the sun is surprisingly constant over a year's time, even during violent disturbances on the sun's surface. The bulk of the energy in the solar spectrum lies between 0.3 and  $4.0 \mu$ , with approximately 1% of the energy lying beyond these limits.

The solar constant, the total solar irradiance at the earth's mean distance (one astronomical unit) from the sun, is given by Johnson (1954, Reference 4) as  $2.0^{\circ} \pm 0.04 \text{ cal/cm}^2\text{-min}$ , or  $1.4 \cdot 10 \text{ ergs/cm}^2\text{-sec}$ ; this is about 433 Btu/ft<sup>2</sup> hour. This figure does not vary by more than 2% during periods of solar activity. The total energy generated by the sun is therefore the area of a sphere of one astronomical unit times the solar constant, or,

$$\begin{aligned}\text{Total energy radiated} &= 4\pi(1.5 \times 10^{13})^2(1.4 \times 10^6) = 4 \times 10^{33} \text{ ergs/sec} \\ &= 4 \times 10^{26} \text{ w}\end{aligned}$$

The electromagnetic radiation of the sun as seen at the earth outside the atmosphere consists of a continuous spectrum in the near-ultraviolet, visible, and infrared regions containing many absorption lines (Fraunhofer lines) and a number of emission lines at shorter wavelengths which contribute only a small amount of energy compared with the continuum. Rocket observations have shown that the continuous spectrum diminishes in intensity very rapidly with decreasing ultraviolet wavelength and that, below 1400 A, the sun radiates a continuous spectrum with emission lines superimposed upon it. This is unlike the visible and near-ultraviolet, where the continuum is crowded with intense absorption lines and there are no emission lines.

The continuous spectrum can be well approximated in various wavelength intervals by blackbody radiation of a specified temperature. For example, the visible and infrared regions show a spectral irradiance corresponding rather closely to that of a 6000°K blackbody source. The temperature of a blackbody that most nearly matches the continuous spectrum of sunlight in total energy output is about 5750°K. (In this connection, see Reference 7.) From 1040 to 912 A, the spectrum consists mostly of emission lines which are not resolved in the plot with 10-A intervals. The extreme ultraviolet shown in this figure originates from higher levels in the sun's atmosphere than does the near-ultraviolet and the visible. The continuum in the ultraviolet region probably comes mainly from the low chromosphere, where the temperature is of the order of 4000 to 5000°K. The emission lines at short wavelengths originate in still higher regions of the solar atmosphere, where the temperature ranges from 5000°K in the chromosphere to millions of degrees in the corona. The exact region of emission depends on the particular line.

An important series of emission lines is the Lyman series in the hydrogen spectrum, with the first line, Lyman alpha, at 1216 A. The Lyman-alpha line carries about 6 ergs/cm<sup>2</sup>-sec near solar maximum and delivers more

energy than the entire solar spectrum from wavelengths shorter than itself. The intensity is probably less at sunspot minimum. The higher members of the series are followed by the Lyman continuum, which is the most important emission below 912 Å. It follows a 6700°K blackbody curve. At 584 and 304 Å, there are intense emissions by neutral and ionized helium, respectively. The two lines produce about 0.5 erg/cm<sup>2</sup>-sec at the earth (Hinteregger, 1960, Reference 8).

A very small portion (~ 0.1%) of the electromagnetic radiation lies in the soft X-ray region of a few kw. This ionizing radiation is absorbed strongly by materials and does not pose a problem to manned space flight. The radiation hazard is discussed further in Section III.

## B. INTERPLANETARY SPACE

The interplanetary medium can be considered as an extension of the sun's corona, with particles and magnetic fields from outside the solar system superimposed. The particles which make up this medium range in energy from a few electron volts to relativistic energies and higher ( $7 \times 10^{19}$  ev). The broad range of energies covered by these particles is shown in Figure 6.

### 1. Interplanetary Gas

The streams of ionized gas that move outward from the sun extend in a continuously diminishing field to at least as far as the earth's orbit. This gas movement, first deduced from an analysis of motion of comet tails (Reference 9) has been established directly from satellite measurements (References 10 and 11) and more recently by Mariner II data, (Reference 33). This efflux of gas particles from the sun across planetary space is called the solar wind. (Other particles, notably solar flares and cosmic rays, accelerate along magnetic lines of force through space.)

The velocity of the solar wind, as measured on Mariner II (Reference 33), varies from 200 to 500 miles/sec, and its temperature is in the neighborhood of 100,000 to a million degrees Fahrenheit with  $2 \times 10^5$  a reasonable average. Its tenuousness is almost beyond comprehension, there being only 1 to 4 protons (hydrogen nuclei) and electrons per cubic centimeter with 88/cu cm a

maximum (Reference 33). These Mariner II data (Reference 33) are compared with observatory (eclipse) and satellite data (Reference 12) in Figure 7. Note that Mariner temperatures are longitudinal temperatures - not the random temperatures of the various theories summarized in the cross-hatched regions. Therefore, whether or not the high Mariner temperatures actually contradict the results of a wide variety of postulated thermal models cannot yet be stated. Furthermore, the Mariner data were found to be both larger and smaller than the Explorer X, with the Mariner providing a vastly larger number of data points in time. The Mariner results therefore represent a better average than the single point location given for example in Reference 12 and shown for comparison in Figure 7.

The rate at which these particles move through space (the solar wind) is evidently closely related with the sun's activity. The Mariner results show that on approximately 20 occasions during the flight, the solar wind velocity increased within a day or two by 20 to 100%. These fluctuations correlate very well with the amount of magnetic disturbance observed on earth. This same effect had been observed earlier from satellite data (References 10 and 13).

Hydrogen particles also occupy interplanetary space with a density of about 500/cu cm. These particles are luminous because of fluorescence (absorption of ultraviolet sunlight and re-emission of it in the form of Lyman-alpha quanta). It is thought (Reference 14) that these hydrogen atoms are driven out of the solar system by radiation pressure and are continually being replenished by the sun.

## 2. Magnetic Fields

The general galactic field is thought to have fields of  $10^{-5}$  to  $10^{-6}$  gauss (Reference 12). Data from Pioneer V revealed a remarkably stable and uniform (nonradial) interplanetary magnetic-field strength of  $2.7 \cdot 10^{-5}$  gauss (Reference 15). Salisbury (Reference 12) has suggested that the spatial uniformity indicates the presence of a galactic-interstellar field.

The solar magnetic fields lie superimposed on the general galactic field. One model of the solar field assumes the solar wind to extend



the lines of force of the general solar field into a radial configuration. Each line of force is drawn out to a location where, far beyond the earth's orbit, the force lines cross the equatorial plane and return to the opposite hemisphere on the sun. This model has been confirmed by Mariner II data. Another type of solar magnetic field has been proposed which is similar to a long tongue (or magnetic "bottle") extending from the sun's surface (Reference 16). Although it has been argued (References 17 and 18) that a magnetic tongue rooted in the sun's surface is necessary to explain certain cosmic ray phenomena, these arguments no longer appear valid in light of the Mariner results.

Mariner II showed that the field transverse to the radial direction from the sun is typically 2 to 5 gammas at quiet times and has some tendency to have its direction approximately parallel to the plane of the earth's orbit. An appreciable perpendicular component exists much of the time, and fluctuations of 10 to 20 gammas are not uncommon. Such fluctuations usually correlate with changes in the solar wind velocity. (For comparison, the earth's magnetic field is approximately 30,000 gammas at the equator and 50,000 gammas at the poles.)

Instabilities and disorders in magnetic field lines can be caused by a number of events, primarily energetic particle motion and field reversal interactions. The region of disordered magnetic fields, thought to lie beyond the earth's orbit, may also produce a clumping of field lines with particles accumulating in the weaker regions.

### 3. Interplanetary Radiation

Both electromagnetic and corpuscular radiation permeate interplanetary space. This radiation varies both with location and time. The electromagnetic radiations span the entire spectrum from radiowaves to high-energy gamma rays. The energy span for corpuscular radiation (Figure 6) also covers a vast range of energies (Reference 16). The principal sources of corpuscular radiation are from galactic cosmic rays, trapped electrons and protons, and solar-flare protons. The general topic of interplanetary radiation, extremely important in space travel, is treated at length in Section III.

## C. ASTEROIDS

The asteroids, or minor planets, are small planet-like bodies in Keplerian orbits about the sun. They are chiefly concentrated between the orbits of Mars and Jupiter. Their discovery came as a result of searching for a planet 2.8 astronomical units from the sun, as predicted by Bode's relation. This belief in Bode's empirical formula came about when the discovered position of Uranus agreed with the value he had predicted 9 years before. Instead of a single planet, many small bodies were detected. Approximately 2,000 have been discovered to date (Reference 19).

Orbits of all sizes, eccentricities, and inclinations can be found among the asteroids, but most lie between 2.1 and 3.5 A.U., near the plane of the ecliptic; all travel in direct motion about the sun. They have average inclinations and eccentricities of  $9.5^{\circ}$  and 0.15, respectively, with periods ranging from 3.5 to 6 years (Reference 14). Some of these orbits are shown in Figure 8.

Recent re-discovery of the close-approach asteroid, Ivar (see Table 5) has highlighted increasing scientific interest in the minor planets. As Dr. Harold C. Urey has pointed out (Reference 25), the answer to some of the major problems of the universe may be found on the asteroids, since the asteroids may retain the best record of the early history of the solar system.

Unlike the planets whose surfaces have been altered by a variety of different weathering forces, the asteroid surface may be reasonably free from such effects. Mars, Venus, and other planets in the solar system are like the Earth in that they have atmospheres, and may in the past have had oceans. Large bodies of the solar system which have neither atmospheres nor oceans, such as the Moon, are also subject to erosion caused by the extremes of temperature and collision with space debris. The small asteroids are expected to be free from most of these eroding forces.

Another major reason for the recent increased interest in the asteroids is related to their use as position indicators in interplanetary navigation. By measuring the celestial coordinates of two bodies belonging to the solar system,

a vehicle's position can be uniquely defined providing that the orbital positions of the near bodies are accurately known. The asteroids are promising candidates since, unlike the planets, they are small in size, and give an accurately defined point source of light. Furthermore, asteroids have another advantage owing to their high average orbital inclination ( $21.0^\circ$ ). Since the planets, with the exception of distant Pluto, lie close to the ecliptic plane, position indication using planets as reference will have a significant uncertainty in the direction normal to the orbital plane; this error would be greatly reduced using the asteroids as guides.

However, the asteroids are faint objects against the bright stellar background, as described below. Locating the asteroids during flight will require sensitive instruments even for the brightest asteroids (Reference 26), and accurate information concerning their orbits.

Orbital elements calculated by various institutions, accurate to four decimal places of an astronomical unit, are collected and published annually by the Institute for Theoretical Astronomy, Leningrad (Reference 27).

Asteroid distribution is not uniform; at distances from the sun which are simple fractions of Jupiter's semimajor axis, there are noticeable drops in asteroid density. Known as Kirkwood Gaps, they are produced by Jupiter's repetitive attraction in an outward direction on bodies in this region.

Jupiter in conjunction with the sun also provides two stable Lagrangian libration points in its orbital plane which form equilateral triangles with these two bodies. Twelve asteroids are found at these points, seven to the east of Jupiter and five to the west, each with a period equal to the Jovian year.

Ceres, Pallas, Juno, and Vesta, with a combined mass of one four-thousandth of that of the earth, account for 75 to 80% of the total mass of all asteroids (Reference 20), both known and unknown. Ceres, the largest asteroid, is only 770 km in diameter and has a surface gravity of only 0.1 g; it could not possibly hold a significant atmosphere (Reference 21).

Since the minor planets are too small to visually determine the size of their disks, their diameters are computed by measuring their brightness.

Assuming that their reflecting power is about equal to that of the moon, it can be shown (Reference 22) that

$$\log d = 3.13 + \log a (a-1) - .012 m + 11 c$$

where  $d$  = diameter in km

$a$  = distance from the sun at opposition in A.U.

$m$  = visual stellar magnitude at opposition

$c$  = variation of brightness in magnitudes per degree phase

Although there must be many small asteroids, those which have been discovered are fairly sizable. Of the 27 known asteroids which cross the Martian orbit, two-thirds exceed 10 km in diameter (Reference 23).

The albedos of the asteroids are highly variable; Vesta is especially bright, reflecting 55% of the sun's light (Reference 24). This leads to the speculation that it has a snow covering. Traces of the heavier gases may be the cause of the high albedos on some of the larger asteroids. A few show large fluctuations in brightness which are due to rotation of their nonspherical shape. One is believed to have the shape of a dumbbell. The periods of rotation are all small, none being greater than 10 hours.

Among the great number of known asteroids, a few are of special interest. Hidalgo has both the highest eccentricity (0.6557) and the greatest inclination ( $42.529^\circ$ ) of any known minor planet (Reference 20). Geographos has the distinction of making the closest predictable approach to the earth's orbit and will come within three million miles of the earth in the near future. One of the most interesting and unusual asteroids, Icarus, is the only body other than comets and meteors which passes within the orbit of Mercury (0.1869 A.U.) at its closest approach to the sun (see Figure 8). Its surface, alternately exposed to the extremes of heat and cold, must be unique in the solar system.

Asteroids will not be explored in the near future, however, since their high inclinations to the ecliptic require large amounts of energy to land a vehicle on one of these bodies. The planets will have priority as well as lower energy requirements, which will result in a much delayed exploration of most

asteroids. A study of the surface of Icarus would be especially interesting, but again, as with the other asteroids, it is highly inclined to the ecliptic, making transfer difficult. In 1968 a vehicle could be sent the four million miles to this asteroid on a minimum energy orbit, but data would have to be gathered rapidly as its velocity relative to Icarus would not allow a very long observation time.

Eventually the larger asteroids may be explored, and some plans have been outlined for probe missions (Reference 25). However, contrary to some popular thinking, the asteroids will not provide rides for vehicles to other planets (Reference 20) nor will they be a great menace to vehicles traveling through the asteroid belt. Even a million asteroids could not clutter the space between the Jovian and Martian orbits (Reference 21). However, a concentration of meteoritic matter in the asteroid belt is probable, and would present an appreciable hazard.

#### D. METEORIODS

Interplanetary space contains many small particles, about the size of sand grains, traveling in elliptical orbits around the sun. These particles and their larger but rarer cousins are classified as meteoroids.

The term "meteorite" is used only for those remnants of meteoroids found on the earth's surface which are not completely burned up upon entry into the atmosphere. Each year the earth collects about  $2 \times 10^9$  kg of meteorites of all sizes (Reference 14). Small meteoric particles are found in the deep sea-bottom oozes, and have also been collected from the upper atmosphere. Although large meteorites are rare, a few have been found which are greater than 10,000 kg. Craters left by meteorites on the order of  $10^6$  kg, such as the Barringer crater in Arizona, must have been produced by bodies which were of asteroidal dimensions prior to atmospheric ablation (Reference 25).

Mason (Reference 27a) defines terms as follows: "A meteor is quite distinct from a meteorite; it is the transitory luminous streak in the sky produced by the incandescence of an extraterrestrial body (a meteoroid) passing through the earth's atmosphere". Observations of meteors as they enter the atmosphere reveal that most, if not all, meteors travel with a speed less than the limiting parabolic

speed of 42 km/sec at the earth's orbit and are therefore part of the solar system. A few have been observed which exceed this value, but it is more likely that they obtained this excess speed from perturbations by the planets rather than that they truly originated outside the solar system. Unlike the asteroids, not all meteors travel in direct motion about the sun. Meteors have been recorded entering the atmosphere at 72 km/sec from a direction opposite to the earth's orbital motion. This results from the addition of the meteoroid's velocity of 42 km/sec to the earth's 30 km/sec orbital velocity.

1. Meteoroids of Asteroidal Origin

A small fraction of observed meteors are of asteroidal origin, although virtually all of the meteorites collected on earth have this origin (References 27b and 291). Very bright meteors, with brightnesses approaching that of the moon, are likely to be of asteroidal origin, while only a few of the fainter meteors have this origin. These asteroidal meteors have relatively high densities, and the resulting meteorites consist of iron or stone. The iron has a high nickel content that distinguishes it from iron of terrestrial origin; the stony meteorites usually contain iron-nickel particles which are indicative of the meteoric origin of the stones. Asteroidal meteors are always sporadic and do not arrive in streams or swarms.

Meteorites have been extensively studied both microscopically and chemically. Indications are that they were formed under the pressure and temperature conditions found inside a planet, supporting the view that meteorites are of asteroidal origin and that asteroids resulted from disruption of a planet (Reference 27b). Meteorites usually are irregularly shaped and frequently have pitted surfaces. The irregular shape is consistent with a collisional origin for these bodies. The asteroidal belt is densely populated with small bodies which may collide with one another causing breakups and orbital changes. Some of the resulting particle orbits intersect the path of the earth and become meteors as they enter the earth's atmosphere.

Many fine dust particles in interplanetary space are also inferred to be of asteroidal origin. For fine particles, radiation pressure and the Poynting-Robertson effect become important. The latter effect is due to a slight relativistic

aberration in the direction of solar radiation incident on the particle which results in a decrease in the particle's angular momentum and a resulting decrease in the particle's orbital radius. A particle 100 microns in radius would spiral into the sun in about 4000 years from a distance equal to that of the earth's orbit (Reference 5). The particles do not drift all the way into the sun, because as they come close to the sun they are vaporized and lose mass. As their size decreases, radiation pressure - which is proportional to projected area - becomes important compared to gravitational pull (which depends on particle mass). Below a certain minimum size, the particles are quickly blown out of the solar system by radiation pressure. This minimum diameter,  $D_m$  (in microns) is given by the relationship

$$D_m = \frac{0.6}{\rho}$$

where  $\rho$  is particle specific gravity (Reference 5).

## 2. Meteoroids of Cometary Origin

Most meteors and nearly all of the fine interplanetary dust is of cometary origin. All shower meteors are inferred to have this origin. (Meteors are somewhat arbitrarily divided into two classes - sporadic and shower - but the shower meteor is not easily distinguished from the sporadic background when the shower is diffuse or depleted.) There are many meteor showers which recur every year with regularity (Table 18) and about eight of the known meteor showers have been identified with comets and are noted below (Reference 12).

<u>Meteor Shower</u>	<u>Comet</u>	<u>Time of Year</u>
Lyrids	1861 I	April 21
Eta Aquarids	Halley's	May 5
Perseids	1862 III	August 12
Giacobinids	Giacobini-Zinner	October 9
Orionids	Halley's	October 20
Taurids	Encke's	November 7
Leonids	1866 I	November 15
Bielids	Biela's	November 23

The shower is usually named after the constellation of stars from which it appears to come (the radiant of the shower).

Cometary meteoroids have, in general, low densities. Whipple (Reference 6) derived an average density of 0.44 for all meteors, and much lower densities have been observed. Many cometary meteoroids may have a dustball or porous structure, agreeing well with the current comet model for which the cometary nucleus is an agglomerate of ices and dust. When the ice sublimates in solar heat, a porous crust is left which breaks irregularly to form meteoroids.

The most serious danger present to space vehicles by space debris is presented by micrometeoroids. Micrometeoroids are small (less than 300  $\mu$  dia) particles in space with masses  $10^{-3}$  and  $10^{-12}$  g. The danger of these particles lies in their much greater frequency than heavier particles, and their hypervelocity impact (up to 72 km/sec) on space vehicles.

In order to protect against the micrometeoroid hazard, it is necessary to know the frequency of collisions expected, the characteristics of the particles encountered (mass, size and velocity), and the characteristics of hypervelocity impact (penetration depth, crater size, etc). These topics are discussed further in Section III.

#### E. COMETS

Comets, although seldom seen, are a part of the solar system. Their orbits around the sun are of two types, depending on their past history. Originally, all comets were long-period in type (i.e., their eccentricities were greater than 0.99 and less than 1). Moving in these extended ellipses with periods ranging from  $10^3$  to  $10^6$  years, they would be fairly frequently perturbed sufficiently by one of the larger planets either to completely remove the comet from the solar system ( $e > 1$ ) or lower its eccentricity, giving it a period comparable to that of the planets (see Figure 9). Thus, over the millenia, a considerable number of short-period comets have accumulated within the orbit of Pluto. The following tabulation lists the distinguishing features of each type for comparison:



Short Period	Long Period
Period 3 to 165 years	Period $10^3$ to $10^6$ years
$e = 0.4$ to $0.9$	$e = 0.99$
Elliptical orbits	Nearly parabolic orbits
Lie near plane of ecliptic	Concentrated at inclinations of $80$ to $150^\circ$
Grouped in families associated with the larger planets	No definite grouping
Usually direct motion	Random distribution between direct and retrograde motion

Since short-period comets are captured by a planet, the resulting new orbits are characterized by an aphelion distance about equal to the semimajor axis of the captor. This brings about a grouping of the short-period comets into families associated with each of the larger planets. Jupiter, because of its large mass, has captured more than 40 comets, with Saturn, Uranus, and Neptune having considerably fewer. Table 6 gives a partial list of the comets in the various families.

In appearance, a comet differs radically from all other bodies in the solar system. It is composed of three parts: the nucleus, the coma, and the tail. The nucleus is small and round, with a diameter of about 1 km. Although small in size, it is very dense, as the average mass varies anywhere from  $6 \times 10^{12}$  to  $6 \times 10^{16}$  tons (Reference 20). Surrounding the nucleus is a gaseous hull known as the coma, with a density less than a good earth vacuum. This mass of gas contains molecules and atoms liberated by the nucleus and usually consists of OH, NH, CH, CN or  $C_2$ . The tail contains molecules of  $N_2$ , CO, and  $CO_2$  which have been driven away from the sun by radiation pressure. At times the tail attains lengths of hundreds of millions of miles, but it usually does not appear until it is within the orbit of Jupiter.

It has been proposed by Whipple that the nucleus is an icy conglomerate of compounds of nitrogen, oxygen, carbon, and hydrogen, with imbedded silicates and metals (Reference 32). As the comet approaches the sun, the ice evaporates,

resulting in gases which form the coma and tail. This model is the one most generally accepted. Recently Robey has proposed the addition of a permanent coma in the form of a magnetized plasma to account for observed excess light emissions, explosive outbursts, and contraction and expansion of the coma (Reference 30).

The vaporization of a comet takes place on its nucleus surface and is a process of melting, boiling, and surface microexplosions which disperse solid surface material. At first these particles form a compact cloud which travels in the same orbit as does the nucleus of the comet. With the elapse of time, radiation pressure (Poynting-Robertson effect), solar wind, and perturbations by planets tend to spread the cloud into a large swarm of meteoroids. These swarms of meteoroids are termed meteoroid showers (upon atmospheric entry) and their common orbital path is similar to that of their parent comet. The effect of this orbital attenuation is to cause these particles to spiral into the sun. This process takes an enormous amount of time. During the process, each meteoroid is dispersed from its cloud to such an extent that it can no longer be associated with the cloud. This leads to the birth of sporadic meteoroids of cometary origin, with a unique orbital path for each particle.

Although meteor showers are noted for greatly increased counting rate, the average contribution per annum is only 20 to 30% of the total mass accumulated by Earth (Reference 31). It is believed that 90% or more of all meteors are of cometary origin (Reference 32).

The probability of a space vehicle hitting the nucleus of comet is extremely small; however, the gases of the coma and tail occupy a considerably larger volume. Ehricke has shown (Reference 20) that traveling through such a tenuous gas for a long period could critically alter a vehicle's velocity. Since most of the comets travel in inclined orbits, however, the probability is low that planetary probes would encounter such difficulties.

## II. PLANETS AND THEIR SATELLITES

Excessive energy requirements prevent exploration in the near future of any but the nearest planets. Exceedingly long times required for the more remote planets are shown in Figure 10. Travel time required to a given planet on the indicated curve assumes a minimum-energy trajectory as indicated by the top curve. If more energy is available, i.e., the energy lies somewhere in the upper shaded region, then a shorter flight time is obtained, falling in the lower shaded region (Reference 34).

Clearly, Jupiter's orbit represents the most optimistic goal for inter-planetary travel, at least for the next few years. Therefore, this study emphasizes those planets, namely Mars, Venus and Jupiter, which could be visited within the foreseeable future. However, consideration of the more remote planets is also important since frequently information pertaining to a particular planet is helpful in understanding observations from another. Each of the planets is therefore individually discussed.

Tabulations of the physical and orbital data of the planets and their satellites were presented in Tables 1 through 4. Note that the orbits of the planets, as well as the orbits of the satellites, are nearly circular, and that most of the orbits are nearly coplanar. All of the planets (except Uranus, and possibly Venus) and the sun rotate in the same direction in which they revolve. Similarly, most of the satellites and the rings of Saturn revolve around their parent planets in the same direction in which the planets revolve around the sun.

According to their physical characteristics, the nine planets fall into separate groups - terrestrial (resembling the earth), and Jovian, or giant (resembling Jupiter). Although Mercury and Pluto are the extreme opposites on the temperature scale according to their relative distance from the sun (Figure 11), they are similar; both have small diameters, high densities, low masses, and long rotational periods characteristic of the earth. Thus, together with Mars and Venus, they are termed terrestrial planets. In contrast, Saturn, Uranus, and Neptune are referred to as Jovian or giant planets because of their

similarity to Jupiter. Their very low densities, rapid rotation, hydrogen-compound atmospheres, and huge diameters suggest an evolution different from that of the earth. Important features of the planets, pertinent to space-propulsion considerations, are presented in sequence of their distance from the sun.

#### A. MERCURY

Mercury is the smallest of the nine planets, with a diameter of 5000 km. Named Mercury by the Romans because of its rapid apparent motion (a motion caused by the fact that it speeds faster in its orbit than any other planet - 29.8 miles/sec), it is not much larger than the moon and is slightly smaller than the two largest satellites of Jupiter. However, its density (0.9 of the earth's and more than twice that of Ganymede) is of planetary dimensions.

As a result of being so close to the sun, it has been constrained to rotate and revolve in the same period of 88 days, just as the moon keeps the same face to earth. Nevertheless, only 30% of the planet is in continual total darkness (Reference 34), since the ellipticity of its orbit ( $e = 0.2$ ) causes rather large librations.

Mercury has received increased attention during the last two years from both observational and theoretical astronomers, as well as from systems engineers considering the feasibility of a space probe flight in the near future (prior to 1980). Since the dark side of Mercury may contain the greatest abundance of light elements in the solar system (elements of importance both for life support and as propellant chemicals), the planet is of interest both as a logistic supply base, in addition to its basic scientific significance (Reference 43). A preliminary analysis showing the feasibility of a Mercury mission has recently been published (Reference 37).

In 1962, the microwave brightness temperature of Mercury's illuminated disk was measured for the first time, and radar contact was established.

These and other measurements are summarized in tabular form below.

<u>Observational Technique</u>	<u>Results and Interpretations</u>	<u>Investigator</u>
(1) <u>Radiometry</u>		
(a) Infrared flux	Average subsolar point temp ~600°K at 8-13 $\mu$ with substantial variation due to eccentricity of orbit	Petit, 1961 Reference 46
(b) Microwave flux	1050 + 350°K near 3.5 cm in illuminated hemisphere.	Howard, Barrett and Haddock, 1962 Reference 45a
(2) Radar	Reflectivity 3-6%	Kotel'nikov, 1962 Reference 53
(3) Photometry	Albedo = 0.056	Harris 1961 Reference 52
(4) Polarimetry	Deduced atmosphere ~1 mm Hg	Dollfus 1950 Reference 50
(5) Visual and Photographic	Occasional reports of veiling of surface features; no photographic mapping	Antoniadi (1935) Reference 44

#### 1. Atmosphere

Lyot's polarization curve of Mercury shows an excess of polarization at the cusps, probably indicating the presence of a weak atmosphere (References 35 and 50). If the atmosphere consisted of air, it would have a thickness of only 25 meters and a surface pressure of 1 millibar. The presence of tenuous dust clouds could account for regional departures in the observed polarization curve. Assuming that the gases of this atmosphere were produced after the planet cooled to its present temperature, its most likely constituents are carbon dioxide, oxygen, sulfur dioxide, and argon (Reference 36). Lighter gases would have long since escaped. An excellent discussion of the possible constituents of the Mercurian atmosphere is presented by Sagan and Kellogg (1963, Reference 38).

2. Temperature

Mercury exhibits the greatest temperature extremes of any planet in the solar system. At the subsolar point, the temperature varies from  $688^{\circ}\text{K}$  at perihelion to  $558^{\circ}\text{K}$  at aphelion (Reference 35), as calculated from its blackbody curve and the solar constant. On the dark side, the temperature approaches absolute zero. Because of the large librations, there is a fairly wide belt near the terminator with earthlike temperatures. Only in this twilight zone would surface landings be feasible.

For the illuminated side, the reported microwave temperatures (Howard, 1962, Reference 45a) appear significantly higher than the infrared observations (Petit, 1961, Reference 46). The temperature differences at various phases are presented below (from Robert, 1963, Reference 45b).

<u>Planetocentric Angle Between Sun and Earth, deg</u>	<u>Disk Temperature Reduced to Mean Solar Distance of Mercury, <math>^{\circ}\text{K}</math></u>	
	<u>Microwave</u>	<u>Infrared</u>
0	~ 1100	~ 600
30	1000	540
60	750	350
90	500	120
120	250	40

Field (Reference 48) has shown that, if the above apparent difference is real, the difference can be interpreted in terms of unexpectedly high temperatures in the unilluminated hemisphere, possibly in the range of  $200\text{--}300^{\circ}\text{K}$ ; radioactive heating from within might also be responsible (Reference 40). Comprehensive discussions of the microwave and infrared temperatures are presented by Rea and Welch (Reference 40, 1963) and Sagan and Kellogg (Reference 38, 1963).

The temperature of the dark hemisphere has been treated theoretically by Walker (Reference 47, 1961). If heat conduction from the illuminated hemisphere is neglected, Walker computes a lower temperature limit of  $25^{\circ}\text{K}$ . When heat conduction is allowed, Walker predicts a temperature of  $28^{\circ}\text{K}$ .

### 3. Interior

Appreciable theoretical evidence is available to indicate that the Mercurian interior is in a molten metallic state (Reference 38 and 39, 1963). Urey (Reference 42, 1963) points out that the density of Mercury at low temperatures and pressures is not consistent with the densities of other planets; he cites references that suggest Mercury consists of iron carbide. The planet's mean density (5.5 g/cu cm) is thought by MacDonald (Reference 39, 1963) to indicate that it does not have a highly radioactive composition similar to that of chondrites, as has sometimes been hypothesized. MacDonald suggests that Mercury is largely metallic, with a low concentration of radioactive elements.

### 4. Surface

In appearance, Mercury's surface is similar to that of our own moon (References 37 and 51). The albedos and polarization curves of both bodies are remarkably alike. Moreover, the increase in the brightness of Mercury from quarter to full phase, produced by the disappearance of shadows, indicates that the topography of Mercury is at least as irregular as that of the moon. In the temperature belt mentioned above, libration will produce a "day and night," causing the surface to be alternately heated and cooled. The surface in this area, therefore, is very probably cracked in many places. These natural crevices and the shadows, if mountainous, could be used to protect an outpost or probe from the heat of the sun while observing that body from the hot side of Mercury (Reference 35). Lyttleton (Reference 41, 1962) in a theoretical work on the origin of mountains, presents arguments showing the Mercurial surface can be expected to resemble that of the moon rather than that of the earth. Hodge (Reference 49) states that meteoritic erosion of the dark side of Mercury is probably insignificant, although the constant meteoritic infall may disturb any anticipated stratification of surface material.

## B. VENUS

Although Venus is the closest planet to earth, and is very similar to earth in its mass and radius, earth-based observations have been hampered by the extremely thick cloud layer covering Venus and the distance separating the two planets. At the closest point to earth, inferior conjunction, Venus is some 26 million miles from earth.

At the time of the Venus flyby, on 14 December 1962, the Mariner II spacecraft was only 21,000 miles from Venus, permitting close observation of the planet for 35 min. These Mariner II data, together with recent radar and spectroscopic studies, have resolved several controversies concerning the physical properties of the planet. While several important considerations are not yet well understood (including the circulation, meteorology, and aspects of the rotation), a good deal is now known, allowing at least the general features of the environment to be described in a realistic way. The following discussion endeavors to concentrate on the most recent concepts rather than elaborate on older formulations that are covered to some extent in the annotated bibliography (primarily References 54 to 120).

1. Physical Properties

The mass, diameter (with cloud cover), and volume of Venus were known fairly well prior to the Mariner flight. Since Venus does not have a satellite, the mass had been calculated using the perturbations of the orbits of other planets (Mars and the earth). This procedure, using data collected for decades, has a probable error of 0.05%. From Mariner tracking data, it will be possible to establish the Venus mass within 0.005%.

The rotation period of Venus is believed to be 230 days ( $\pm 40$  to 50 days) retrograde, based on 1962 radar experiments (Reference 33). The fact that the rotation is very slow is confirmed by at least four different measurements: Doppler smearing, signal-strength variation with time, Doppler shifts from several range "slices" of the planet, and observation of a bright reflecting spot moving across the face of the planet.



The conclusion that the rotation is retrograde is, however, based on the assumption that the axis of rotation is perpendicular to the radar line of sight from the earth (or nearly perpendicular to the orbital plane). Kopal (Reference 55) warns that even a  $30$  or  $40^\circ$  inclination would change the interpretation from direct to retrograde. Consequently, statements as to whether the motion is direct or retrograde cannot be made until estimates of the angle of inclination are known. Further, some care should be used in applying the 230-day period, since it is conceivable that libration or wobble of the planet could seriously confuse the observed data. Improved experimental techniques should result in data of higher certainty in the near future.

It is possible that lightning and other atmospheric disturbances occur on Venus. Kraus studied radio signals at 11 cm and concluded that lightning could have produced the observed intensities; more recently (in 1960), he re-examined the data (Reference 97) and concluded that the quasi-coherent radiation did not come from Venus but from interference of terrestrial origin. Recent observations by Carr (1961, Reference 87) failed to show any such disturbances over a 330-hour period of continuous monitoring.

## 2. Albedo

Evidently, the planet reflects the greater part of the incident solar radiation in the visible region, and a much smaller fraction in the violet and near ultraviolet. The albedo of Venus has been measured and found to be between 0.55 and 0.90 in the visible and infrared; it also varies markedly with wavelength. Kuiper (1957, Reference 110) has estimated the effective albedo as  $0.67 \pm 0.03$ . Kuiper's value is probably the most accurate, since the wavelength for which it was determined (5500 A) is representative of the peak radiant energy of the sun.

## 3. Surface Characteristics

Almost nothing is known about the structural surface characteristics of Venus. The high surface temperatures measured by Mariner II ( $700^\circ\text{K}$ , discussed under 6 below), higher than the melting point of lead, confirms the

absence of any life of the kind known on earth. It has been inferred from radar data that the surface characteristics may be very similar to those of the earth (Reference 74). The surface was shown to be rough by cross polarization measurements (Reference 33), with the average dielectric constant of the surface material similar to that of dust or sand. No indication of major volcanic activity has ever been observed. Lyttleton (Reference 41, 1963) predicts the presence of mountains similar to those found on earth.

#### 4. Clouds

A yellow cloud cover, fluctuating in optical depth in place and time, obscures the solid surface. The nature of these clouds is still disputed among authorities. Sagan (Reference 94) proposes that the clouds are ice crystals, while Öpik (Reference 89) suggests they are dust stirred up by strong surface winds. More recently, Kaplan (1963) has suggested hydrocarbons similar to smog (Reference 61).

The preponderance of physical evidence favors the ice crystal or water vapor theory. Kopal (Reference 55) recently suggested this viewpoint, mentioning the probability of dust particles at the lower cloud layers. Evans (Reference 58) also arrived at the water-vaporcloud conclusion by a detailed study of the variation of albedo of Venus with wavelength. While the variation of frequency with wavelength, reported by Evans (Reference 58) and attributed to Sinton, differs somewhat from Sinton's original measurements (Reference 56), and while Sinton's measurements cannot be satisfied completely on the basis of a water vapor assumption, many similarities between water vapor cloud absorption (e.g., Hewson, Reference 64 and Moreland, Reference 65) are apparent.

From Mariner II data (Reference 54) it is estimated that the cloud layer is 15 to 20 miles thick, with a ceiling of about 45 miles. The temperature is about  $+200^{\circ}\text{F}$  at the bottom decreasing to about  $-30^{\circ}\text{F}$ , somewhere in the middle of the cloud layer. However, the probe found no evidence of breaks in the clouds as were previously thought to exist because of observed shifting, irregular markings observed from earth. One cold spot in the cloud layer, (at least  $20^{\circ}$  cooler than the surrounding clouds) was found, indicating a region of

higher clouds, or a more opaque area, or both. Temperatures in the cloud layer were found to be the same on the dark side as on the light side.

These Mariner data are in reasonable agreement with observatory data as far as comparisons can be made. Spectroscopic temperatures of  $300^{\circ}\text{K}$  ( $80^{\circ}\text{F}$ ) have been reported by Chamberlain and Kniper (1956, Reference 114) and others. Spinrad (1962, Reference 70) calculated a rotational value of  $240^{\circ}\text{K}$  from  $\text{CO}_2$  spectra; a thermal emission temperature of  $234^{\circ}\text{K}$  in the cloud layer was found by Strong and Sinton (1960, Reference 91). These correspond roughly to the  $+200$  to  $-30^{\circ}\text{F}$  range measured by Mariner II.

Temperature calculations of  $207$  to  $215^{\circ}\text{K}$  have been computed from the occultation of Regulus (Reference 59a), data which is usually taken to be about 50 km above the cloud layer.

Although the corresponding pressures can usually be determined by line-broadening from the spectra, the major difficulty, for the purposes of calculating model atmospheres, is in determining corresponding elevations.

#### 5. Atmospheric Constituents

Until 1954,  $\text{CO}_2$  was the only known specific molecule present in the Venusian atmosphere (Dunham, 1952, Reference 120). Molecular nitrogen and other molecules were identified by Kozyrev (1954, Reference 118). Until recently,  $\text{CO}_2$  was thought to be the major constituent. Kopal (Reference 90) suggested in 1960 that  $\text{CO}_2$  was probably only a small part of the atmosphere and that molecular nitrogen formed the major portion. Recently, these ideas were verified by Spinrad (1962, Reference 70).

Spinrad studied the ten best Mt. Wilson plates and by careful analysis found the total pressures in the atmosphere to be substantially higher than previously computed. The percentage of  $\text{CO}_2$  is therefore substantially reduced (to about 5%, with an uncertainty factor of 2), making  $\text{CO}_2$  only a minor constituent of the atmosphere. In the absence of positive spectroscopic identification, the major constituent creating the high total pressures must therefore be a gas whose emission lines are absorbed in the earth's atmosphere. Nitrogen would appear to be the possible answer.

Spinrad calculated the  $\text{CO}_2$  absorption to originate in a region in which

$$T_{\text{rot}} = 440^\circ\text{K with } P \sim 5 \text{ atm.}$$

Mariner II data failed to show the presence of either water vapor or  $\text{CO}_2$ , the concentrations being too small to be detected with the probe instrumentation. Evidences of water vapor have been found by Sinton and Strong (1960, Reference 93), although there are questions to the accuracy due to the uncertainties in the amount of water vapor present in the earth's atmosphere. A detailed discussion of the literature on the constituents of the Venusian atmosphere is given by Sagan and Kellogg (Reference 38, 1963).

#### 6. Thermal Structure of the Venus Atmosphere

The temperature of the Venus atmosphere varies over extreme ranges with height but does not vary appreciably with longitude or latitude location; the temperatures at any given height are similar whether on the sunlit or dark sides of the planet (Mariner II, Reference 33 and 54).

Even before the Mariner II data was available, it had been established from radio signals that the surface temperature was high (about  $600^\circ\text{K}$ ), by Mayer, McCullough, and Sloanaker (1958, Reference 107), and more recently by Lilley (1961, Reference 83). A radiometric temperature of  $700^\circ\text{K} \pm 140^\circ$  is usually quoted (Drake, 1962, Reference 59). The average of this value is identical to the Mariner II measurement. A comprehensive discussion of recent radiometric and infrared temperature measurements is given by Rea and Welch (Reference 40), 1963.

Kaplan (Dec. 1962, Reference 76) calculated a "standard" and an extreme model atmosphere for Venus presenting the temperature, density and pressure as functions of height as shown in Fig. 12. Kaplan's model correlates Spinrad's analysis of the old Venus  $\text{CO}_2$  spectra with the occultation of Regulus data and radiometric data (8 to  $13\mu$ ). The "standard" surface temperature was taken as  $700^\circ\text{K}$ , at that time based on radar results but since verified by Mariner II.

Kaplan's calculation was based on the familiar hydrostatic equation of state taking into account the variation of the acceleration of gravity, taken as 900 cm/sec at the surface. Between the significant levels, the pressure-temperature relation was assumed to be

$$T_1/T_2 = (P_1/P_2)^k$$

where k was assumed to be constant for each layer (Table 7).

The results of Kaplan's work are contained in Table 7 and in Figure 12. The standard model is considered adequate for re-entry heating calculations. Owing to current uncertainties in pressure variation near the surface, the curves should not be used to determine flight time between re-entry and ground contact. However, the high surface temperatures make this limitation of little practical importance.

#### 7. Physical Mechanisms of the Thermal Environment

The description of the Venus atmosphere presented above is an attempt to assemble, in a systematic way, the various observed parameters without investigating actual physical mechanisms that could produce these parameters. In light of Mariner II data, it appears reasonable to construct at least a rudimentary model of the Venusian thermal processes. The now-familiar schematic diagram of the thermal environment is shown in Figure 13. In this model, the incident visible and infrared sunlight permeates the clouds but the resulting thermal emission from the surface is blocked by the cloud layer. Quite probably, strong convective currents dominate the surface environment, equalizing the surface temperature around the planet. This process of heating the dark side would be aided by the complete cover of the insulating cloud layer.

The above description would appear to be a combination, with certain modifications, of two well-known theories: the greenhouse model and the aeolosphere model.

The greenhouse model (Sagan, 1960, Reference 94) explains the high surface temperatures by assuming that the cloud layer, composed of  $\text{CO}_2$  and  $\text{H}_2\text{O}$ , is transparent to the incident sunlight in the visible and infrared, but opaque to the far-infrared (thermal) emission from the surface. A sketch of this effect is shown in Figure 14. Verification of the presence of water vapor was found by Strong and Sinton (1960, Reference 93) although the amount was not established. Calculated values of cloud-layer depth, temperature rise, necessary to support this theory are found to be consistent with observations.

There is disagreement between the calculations of Sagan and Öpik (1956, Reference 112) regarding the amount of water vapor necessary to support the greenhouse effect. Until better measurements are available (Sinton's observed  $2 \times 10^{-3}$  g/cu cm of water vapor is in question), the problem cannot be resolved. Spinrad (1962, Reference 72), by calculating Doppler shift calculations on Dunham's Mt. Wilson plates, has recently confirmed the belief that the water vapor is far less than that reported by Sinton.

The expected surface of Venus, consistent with the greenhouse model, would be dry, calm, overcast, and very hot, with the sun visible through high cirrus clouds.

The aeolosphere model, suggested by Öpik (1961, Reference 99) suggests that the clouds are composed of dust which is stirred up by winds. The surface is, therefore, a perpetual dust storm, with no sunlight but intense heat resulting from the imposed adiabatic heat lapse rate through the stirred up atmosphere. A schematic sketch of the proposed aeolosphere is shown in Figure 15. This theory has been challenged on several points, including possible inconsistencies in the albedo and phase variation of the microwave emission.

Kopal (Reference 55) has suggested the actual situation may consist of a greenhouse effect in the cloud layer, much as Sagan (Reference 94) described the mechanism but with the atmosphere under the cloud layer consisting of an aeolosphere as Öpik (Reference 89) described, with hot, perpetual dust storms.

### 8. Magnetic Fields and Radiation

The Mariner II probe magnetometer did not detect the presence of a magnetic-field (within the 5-gamma limit of sensitivity). At an altitude of 21,000 miles above Venus, the magnetic field would have been about 100 to 200 gammas if the Venus magnetic field were similar to that of the earth. These data tend to confirm the theory that the strength of the magnetic field is related to the rate of rotation. Since other experiments have shown that Venus rotates very slowly, if at all, Venus could be expected to have a small magnetic field. Of course, it is possible that Venus might have a complicated magnetic field structure that would produce high magnetic field intensities locally on the surface without being apparent at the 21,000-mile fly-by distance.

With regard to theoretical efforts, Kopal had previously pointed out (1960, Reference 90) that since Venus is approximately the same size and density of the earth, Venus could reasonably be expected to have a similar core and a similar field, and quoting the results of Houtgast (Nature, 1956) shows a 1- to 2-gauss field likely. Recently, however, Kopal (Reference 55) expressed the view that the magnetic field strength was related to the rotation speed; this would greatly reduce the probability of a Venusian magnetic field. Naroyana (1959, Reference 103) calculated a 0.4 gauss field, based on statistical plots of daily planetary amplitude. The most recently accepted thesis appears to be that expressed by Newburn (1962, Reference 76), that the field is much less than that of the earth and is very unlikely to be more than a few gauss.

### C. THE EARTH-MOON SYSTEM

The earth's moon is the largest of all moons in relation to the parent planet. Several moons (e.g., Ganymede) are actually larger. Ganymede, however, is only  $1/28$  the size of Jupiter, while the earth's moon is  $1/4$  the earth's size. This fortuitous situation provides an excellent training ground for practicing the techniques of space flight necessary for exploring the solar system.

### 1. The Lunar Environment

Although the nature of the lunar surface has been described in many places [see, for example, Fielder (1961, Reference 133); Kopal (1960, Reference 134); and Buwalda (1960, Reference 135)], a new evaluation of some of the experimental results is in order for this report since the application of the results will be new. This report is particularly concerned with the influence of lunar environmental conditions on propulsion systems.

The environment encountered by a propulsion system in the neighborhood of the moon is similar to that in interplanetary space with a few important exceptions. Thermal, gravity, and radiation conditions differ from those found in space. Magnetic, electrical, and gravitational fields differ, and the density of charged and neutral particles, including meteors, is probably not the same as that in space. Dust may be stirred up from the moon's surface and interfere with operations on the surface. On the other hand, presence of solid materials and resources may prove to be advantageous to these operations.

As a first step in describing the lunar environment, a few important constants should be listed to provide a frame of reference for the discussion. The constants are shown in Table 8.

As the table shows, the moon's albedo is low. Only 7% of the sunlight received is reflected. The rest is absorbed. The moon itself radiates heat, known as planetary heat; from this radiated heat may be inferred the temperature of the surface and of deeper layers. Infrared measurements yield the surface temperature which ranges from 400°K at the subsolar point (the point on the moon's surface directly below the sun at any instant) to below 120°K in the shade. This temperature range, from above boiling water, down to nearly liquid-air temperature, is tremendous. Materials and systems will not survive and operate properly under these conditions unless specially designed or thermally protected.



The problem of thermal control is different on the lunar surface than in space. Instead of radiating to cold outer space and receiving essentially no heat in return, a device on or near the moon receives radiation from the moon. It is exposed to cold outer space over only about a hemisphere. The device may be shaded by the moon from solar radiation, and, alternatively, may shade from the sun a small area of the moon's surface, changing its surface temperature. Maintaining the temperature of the device on the moon's surface within a reasonable range may require even more ingenuity than does thermal control in space.

In contrast to the extremes of temperature encountered on the lunar surface, the temperature a short distance below the surface - a foot or two - remains nearly constant at a temperature a little below that of freezing water. (This result was obtained by studying radio microwave radiation from the lunar surface.) The surface temperature changes because the moon rotates with respect to the sun, although it continually keeps one face toward the earth as it revolves in its orbit. A point on the moon's surface is sunlit for half a month (one month equals 27.32 days, as shown in Table 8) and shaded for the other half-month. The surface temperature drops rapidly as the area passes into shade, while the temperature of layers below the surface changes slowly. Even more striking, the surface temperature during an eclipse almost directly follows the insolation, while the deeper temperatures lag severely. These results have important bearing on the nature of the surface materials. An extremely low thermal conductivity is indicated for the surface layer. In fact, the indicated thermal conductivity is so low that only fine powders in vacuum can be considered as surface materials. These results apparently demonstrate that there is fine dust over much of the moon's surface, but they also indicate that the dust layer probably isn't very thick, probably less than an inch or a few inches thick. Other lines of evidence support this estimate of thickness although claims have been made for much greater thicknesses. The heat capacity of the surface layer is probably low, while that of material lying below the surface is closer to the heat capacity of common terrestrial rocks. All of these results have bearing on the thermal design of a device for use on the moon.

Radiation other than thermal will offer problems for lunar operations. The ultraviolet, X- and gamma-radiation from the sun will damage some materials if exposure to these rays is sufficiently long. The radiations are exactly the same as those measured in nearby space and for that reason will not be discussed in this section. All of the electromagnetic radiation from the sun travels in straight lines and will fall upon the sunlit side of the moon and not on the dark side.

Charged-particle flux, on the other hand, does not necessarily travel in straight lines, but may be deflected by magnetic or electric fields, and hence presents an extremely complex problem. Solar-flare flux of high-energy particles is particularly complex and is of great concern, since it may damage such materials as solid propellants, electronic components, and plastics. The nature of these solar-flare fluxes will be discussed elsewhere, but it should be pointed out here that many of these particles may reach the side of the moon away from the sun. There is no real assurance that hiding from sunlight will enable one to escape solar-flare particles. Charged particle streams from the sun, including the solar wind (which probably "blows" rather gently most of the time) and particle streams from flares, have many other effects. They may affect the charge on the moon's surface or on a vehicle and influence electric fields in the neighborhood of a vehicle. (Photoelectrons generated by ultraviolet light will also contribute to the charge conditions.)

Dust and meteor flux will be important to systems operating on the moon. The flux will resemble that in interplanetary space in the neighborhood of the earth's orbit and will be little influenced by the moon's gravitational field. However, the flux may vary with position on the moon's surface since the flux is isotropic neither for the moon nor the earth. Detailed discussion of the fluxes, masses, and expected damage will not be repeated here since these subjects are covered in the description of the interplanetary environment.

Another important environmental feature is the atmosphere. Almost all attempts to measure any atmosphere near the moon's surface have failed. In fact, Dollfus (1956, Reference 138), using refined techniques,

found that the density of the atmosphere at the surface of the moon must be less than  $10^{-9}$  of the density of the earth's atmosphere at sea level. Elsmore and Whitfield (1955, Reference 139) detected the presence of a tenuous atmosphere of charged particles by observing occultation of radio stars. Elsmore (1957, Reference 136) estimated the surface density of electrons to be  $10^3$  particles cu cm and the total density of the atmosphere at the surface of the moon to be less than  $6 \times 10^{-12}$  of terrestrial sea level density. The gases present in minute quantities in the atmosphere may be heavy gases, such as Kr and Xe, or there may be some light gases, temporary visitors from the sun, just as there are throughout interplanetary space, or there may even be a little water vapor (Watson, Murray, and Brown, 1961). In any case, the atmosphere is extremely rarefied and represents a vacuum better than a laboratory high vacuum. High vacuum introduces difficult and challenging materials problems. Many plastics, for example, are useless for vacuum applications. Thermal control paints, electronic potting compounds, lubricants, and seals must all be studied carefully for they are likely to be altered by the vacuum environment and fail to perform satisfactorily.

Gravity on the moon is one-sixth that on the earth; this will influence mechanical design on some systems, although the changes introduced will not be drastic. Suspension systems, for example, that balance a spring force against a weight force will require design different from that on earth.

The magnetic field of the moon, which may be important in some control units, is very small if it exists at all. It is probably less than 100 to 200 gammas. (A gamma is  $10^{-5}$  gauss; the earth's field is about half a gauss.)

## 2. Van Allen Radiation

Our understanding of the Van Allen radiation belts has changed significantly during recent months, due primarily to results of Explorer XII (e.g., References 141 to 143). The Van Allen radiation consists almost entirely of protons and electrons trapped in belt-like regions about the earth over very extensive areas extending out toward the limit of the geomagnetic field in the direction of the sun. To a first order approximation, these regions have rotational symmetry about the geomagnetic axis and, in terms of geocentric distance in earth radii, form a hard electron belt at about three earth radii ( $2 \times 10^4$  km) and a hard proton belt somewhat closer at about 2 to 2.5 earth radii, with softer electron and proton belts extending out to 8 to 10 and 10 to 12 earth radii, respectively.

The accepted electron flux of  $10^8$  electron/cm<sup>2</sup> sec for energies greater than 20 kev, based on Explorer XII data (Reference 141) agrees with that predicted previously by Gringauz et al. (Reference 144) but is substantially less than predicted by Van Allen and others (e.g., References 145, 146) -  $10^{10}$  or  $10^{11}$  electrons/cm<sup>2</sup> sec. Further, the presence of a generally unsuspected flux of electrons of about  $10^5$  electrons/cm<sup>2</sup> sec with energies near 2 Mev has been detected.

Schematic diagrams of the location and energy-flux levels of the belts prior to Explorer XII are shown in Figures 16, 17, and 18 respectively. These data were obtained from Johnson (1962, Reference 141), Dessler (1961, Reference 147), which was in turn based on work of Freden and White (1959, 1960, References 148 and 149) and the work of Vernon, et al. (1959, Reference 150) and Walt et al. (1960, Reference 151). Spatial distributions and energy levels based on Explorer XII data are given in Figure 19, based on work by Johnson (1962, Reference 141).

The complex structure of trapped-particle belts is due to the different source mechanisms which inject protons and electrons into different regions of the earth's magnetic field. As soon as these mechanisms are thoroughly understood, the space distribution and spectrum of the trapped particles can be given in terms of the sources. The decay of neutrons produced by interaction of cosmic rays and solar-flare protons with the atmosphere is a source of the

higher-energy protons and electrons. Direct injection of solar protons and electrons, and local acceleration of thermal protons and electrons, are possible sources for the soft-proton belt, the low-energy part of the electron belt, and the "auroral" belt. The neutron-albedo decay, previously thought to be a source of the hard electron and proton belts is no longer accepted, as discussed recently by Johnson (1962, Reference 141) and Pizzella et al. (1962, Reference 143).

The best description of the spatial distribution of the geomagnetically trapped (Van Allen) protons and electrons, based on their relation to the earth's magnetic field, involves the theory of the motion of trapped particles. This motion divides naturally into three components:

a. A particle moves in a circle of radius

$$a = mv_n(c/eB) \text{ with a frequency } W_c = eB/mc,$$

where  $m$  is the mass of the particle,  $v_n$  is the component of its velocity perpendicular to the direction of the magnetic field,  $e$  is the particle's electric charge, and  $B$  is the magnitude of the magnetic field (the units are gaussian). The radius,  $a$ , is small compared to distances over which the magnetic field changes by an amount comparable to itself. The center of this circular motion is called the guiding center of the particle.

b. The guiding center of the particle moves along a magnetic field line with a velocity equal to  $v_p$ , the component of the particle's velocity along the direction of the magnetic field. This motion satisfies the condition  $B/\sin^2 \theta = \text{constant}$ , where  $\theta$ , the "pitch angle" of the particle, is the angle between the direction of the magnetic field and the velocity of the particle. Therefore, when the guiding center reaches the maximum magnetic field,  $B_m = B/\sin^2 \theta$ , the pitch angle will be  $90^\circ$  and the particle will be reflected. Thus, the guiding center of a trapped particle moves along a field line, bouncing back and forth between northern-hemisphere and southern-hemisphere mirror points.

c. In addition to bouncing back and forth between mirror points, the guiding center drifts slowly in longitude. Positively charged particles drift westward and negatively charged particles drift eastward. The guiding center traces out a surface which, for a perfect dipole field, would lie on the surface defined by rotating a magnetic-field line about the magnetic dipole axis. This surface is called the longitudinal invariant surface.

The use of adiabatic invariants in describing the motion of a particle in a magnetic field has been discussed by Northrup and Teller (1960, Reference 152). One such adiabatic invariant, the integral or longitudinal invariant, can be defined as

$$I = \int_{\vec{r}}^{\vec{r}'} \left[ 1 - \frac{B(s)}{B(\vec{r})} \right]^{1/2} ds$$

where  $ds$  is the element of path length along a line of force connecting the point  $r$  with its conjugate point  $\vec{r}'$ ,  $B(s)$  is the magnitude of the magnetic field on this element of path length  $ds$  and  $B(\vec{r})$  is the magnitude of the magnetic field at the point  $\vec{r}$ . The integral is taken along the line of force between the conjugate points. Defined in this manner,  $I$  has a definite value at each point in space, and specifying  $I$  determines a surface. If  $\vec{r}$  and  $\vec{r}'$  refer to the mirror points of a trapped particle, and if there are no electric fields,  $I$  is an adiabatic invariant of the motion of the guiding center. Also, if there are no electric fields, the particle will always reflect at the same magnitude of the magnetic field. The points in space that have the same values of  $B$  and of  $I$  for a ring in each hemisphere. A particle mirroring at this  $B$  and  $I$  will remain upon the surface described by the lines for force that connect these rings. Thus the values of  $I$  and  $B$  are the same at every point in space at which a given particle mirrors. The coordinate system consisting of the magnitude of the magnetic field,  $B$ , the integral invariant,  $I$ , and the longitude has been found to adequately organize measurements made at different geographic locations. If the energy and the mirror-point distributions of a set of trapped particles do not change significantly during the time the slowest particles drift once around the earth, then the directional intensity perpendicular to the line of force will be the same at all points in space having the same values of  $B$  and  $I$ . In general, two particles that initially mirror at different values of  $B$  along a particular line of force will not drift in longitude to the same lines of force. For the earth's magnetic field, however, the shells described by the trajectories of the two particles may be considered to coincide. One important consequence of this fact is that the omnidirectional intensity as well as the directional intensity is constant along the loci of constant  $B$  and  $I$ .

The fact that all particles that drift through a given line of force will remain on approximately the same shell or surface throughout their motion leads immediately to the desirability of labeling all points in space with a number that is unique for each shell. The use of such a parameter would organize measurements along lines of force. C. E. McIlvain (1961, Reference 153) has defined a parameter,  $L$ , called the "magnetic shell" parameter, which, together with the magnetic field magnitude  $B$  and the longitude, can be used as coordinates for mapping the distribution of magnetically trapped particles.

In general,  $L$  is a parameter that retains most of the useful properties of  $I$  and is also approximately constant along lines of force. As pointed out above, a magnetic shell or longitudinal invariant surface for a dipole field is simply the surface obtained by rotating a field line about the magnetic axis. In this case, it should be noted that the magnetic-shell parameter,  $L$ , is just the equatorial radius of a magnetic shell. For most studies,  $B$  and  $L$  can be used as the principal space coordinates.  $L$ , usually given in units of earth radii, can be computed using a spherical harmonic expansion of the earth's field. A complete definition of the magnetic-shell parameter is given in Reference 153.

Dipole representations of the earth's magnetic field have been found to have insufficient accuracy for the study of magnetically trapped particles. However, for the present purpose, it is sufficient to relate the coordinates  $B$  and  $L$  to polar coordinates, using the relations for a dipole field.

$$B = \frac{M}{R^3} \left( 4 - \frac{3R}{L} \right)^{1/2}$$

$$R = L \cos^2 \lambda$$

where  $R$  is the geocentric distance;  $\lambda$  the magnetic latitude; and  $M$  is the dipole moment of the earth, which may be taken as  $0.311635 \text{ gauss-R}_e^3$  ( $R_e = 6371.2 \text{ km}$ ). This relationship between the polar coordinates  $R$  and  $\lambda$  and the  $B$  and  $L$  coordinates, is shown in Figure 20.

d. The paths described by mirror points for particles trapped in the earth's field and chosen to mirror at about 1500 km of altitude at  $120^\circ\text{E}$  longitude were constructed by Dessler (1961, Reference 147), and are shown in Figure 21.

The path followed by a particle whose conjugate mirror points coincide is called the integral invariant equator. It is a curve of approximately constant magnitude of magnetic field and is given for two different values of B in Figure 22 from Dessler (1961, Reference 147). The density of trapped particles is approximately symmetric with respect to the integral invariant equator appropriate to their L-value or shell, but it is sufficiently accurate for many environmental calculations to take the trapped particle belts as symmetric to the integral invariant equator as given in Figure 22.

## 2. Particle Flux

Reliable values for the proton flux at higher energies have been known for some time. While the Explorer XII data shows the proton belt to extend over a much wider range than had been previously believed, this extended proton range is of low radiation intensity, the protons having only a few Kev or less, so that the effective radiation zone is not much larger than originally predicted.

Johnson (1962, Reference 141) points out that since the flux of the trapped protons is comparable to or even exceeds that of the trapped electrons, and since the average energy per particle is greater for protons, then the energy content of the trapped protons is much greater than that of the electrons. Consequently, the geophysical importance of the newly discovered outer proton belt is great, even though from radiation intensity considerations the inner-proton belt is of immediate concern. Proton flux contours for the hard-proton belt are given in Figure 16; according to Dessler (Reference 147) these values are probably correct within a factor of 2 within  $10^4$  km of the earth's center and within a factor of 10 beyond  $10^4$  km. A curve of proton integral flux near the integral invariant equator vs altitude is given in Figure 23, representing a plot of the flux values of Figure 16 vs altitude above the integral invariant equator. Figures 16 and 23 are to be used in conjunction with Figure 22. Thus, by placing the dot of Figure 16 at the altitudes along the integral invariant equator indicated in Figure 22a, a three-dimension description of the proton belt is obtained. Accordingly, the ordinate of Figure 23 begins at the various altitudes of the integral invariant equator indicated in Figure 22a.

Results from measurements by means of a scintillation-counter on Explorer XII indicate an intense proton belt from about 10,000 to 55,000 km



(Reference 154). This soft-proton belt showed maximum flux at values of from 3 to 4 earth radii and a fairly sharp outer edge at about 10 earth radii, which was about the limit of the earth's field as observed by Explorer XII. The proton flux values in the energy range from 120 Kev to 4.5 Mev are between  $10^6$  and  $10^7$  cm<sup>2</sup>-sec<sup>-1</sup> for L values between 2 and 3 earth radii. These are maximum intensities. The high-latitude belt of low-energy protons probably has a source different from that of the hard-proton belt of Figure 16.

Until Explorer XII, measurements of the electron flux were uncertain. Various theories placed the flux at  $10^{10}$  or  $10^{11}$  electrons/sq cm-sec (e.g., References 145 and 146), while others (Reference 144) placed the flux at  $10^8$  electron/sq cm-sec.

The flux of electrons as determined by Explorer XII with the energies above 40 Kev is only about  $10^8$  electrons/sq cm-sec. The flux of electrons with energies greater than 20 Kev is probably not more than twice the flux above 40 Kev. For energies greater than 0.2 Kev, Gringauz (Reference 144) had previously predicted a flux of  $2 \times 10^7$ . In addition, Explorer XII uncovered a flux of electrons in the 2 Mev range at about  $10^5$  electrons/sq cm-sec.

Prior to Explorer XII, Dessler (1961, Reference 147) had taken the electron-flux contours shown in Figure 17 but gave lower flux values than those of any other author. For example, Van Allen's older estimates are given in Table 9 (Naugle 1961, Reference 155). The higher flux values reported by other investigators are obtained by multiplying Dessler's flux values of Table 9 by  $10^2$  for the outer zone and  $10^4$  for the inner zone. This uncertainty in electron flux existed because virtually all measurements had been Bremsstrahlung experiments involving low-efficiency detection (wherein the electron-energy spectrum is uncertain) and because the number of particles in the outer zone varies sometimes by even more than an order of magnitude in a matter of hours (Vernov and Chudakov 1960, Reference 156).

A summary of the Explorer XII flux and energy data as presented by Johnson (1962, Reference 141) is shown in Figure 19. Further highly detailed electron flux data have recently been presented by Hoffman et al. (1962, Reference 157). The importance of spectral changes due to magnetic storms has recently been discussed by Rosser et al. (1962, Reference 142).

The electron experiments can be divided into three categories: (a) energy-flux measurements, (b) electron-spectrum measurements, and (c) Bremsstrahlung experiments (Geiger tubes). Dessler considers that the most reliable value for the electron flux is obtained by combining available measurements (a) and (b); he used the electron-energy flux of  $2 \times 10^{11}$  ev/sq cm-sec measured by Vernov et al. (1959, Reference 150) and the electron spectrum measured by Walt et al. (1960, Reference 151) to infer the electron-particle flux in the heart of the outer zone. On the other hand, the scintillation-counter on Explorer VI, which probably responded primarily to electrons directly and not appreciably to electron-Bremsstrahlung, gave a flux of from  $2.2$  to  $2.7 \times 10^9$  particles/cm<sup>2</sup>-sec with energies greater than 200 Kev at  $25$  to  $30 \times 10^3$  km from the earth's center in the equatorial plane (Rosen and Farley, 1960, Reference 158). This value assumes a steep spectrum between 200-500 Kev, as is shown by the spectrum of Walt, used by Dessler as mentioned above. The Explorer VI scintillation-counter electron flux of about  $10^9$  particles/sq cm-sec (with energies greater than 200 Kev) is considerably higher than would be expected from Figure 17. However the preliminary results of the Explorer XII experiments apparently have resolved this uncertainty in electron fluxes in favor of the values given by Dessler. Therefore, the electron flux values shown in Figure 17 can be assumed to represent the best estimate for quiet-day fluxes.

The bifurcation in the maximum of electron flux vs radial distance in the equatorial plane shown in Figure 17 has been attributed to the Cape-town anomaly in the earth's magnetic field. The suggestion is also made that the two peaks in electron flux are evidence of two separate sources for these two branches of the electron belt, namely neutron albedo decay for the inner branch and solar particles for the outer branch (Reference 159). The greater stability of the inner branch supports this idea.

The scintillation counter on Explorer XII observed large fluxes of electrons in the energy range between 10 and 100 Kev (Reference 154). Between 3 and 4 earth radii, a flux as high as  $4 \times 10^8$ /cm<sup>2</sup>-sec-ster was observed. Between 6 and 7 earth radii, the electron flux was between  $10^6$  and  $10^8$ /cm<sup>2</sup>-sec-ster. From these and other observations (Reference 144), it seems that large fluxes of soft electrons form part of an "auroral" belt extending out to about 10 earth radii.

"Auroral" means only that these particles, electrons, and protons are on field lines meeting the earth in or near the auroral zones. They are not necessarily the primary source of particles causing auroras.

### 3. Energy Spectra

Previously, the neutron-albedo theory has been accepted as a dominant source of electrons and protons in the inner radiation belts. Recently, Pizzella et al. (1962, References 143 and 160) presented data received from an Injun I satellite experiment; in the same reference, he discussed a correlation analysis which showed that neutron-albedo theory cannot be the dominant source.

However, a surprisingly good case has been made for the neutron-albedo decay theory. Realizing that some objections are now being expressed to this theory, some of this background information is presented below.

The energy spectrum of the hard-proton belt shown in Figures 16 and 23 agrees in certain respects with that calculated, assuming a cosmic-ray neutron albedo decay source. If the calculated differential-energy spectrum is expressed as  $N(E)dE \sim E^{-n(E)dE}$ , the exponent  $n(E)$  is calculated to be 0.72 from 40 Mev to 80 Mev, then to increase monotonically to 1.4 at 150 Mev and to 2.65 at 650 Mev. The calculated spectrum (solid line), together with measured values, is given in Figure 24 (Freden & White, 1960, Reference 149). Recent nuclear emulsion measurements by Armstrong et al. (1961, Reference 161) and those reported by Kniffen and Naugle (1961, Reference 162) indicate fluxes higher than those calculated, assuming a cosmic-ray neutron albedo source, for energies below 100 Mev and for L values greater than about 1.6 earth radii. Most of the emulsion data are accumulated over the trajectory of the rocket payload, but a series of separate time exposures was obtained on one flight reported by Kniffen and Naugle (1961, References 163 and 164). The fluxes determined by nuclear emulsion exposures at four different positions on the trajectory are shown in Figure 25. It is apparent that the shape of the spectrum and the flux change with latitude and that the lowest latitude curve of Figure 25 agrees with the calculated flux based on a cosmic-ray neutron albedo source (Figure 24).

It is apparent that for L values greater than about 1.6, high fluxes of low-energy protons below 100 Mev are encountered. It is now believed

the source is definitely not cosmic-ray albedo neutron decay. It is possible that this high latitude belt of low-energy protons is due either to solar protons trapped in the geomagnetic field or to protons produced by the decay of albedo neutrons resulting from nuclear interaction of solar protons with the atmosphere over the polar regions. In any case, the low-energy protons observed by Naugle and Kniffen (Reference 164) appear at about the same L values as do those measured by the Explorer XII scintillation counter and are considered in this report as part of the soft-proton belt defined by Explorer XII.

Assuming that the low-energy protons are associated with solar activity, their flux should decrease as the number of solar proton events per year decreases during the solar cycle.

Spectra of protons observed at low altitudes over the auroral zones are shown in Figure 26, curves (4) and (5). These particles may come from an "auroral" belt, or they may be solar particles directly entering the polar regions.

Solar activity apparently has very little effect on the proton flux of the inner belt, which always seems to remain within a factor of 2 or 3 of an average value.

The energy spectrum of the outer-zone electrons is uncertain and, probably, variable with time. The electron-energy spectrum was measured by Cladis et al. (1961, Reference 165), by means of a collimated magnetic-deflection spectrometer carried in a Javelin rocket which reached a maximum altitude of 1045 km at about 37°N geomagnetic (Figure 27). At apogee, the intensity of electrons of energy greater than 50 Kev was reported to be  $4.2 \pm 0.8 \times 10^6$  electrons/sq cm-sec. No change in spectrum shape was observed at altitudes greater than about 600 km. Any boundary phenomena associated with the atmosphere or a magnetic anomaly effect which would radically alter the energy spectrum at low altitude would introduce an altitude dependence to the spectrum which would be expected to be more pronounced in the 600- to 1000-km region than at higher altitudes. This and other arguments given by Walt et al. (1961, Reference 166) lead one to believe that the measured spectrum is also characteristic of fluxes at somewhat higher altitudes. In the heart of the outer zone, the electron spectrum certainly becomes much harder. Preliminary results from Explorer XII are given in Figure 28. These measurements were made with a combination of Geiger counter, electron magnetic

spectrometer, and CdS energy-flux detectors (O'Brien et al., 1962, Reference 167). The designations SpL, SpH, and SpB refer to the three channels of the spectrometer; the cadmium sulfide (CdS) total-energy detector and Anton 302 Geiger-Mueller tube measurements are also labelled. The sensitivity limits of the detectors are indicated by the vertical arrows.

Electron fluxes have been measured on rocket flights through auroral displays (Davis et al. 1960, Reference 168). The flux is generally isotropic above the atmosphere but appears to be strongly focused, producing the arcs and curtains characteristic of auroras. Rocket flights which did not penetrate visible auroras detected no electron flux. This is to be contrasted with "auroral" protons, curves (4) and (5) of Figure 26, which are observed uniformly over the auroral zones and perhaps down to about  $40^\circ$  geomagnetic latitude. The auroral electrons show an extremely variable spectrum with the number of electrons with  $E \geq 10$  Kev between  $2$  and  $6 \times 10^7$  electrons/sq cm-sec-ster. The integral spectrum above 5 Kev was found on one flight to vary as  $1/E$ ; few electrons were found to have  $E > 50$  Kev.

The origin of the trapped electrons is unknown. The ability of the cosmic-ray neutron-albedo mechanism to account for geomagnetically trapped electrons has been investigated quantitatively by Lencheck, et al. (1961, Reference 169). They conclude that cosmic-ray neutron albedo may contribute most, if not all, of the high-energy electrons above 400 Kev, and possibly above 200 Kev. At higher altitudes and latitudes, corresponding to L values of two or more earth radii, an additional component contributes electrons of lower energies, typically from 20 to 50 Kev, with a very steep spectrum and very large intensity. Their energy is not derived from cosmic rays but most likely from the sun through the medium of acceleration in the geomagnetic field.

During magnetic storms, the electron intensity of the outer belt has been observed to change drastically. Van Allen and Wei Ching Len (1960, Reference 170) observed in Explorer VII data the almost complete disappearance of the outer zone at low altitudes, following a large magnetic storm, and its recovery during the following week to an intensity 30 times its quiescent value. Farley and Rosen (1960, Reference 171) observed in Explorer VII data, intensity fluctuations of as much as three orders of magnitude in the outer zone during the beginning

of the main phase of a geomagnetic storm. Forbush et al. (1961, Reference 172) investigated changes in the intensity of the outer Van Allen radiation belt over the period from 26 October to 9 December 1959, using data from Explorer VII. During this period, the intensity variations were negatively correlated with geomagnetic activity, and the reduction in intensity generally occurred in the outer part of the zone. The decrease in measured intensity is consistent with the idea that some of the particles are "dumped" into the auroral and subauroral zones.

The "dumping" of the outer Van Allen radiation belt during the main phase of a magnetic storm may be only apparent, however; Dessler and Karplus (1961, Reference 173) propose the following partial explanation of the observed changes in the outer belt: "(1) The geomagnetic field in the region of the outer zone of the Van Allen radiation belt is normally distended by a band of trapped low-energy radiation between 6 and 11 earth radii. Electrons from neutron decay are deposited throughout the entire geomagnetic field with a trapping time of the order of  $10^9$  seconds. (2) The arrival of plasma from the sun causes a geomagnetic storm with a diamagnetic current ring set up in the 3 to 5 earth radii region. The reduction in field strength in this region due to the diamagnetism causes a deceleration of the trapped radiation and a resultant decrease in counting-rate in instruments flown through the outer zone. (3) The distortion of the geomagnetic field due to the geomagnetic storm causes the low-energy radiation which is normally present between about 6 and 11 earth radii to be lost into interplanetary space. Therefore, after the decay of the magnetic-storm ring current, the magnetic field will contract beyond its pre-storm configuration. This 'adiabatic compression' of the trapped Van Allen electron 'gas' will cause a 'heating' or increase in energy, and hence an increase in counting rate. The recovery of the Van Allen radiation to its pre-storm conditions is then ascribed to the replenishment of the low-energy radiation found between 6 and 11 earth radii."

A complete and up-to-date discussion by Van Allen of the radiation belts around the earth is to be found in Reference 174.

#### 4. Radiation from the Earth

Radiation from the earth contributes significantly to the space environment near the earth. This energy consists of thermal radiation emitted by the earth's surface and atmosphere and that portion of the incident solar radiation

which is scattered and reflected back into space (Figure 29). The scattered and reflected portion of the incident solar radiation is usually referred to as "albedo."

The albedo varies with the sun's zenith angle, the earth's distance from the sun (season), the state of the atmosphere over which it is observed, and whether it is observed over land or water. Extreme limits of the earth's reflectivity are about 0.15 to 0.85.

The thermal radiation is also variable, depending greatly on the degree of cloudiness of the atmosphere which screens the earth's surface and on the temperatures of the surface and atmosphere for the position and time of observation. The atmospheric transparency varies considerably because of varying amounts of water vapor present, as well as the obvious effect of clouds.

The input of solar energy to the earth (the insolation) can be calculated as a geometrical problem for various latitudes if the solar constant is corrected according to the season. Figure 30 plots the result of such calculations for the northern hemisphere, where the values shown result from time-averaging the insolation over the period of 1 day or longer. The values shown in Figure 30 were calculated by List (1951, Reference 175). Figure 31 shows the average values for the energy absorbed in the earth's atmosphere and at the earth's surface, as determined by Baur and Philipps (1934, 1935, Reference 176) from meteorological studies of the heat balance of the earth. The values of Figure 31 are also averages over periods longer than 1 day. Average values of the earth's albedo are obviously the difference between Figures 30 and 31; these values are plotted in Figure 32.

The spectral-irradiance curve for the earth's thermal emission can be obtained semiquantitatively by assuming that the earth's surface emits practically as a blackbody and the atmosphere has the emission spectrum of an absolute blackbody at a stratospheric temperature of about  $218^{\circ}\text{K}$ . Taking into account the fact that the atmosphere absorbs certain bands partially or completely because of the presence of water vapor and carbon dioxide, the net spectral radiation to space can be obtained. For example, Figure 32 in which the earth's surface is taken as a blackbody at  $280^{\circ}\text{K}$ , shows the earth's thermal-emission spectrum (solid line) as the sum of the  $218^{\circ}\text{K}$  atmospheric-emission curve and the  $280^{\circ}\text{K}$  surface-

emission curve minus that part absorbed by the atmosphere (Belinski, 1948, Reference 177). (If there are clouds or other suspended admixtures which are able to reflect the earth's emission back or to absorb it, the net emission out to space is further modified.) The main feature of Figure 33 is that it shows the spectral region in which the maximum intensity of the earth's radiation falls.

For the purpose of satellite thermal calculations, an average value of the earth's albedo is generally taken to be about 0.38. The average insolation incident on the earth's atmosphere is also usually taken as the solar constant (443 Btu/hour-sq ft) on a plane normal to the earth-sun line. The insolation on a given surface is proportional to the cosine of the angle between the normal to the surface and the earth-sun line. This gives a maximum reflected hemispherical radiant intensity of 168 Btu/hour-sq ft or 0.76 cal/min-sq cm for the above albedo. The earth's absorptance corresponding to this albedo is then 0.62, which gives 275 Btu/hour-sq ft as the rate at which the earth absorbs solar energy per unit of projected area. For thermal balance, this energy must be re-radiated by the earth at the rate of about 68.7 Btu/hour-sq ft, since the radiating area is four times the projected area exposed to solar radiation. The earth's thermal emission of about 68.7 Btu/hour-sq ft, on the average, is often considered to have the shape of the emission spectrum of a gray body at 250°K with an emittance very nearly equal to unity (see Figure 33).

##### 5. The Earth's Exosphere

The composition, density, and temperature of the medium near the earth, but above from 500 to 600 km of altitude, have been estimated on the basis of models derived from theoretical considerations and from a variety of measurements made primarily below 250 km. Many balloon and rocket experiments have measured temperature, density, and concentrations of various neutral-gas-constituents in the atmosphere below 250 km. Because the atmospheric composition changes above 100 km and because these changes vary during the day and with solar activity and latitude, more measurements are needed at various latitudes and throughout the sunspot cycle. Satellite drag-calculations have provided data on the average density at altitudes up to 700 km and higher for day and night conditions near solar maximum. Direct satellite measurements of electron concentration and temperature, positive-ion concentration, and mass at high altitudes are currently being made by instruments aboard Explorer VIII (Bourdeau, 1961, Reference 178).



## a. Temperature and Pressure Profiles of the Exosphere

The exosphere is the outermost portion of the atmosphere, in which the gas is so rarified that collisions between neutral particles can generally be ignored. It may extend outward to about 100 earth radii in the form of a geocorona. The base of the exosphere is called the critical level, which is defined as the height at which a fast neutral particle moving upward has a probability of  $1/e$  of escaping from the atmosphere without collisions. The altitude of the critical level varies from 450 to 650 km as the temperature and density vary during the solar cycle.

The exosphere probably merges into and mingles with interplanetary gas from a slowly expanding solar corona. If energy losses by radiation are low, the interplanetary medium at the earth may be extremely hot. The temperature of the interplanetary gas at the earth's orbit may range from 15,000 to 20,000°K on the model of Chamberlain (1961, Reference 179). Chapman (1959, Reference 180) suggested that heat may be conducted from this interplanetary gas to the upper atmosphere and the exosphere. If the exosphere were heated by downward conduction, the temperature would increase with height; however, Bates (1959, Reference 181) has maintained that such a situation is not realistic, since the exosphere, by definition, is confined to particles belonging to the atmosphere for which collisions are not significant and the energy of which is determined by collisions below the critical level.

It seems most reasonable to assume that any high-energy-interplanetary gas will have few collisions with terrestrial atoms in the exosphere and that the exosphere will show a temperature profile determined by the temperature at the critical level. The region above the critical level is above the height where emission and absorption of radiant energy is important; it is also above the height of the other less important heat inputs such as hydromagnetic heating, high-energy particle bombardment, and joule heating from ionospheric currents. Thus, from an altitude of about 500 km or the base of the exosphere up to altitudes of about 1000 km, the medium is probably isothermal (Nicolet, 1961, Reference 182). Beyond these altitudes, particles escaping from the exosphere cause its average energy to drop. On the other hand, the hot interplanetary gas may become a relatively important constituent, so that the average energy of the medium may rise.

The variation of pressure,  $p$ ; density,  $\rho$ ; temperature,  $T$ ; and particle mass,  $m$ , is determined by the ideal-gas law and the hydrostatic equation. The hydrostatic equation in differential form is:

$$dp = -\rho g dh$$

where  $g$  is the acceleration of gravity and  $h$  is altitude. On using the ideal-gas law in the form  $p = \rho kT/m$ , the hydrostatic equation becomes

$$\frac{dp}{p} = -\frac{dh}{H}$$

where  $H = \frac{kT}{mg}$ , and is called the scale height. Integrating the hydrostatic equation gives

$$p(h) - p(h_0) = - \int_{h_0}^h \rho g dh$$

whereupon it is clear that, if the density profile as well as the pressure at  $h_0$  are known, the pressure at  $h$  can be found by numerical integration. The other form gives

$$\frac{p(h)}{p(h_0)} = \exp \left\{ - \int_{h_0}^h \frac{dh}{H} \right\}$$

If the change in scale height  $kT/mg$  with altitude and pressure at  $h$  are known, the pressure at  $p(h)$  can be obtained. The scale height varies both because of changes in temperature and in composition, i.e., mean particle mass,  $m$ . (The scale height also varies because  $g$  is a function of altitude.) In order to calculate the pressure, a variation of scale height with altitude is generally assumed. Of course, knowledge of either the pressure and density profiles or the pressure and scale-height profiles determines the altitude temperature distribution, assuming that the mean particle mass is known as a function of altitude.

Satellite-drag calculations have provided good data on density at high altitudes. Data from 29 satellite have been used to obtain the density curves shown in Figure 34 (King-Hele, 1961, Reference 183). The curves of density vs height are divided according to date; that is, the particular year of the sunspot cycle and day and night values are distinguished. The error in

the majority of values is estimated at about 15%. If the values of the scale height at various altitudes are determined by the equation:

$$\rho = \rho_0 \exp \left\{ - \frac{(h - h_0)}{H} \right\}$$

where  $\rho$  is the measured density according to Figure 34, then the temperature at these altitudes is determined if the average particle mass is known. At these altitudes,  $m$  is not known exactly, but if the molecular weight is assumed to fall from 25 at 200 km of altitude to 16 at a height of 500 km and then to be constant up to 700 km, the temperature so determined shows a tendency to become constant at heights above 400 km in accord with the assumption mentioned above of an isothermal exosphere. (The above equation follows to a good approximation from the hydrostatic equation and the perfect-gas law.) The temperature between 400 and 600 km so obtained was, by day, 1600°K in 1958 and 1450°K in 1960. By night it was 900°K in 1959-60. The error in these figures is also about  $\pm 15\%$  (King-Hele, 1961, Reference 183).

#### b. A Model of the Exosphere

Johnson (1961, Reference 256) has given a dynamic model of the upper atmosphere, which is the one presented here as giving the best available description above the critical level. It is based on the assumption that the atmosphere becomes isothermal at the base of the exosphere. Johnson takes the temperature above 400 km of altitude to be 1000°K at sunspot minimum and to be 1500°K at sunspot maximum, agreeing with the values, mentioned above, obtained from satellite density measurements. Above about 200 km, sounding rockets have shown that diffusive equilibrium exists (Meadows and Townsend, 1960, Reference 184). In other words, each component of the atmosphere is distributed independently of the others, and the vertical distribution of each component is just that which would prevail in the absence of all the others which have the same temperature profile. Consequently, the distribution of each component can be calculated individually from the hydrostatic equation and the perfect-gas law. Assuming that diffusive equilibrium exists, and making use of available data on atmospheric composition, Johnson (1961, Reference 25) has calculated the curves showing atmospheric composition out to 60,000 km (see Figures 35 and 36).

These curves are tentative, since many uncertainties exist regarding the degree of dissociation of the various molecular gases. More recent calculations of density at 1500 km from Echo I orbital data give between 1 and  $5 \times 10^{-18}$  g/cu cm for maximum daytime conditions in 1960 (King-Hele, 1961, Reference 183), which is about an order of magnitude higher than indicated by Figure 37. This corresponds to a concentration of atomic hydrogen of about  $10^6$  particles/cu cm. Nicolet suggests that atmospheric properties above 750 km are explained by the presence of helium (Nicolet, 1961, Reference 185). A source of He exists through the decay of uranium and thorium in the earth's crust. Diffusive equilibrium calculations by Nicolet give concentrations of He at 750 km of about  $5 \times 10^5$  cm<sup>-3</sup> for solar minima and about  $1 \times 10^6$  cm<sup>-3</sup> for solar maxima. Thus the Echo I drag data can be explained by the presence of an atmosphere of atomic oxygen and He at these altitudes rather than by the atomic oxygen and hydrogen atmosphere of the model shown in Figures 35 and 36. The presence of a dust component with a density of  $4 \times 10^{-19}$  g/cu cm at 1600 km cannot explain the Echo I drag data, since atmospheric drag perturbations were observed during the November 1960 solar-flare events (Jacchia, 1961, Reference 186).

However, the presence of about  $10^{12}$  hydrogen atoms above each cm<sup>2</sup> of the earth's surface is required by the diffuse Lyman-Alpha radiation present in the night sky, discovered in 1958, and part of the absorption present in the solar Lyman-Alpha line. It was at first thought that this absorption and re-radiation was by interplanetary hydrogen; densities of neutral hydrogen required to produce this level of absorption were computed. Now, the ionizing flux for hydrogen has recently been found to be an order of magnitude higher than previously supposed, and these densities of interplanetary neutral hydrogen could not permanently exist in this flux. It was then proposed that this neutral hydrogen exists as a cloud around the earth. According to Johnson's Model, this hydrogen is distributed as in Figure 36.

Combining the densities of the atmospheric components, Johnson (1961, Reference 256) gives the average daytime atmospheric density shown in Figure 37. The corresponding pressure and other parameters vs altitude are given in Tables 10 and 11.

Figure 38 shows the pressure to an altitude of 50,000 km. It assumes that the isothermal condition of Johnson's model extends out this far,

and that the hydrogen composition is as shown in Figure 36. The temperature drop due to escaping particles is ignored in view of the uncertainty of existing knowledge of hydrogen concentration, and the curve probably gives maximum values.

Electromagnetic radiation from the sun causes appreciable photoionization of the upper atmosphere and the formulation of the ionosphere. Ultraviolet wavelengths produce most of the ionization by far, but during solar flares X-ray bursts also contribute significantly. Corpuscular radiation in strong aurorae makes a very small contribution to the formation of the ionosphere.

The concentration of positive ions is essentially equal to the concentration of electrons at altitudes of 100 km or greater. Estimates of electron densities have been obtained from propagation measurements between ground stations and rockets or satellites, and also by direct satellite measurements using r-f impedance probes. However, at large distances from the earth, the main source of information about electron densities has come from a study of whistlers. These are low-frequency signals generated by lightning strokes and propagated along the lines of the earth's magnetic field from one hemisphere to the other. Locating the field line along which the whistler has propagated is a serious problem in this method. The electron density at high altitudes as determined by this method is shown in Figure 39 (Hanson, 1961, Reference 187). The cause of the annual variation shown is unknown.

The concentration of the principal ions at altitudes above 500 km is shown in Figure 40 (Hanson, 1961, Reference 187). These curves are consistent with mass-spectrographic rocket experiments made at lower altitudes.

## D. MARS

Mars may be the only planet, other than the earth, on which instrument packages and scientific exploration teams can be based to study the solar system in more detail. Venus has a surface temperature too high to make landing feasible ( $700^{\circ}\text{K}$ ) and further; since it has a thick cloud layer, is less suitable as an observation platform. The atmosphere of Mars is highly transparent in most optical frequencies, making it a good choice for an astronomical base.

The most exhaustive analysis of Martian data available covering work prior to 1954 is the extensive work of De Vaucouleurs (Reference 243). Later, more limited reviews have been written by Hess (Reference 199d, 1961) and Öpik (1962, Reference 199e). A 1960 conference on planetary atmospheres produced a report, summarizing the state of the knowledge of the atmospheres of Mars and Venus, by Kellogg and others (1961, Reference 203). Two excellent recent surveys available are those of Sagan and Kellogg (1963, Reference 38), and Rea and Welch (1963, Reference 40).

Of particular importance, regarding the constituents and properties of the Martian atmosphere, is the recent work of Spinrad and Kaplan (1954, Reference 188) which has significantly altered earlier concepts. A review of these and other important contributions is presented below, with a partially annotated bibliography (References 188 to 247).

1. Physical Properties

The diameter of Mars is approximately 6626 km, making this planet about one-half as large as the earth, while its mass is only 10.8% of that of the earth. As a result, the mean gravitational acceleration on the surface of Mars is only about  $1/3$  that of the earth.

More precisely, the limiting values of the mass and radius (earth units) range from 0.1069 to 0.1080 and 0.521 to 0.539. Using these values, the calculation of surface gravity yields 0.368 to 0.398 of that of the earth (Reference 220).

The only serious uncertainty concerns the ellipticity of Mars. This has been measured in two ways which give different results: observations of the Martian satellite orbits give the dynamic ellipticity usually quoted of

0.00522, while the optical measurements (determined by measuring the flattening of the disk with a micrometer) give a value two or three times larger, or about 0.013. The reason for this discrepancy has not yet been found.

The two satellites observed in the ellipticity measurement are located at distances of 9000 and 23,000 km from the Mars center, respectively. The inner satellite, Phobos, has approximately twice the diameter of the outer satellite, Deimos. Both are probably less than 10 miles across. Little information is available concerning their natural environment. Shaw (1961, Reference 207) reports that "it is inferred they will have no atmosphere, a mean temperature similar to Mars but of greater extremes and a rough irregular surface covered with dust."

## 2. Surface Characteristics

In order to draw conclusions about the surface features from observed data, the effects of the atmosphere must be eliminated. De Vaucouleurs (1954, Reference 243) has discussed in detail the gross uncertainties and assumptions in this procedure. Nevertheless, certain distinguishing features have been observed and can be delineated, at least from a descriptive viewpoint.

The distinguishing surface features are: dark areas, predominantly neutral-grey in color, localized near the equatorial regions; bright areas of orange ochre covering most of the remainder of the planet; and a white polar cap. Mars usually has a polar cap at all times in one hemisphere or the other. The polar caps are time-variable; they diminish in area as local summer approaches and one or the other sequentially disappears entirely before reforming the following winter; the propagation of these darkening waves has been measured to be about 35 km/day (Focas, 1962, Reference 199a). It is now well established that the polar caps are not frozen  $\text{CO}_2$  but are probably ice.

Surface relief on Mars is generally believed to be moderate. No definite shadows have ever been observed, implying that there are no abrupt linear features extending more than 7000 or 8000 ft above the surrounding terrain. A lone peak like Mt. Shasta, of even 12,000 to 15,000 ft elevation, would almost certainly have escaped detection, however (Framen, 1962, Reference 199f). Lyttleton (1962, Reference 41) presents a theoretical argument predicting a Martian surface of plateaus and crevices but without mountains.

It has been inferred from the irregular retreat of the polar caps and the advance of the darkening waves that some areas are significantly higher than others, forming plateaus. Shilling (Reference 208) has suggested that a study of the Chang Tan desert in Tibet may offer some clues about the nature of the Martian surface.

Some of the most provocative observations of the dark areas were made in the infrared by Sinton (1961, Reference 198); he interprets these spectra, which have features that are more pronounced for the dark areas than for light areas, to be absorption bands, and suggests they are due to organic material, including carbohydrates. Colthrup (1961, Reference 196) has suggested one of Sinton's bands may be acetaldehyde; this view has been criticized by Rea (1963, Reference 195), who notes that acetaldehyde is very volatile and would be expected to be in the gas phase atmosphere, producing bands of similar intensity over both light and dark areas. It is also possible that these features are caused by surface organic matter.

The bright areas are thought by Kuiper (1952, Reference 245) to consist of igneous rock, similar to felsitic rhyolite; this tentative conclusion is the result of a study of the reflectivity in the visible and infrared (uncorrected for atmospheric effects). Visual polarization measurements, on the other hand, have led Dollfus (1961, Reference 199g) to the conclusion that the bright covering is finely powdered limonite,  $\text{Fe}_2\text{O}_3 \cdot 3\text{H}_2\text{O}$ . The discrepancy between these two conclusions indicates the limitations of visual observations for obtaining compositions.

### 3. Clouds and Haze

Observers have identified three general categories that have different colors and somewhat different properties: yellow clouds, presumably dust, which form in limited areas and move with the wind; white clouds, probably composed of ice crystals or possible  $\text{CO}_2$  crystals; and blue haze, which covers extensive areas and is the subject of considerable speculation. Possible explanations of the haze include: a gravitational settling of suspended particles; a phase change of a condensable or sublimable substance, a layer of ice-crystals of a particular diameter, that produce special back-scattering properties; trapped



solar protons; and others. The blue haze (probably red to eye, since it extinguishes blue light) remains one of the Martian enigmas. The question of the blue haze is not wholly academic, since the albedo is strongly influenced in this short-wave region, making accurate heat balance of space vehicles difficult.

Wind-velocity measurements of the yellow clouds indicate an average velocity of 4 to 10 m/sec, with the largest observed velocity being about 25 m/sec; these measurements summarize observations since 1911 (DeVaucouleurs, 1954, Reference 243).

#### 4. Atmosphere

Radical changes have occurred in our concept of the Martian atmosphere during the last few months, due principally to a single high-dispersion spectrogram taken at Mount Wilson by Spinrad and Kaplan (1964, Reference 188). The two important results from this work are:  $H_2O$  was definitely detected, with an abundance of  $14 \pm 7$  microns; and  $CO_2$  was detected, with an abundance of  $55 \pm 20$  meter-atmospheres implying an extremely low surface pressure of about  $25 \pm 15$  mb.

This low surface pressure has now been generally accepted in place of the older values of 100 mb or larger. Much of the earlier work in constructing model atmospheres (such as Schilling, References 200 and 211, and Chamberlain, Reference 199b) is in need of extensive revision, since these lower pressures also indicate rather different chemical compositions than was believed to exist previously.

In attempting to specify the abundances of gases present in the Martian atmosphere, the only quantitative information available is the partial pressure of  $CO_2$  and the observed total pressure, the difference between the two pressures being presumably made up by some unobservable gas such as nitrogen and/or argon. Regarding argon, two assumptions seem reasonable: the net  $A^{40}$  content of the Martian atmosphere in the same (19 mb) as the earth (Brown, 1952, Reference 199h, and Urey, 1958, Reference 223); alternatively, the net content of  $A^{40}$  of the Mars' atmosphere may be taken as proportional to that of the Earth by the ratio of corresponding planetary masses, giving a partial pressure for argon of 2 mb. Whatever portion of the total pressure (if any) remains after the assumed argon is subtracted would presumably be nitrogen.

Calculations based on the above assumptions regarding the constituents were carried out by Kaplan, Munch, and Spinrad (1964, Reference 188) with some surprising results. For the three assumed argon cases [(a) no argon, (b) argon equal to that of the Earth, and (c) argon in proportion to the Earth-Mars planetary mass ratio], and for the lowest, mean and highest pressure models consistent with the observations, the following compositions are obtained:

		Pressure, mb		
		Low	Mean	High
CO <sub>2</sub> (measured)		6	4	3
Total (measured)		<u>10</u>	<u>25</u>	<u>40</u>
Difference between total and CO <sub>2</sub> to be made up by other constituents		4	21	37

Model	Constituents	Pressure, mb		
		Low	Mean	High
a) no argon	CO <sub>2</sub>	6	4	3
	N <sub>2</sub>	4	21	37
b) argon content equal to that of the earth	CO <sub>2</sub>	6	4	3
	A	-	19	19
	N <sub>2</sub>	-	2	18
c) argon content proportional to the ratio of Mars-Earth planetary masses	CO <sub>2</sub>	6	4	3
	A	2	2	2
	N <sub>2</sub>	2	19	38

If the low-pressure model is assumed to be the correct one, then CO<sub>2</sub> is the major constituent. If the argon content is taken as being equal to that of the Earth, then, for the mean pressure model, argon would be the major constituent. However, under the more logical hypothesis, that the concentration of argon is proportional to the planetary mass ratio (and that degassing has occurred in both planets to the same extent), then nitrogen would be the same major constituent for both the mean and high pressure models.

Nitrogen appears grossly underabundant with respect to the earth's atmosphere. Kaplan, *et al.* (Reference 188) point out that this conclusion supports the conjecture, advanced by Urey (1959, Reference 223) regarding the likelihood of nitrogen escaping from Mars.

While model atmospheres based on the new Martian pressure data have not yet appeared in the open literature, some preliminary calculations have been made available assuming (a) no argon content, and (b) an argon content midway between that found on Earth and that corresponding to the planetary mass ratio value. For each argon model, five possible atmospheres are suggested corresponding to appropriate combinations of maximum and minimum surface pressures (taken as 11-30 mb) and temperature (130-230°K) values. These computations are presented in Tables 12 and 13.

#### 5. Temperatures

Infrared, radiometric, and microwave temperatures have been measured by a number of investigators; these values are summarized below:

<u>Experimental Technique</u>	<u>Temperature, °K</u>	<u>Investigator</u>
Infrared	237-254	Menzel, 1926
Infrared	217	Kuiper, 1952
Radiometric, 8-13μ	220-300	Gifford, 1956
Radiometric, 8-13μ	248-288	Strong & Sinton, 1960
Microwave, 3.15 cm	218 $\pm$ 50°	Mayer, 1956
Microwave, 3.14 cm	211 $\pm$ 20°	Giordmaine, 1959
Microwave, 10 cm	177 $\pm$ 17°	Drake, 1963

Mayer (1961, Reference 199c) suggests the difference between the microwave and infrared values is significant; he believes that the lower microwave temperature corresponds to a location further below the Martian surface than that from which the infrared emanates. Drake (1963, Reference 197) attributes the even lower 177° obtained at 10 cm to the effect of surface emissivity changing with wavelength. At the longer wavelengths, the surface is effectively smoother so that the emission from the region near the limbs is less, and the integrated temperature is lower. Rea and Welch (1963, Reference 40) point out that this effect is

reasonable in view of the visible observations that dust must cover large areas of Mars; however, it is interesting that this same effect was not detected in the 10-cm observation of Venus, since the Venusian surface is thought to be even dustier than Mars.

#### 6. Albedo

The albedo of Mars is a strong function of wavelength at 7000 Å; the albedo is about 0.3 declining rapidly to about 0.04 below 4700 Å; the region of the blue haze (Reference 203). The reflectivity at any given wavelength varies with position on the surface; representative albedoes of the bright and dark areas are 0.15 and 0.05.

An average albedo of 0.15 is generally accepted (Reference 222); variations of this mean from 0.148 to 0.154 are given by Kirby (Reference 220).

#### 7. Absence of Magnetic Fields and Radiation Belts

No indication of a Van Allen belt of any significant intensity has been observed on Mars. If a magnetic field exists, it is probably substantially weaker than that of the earth (Reference 226). Kopal originally felt that the magnetic field was negligible (Reference 221) but has recently conjectured higher intensity fields (work to be published).

### E. JUPITER

Although no flights to Jupiter are planned for the immediate future, such explorations will eventually be made. It is therefore appropriate to consider briefly some of the characteristics of Jupiter in order to ascertain, in at least a preliminary way, what some of the propulsion problems might be.

During October 1962, approximately 40 astronomers and physicists met at the Institute for Space Studies in New York City to discuss the properties of the planet Jupiter. The proceedings of this meeting were published in May 1963 (Reference 140). Much of the data presented below has been abstracted from this conference proceedings, as well as from other reference material (References 121 to 132), including the particularly extensive survey of Trafton (1962, Reference 122).

### 1. Physical Properties

Jupiter is the largest planet in the solar system, larger in fact, than all the other planets put together. Because of its great size, Jupiter causes serious perturbations in the orbits of other planets and planetoids. Its influence on the motion of other bodies makes the study of Jupiter extremely important in celestial mechanics.

Jupiter has 12 known satellites. It has been suggested that one of the larger satellites might be used as an observation base. Of these, the four largest, called the Galilean satellites, have been studied in some detail because of their densities; the first two are believed to be of rock, while the third and fourth may be solid carbon dioxide or ice. Characteristics of the satellites are given in Table 4.

### 2. Clouds

Jupiter is covered with brilliantly colored clouds, ranging from red and brown to bluish white. Different cloud altitudes are observed to have different rotation periods. The violent cloud motions and high-level turbulence observed in the atmosphere are believed to be associated with the high speed of rotation of the planet coupled with a very thick atmosphere.

These clouds have been the subject of much speculation; considerable factual information concerning their development, motion, relative velocity, and color has been gathered. It has been proposed that the colors may be due to various solutions of metallic sodium in liquid or solid ammonia. Recently, Spinrad (1962, Reference 121) found that the Jovian ammonia rotates at a much slower speed than the cloud layer - slower by 7 or 8 km/sec. Depending on the extent of the vertical distance out from the planet covered by this motion, a jet stream of sizable proportions could exist. This effect however seems markedly variable with time and perhaps with Jovian latitude; some recent plates did not show it at all (Reference 140).

### 3. Surface Characteristics

It is inferred that beneath the turbulent atmosphere, a solid surface exists. Although no surface features are visible, certain semi-permanent

markings have been observed. The Great Red Spot is the most prominent. This large area, about 30,000 miles long and 7000 miles wide, has gradually faded away, losing its red color and becoming rounder in form. Observation has indicated, however, that the Great Red Spot, as well as other semi-permanent markings, may not be permanently attached to a solid surface but instead may behave more as a solid floating in a liquid medium. Hide (1963, Reference 140), however, has presented an analysis showing that the spot could result from a large surface discontinuity over which the atmosphere flows, setting up a vertical Taylor column (at a much greater height than the surface discontinuity) on the rotating planet.

#### 4. Atmosphere

Methane, ammonia, and hydrogen have been identified spectroscopically in the Jovian atmosphere. Helium has not yet been detected, although its presence is inferred from studies of Uranus and Neptune. Nitrogen is not believed to be present because of inconsistencies with molecular weight calculations. The abundance of these constituents is not known. It is thought that approximately three times as much helium as hydrogen is present (Reference 121) but Zabriskie (Reference 123) warns that this concept of Jovian atmosphere may require substantial revision. Based on reference data of Uranus and Neptune, the following composition is computed by Trafton (1962, Reference 122) using a method suggested by Kuiper (see Reference 122 sub-listing):

135 km-atm of hydrogen

373 km-atm of helium

3 km-atm of ammonia.

The abundance of these elements except helium, has been measured above the cloud layer. Based on these measurements (and estimating the helium concentration), the total pressure above the clouds was computed by Trafton to be as follows:

Elements and Compounds	NPT Density <u>g/cu cm</u>	Jovian Abundance <u>km-atm</u>	Partial Pressure <u>Atmospheres</u>
H <sub>2</sub>	8.9 x 10 <sup>-5</sup>	5.5	0.048
He	17.8 x 10 <sup>-5</sup>	16.5	0.285
CH <sub>4</sub>	71.4 x 10 <sup>-5</sup>	0.15	0.010
NH <sub>3</sub>	75.9 x 10 <sup>-5</sup>	0.007	<u>0.001</u>
		Total	0.36 atm

R. M. Gallet (1963, Reference 140) has recently suggested that previous models of the Jovian atmosphere cannot be correct because they neglect the changes produced by the condensation of ammonia and water vapor on the structure of the atmosphere. With allowance for the heat released in this condensation, Gallet calculates a marked reduction in temperature gradient, but a sharp increase in the pressure gradient for an atmosphere in adiabatic equilibrium. The next effect is to reach high densities and pressures at relatively low temperatures and relatively small distances below the top of the apparent cloud deck. This implies the presence of ammonia ice-crystal clouds, probably about 50 km thick. Below these clouds lies a region in which ammonia rainstorms may be a prominent feature. At still deeper layers the ammonia may be gaseous. A few kilometers below the ammonia clouds, a similar phenomena occurs with water, so that there may be a certain thickness of water clouds with water vapor below.

If the interior of Jupiter is warm enough to produce an appreciable outward flow of heat, the atmosphere would have to have an approximately adiabatic temperature gradient. According to Gallet's calculations, it is possible to reach high enough pressures and low enough temperatures so that the surface of the solid mantle would occur a few hundred kilometers below the tops of the clouds.

#### 5. Temperature and Thermal Structure

Little is known concerning the temperature distribution in the atmosphere or the energy balance of Jupiter. The maximum radiation temperature is  $120^{\circ}\text{K}$ . Temperatures above the cloud layer have been determined as 170 to  $200^{\circ}\text{K}$  (Zabriskie, 1960) and 165 to  $168^{\circ}\text{K}$  (Kuiper, 1949). Microwave radiation yields various temperatures depending on the wavelength:

<u>Wavelength</u>	<u>Disk Temperature</u>	<u>Source</u>
10 $\mu$	$140 \pm 10$	
3.03 cm	$171 \pm 20$	
3.15	$145 \pm 18$	Mayer (1959)
3.17	$173 \pm 20$	Giordmaine (1959)
3.36	$189 \pm 20$	Giordmaine (1959)
3.75	$200 \pm 200$	Drake and Ewen (1958)

<u>Wavelength</u>	<u>Disk Temperature</u>	<u>Source</u>
10.2	640 $\pm$ 85	Sloanaker (1959)
21	2500 $\pm$ 450	McClain (1959)
22	3000 $\pm$ 1700	Drake and Hvatum (1959)
31	5500 $\pm$ 1500	Roberts and Stanley (1959)
32	7500 $\pm$ 2500	McClain (1959)
68	70,000 $\pm$ 30,000	Drake and Hvatum (1959)

Various theories have been proposed to account for these high temperatures; cyclotron and synchrotron theories account for both the radiation intensity and for the strong polarization (Reference 125). Another theoretical model proposes that Jupiter produces heat internally by gravitational contraction. Much additional information is needed before the problem is resolved.

#### 6. Albedo

The albedo of Jupiter is believed to have a value of not less than 0.64 nor more than 0.82. The most recently calculated value (Traften 1962) is 0.73. The older values of 0.51 (Kuiper and Harris, 1949) and 0.44 (Schonberg, 1921) are considered too low. The reflectivity was recently measured by an Aerobee rocket experiment to be  $0.26 \pm 0.04$  at 2700 A.

#### 7. Magnetic Fields and Radiation

It has been reasonably well established that Jupiter has a Van Allen radiation belt many orders of magnitude greater than that of the earth. This is verified by the extremely high intensity radiation measured from radio waves (Reference 128) and as in agreement with cyclotron theory predictions. While agreement has not yet been reached as to the value of magnetic field (maximum value may be as high as 10,000 gauss, with radiation intensity a trillion times that of the earth), there appears to be little doubt that the fields are very large, posing serious problems.

#### F. SATURN

Saturn's size is deceptive, for although its diameter is almost equal to that of Jupiter, it is not even a third as massive. Its density is extremely low (0.71); it is the only planet that would float if it were placed in an ocean.



Like Jupiter, this suggests a much smaller solid core than its visual disk indicates, surrounded by large quantities of lighter material such as ice and frozen ammonia.

1. Atmosphere

Absorption bands of great intensity indicate large quantities of ammonia and methane. The former is not nearly so abundant as on Jupiter, since the cooler temperatures of the ringed planet cause more of the ammonia to freeze out. This results in a greater penetration of sunlight into the methane of the atmosphere (Reference 248). More regular than those of Jupiter but less distinct, the bands of Saturn range in color from the broad yellowish band around the equator to the greenish caps of the poles. The atmosphere is fairly deep, but its precise depth thickness is not yet known.

In 1962, Guido Munch of the Mt. Wilson and Palomar observatories, and Hyron Spinrad of the Jet Propulsion Laboratory, discovered molecular hydrogen in the atmosphere of Saturn. This evidence supports the widely held opinion that the atmosphere of Saturn is largely hydrogen and helium, similar to the primordial sun. They also detected evidence of very high winds causing the gases to be swept into the three observable bands.

2. Temperature

Infrared radiometric observations yield a surface temperature of  $123^{\circ}\text{K}$ . This is in close agreement with the recent blackbody disk temperature of  $106 \pm 21^{\circ}\text{K}$  obtained from radio emissions at 3.4 cm by the University of Michigan.

3. Rings

The reflection spectrum of the rings appears to be very similar to that of the Martian polar cap. This leads Kuiper to conclude that the particles are either covered by frost or made entirely of ice (Reference 248). They, along with the inner satellites, are considered to be atmospheric condensations, the rings not having formed a satellite because they are within the Roche limit of Saturn.

Because of uncertainty regarding the depth of the atmosphere and the existence of a solid surface coupled with the high escape velocity of the

planet, exploration will be limited to observation of the ringed planet from one of its nine satellites for some time to come.

#### 4. Satellites

The physical data of Saturn's satellites is presented in the general tables on the solar system. Of the nine satellites, the first five are grouped close to the planet. ~~Mimas~~ Enceladus, and Tethys are probably made up largely of snow, since they are less dense than water (Reference 248). Their surfaces, therefore, may not be very firm. Yet Mimas would provide a good observation base for observing Saturn at close quarters, as it makes a complete circuit of the planet in less than a day.

Dione, Rhea, and Hyperion probably have a rock core surrounded by ice, snow, or even solid ammonia. Traces of methane gas probably make up tenuous atmospheres on these small globes (Reference 249).

Although Mimas has the advantage of being close to Saturn for observational purposes, it has the disadvantage of Saturn's static and electromagnetic field effects on earthbound radio signals. Titan, Saturn's largest satellite, is far enough from its primary to alleviate this and is in view of the earth for as long as a week at a time. It could provide a stable platform, as it is comparable in size to the planet Mercury. Its methane atmosphere makes it unique and provides a definite source of fuel for rockets in the area. It might be profitable to establish a permanent refueling base on this satellite in the distant future to service vehicles exploring the outer reaches of the solar system. Such a refueling capability would enable the use of shorter hyperbolic trajectories in preference to the slow minimum-energy orbits. Titan's planetary-sized atmosphere would help in its own exploration since it could support aircraft. Estimates of Titan's diameter vary from the standard 4200 km, to 5050 km, measured by Carmichael (Reference 248).

Beyond Titan, two more satellites, Japetus and Phoebe, complete Saturn's known satellite system. Japetus is of interest because one side shines five times brighter than the other, indicating that an anomaly exists in its surface structure. Phoebe, on the other hand, is distinguished by its retrograde motion about Saturn.

Since all of the above nine satellites are larger than Jupiter's smallest six, it seems likely that a few small satellites have yet to be detected.

#### G. URANUS AND NEPTUNE

Uranus and Neptune are very similar in all observable characteristics. Both appear as green disks in the telescope because of the many intense absorption bands in the red region of the spectrum. They are typical of Jovian planets having low densities and large diameters. Neptune, though slightly smaller, has a density of 2.47, compared to a density of 1.56 for Uranus. Bidurnal variations in the brightness of Neptune suggest two more or less antipodally situated regions of high albedo, a condition which could be due to an anomaly in Neptune's structure (Reference 248).

##### 1. Atmosphere

The spectra of the two planets reveal large quantities of methane, with little or no ammonia. Kuiper, however, holds that the methane of Uranus is not methane at all, but something resembling formaldehyde (Reference 248). Our telescopes can penetrate farther into these atmospheres than those of Jupiter and Saturn, due to the fact that it is too cold in the region of Uranus and Neptune for ammonia to remain in the gaseous state. While it had been assumed that all of the giant planets contain large quantities of hydrogen and helium (because of their low density), none had been observed. Studies of Neptune, and more recently of Saturn, have spectroscopically detected hydrogen, giving support to the above assumption (Reference 248).

##### 2. Temperature

Because of their great distance from the sun, Uranus and Neptune have average temperatures of  $49^{\circ}\text{K}$  and  $40^{\circ}\text{K}$ , respectively. As in the case of the other giants, their surfaces are not visible and it is unlikely that vehicles will be landing on these two planets for some time to come, if ever. A final determination will have to await further information on the planets' surface characteristics.

### 3. Satellites

The small size and great distance of these satellites makes it difficult to gather much information on their characteristics. Uranus has five satellites that are about the size of Saturn's inner group. They technically revolve in a retrograde direction, since the equator of Uranus is inclined  $98^{\circ}$  to its orbital plane. As a result of this unusual configuration, direct line-of-sight radio communication will be possible with the earth most of the time. Radio travel time, however, will be extended because of the great distance.

Of Neptune's two satellites, Triton and Nereid, the former is more interesting as it is closer to its primary and as big as Titan. No atmosphere has been detected; its physical dimensions are not certain, but its surface is considered to be similar to that of Pluto.

#### H. PLUTO

The discovery of Pluto in 1930 was the result of a careful search organized following a mathematical prediction of its existence. Little is known about this remote world other than its orbital elements. Its highly eccentric orbit carries it closer to the sun than Neptune at perihelion and more than 40 A.U. distant at aphelion, in a plane making an angle of  $17^{\circ}$  with the ecliptic.

The planet's brightness, according to available measurements, shows a periodic variation of 0.11 mag every  $6.390 \pm 0.003$  days and is believed to indicate the duration of Pluto's day (Reference 248). The 0.16 albedo is probably due completely to surface reflection, as all atmospheric components but hydrogen would freeze out and cover the surface in its  $45^{\circ}\text{K}$  temperature (Reference 249). Pluto's surface is believed to be fairly rough because of collisions with meteors, comets, and the effects of its cold environment.

Such basic quantities as the mass, diameter, and density, however, are more difficult to determine in the case of Pluto. Because it has no satellites, its mass must be determined by its perturbations on Uranus and, especially, on Neptune. All such determinations depend on doubtlessly inaccurate observations of Neptune made by Lalande in 1795 (Reference 248). As a result no reliable, gravitationally determined estimate of the mass of Pluto is now available. The mass estimate generally favored puts it between the values of the earth and Venus.

Kuiper has measured Pluto's diameter as  $3600 \pm 200$  miles by use of a 200-in. telescope. This value, coupled with a high mass value, could mean that Pluto is the densest planet in the solar system (Reference 36). Surely it is terrestrial in type and bears no relation to its Jovian companions.

As in the case of Uranus and Neptune, the most severe requirements placed on the vehicle will be the long transit times and the intense cold. Pluto's high inclination to the ecliptic will necessitate the use of extra energy during transfer, even though it will be about as close as Neptune for the rest of the twentieth century (Figure 2). Specific vehicle requirements for landing on Pluto will remain unknown until the planet can be observed from closer range, possibly from a probe traveling as far as the orbit of Uranus.

### III. RADIATION AND SPACE DEBRIS HAZARDS

The two major hazards of the interplanetary environment, aside from the vacuum difficulties, are (a) damages due to the interception of various types of radiation, and (b) collisions with space debris. Although initial predictions tended to overestimate the severity of the radiation and collision hazards, newer data still show the problems to be formidable.

The principal types of radiation to be encountered consist of the continuous electromagnetic radiation from the sun and various types of particle radiation, including galactic cosmic rays, solar flares, and trapped radiation such as that found in the Van Allen belts. The principal space debris hazard lies in the abundance of hypervelocity micrometeoroids.

Present knowledge of the interplanetary environment is so quantitatively incomplete - and concepts and ideas develop or change so rapidly - that a description of this environment, as now understood, cannot be presented simply as a collection of formulas, tables, and graphs. Therefore, the description of the space environment is given in the form of a concise discussion combined with tables and graphs showing the best, or otherwise typical, quantitative information. In this way, the most intelligent use of existing data can be made. Before use is made of any particular figure or table, it is recommended that the relevant discussion be read.

#### A. INTRODUCTORY COMMENTS

The task of putting together all the data acquired from space probes, satellites, and earth-based observatories has been likened to a cosmic jigsaw puzzle (Reference 250). Bits and pieces of data are assembled, as they are obtained, by many people throughout the scientific community; this jigsaw puzzle goes together so gradually from so many different viewpoints that frequently the design engineer finds himself both overwhelmed with descriptive literature and bewildered by conflicting interpretations.

With the acquisition of newer data and a more detailed study of older work, many of the apparent conflicts have been resolved and a greater confidence developed in an understanding of the space environment. For

example, M. Neugebauer and C. Snyder (Reference 251) show that the Mariner II data on the plasma flux is in good agreement with the earlier Explorer X and Lunik results, with the Mariner giving a much superior "average" value owing to the extremely long sampling time. Furthermore, Johnson (Reference 252) reports that the Explorer XII resolved the problem which existed regarding the magnitude of the Van Allen belt electron flux in favor of the lower value of  $10^8/\text{cm}^2\text{-sec}$ . With regard to micrometeoroid flux, Whipple (Reference 253) in summarizing flux and penetration problems points out the improvements now possible due to better measuring techniques and more abundant data.

Further study and research can usually be expected to uncover a number of new problems, some of which may prove more complex than those solved. In general, though, the process of acquiring and evaluating new data and comparing it with previously determined concepts soon establishes meaningful physical models on which realistic design criteria can be established. Although it is true that improvements are needed in our understanding of the basic physics of the sun before the problem can be resolved completely, it is also apparent that the statistical studies of measurements obtained since 1956 have greatly increased our confidence in predicting major solar flare events. Conversely, the systematic collection of solar flare data did not lead at once to any unified agreement on the structure of the interplanetary magnetic fields, since as Warwick (Reference 255) points out, the magnetic models derived by various research workers depended in many cases on which of the relations the authors chose to summarize. It might be pointed out that the Mariner II data has done much to resolve this controversy (Reference 251).

Therefore, even though much essential data is not yet available and our understanding of many important processes is grossly inadequate, it must be admitted that the amount of meaningful information available for evaluating practical design problems is quite substantial. In most cases it is not possible to present this work in compact form, since the necessary "similarity" relations are not yet known. Many charts and tabulations must therefore be included.

## B. ELECTROMAGNETIC RADIATION

The total flux of electromagnetic radiation from the sun is surprisingly constant over a year's time, even during violent disturbances observed on the sun's surface. The energy output of the solar surface into space is about 44 megawatt/sq meter. At the earth's distance the value is about 1.36 kw/sq meter. The solar radiation energy varies inversely with the square of the distance from the sun and can be computed from.

$$S = \frac{9.05 \times 10^{25}}{4\pi R^2}$$

where  $9.05 \times 10^{25}$  cal/sec is the bolometric luminosity of the sun, and R is the solar distance. Values for this radiation as a function of distance from the sun are shown in Figure 41. The radiation equilibrium temperature of a blackbody depends only on the solar radiation intensity (distance from the sun) and on the body shape, assuming that no other heat sources are present. Typical radiation equilibrium temperatures for a spherical blackbody are shown as a function of distance from the sun in Figure 42. The extremely limited temperature range tolerable by humans is noted; propulsion system components, of course, can withstand a much wider temperature range.

The bulk of the energy in the solar spectrum lies between 0.3 and 4.0 $\mu$  with approximately 1% of the energy lying beyond each of these limits.

The electromagnetic radiation of the sun as seen at the earth outside the atmosphere consists of a (1) continuous spectrum in the near-ultraviolet, visible, and infrared regions containing many absorption lines (Fraunhofer lines), and (2) a number of emission lines at shorter wavelengths which contribute only a small amount of energy, compared with the continuum. Rocket observations have shown that the continuous spectrum diminishes very rapidly in intensity with decreasing ultraviolet wavelength and that, below 1400 A, the sun radiates a continuous spectrum with emission lines superimposed upon it. This is unlike the visible and near-ultraviolet where the continuum is crowned with intense absorption lines and there are no emission lines.



The continuous spectrum can be well approximated in various wavelength intervals by blackbody radiation of a specified temperature. For example, the visible and infrared regions show a spectral irradiance corresponding rather closely to that of a  $6000^{\circ}\text{K}$  blackbody source. The temperature of a blackbody that most nearly matches the continuous spectrum of sunlight in total energy output is about  $5750^{\circ}\text{K}$ . The distribution of energy in sunlight outside the earth's atmosphere is shown in Figure 43 (Johnson, 1961, Reference 256). The ultraviolet region where emission lines become prominent is shown in more detail in Figure 44 and is taken from the work of Detwiler, Purcell, and Tousey of NRL (Tousey, 1961, Reference 257). From 1040 to 912 Å, the spectrum consists mostly of emission lines which are not resolved in the 10-Å interval plot. The extreme ultraviolet shown in Figure 44 originates from higher levels in the sun's atmosphere than does the near-ultraviolet and the visible. The continuum in the ultraviolet region of Figure 44 probably comes mainly from the low chromosphere, where the temperature is in the range of about 4000 to  $5000^{\circ}\text{K}$ . The emission lines at short wavelengths originate in still higher regions of the solar atmosphere, where the temperature ranges from  $5000^{\circ}\text{K}$  in the chromosphere to millions of degrees K in the corona. The exact region of emission depends on the particular line.

An important series of emission lines is the Lyman series in the hydrogen spectrum, with the first line, Lyman alpha, at 1216 Å. The Lyman-alpha line carries about  $6 \text{ erg/cm}^2\text{-sec}$  near solar maximum and delivers more energy than the entire solar spectrum from wavelengths shorter than itself. The intensity is probably less at sunspot minimum. The higher members of the series are followed by the Lyman continuum, which is the most important emission below 912 Å. It follows a  $6700^{\circ}\text{K}$  blackbody curve. At 584 and 304 Å, there are intense emissions by neutral and ionized helium, respectively. The two lines produce about  $0.5 \text{ erg/cm}^2\text{-sec}$  at the earth (Hinteregger, 1960, Reference 258).

The solar constant, the total solar irradiance at the earth's mean distance from the sun, as given by Johnson (1954, Reference 260) is  $2.00 \pm 0.04 \text{ cal/cm}^2\text{-min}$  ( $1.39 \times 10^6 \text{ erg/cm}^2\text{-sec} = 443 \text{ Btu/ft}^2\text{-hour}$ ) and does not

vary significantly with the solar cycle. The solar spectrum in 50-A steps from 0.22 to 7 microns (1 micron =  $10^4$  A =  $10^{-4}$  cm) is given in Table 14 where  $H_\lambda$  is spectral irradiance and  $P_\lambda$  is the percentage of the solar constant associated with wavelengths shorter than  $\lambda$  (Johnson, 1954, Reference 260).

The region below 3000 A is shown in great detail in Tables 15 and 16, which are taken from Hinteregger (1961, Reference 259), who has evaluated recent measurements. Table 15 shows rounded-off values taken or averaged from work published through 1960. In the region where the table of Johnson and that of Hinteregger overlap, Johnson's values are lower by as much as 40%. Johnson's values are based on early NRL rocket data and are considered by Tousey (1961, Reference 257) to be too low at lower wavelengths. Hinteregger's data should be considered the more accurate of the two.

The comments below apply to Tables 15 and 16 and give definitions and explanations of the notation used.

The radiation spectrum is described both in terms of photon-flux density,  $\Phi$ , and in terms of energy-flux density,  $I$ . The dimensions of  $\Phi$  and  $I$  are given in the column headings.  $\Phi(\lambda)$  and  $\Phi(\lambda_1/\lambda_2)$  are integral fluxes of photons defined as

$$\Phi(\lambda) = \int \Phi_\lambda d\lambda$$

(integral over the specific line around  $\lambda$ )

$\Phi(\lambda)$  has dimensions of photons/cm<sup>2</sup>-sec and

$$\Phi(\lambda_1/\lambda_2) = \int_{\lambda_1}^{\lambda_2} \Phi_\lambda d\lambda$$

(integral over all lines and/or continua)

$\Phi(\lambda_1/\lambda_2)$  has dimensions of photons/cm<sup>2</sup>-sec, where  $\Phi_\lambda$  designates the differential spectral photon-flux density. For example, from Table 15, the

flux of photons in the interval 2800 to 3000 Å is  $1.5 \times 10^{15}$  photons/cm<sup>2</sup>-sec and from Table 16 the photon flux for the Si-III line is  $4 \times 10^9$  photons/cm<sup>2</sup>-sec. These are values estimated for the top of the atmosphere. It should be noted that the convention that  $a \times 10^b = a^b$  is followed in both Tables 15 and 16. Similarly, the intensities are also defined as integral fluxes

$$I(\lambda) = h\nu \cdot \Phi(\lambda),$$

where  $h$  is Planck's constant and  $\nu$  is the frequency corresponding to the wavelength  $\lambda$ . The dimensions of  $I(\lambda)$  are erg/cm<sup>2</sup>-sec. In an analogous way

$$I(\lambda_1/\lambda_2) = \int_{\lambda_1}^{\lambda_2} h\nu \cdot \Phi_{\lambda} d\lambda$$

In using the tables it is important to notice that photon flux  $\Phi$  or intensity given for a particular wavelength interval includes certain lines indicated (only the continuum, or both lines and continuum in the interval). For example, the intensity in the interval 1200 to 1300 Å including only the continuum is 0.08 erg/cm<sup>2</sup>-sec. The total intensity including lines and continuum is 3.5 erg/cm<sup>2</sup>-sec.

Both tables list more-or-less empirical values of a certain altitude  $h^*$  in the earth's atmosphere, defined as the level at which the specified solar photon-flux is reduced to the fraction  $1/e$  of the corresponding flux on top of the atmosphere for an overhead sun. Both of Hinteregger's tables are reproduced intact, and they contain much information beyond simply specifying what is known about the solar spectral intensities.

The basic measurements for Tables 15 and 16 come from rocket-borne experiments at various altitudes high in the atmosphere, and the estimates given for the top of the atmosphere are based primarily on simple extrapolations of the observed vertical-attenuation profiles rather than on any assumed "atmospheric models." When satellite solar-spectral observations are made, this uncertainty will be removed and in addition much information about the atmosphere can then be inferred.

The average incident fluxes of solar photons from the visible to the nearer-ultraviolet region are known to be more or less constant throughout a full solar cycle. This includes the data of Table 15. The extreme ultraviolet region ( $\lambda \sim 1300$  A, Table 16) shows both long-term variations over a solar cycle and short-term variations during solar flares. Empirical data on these variations is extremely meager. Transient variations produced by flares are probably much more pronounced in the X-ray region than for longer wavelengths of approximately 100 A. This distinction has been experimentally established for the Lyman-alpha line by Friedman, who has shown that the total solar Lyman-alpha flux remains more or less constant even during major solar flares (Friedman, 1961, Reference 261). The long-term variation of the Lyman-alpha line over a solar cycle is, however, not well-known. The situation is even less satisfactory for the other emission lines, and no reliable picture of systematic variations of  $\Phi$  (100/1300 A), i.e., the integrated photon-flux from 100 to 1300 A, can be given as yet.

Upper limits for the intensities of solar-flare X-rays are given in Table 16. Also to be mentioned when considering the time variation of the solar spectrum are the radio-noise bursts which occur around several hundred megacycles. These have been classified as Types I through IV and are of great complexity.

As emphasized above, these variations have no significant effect on the solar constant. References mentioned in Tables 15 and 16 are listed separately in the bibliography.

#### C. SOLAR FLARES

Solar flares are explosive outbursts of electromagnetic radiation (including radio, ultraviolet, and X-ray wavelengths) and ionized matter (primarily protons and electrons) from the vicinity of sunspot groups. They are catastrophic disturbances having a sudden onset and a gradual decay, usually taking less than an hour. On reaching the earth in approximately 8 min, the ultraviolet- and X-radiation greatly increase the ionization in the D-layer of the ionosphere (50 to 100 km above the earth).

### 1. Observation of Flares

To investigate such abnormal ionization, data on  $W_{\min}$  in ionograms are useful.  $W_{\min}$  is defined as the minimum frequency of radio waves at which ionospheric echoes are observable; its time variation depends on the electronic density in the lower ionosphere. The value of  $W_{\min}$  increases when the excess X-radiation reaches the earth (SID or Sudden Ionospheric Disturbance effect). Solar-flare particles frequently follow the enhanced X-radiation, reaching the earth some time after the visible flare and producing increased ionization over the polar-cap regions. As a result, all ionospheric echoes may be completely masked, causing "polar blackouts." Unlike ordinary auroral-zone ionizations, these abnormal ionizations indicate the precipitation of particles over the whole polar cap, which suggests an isotropy of incoming particles.

Another technique for observing the ionospheric effects due to ionization by solar-flare energetic charged particles has been developed primarily by Little, Leinbach, and Reid (1958, 1959, References 262, 263 and 264). The absorption of incoming cosmic radio noise at 27.6 mc is observed after passing through the ionosphere, and the changes in the absorption due to increases in ionization of the 50-to-100-km level are recorded and interpreted as the arrival of protons in the energy range of 10 Mev and higher. This is called Type III absorption (or "polar-cap absorption") and has been observed over a wide range of longitudes in the polar regions. Within the last 2 years, solar flare particles have also been observed directly by means of high-altitude balloons, rockets, and satellites.

### 2. Energy Levels

The great majority of solar flares which produce bursts of particles reaching the earth do not produce particles attaining relativistic energies. Comparatively rare, large-scale events do, however, produce a spectrum of particles reaching cosmic-ray energies of 40 Bev. Protons of energy greater than about 2 Bev produce secondary nucleonic components observable at ground level, and relativistic solar flare events are now immediately detected by many neutron-monitor stations and meson detectors throughout the world.

There seems to be a gradual transition between the relativistic and the non-relativistic solar-flare events, with the latter much more frequent.

### 3. Sequence of Events

The sequence of events following a major relativistic solar flare (23 February 1956) is described by J. A. Simpson (1961, Reference 265) as follows: "The first arriving particles come to the earth from a limited-source direction in the sky.\* The apparent source is a relatively large area which includes the sun. Initially the particles are of the highest energies in the flare spectrum. Subsequently the whole sky becomes 'illuminated' with particles extending to lower energies; for these low-energy particles, and late-arriving high-energy particles, there appears to be remarkable isotropy. Following the onset of isotropy, the particle intensity gradually diminishes with the flare spectrum essentially unchanged . . . The intensity at the earth is observed to diminish to its preflare level within a period of 15 to 20 hours."

Simpson also describes the sequence of events for a non-relativistic flare in the following words: "The first high-energy particles (on the order of  $10^2$  Mev) arrive within 1-5 hours following the solar flare. On only a few occasions has the first arrival of high-energy radiation been delayed more than 4 or 5 hours. . . The particles are observed to arrive over the entire polar cap and down to latitudes limited only by the prevailing geomagnetic cutoff. Particles continue to arrive for a period of many hours to several days following a solar flare. In a manner typical of large solar flares, a low-energy beam or plasma region independently reaches the earth within about a day following the flare to produce a geomagnetic storm. The low-energy particles continue to arrive throughout the geomagnetic storm effect and, in addition, are observed at geomagnetic latitudes which normally forbid their arrival . . . An outstanding feature of these low-energy bursts is the very high flare-values attained on some occasions."

---

\*The first particles arrived about 10 min following the onset of the flare.

#### 4. Frequency of Flares

The annual frequency of the nonrelativistic solar-flare events is indicated in Figure 45, which covers an 11-year period (Geodeke, 1961, Reference 266). The frequency of occurrence is in phase with the solar cycle and shows maxima near the equinoxes (22 March and 22 September) and minima in June and December in the northern hemisphere.

There have been ten relativistic events observed since the first one was detected on 28 February 1942. Figure 46 gives the frequency of both relativistic and nonrelativistic events over a solar cycle (Dessler, 1961, Reference 267). The frequency of the nonrelativistic events in Figure 46 was inferred from polar-cap absorption studies.

#### 5. Flux and Spectrum

It has been mentioned in the preceding paragraphs that the sun emits various kinds of particles - primarily protons and electrons - ranging from thermal to relativistic energies. The knowledge of the energy spectrum of particles ejected from the sun is still incomplete. Of special importance is the uncertainty in the maximum particle-flux one can expect from a solar flare. Obayashi and Hakuha (1960, Reference 268) have combined the observations of many investigators and their resultant integral energy-spectrum of solar particles is presented in Figure 26. The positions of flares on the solar disk and the magnetic type of their associated sunspots have an important bearing on the magnitude of the particle flux reaching the earth, as does the state of the magnetic field between the earth and the sun. A certain range in observational results is therefore expected and is indicated in Figure 26 by the shaded area. Associated with general solar activity and included in the figure are spectra for interplanetary thermal particles near the earth of temperature  $2 \times 10^5$  °K, according to Chapman (1957, Reference 269). The fluxes are computed using this temperature and densities of about 600 particles/cm<sup>3</sup>, from observations of zodiacal light (Siedentopf, 1953, Reference 270). Also included are proton spectra of solar plasma clouds and the solar wind which are labeled solar corpuscles in the figure. A plasma cloud of this energy

(about 1000 km/sec) emitted by a solar flare penetrates into the geomagnetic field until the particle energy density approximately equals the energy density of the magnetic field. This theoretically occurs around ten earth radii. Plasma particles then appear to contribute to the development of a diamagnetic-ring current at about five earth radii. This current causes the main phase of geomagnetic storms. However, these particles do not directly form a part of the space environment within at least five earth radii.

The following comments apply to Figure 26. The information about solar particles of the highest energy is derived from the cosmic-ray intensity increases associated with the great solar flare of 23 February 1956, which yields the spectrum of relativistic protons (Meyer, 1957, Reference 271). This is indicated by the curve labeled (1) in the figure and, for comparison, the energy spectrum of normal cosmic rays is also shown (Van Allen and Singer, 1950, Reference 272). The late effect of the flare gives information about the spectrum for nonrelativistic particles. Abnormal ionization of the polar ionosphere began gradually and reached a maximum a few hours after the flare. D. K. Bailey (1959, Reference 273) showed that protons of  $10 \sim 1000$  Mev are responsible for this and, on the basis of balloon observations of the spectrum at about the 1-Bev range (Van Allen and Winckler, 1957, Reference 274), he constructed the curve labeled (2) in Figure 26. Thus, curve (1) gives the flux first reaching the earth from the relativistic flare of 23 February 1946 and curve (2) gives the flux 18 hours later for this same flare. The spectrum in the energy range  $1 \sim 100$  Mev is obtained from polar-cap blackouts, Type III absorption of cosmic radio noises, and satellite observations (e.g., Rothwell and McIlwain, 1959, Reference 275). The curve labeled (3) is due to Anderson et al. (1959, Reference 276) from balloon observations. Most other values mentioned by investigators lie between curves (2) and (3) for nonrelativistic events. Below 1 Mev, the curve (4) was obtained from observations of the hydrogen alpha auroral spectral lines (Chamberlain 1954, Reference 277). Curve (5) represents rocket observations of auroral particles (protons). (See Van Allen, 1958, Reference 278 and Meredith, 1958, Reference 279.)



The label "auroral particles" attached to curves (4) and (5) implies only that these proton fluxes were calculated from observations in or near aurorae. It is believed that the primary source of the luminosity of aurorae is electrons incident on the upper atmosphere; electron fluxes are not presented in Figure 26. The curves (4) and (5) give proton fluxes contributing to the environment over the auroral zones, or about 60 to 80° geomagnetic latitude. For a long time the aurorae have been thought to be produced by the bombardment of the earth's upper atmosphere by high-speed particles ejected from the sun during periods of solar activity. Thus, auroral particles are included in Figure 26 as particles of solar origin. However, the manner in which these particles coming from the sun interact with the earth's magnetic field and finally make their way into the atmosphere to produce the aurora is unknown. It is possible that these soft-proton auroral fluxes are part of the geomagnetically trapped radiation, in which case they will be observed within a belt bounded very roughly by the 60 to 80° geomagnetic field lines.

Also presented in Figure 26 are the vertical atmospheric-penetration depths due to Bailey (1959, Reference 273) and magnetic cutoffs for an ideal geomagnetic dipole.

The condition, whether particles entering the geomagnetic field behave like a single particle or a conducting plasma, is indicated by the dotted line, cutting across Figure 26 (Ferraro, 1952, Reference 280). This limit for plasma behavior crosses over the spectrum of solar particles at the 1 to 100 Mev range. Therefore, above this range, solar particles can be treated as independent particles while, for particles significantly below this limit, the inter-particle electromagnetic interactions become important.

The time decay of the high-energy end of the solar-flare spectrum typically follows the form  $t^{-n}$ , where  $n$  varies between 1.5 and 3. However, because of the existing dispersion, these decay laws should not be applied to the entire solar-flare spectrum. Also, it is generally unreliable to extrapolate observed fluxes backward in time using a  $t^{-n}$  decay in order to estimate maximum expected fluxes. A schematic of what must occur in the time development of the solar-particle spectrum at the earth is shown in Figure 47.

Spectral measurements by other investigators give results lying between curves (1) and (2) of Figure 26 for relativistic solar particles and between curves (2) and (3) of Figure 26 for nonrelativistic solar particles. For example, K. A. Anderson and D. C. Enemark (1950, Reference 281) give the following spectrum including the time dependence from observations on 15 July 1959:

$$\left\{ \begin{array}{l} 85 \text{ Mev} < E < 300 \text{ Mev} \\ t > 1 \text{ to } 2 \text{ days} \\ n(E, t) = \frac{15 \times 10^{10} t^{-3} E^{-4}}{\text{cm}^2\text{-sec}} \end{array} \right\}$$

However, Van Allen (1961, Reference 282), using data from Explorer VII following the flare of 12 November 1960, found intensities as high as  $2.4 \times 10^4$  particles/cm<sup>2</sup>-sec for  $E > 30$  Mev, and a time integral of this intensity for 12-16 November of  $\sim 10^9$  particles/cm<sup>2</sup>. This is somewhat higher than curve (2) of Figure 26. For the same flare, Wasson (1961, Reference 283) calculated intensities agreeing with Van Allen (1961, Reference 282) from the production of radioactive Ag<sup>106</sup> in an emulsion block carried by Discoverer XVII. Also, Winckler (1961, Reference 284) reported a proton flux of  $1.5 \times 10^7$  particles/cm<sup>2</sup>-sec for  $E > 40$  Mev, obtained by extrapolating a balloon measurement to free space. Winckler (Reference 284) regards this value as highly uncertain.

In conclusion, the integral intensities of solar cosmic rays indicated in Figure 26 are considered fairly reliable, but intensities of non-relativistic solar-flare protons possibly can reach values as high as  $10^4$  particles/cm<sup>2</sup>-sec for  $E > 20$  Mev, on some occasions. It seems probable, however, that fluxes this high have never actually been observed. The intensities presented apply to solar-particle beams with little or no geomagnetic cutoff effects included. They apply to free space and regions over the polar caps. For regions near the earth at low latitudes, the spectrum observed is cut off at higher energies to an extent which depends on geomagnetic activity.

## 6. Prediction of Flares

The extent to which it is possible to predict the occurrence of solar flares producing the most intense proton-beams is currently being investigated. The present status of these studies is indicated by Robey (1961, Reference 285) and K. A. Anderson and E. C. Fichtel (1961, Reference 286). No quantitative formulas for predicting the occurrence of flares exist, but long-range studies give estimates of conditions to be expected over long periods during the solar cycle. Also for short-duration trips of less than 1 week, favorable launching dates can be recognized.

### D. PRIMARY COSMIC RADIATION

The primary cosmic radiation evidently fills interstellar space as an isotropic flux of high-energy particles, mostly protons. Eighty-five percent of the primary particles are hydrogen, 14% helium, approximately 1% are in the carbon-nitrogen-oxygen group, and 0.25% in the group are heavier than neon. There is a small flux of lithium, beryllium, and boron which is approximately 0.25% of the total flux. It is presently believed that high-energy electrons and gamma rays constitute less than 1% of the total flux.

A few of these primary cosmic particles possess energies as high as  $10^{18}$  electron volts. The cosmic-ray integral spectrum is indicated in Figure 26, but near the earth a strong latitude effect is introduced by the geomagnetic field. Incoming particles are deviated toward the east and may be completely deflected by the geomagnetic field before reaching the top of the atmosphere. The minimum energy of a vertically incident particle able to reach the top of the atmosphere at a particular geomagnetic latitude is called the geomagnetic cutoff energy at that latitude. For protons, this is indicated in Figure 26.

The flux of cosmic rays is not constant; the two most important types of modulation are the 11-year solar-cycle variation and the Forbush or magnetic-storm decrease. Above 20 Bev/nucleon, the cosmic-ray intensity is steady in time to within  $\pm 2\%$ . Below 20 Bev/nucleon, the cosmic-ray intensity follows the 11-year solar cycle, being higher at times of solar minimum. Presumably when the sun is inactive the cosmic rays reach the earth unhindered,

and when the sun is active it sweeps back the cosmic rays with its magnetic field, thereby excluding low-energy particles from the vicinity of the earth. However, none of the proposed mechanisms for modulating the primary cosmic-ray intensity appear to fit the experimental data.

The total flux of cosmic rays for energy greater than 1 Bev is 0.2 particles/cm<sup>2</sup>-sec-ster at sunspot maximum. The energy density is approximately 1 ev/cu cm compared to about 0.05 ev/cu cm for starlight (Reference 287). The details of the integral spectrum over the range 0.15 to 10<sup>10</sup> Bev for primary cosmic rays near sunspot maximum is given in Table 16 (Singer, 1958, Reference 288; Noon, 1957, Reference 289). The total intensity is decreased by a factor of about 2 from solar minimum to solar maximum, and the lower-energy particles are affected most (McDonald and Webber, 1960, Reference 290). Therefore, the total flux of particles of energy greater than 1 Bev can be expected to be about 0.4 particles/cm<sup>2</sup>-sec-ster at sunspot minimum. The shielding of cosmic-ray primaries is not a rewarding operation because of the very high penetrating characteristics of these relativistic ions.

Even with generous allowances for the high relative biological effectiveness of heavy particles, the estimated integrated dose delivered to an unprotected man in space would be on the order of only 1/2 rem (roentgen equivalent man) per week, and is therefore of negligible effect except for journeys of several years. The galactic cosmic radiation will have essentially no effect on materials, except for certain photographic emulsions.

#### E. METEOROID ENVIRONMENT

Micrometeoroids present the principal particle hazard to a space vehicle since the flux of larger particles is so low that the danger of collision with a vehicle is negligibly small (Reference 292 and 293). Extremely small particles, having masses much less than 10<sup>-6</sup> g will not have enough energy to do great damage even when they impact at very high speeds. Particles with masses in the range 10<sup>-6</sup> to 10<sup>-3</sup> g are the most dangerous since fluxes are high enough to give finite collision probabilities and since the particles are large enough to do appreciable damage on hypervelocity impact. Unfortunately, fluxes

are not well known for particles in this size range; the fluxes are obtained by extrapolation from measurements made on other sizes (Reference 304). Satellite measurements have been largely confined to particles lighter than  $10^{-6}$  g, while visual and radar studies best define fluxes for particles larger than  $10^{-3}$  g, although radar measurements of smaller particles have been made.

To assess the potential damage to a space vehicle, particle fluxes must be accurately determined. In the following section, the experimental methods for measuring these fluxes and the results obtained will be discussed.

#### 1. Experimental Techniques

Sounding rockets and space probes have ushered in a new era in meteoroid measurement. There is a new widespread interest in meteoroids and their effects on space vehicles. Furthermore, spacecraft have the ability to measure directly characteristics of meteoroids: fluxes, directions and magnitudes of velocities, sizes, densities, and compositions. To date, the principal measurements have been of fluxes as functions of time and position in space. Microphone type sensors have recorded numbers of impacts of meteoroids with momenta (or energies) above chosen levels. Approximate mass ranges are obtained by assuming average meteoroid velocities and by sensor calibration. Calibration has been principally with low-speed particles with extrapolation to hypervelocities, assuming a mechanism for response of the sensor to hypervelocity impact. Calibrations with particles of micrometeoroid size and density and having realistic speeds are becoming possible and will help to eliminate one of the unknowns in the measurements. Other types of sensors, such as skin penetration indicators, wire grids, etc, have also been used to record numbers of impacts by particles with energies (or momenta) greater than chosen values. At present, sensors are being designed to specifically measure momentum (or energy), and in some cases also to measure particle size or mass. Recoverable rockets and satellites have also permitted study of the nature of particles.

Nevertheless, the bulk of our knowledge about meteoroids has been obtained from ground-based measurements. Fluxes close to earth, and velocities and compositions, have been obtained by analysis of visual, photographic, and radar measurements of meteors. Fluxes in the earth's neighborhood

are also inferred from analyses of marine sediments and of particles collected from the atmosphere. Micrometeoroid spatial densities far from the earth are obtained from zodiacal light and solar corona measurements. The nature and composition of meteoroids is obtained from detailed study of meteorites, and from spectroscopic analyses of meteor trails.

Meteors have been studied visually for many years, and measurements techniques have been refined to yield good values of variables of interest. Trained observers are able to measure positions of the ends of the visible meteor trails and the angular direction of the paths to a few degrees. Such observers also are able to measure the angular speed to within 20 to 30%, and to estimate the brightness to better than one stellar magnitude. With simultaneous observations at separated localities on the earth's surface, meteor altitudes and the three-dimensional geometry of the paths can be measured. Fluxes of meteors brighter than about the fifth magnitude can be measured, with flux errors increasing with decreasing brightness. The brightness range is extended down to about the eleventh magnitude with telescopic aids (Reference 27b).

More accurate and reliable are the photographic techniques that have been developed, particularly during the past few years. For efficient study of meteors, a camera with wide sky coverage is required. Camera optical systems which have been used on meteor programs may be grouped into three broad categories: (a) lenses with  $f/4$  to 8 and focal length of 100 to 500 mm; (b) lenses with  $f/1.0$  to 3.5 and focal length of 50 to 200 mm; (c) lenses with  $f/0.5$  to 1.0 and focal length of 100 to 300 mm. The choice of category depends upon the application, but category (c) has proven particularly effective (also expensive). The most efficient camera of the category that has been developed has a super-Schmidt optical system with  $f/0.65$  and focal length of 200 mm, designed by J. G. Baker. A rotating shutter is an important item of auxiliary equipment for a meteor camera. This shutter serves primarily to measure the angular velocity of a meteor, but also serves to suppress sky-fog intensity relative to meteor image and aids in the study of distribution of luminosity behind the meteor head (Reference 27b).

Multiple observations from photographic stations separated by appreciable distances on the earth's surface are used to measure meteor altitudes and the three-dimensional paths, just as they are for visual observation. Altitudes are also measured by decay of luminosity or ionization. At low altitudes, density is relatively high and decay is fast, while at high altitudes the reverse is true. Many meteors are seen at an altitude of about 90 km, and are nearly all observed within the band 60 to 110 km - the observed altitude depending particularly on meteoroid size and density, speed, and path angle.

Meteoroid masses and densities may be inferred from photographic measurements. An empirical direct relation between meteor luminosity and particle mass has been established, and recently has been refined by measurements of luminosities of particles of known masses and speeds ejected from Trailblazer I. Densities are established by measuring decelerations along the paths.

Photographic techniques are also used to measure compositions spectrographically; slitless spectra, with a dispersing element mounted in front of the lens, are satisfactory for meteor spectroscopy and cover a wide sky field.

In the past few years a powerful new technique for observing meteors has come to the fore. This technique is radar. It will measure expeditiously many of the important meteor parameters and will do so for relatively faint meteors, down to the fifteenth magnitude or fainter. Radar primarily measures ranges and echo amplitudes, but will also measure direction and many other variables. Range is measured to within 0.05 to 5 km, echo amplitude with error of 10 to 500%, echo duration and decay with good accuracy, and echo phase to a few electrical degrees if a continuous wave system is used. Secondary data may be computed from the measurements as follows: (a) velocity within 1 to 10%; (b) angle of elevation of meteor target with optimum error of  $1^\circ$ , (c) height with average error of 1 km, (d) radiant with positional error of  $2^\circ$ , and (e) electron line density to about an order of magnitude. The speed may be computed, for example, from range observations by applying the formula

$R^2 = R_0^2 + V^2(t-t_0)^2$ , where  $R$  is the range,  $R_0$  is the range at closest approach to the observer,  $V$  is the meteor speed,  $t$  is time, and  $t_0$  is the time of closest approach (Reference 27b).

Radar observes meteors through the sheath of electrons created as the meteor passes through the air. The amplitude of the reflected echo depends upon the number of electrons in the sheath, which in turn has been found to be roughly proportional to meteoroid mass for a given velocity, within a rather wide mass range. Radar most efficiently detects meteors whose paths are nearly at right angles to the line of observation.

Radio wavelengths of 3 to 11 meters have been used for a majority of the observations; pulsed- or continuous-wave or modulated continuous wave systems are used, depending on the aim of the experiment. Wide-area-coverage antennas or narrow-beam antennas are chosen, depending on the application. Multiple station radar, often coupled with visual or photographic observations, is widely used.

In the past 15 or 20 years, radar has yielded new insights into meteor problems and particularly into the flux of meteoroids close to the earth. Far from the earth, meteoroid spatial densities are found from zodiacal light, solar corona, and space-probe measurements. The faint glow in the sky - best seen in the west shortly after sunset or in the east before sunrise, and called the zodiacal light - is ascribed to scattering of sunlight from dust particles in interplanetary space, concentrated in the plane of the ecliptic. From eclipse observations of the solar corona, this cloud of particles is inferred to extend into the sun. From these measurements, the estimated density in interplanetary space is  $10^{-15}$  per cu cm, or about  $10^{-3}$  of that observed close to the earth for particles larger than a few microns (Reference 301 and 302).

## 2. Meteoroid Densities

Densities derived from observation of photographic meteors indicate a rather porous structure for most particles of cometary origin. These range from 0.01 to 1 g/cu cm, depending on "reasonable" estimates of luminous



efficiencies. Whipple (1963, Reference 293), using improved luminous efficiency measurements from the Trailblazer I (analyzed by McCrosky and Soberman, 1962, Reference 308) and by independent determinations (from three asteroidal meteors by Cook, Jacchia, and McCrosky, Reference 309), concludes a meteoroid density of 0.44 g/cu cm.

Deceleration measurements on photographic meteors have also indicated a porous, lacy structure of low density for particles fainter than about magnitude 0. Verniani (1961, Reference 294) calculated the density of photographic meteors, most of which were fireballs, using Whipple's older data and ablation theory with the following results: about 44% had a density of 3.38 g/cu cm, 35% were porous bodies with an average density of 0.67 g/cu cm, and 21% were dustballs with an average density of 0.15 g/cu cm. Collection of small particles in a rocket-borne device (the "Venus Flytrap" equipment) also indicates low-density, weak structures (Reference 295 and 296). These densities and types of structures observed are consistent with the cometary-origin hypothesis.

It is generally believed that micrometeoroids belong to the same population as the particles which cause the meteoric phenomena studied by ground-based techniques. Therefore, the concepts of meteoroid characteristics gained from the study of larger particles of mass greater than about  $10^{-5}$  g have generally been applied also to the micrometeoroids. They are assumed to be in heliocentric orbits with masses ranging upward from a lower limit set by solar radiation pressure of about  $4 \times 10^{-10}$  g for a density of 0.05 g/cu cm, and about  $7 \times 10^{-14}$  g for a density of 3.5 g/cu cm. At the upper end, micrometeoroid masses approach the masses of those which cause radio meteors. Flux intensities for radio and photographic meteors as a function of mass have been extrapolated toward the micrometeoroid range.

It has been proposed that smaller particles of cometary origin would be of greater density than the larger ones, and that the density of the smallest particles would approximate that of stone. Thus, a density of about 3 g/cu cm is often assigned to those particles of mass less than about  $10^{-4}$  g.

This proposal is based on the assumption that, in the formation of cometary material, the condensation of the less volatile materials occurred first, with later condensation and accumulation of the more volatile "ices." However, the "Venus Flytrap" experiment mentioned above (Reference 296) suggested that low-density weak structures were still prevalent among particles with dimensions on the order of microns.

### 3. Meteoroid Flux

Figures 48 and 49 summarize present data on flux intensities of meteoroids close to the earth as a function of meteoroid mass. The cumulative flux for a given mass is the number of particles with a mass greater than the given value which cross 1 sq meter each second. It is given for  $2\pi$  ster (i.e., a hemisphere) and thus counts particles coming from one side only. The uncertainty in determining the mass of a zero-magnitude meteor results in the spread indicated by the lines labeled  $m_0 = 1$  g and  $m_0 = 30$  g in Figure 49 for the flux of photographic and radio meteors. Whipple has assigned the range 1 to 30 g, and first suggested a preferred value of 25 g for the zero-magnitude particle, but in 1963 revised the preferred value to 1 g.

A summary of meteorite information based on photographic and radar data is given in Table 19, prepared by Whipple (1958, Reference 303). It assumes that a zero-magnitude meteor has a mass of 25 g and that the magnitude and mass are related by the formula  $M = 2.5 \log_{10} m_0/m$ , where  $M$  is the magnitude,  $m$  is the meteor mass, and  $m_0$  is the mass of a zero-magnitude meteor. The flux values are for all particles with masses greater than the given mass. The values in the last column are for  $4\pi$  ster, and those in the next-to-last column assume a 50% shielding by a planet. Whipple assigned different values of average velocity to different sizes of dust particles. The velocities assigned varied from 28 km/sec for the visual meteorites to 15 km/sec for small dust particles of the direct-measurement size range. These values should be adjusted to conform with the now-preferred 1 g mass of a zero-magnitude meteor (Whipple 1963).

McCracken and Alexander (Reference 305) have discussed the distribution of micrometeorites in the vicinity of the earth as directly measured by microphone systems carried by rockets, satellites, and space probes. The available direct measurements that have been obtained from these systems are shown plotted in Figures 48 and 49; relevant data for several American spacecraft systems are listed in Table 20. An average particle velocity of 30 km/sec was used in computing the threshold mass sensitivities for the microphone systems for the spacecraft listed in Table 20.

Direct measurements from the microphone systems mounted on Soviet satellite and spacecraft are given in Table 21 (Reference 305). Corrections are not made for the shielding effect of the earth for measurements made at large geocentric distance.

A set of direct measurements obtained by means of the Explorer VIII satellite (Nov-Dec 1961) is presented in Figure 48. The three data points obtained with the Explorer VIII microphone system were corrected for the shielding effect of the earth, and represent the impacts of more than 3100 micrometeoroids registered during an interval of 40 days. An average particle velocity of 25 km/sec was assigned in obtaining detector mass sensitivity. The three Explorer VIII data points establish the shape of a segment of an average distribution curve that extends over approximately three orders of magnitude in particle mass.

The micrometeoroid distribution curve shown in Figure 39 (largely based on Explorer VIII results) can be approximated by a straight-line segment with the equation

$$\phi = 10^{-17} m^{-1.70}$$

where  $\phi$  is the hemispherical flux intensity (per sq meter-sec- $2\pi$  ster) in number of particles with mass  $m$  or greater, and  $m$  is in grams. Caution must be used in extrapolating this distribution curve out of the range of particle mass for which direct measurements have actually been obtained. The above distribution

holds approximately for  $m$  in the range  $10^{-10}$  to  $10^{-6}$  g, and is applied for an average velocity of 30 km/sec. The portion of the distribution curve defined in this range by Explorer VIII joins the straight-line extrapolations from radar and photographic data. (For example, compare Whipple's 1963 extrapolation with Explorer VIII points in Figure 49.)

In 1963, Whipple (Reference 253) revised his previous work suggesting a slope of -1.34 (very close to Hawkin's and Upton's value) but at a different location on the mass-flux graph. Whipple (1963) suggests the following numerical expression for his 1963 curve (which he considers a "pessimistic" estimate) for the photographic and radio meteors of Figure 49.

$$\log \phi = -1.34 \log m + 2.68 \log (0.443/\rho) - 14.48$$

The flux intensity in the region of primary importance for penetration calculations ( $10^{-3}$  to  $10^{-6}$  g) must, at present, be obtained by extrapolation to larger masses from satellite data or to smaller masses from radio and photographic values. It has been customary to approximate the entire spectrum including the satellite data by the formula

$$\phi = 10^{-12} m^{-10/9}$$

where  $\phi$  is the flux intensity in number of particles with mass  $m$  or greater per sq meter-sec (e.g., Bjork, 1961, Reference 307). This formula provides a conservative estimate for meteoroid flux in the important region of  $10^{-4}$  to  $10^{-8}$  g.

These curves present average fluctuations; large fluctuations can occur, particularly during meteor showers.

Predictions have been made, on theoretical grounds, of increased dust concentration around the earth by both American (References 277 and 298) and Russian writers (Reference 312). Using data from Explorer I, Sputnik III, Vanguard III, Explorer VI, and Pioneer I, Whipple (1961, References 295 and 299) derived an altitude dependence for flux intensities for the mass threshold of  $10^{-9}$  g. This assumes a straight-line function of log-flux vs log-mass, which is strongly indicated by Figure 49, if Explorer VII data points

are eliminated. The deviations from the straight line are then assumed by Whipple to be due to altitude differences and plotted against the altitude. Whipple's results indicate that at a distance of about  $10^5$  km the concentration falls off roughly as the inverse 1.4 power of the distance from the earth's surface. Whipple ascribes the apparent dust cloud to the impact on the moon of meteoric bodies of cometary and asteroidal origin at high velocities (up to 72 km/sec), with ejection of dust and droplets. A portion of this dust is assumed to be ejected into cislunar (earth) orbits. The higher concentration near the earth would be caused by convergence of the orbits and atmospheric drag effects.

Measurements from the Midas II, Pioneer I, and Vanguard III data (taken from Soberman and Della Lucca, Reference 312), together with the Explorer VIII data, show the flux dependence on altitude, Figure 50. Russian satellites show similar results, excepting that the largest concentration is interpreted to be 100 to 300 km above the earth's surface (Reference 313).

T. N. Nazarova, using more extensive data obtained in the USSR, supports the basic concept of the dust belt, but postulates a slower fall-off (Nazarova and Moroz, 1961, Reference 306); Hibbs (1961, Reference 300), from a statistical analysis of Explorer I data, concluded that an altitude dependence was indicated to a 90% confidence level.

The Mariner II data have shown four orders of magnitude difference between near-earth and interplanetary environments. Only two impacts were recorded by the Mariner II during 109 days of flight, as compared to 3,700 impacts in one month by an earth satellite. No observations of the zodiacal cloud and solar corona tend to confirm this low concentration of dust particles in interplanetary space.

#### 4. Velocity Variations

It known that from 80 to 90% of the micrometeoroids are sporadic, no two having a common radiant (References 316, 317, and 318). The particles are concentrated in heliocentric orbits distributed about the

ecliptic plane (Reference 319). Gill and Davies (Reference 320) determined from their measurements that more than 60% of all meteor radiants are within  $20^{\circ}$  of the ecliptic plane. Mlodnosky (Reference 321) has estimated that approximately 50% of the sporadics have radiants within  $13^{\circ}$  of the ecliptic. Figure 51 (taken from Reference 79) shows the relative number of visual radiants of sporadic meteors in the ecliptic plane. Lovell (Reference 310) has indicated that another group of sporadic meteoroids, composing 15% of the total, moves in rather circular orbits with inclinations grouped around  $60$  to  $120^{\circ}$ .

Most of the meteoroids are in direct heliocentric orbits, although the exact percentages of those in direct and retrograde orbits are not known. Hawkins and Upton (Reference 254) have made a radio-echo survey of sporadic meteors, showing the earth's influx pattern for a 24-hour period. Figure 52 shows, for the plane of the earth's orbit, the direction of incoming particles as a vector, the length of which is a measure of the number of particles from that vector direction. Hawkins constructed a heliocentric distribution of his observations at a point of the earth's orbit, adding the earth's heliocentric velocity of 30 km/sec to his observed particle velocity (relative to the earth), and assuming that all particles possessed a heliocentric velocity of 40 km/sec. This can be seen in Figure 53, but, because of Hawkins' assumption, Figure 53 should be taken as a model rather than the actual prevailing pattern. Figure 53 shows that most meteoroids approach the earth from behind but, since their heliocentric velocity is of the same order as the earth's, more are captured by the earth on its front side (Figure 52). The earth can be said to strike or overtake many more meteoroids than strike or overtake it.

Also noticeable in Figure 52 is a trinodular distribution on the front (apex) side of the earth. The explanation of this comes from Mlodnosky (Reference 321). In his evaluation of data taken by Gill and Davies (Reference 320), Mlodnosky deduced from Figure 54 which shows somewhat more pronounced lobes than does Figure 52, that there exist two conical null zones (antiradiant cones). No radiants were said to lie in these zones because of the capture and dissipative power of the sun on low-perihelion (10 sun radii or less) particles.

Mlodnosky deduced that the antiradiant concept also explains the characteristic bimodal velocity-distribution histograms observed by Millman and discussed in Reference 79 (Figure 55). Mlodnosky has shown that the limiting perihelion does not allow geocentric velocities between 40 and 53 km/sec and that there is a sparsity of meteors with heliocentric velocities below 30 km/sec. He has also observed that meteoroids have a preponderance of nearly parabolic orbits. This indicates a highly eccentric orbit. The aphelion velocity of such a particle is about  $1 \times 10^{-5}$  km/sec (1 cm/sec) and the perihelion velocity is about 195.7 km/sec.

There are seasonal shifts as well as daily variations in the meteor statistics. The daily maximum occurs about 6 am. It occurs later in the spring and earlier in the winter, over a range of about 2 hours. The mean hourly rate is also seasonally influenced, lessening in the spring and increasing markedly in the fall. The minimum is 50% of the average. Reference 314 and 315, which agree that there is a seasonal variation, give different numbers and also indicate a hemispherical (north-south) variation.

REFERENCES

(Partially Annotated)

1. G. P. Kuiper, The Sun, Univ. of Chicago Press, 1953.
2. H. Friedman, "Solar Radiation," Astronautics, August 1962.
3. H. W. Newton, "The Face of the Sun," Pelican Books, 1958.
4. F. S. Johnson, J. Meteorol., 2, 431, 1954.
5. David R. Beard, "Comets and Cometary Debris in the Solar System," Rev. of Geophysics, 1 (1963) 211-229.
6. Fred L. Whipple, "On Meteoroids and Penetration," Proceedings, Ninth Annual American Astronautical Society Meeting, Los Angeles, California (Jan. 1963).
7. R. Tousey, "The Solar Spectrum in Space," Astronautics, July 1961, p. 32.
8. H. E. Hinteregger, Astrophs. J., 132, 801, 1960.
9. L. Biermann, Astrophs. J., 25, 161, 1949.
10. H. S. Bridge, A. J. Lazarus, B. Rossi and F. Scherb, "Explorer X Interplanetary-Plasma Observations," Trans. of American Geophysical Union, 43, 1, March 1962.
11. H. J. Goett, Scientific Exploration of Space, presented at the Aviation and Space Writers Association, 25 May 1962, San Francisco.
12. M. L. White and A. A. Wyller, "Interplanetary Gas and Magnetic Fields," from Space and Planetary Environments, ed. S. L. Valley, Air Force Cambridge Research Lab. Rept. 139, January 1962.
13. C. P. Sonnett, "Magnetic Fields in Space," Aeronautics, August 1962.
14. Otto Struve, Elementary Astronomy, Oxford University Press, New York, 1959.
15. P. S. Coleman, L. Davis, and C. P. Sonnett, Phys. Rev. Letters, 5, 43, 1960.
16. L. V. Berkner and H. Odishaw, Science In Space, McGraw-Hill, 1961.
  - a. J. A. Simpson, "The Acceleration and Propagation of Particles Within the Solar System," pp. 239 ff.
  - b. J. A. Simpson, "Physics of Fields and Energetic Particles in Space," pp. 221 ff.



REFERENCES (cont.)

- c. E. N. Parker, "The Interplanetary Gas and Magnetic Fields," pp. 229 ff.
- d. L. Goldberg and E. R. Kyer, Jr., "The Sun," pp. 307 ff.
- 17. Thomas Gold, "Cosmic Rays and the Interplanetary Medium," Astronautics, August 1962.
- 18. McCracken, "The Cosmic Ray Effect, Deductions Regarding the Interplanetary Magnetic Field," Jour. of Geophysical Research, 67, 2, February 1962.
- 19. H. M. Jeffers, "Observations of Comets and Asteriods," S. Vasilevskis and E. S. Roemer, Astron. J., 5, 8, September 1954.
- 20. Krafft A. Ehricke, Space Flight (I. Environment and Celestial Mechanics), Van Nostrand, New York-London, 1960.
- 21. Arthur C. Clarke, The Exploration of Space, Harper, New York, 1959.
- 22. E. J. Opik, "Diameters of the Asteriods," Irish Astron. J., 1, 5, March 1951.
- 23. E. J. Opik, "Mars and the Asteriods," Irish Astron. J., 1, 1, March 1950.
- 24. Felix Godwin, The Exploration of the Solar System, Plenum Press, New York, 1960.
- 25. D. M. Cole, "Asteroids Stir Growing Interest," Missiles and Rockets, February 25, 1963.
- 26. R. J. Levy, "On the Possibility of Using Asteroids as Position Indicators in Interplanetary Navigation," Report Number 61-27-A, Geophysics Corporation of America, June 1961.
- 27. "Ephemerides of Minor Planets," Institute for Theoretical Astronomy, Leningrad (annual).
- 27a. Brian Mason, Meteorites, John Wiley and Sons, Inc., New York, 1962.
- 27b. Middlehurst, Barbara M, and Kuiper, Gerard P. (Editors), "The Moon Meteorites and Comets," The University of Chicago Press, Chicago, 1963.
- 28. E. J. Opik, "Physics of Meteor Flight in the Atmosphere," Interscience Tracts on Physics and Astronomy, No. 6, Interscience Publishers, 1958.
- 29. R. E. Lyttleton, The Comets and Their Origin, Cambridge Univ. Press, 1953.

REFERENCES (cont.)

30. D. H. Robey, "A New Model for Comets - The Cold, Partially Condensed, Magnetized Plasma," J. of the Astronautical Sciences, 9, 2, American Astronautical Society, New York, 1962.
31. A.C.B. Lovell: "Geophysical Aspects of Meteors," Encyclopedia of Phys., S. Fliigge, Ed., Vol. XLVIII - Geophysics II. Springer-Verlag, 1957, pp. 427-454.
32. Fred L. Whipple, and Robert F. Hughes: "On the Velocities and Orbits of Meteors, Fireballs, and Meteorites," Meteors, T. R. Kaiser, Ed., Pergamon Press Ltd., 1955, pp. 149-156.
33. Conway Synder, personal communication, Jet Propulsion Laboratory, April 1963.  
See Also: News Releases, Mariner II Data Evaluation, Office of Public Education and Information, California Institute of Technology, Feb. 26, 1963.
34. Arthur C. Clarke, The Exploration of Space, Harper, New York, 1959.
35. Gerard P. Kuiper, The Solar System: Vol. III - Planets and Satellites, University of Chicago Press, Chicago, 1961.
36. Felix Godwin, The Exploration of the Solar System, Plenum Press, New York, 1960.
37. D. M. Cole, "Mercury Missions Seen More Useful than Mars, Venus Probes," Missiles and Rockets, June 24, 1963.
38. Carl Sagan and W. W. Kellogg, "The Terrestrial Planets," published in the Annual Review of Astronomy and Astrophysics, Vol. I, 1963.
39. G.J.F. MacDonald, "The Internal Constitutions of the Inner Planets and the Moon." Space Science Reviews, Oct. 1963.
40. D. G. Rea and W. J. Welch, "The Reflection and Emission of Electromagnetic Radiation by Planetary Surfaces and Clouds," Space Science Reviews, October 1963.
41. R. A. Lyttleton, "On the Origin of Mountains," Proceedings of the Royal Society, Vol. 275, 1963.
42. Harold C. Urey, "The Origin and Evolution of the Solar System," published in Space Science, edited by Donald P. Le Galley, Wiley Books, 1963.
43. I. M. Levitt and D. M. Cole, "The Forgotten Planet," from Exploring the Secrets of Space, Prentice Hall, 1963.

REFERENCES (cont.)

44. E. M. Antoniadi, Astronomi, 49, p. 449, 1935.
- 45a. W. E. Howard, A. H. Barrett and F. T. Haddock, Astronomical Journal, 66, p. 287, 1961.
- 45b. J. A. Roberts, Planet Space Science, Vol. II, p. 221, 1963.
46. E. Petit, Planets and Satellites, Chapter 10, 1961.
47. J.C.J. Walker, Astrophysics Journal, 133, p. 274, 1961.
48. G. B. Field, Astronomical Journal, 67, p. 575, 1962.
49. P. Hodge, Proc. Inter. Astrophysical Colloq. 11th, Siege, 1963.
50. A. Dollfus, Compt. Rend., 231, p. 1430, 1950.
51. A. Dollfus, Planets and Satellites, Chap. 8, 1961.
52. D. L. Harris, Planets and Satellites, Chap. 8, 1961.
53. V. P. Kotel'nikov, et al. Doklady Akad Nauk, 147, 1962.
54. Staff, Jet Propulsion Laboratory, Mariner, Mission to Venus, McGraw Hill Book Co., 1963.
55. Z. Kopal, personal communication, April, 1963.
56. W. M. Sinton, personal communication, August 1962.
57. C. E. Anderson, Physical Properties of the Planet Venus, Douglas Aircraft Co., SM-41506, July 1962.
58. D. C. Evans and C. E. Anderson, The Nature of the Venus Cloud System, Institute of Aerospace Sciences, June 18-22, 1962.
- 59a. G. de Vaucouleurs, and D. H. Menzel, "Results of the Occultation of Regulus by Venus," Nature, London, Vol. 188, pp. 28-33, 1960.
- 59b. F. D. Drake, "10 Cm Observations of Venus in 1961," Publ. Natl. Radio Astron. Observatory, Vol. 1, pp. 165-178, 1962.
60. V. Radhakrishnan, Radio Astronomy of the Solar System, American Astronautical Society, Jan. 1963.
61. L. D. Kaplan, Application of Spectroscopy to Chemical and Structural Analysis of Planetary Atmospheres, Proc. International Symposium on Molecular Structure and Spectroscopy, Tokyo, 1962.

REFERENCES (cont.)

62. R. L. Jenne, Reflection, Absorption and Transmission of Solar Radiation Through Clouds, Breaks in Clouds and Water Vapor, M. S. Thesis, Univ. of Wash., 1960, Astia Doc. No. 239846.
63. L. B. Aldrich, "The Reflecting Power of Clouds," Smithsonian Miscellaneous Collections, Vol. 69, No. 16, pp. 1-9, 1919.
64. E. W. Hewson, "Reflection Absorption and Transmission of Solar Radiation by Fog and Clouds," Quarterly Journal of the Royal Meteorological Society, Vol. 69, pp. 47-62, 1943.
65. W. B. Moreland, Reflectivity of Cumulus Clouds in the Near Infrared, American Geophysical Union reprint, 43rd Annual Meeting, Wash. D.C., April 25-28, 1962.
66. D. H. Menzel and F. W. Whipple, "The Case for Water Clouds on Venus," Astronomical Journal, Vol. 59, pp. 329-330, Oct. 1954.
67. M. Neuburger, "Reflection, Absorption, and Transmission of Insolation by Stratus Clouds," Journal of Meteorology, Vol. 6, pp. 98-104, 1949.
68. N. P. Barabashev, (a J.P.L. Translation by K. N. Trirogoff) "Investigation of the Physical Condition of the Moon and the Planets," Pub. Kharkov Obs., 1952.
69. Proceedings of the Lunar and Planetary Exploration Colloquialism, North American Aviation, Space and Information Systems, Pub 513-W-11, May 1962.
70. H. Spinrad, "Spectroscopic Temperature and Pressure Measurements in the Venus Atmosphere," Jet Propulsion Laboratory. To be published, Astronomical Society of the Pacific, late 1962.  
  
In a detailed examination of the Mt. Wilson Venus plates (Dunham), Spinrad shows that the total pressure is considerably higher than previously believed and demonstrates that CO<sub>2</sub> is not more than 5 to 10% of the atmosphere, the remaining 90 to 95% being presumably molecular nitrogen. Total pressure and rotational temperatures are computed from ten plates and model atmospheres proposed.
71. Carl Sagan, "Structure of the Lower Atmosphere of Venus," Berkeley, California, March 1962, to be published in the Astronomical Journal, late 1962.  
  
An extensive study of the lower atmosphere of Venus is presented utilizing the most recently available data and analysis.
72. H. Spinrad, "A Search for Water Vapor and Trace Constituents in the Venus Atmosphere," Jet Propulsion Laboratory. To be published, Astronomical Journal, late 1962.

Previous analysis and data on the abundance of water vapor on Venus are reviewed. New calculations based on the Doppler shift method on Mt. Wilson

REFERENCES (cont.)

plates show that the amount of water vapor is too small to support the Sagan greenhouse theory. It is shown that the amount of water vapor to the total atmosphere (ratio) is  $9 \times 10^{-7}$  by mass. Spinrad concludes that the greenhouse effect may be due to molecular absorption other than water.

73. Peter Wegener, "Estimates of the Flight Regimes of the Venus Atmosphere," Rand Corporation RM 2946. To be published, June 1962.  
This recent paper includes flight analysis data based on recent (late 1961) atmosphere models but does not include the Spinrad work (1962).
74. "Radar Probes of the Venus Indicate Its Surface Similar to Earth," Aviation Week and Space Technology, 14 May 1962.  
A short article covering the May COSPAR meeting in Washington, D.C. discussing the radar measurements obtained from the Goldstone transmitter by Victor and Stevens. It is inferred from these measurements that the surface roughness and composition of Venus may be similar to that of the earth.
75. C. R. Grant and H. H. Corbett "Observations of Venus at 4.3 mm," U.S. Naval Research Laboratory, (Abst.) Astronomical Journal, March 1962.  
Reports of measurements of temperature by shorter wavelength than used previously. Mean temperature of  $352^{\circ}\text{K}$  with an estimated upper value of the probable error of  $\pm 50^{\circ}$ . This mean brightness temperature compares well with the  $340^{\circ}\text{K}$  by Öpik for the top of the visible clouds. This is considerably lower than the brightness temperature measured by longer wavelengths, typically  $585^{\circ}\text{K}$  at 3.15 cm by Mayer, McCullough, and Sloanaker.
76. L. D. Kaplan, A Preliminary Model of the Venus Atmosphere, Technical Report No. 32-379, Jet Propulsion Lab., Dec. 12, 1962.  
"Standard" and extreme model atmospheres of the planet Venus are calculated with temperature, density, and pressure given as functions of height. Use is made of the Spinrad total pressure and rotational temperatures, (based on Dunham's  $\text{CO}_2$  spectra), the occultation of Regulus, and a surface temperature of  $700^{\circ}\text{K} \pm 140^{\circ}$ , (originally from radar data but in good agreement with Mariner II results).

REFERENCES (cont.)

77. J. F. White (Editor), "Flight Performance Handbook for Powered Flight Operations," prepared by the Space Technology Laboratories for JPL, March 1962.  
With reference to Venus, model atmospheres are suggested in Chapter 7, "Planetary Entry." Three exponential models are suggested (based on the work of De Vaucouleurs and D. Menzel, 1960) and are based on the assumption that  $\text{CO}_2$  is the major constituent. Despite the recent publication date, the work of Spinrad, Newburn, (both 1962) and Kopal (1960) is not taken into account, showing the major constituent to be  $\text{N}_2$ .
78. V. A. Firsoff, "On Carbon Dioxide in the Atmospheres of Venus," National Academy of Sciences, Publication 944, Washington, D.C., 1961.  
An excellent discussion of the status of Venus as of late 1961 presenting various opposing theories and evaluations and reviewing pertinent data. Experiments to distinguish among the alternative models are discussed. Several appendices are included: "The General Circulation of Planetary Atmospheres," by Mintz, "Interpretation of the Near-Infrared Bands of Venus," by Chamberlain, and others.
79. J. E. Duberg, The Meteorite Hazard of the Environment of a Satellite, NASA TN-D1248, May 1962.
80. J. H. Shaw and N. Y. Bobrovnikoff, "Preliminary Planetary Investigation of Interplanetary, Lunar and Near Planet Environments and Methods of Simulation," Ohio State University, ASD Technical Report 61-267, July 1961.  
With regard to Venus, the pertinent physical properties are summarized with a concise review of the literature. The bibliography includes 101 papers, all prior to 1958. This section of the report is a summary of the more extensive work, by the authors in February 1959, cited below.
81. L. Hobbs, "An Annotated Bibliography of Articles on the Atmosphere of Venus and Mars," The General Electric Co. Report R61SD175, November 1961.  
Forty-four papers are reviewed covering the most prominent papers prior to 1960. The annotated bibliography is well written with many interesting comments by the author. Certain of the descriptive passages were utilized here. Most of the recent Venus work was, of course, not included. Kopal's article (Ref. 90, published December 1960), pointing out the Venus atmosphere to be largely nitrogen with only small amounts of  $\text{CO}_2$ , was not cited.

REFERENCES (cont.)

82. L. D. Kaplan, "The Structure and CO<sub>2</sub> Content of the Venus Atmosphere," Astronomical Journal, September 1961.  
The fraction of CO<sub>2</sub> in the Venus atmosphere is shown to be 15  $\pm$  7% by volume at 400 mb. This figure resulted from an analysis of the Venus spectra of Kuiper and of Strong and Sinton and the Regulus occultation measurements.
83. A. E. Lilley, "The Temperature of Venus," Astronomical Journal, September 1961.  
Substantial new evidence for high surface temperature of 600°K is presented based on measurements at wavelengths of 21 cm.
84. Carl Sagan, "On the Origin of the Venus Microwave Emission," Astronomical Journal, March 1961.  
Theoretical models are proposed to account for the apparent change in brightness temperature from 600°K to about 300°K with wavelength. The low surface temperatures are shown to be inconsistent with the greenhouse effect. The likelihood of a 1 gauss magnetic field is also mentioned.
85. Y. Mintz, "Temperature and Circulation of the Venus Atmosphere," Planetary and Space Science, Vol. 5 No. 2, p. 141 (1961), (also see Rand Corporation Report RM-2711-JPL).  
With radiative equilibrium the atmosphere is shown to be convectively stable and a mean temperature of 235°K. The circulation system is inferred from the appearance of the Venus clouds in visible and ultraviolet light. Mintz infers that the different appearance in the visible and ultraviolet may result from the fact that different levels are being observed; he suggests a possible way in which a symmetrical circulation regime centered on the sub-polar point at lower levels could change to a different centered circulation at high levels.
86. C. H. Mayer, "The Temperatures of the Planets," Scientific American, Vol. 204, No. 5, p. 58 (1961).  
Radiometric data and analysis are presented for Mars, Venus, Jupiter, and Saturn. With respect to Venus, the high radio predicted temperatures (600°K) are compared with the low (320°K) infrared temperatures. The various theories which attempt to account for this difference are briefly discussed.

REFERENCES (cont.)

87. J. D. Carr, A. G. Smith, H. Bollhagen, N. F. Six, and N. E. Chatterton, "Recent Decameter-Wave-Length Observations of Jupiter, Saturn, and Venus," Astrophysical Journal, Vol. 134, p. 105 (1961).  
Intensive monitoring of Venus failed to detect any decameter-wavelength radiation, in agreement with earlier observations.
88. A. H. Barrett, "Microwave Absorption and Emission in the Atmosphere of Venus," Astrophysical Journal, Vol. 133, p. 281 (1961).  
A model atmosphere is proposed assuming 75% CO<sub>2</sub>, now thought to be unrealistic. However, the paper contains a comprehensive summary of radiometric data.
- 88A. B. Warner, "The Emission Spectrum of the Night Side of Venus," Monthly Notices of the Royal Astronomical Society, Vol. 121, No. 3, p. 279 (1960).  
The measurements given by Kozyrev of features in the spectrum of the night side of Venus are examined. The existence of nitrogen bands is confirmed, and evidence is presented identifying emission lines of neutral and ionized oxygen.
89. E. J. Öpik, "The Aeolosphere and Atmosphere of Venus," J. Geophysical Research, 1961.  
The aeolosphere concept of the Venus atmosphere is described in rejecting the greenhouse effect. The aeolosphere model assumes the yellowish clouds to be dust kept in motion by high-velocity winds. Since the stirred up atmosphere will maintain an adiabatic lapse rate, the temperature will increase with increasing depth below the cloud tops, reaching the high surface temperatures observed by radio measurements.
90. Zdenek Kopal, "Aerodynamic Effects in Planetary Atmospheres," Aerospace Engineering, December 1960.  
A brief summary of the physical and chemical characteristics of Mars and Venus are presented. With reference to Venus, Kopal states that the atmosphere is probably made up mainly of molecular nitrogen and only a small amount CO<sub>2</sub>. This was the first mention found in the open literature. Kopal cites analysis which indicates that Venus might have a magnetic field of 1 to 2 gauss but warns that this result is by no means conclusive.



REFERENCES (cont.)

91. J. Strong and W. H. Sinton, "Radiometric Observations of Venus," Astro-physical Journal, Vol. 131 p. 470 (1960).  
With regard to Venus, measurements in the far-infrared (thermal) emission indicate an effective temperature of  $234^{\circ}\text{K} \pm 10^{\circ}$ . It is generally believed this reflects the temperature of a cloud layer somewhere in the atmosphere.
92. G. De Vaucouleurs, "Remarks on Mars and Venus," in The Exploration of Space, edited by Robert Jastrow, published by the Macmillan Co., 1960.  
An excellent summary article comparing orbital and atmospheric information of Mars, Venus, and earth. The discussion pertains mainly to Venus. Measurements of Kozyrev on the spectral reflectivity and the spectrum of the dark side of Venus (Newkirk) are presented and discussed.
93. J. Strong, "Discovery of Water Vapor on Venus," La Nature (France), Vol. 3298, p. 61 (1960).  
Absorption lines due to water vapor were identified from balloon observations. The abundance could not be accurately established from these data.
94. C. Sagan, "The Radiation Balance of Venus," Technical Report No. 32-34, Jet Propulsion Laboratory, Pasadena, California, 1960.  
It is shown that a greenhouse effect could be responsible for the high surface temperature of  $600^{\circ}\text{K}$ . Opik (1961) criticizes this greenhouse theory primarily on the basis that sufficient water vapor has not been observed consistent with the proposed model.
95. D. H. Menzel, and G. De Vaucouleurs, "Results of the Occultation of Regulus by Venus," Nature, Vol. 188, p. 28 (1960).  
A detailed discussion is given of the results obtained from visual, photographic, and photoelectric observations of occultation of Regulus made by teams of observers from Harvard College Observatory and the Smithsonian Astrophysical Observatory.
96. A. D. Kuz'min and A. E. Salomonovich, "Radio Emission from Venus in the 8-mm Bandwidth," Soviet Astronomy AJ, Vol. 4, p. 279 (1960).

---

\* Translated from Astronomical Journal (USSR), Vol. 37, p. 297 (1960).

REFERENCES (cont.)

The results measurement of radio emission from Venus at 8 mm, made at Lebedev Physics Institute are reported. The brightness temperature, following inferior conjunction, was  $315 \pm 70^{\circ}\text{K}$ . The temperature increased to  $430 \pm 130^{\circ}\text{K}$  after conjunction.

97. J. D. Kraus, "Apparent Radio Radiation at 11-m. Wavelength from Venus," Nature, Vol. 186, p. 462 (1960).  
It is shown that the quasi-coherent radiation reported earlier was not from Venus but was, in all cases, probably interference of terrestrial origin. References to these earlier reports of the burst-type radiation are included [in particular, see Nature, 178, 33 and 687 (1956)]. Recent work by Carr, et al. (1961, Ref. 87) failed to show any intense disturbances from Venus.
98. D. E. Jones, "A Microwave Radiometer Experiment from the Planet Venus," Technical Report 34-112, Jet Propulsion Laboratory, Pasadena, California, 1960.  
The high brightness temperature of nearly  $600^{\circ}\text{K}$  measured in the centimeter region is generally considered to be that of the surface of the planet.
99. H. C. Urey, "The Atmospheres of the Planets," Handbrich der Physik Berlin, Springer-Verlag, Vol. 52, p. 363 (1959).  
Chemical composition, temperature, structure, and evolution of the Venus atmosphere are considered based on the earlier  $\text{CO}_2$  dominated environment at total pressures considerably lower than now believed to exist.
100. G. Newkirk, "The Airglow of Venus," Planetary and Space Science, Vol. 1, No. 1, p. 32 (1959).  
Low-dispersion, high-speed spectra of the unilluminated portion of Venus show emission features, in agreement with Kozyrev's observations. Kozyrev's other emission bands are not corroborated by these spectra.
101. F. J. Heyden, C. C. Kiess, and Harriet K. Kiess, "The Spectrum of Venus in the Violet and Near-ultraviolet," Science, Vol. 130, No. 3383, p. 1195 (1959).  
Observations of the spectrum of the planet Venus, show that a wide, continuous absorption band is present in the violet and near-ultraviolet. It is similar

REFERENCES (cont.)

- in structure to the strong absorption, reported by others, for gaseous nitrogen tetroxide. However, Su-Shu Hong (Dec. 1961, Publications of the Astronomical Society of the Pacific) demonstrates that the existence of nitrogen tetroxide cannot be substantiated by theoretical analysis at this time.
102. J. H. Shaw, and N. T. Bobrovnikoff, "Natural Environment of the Planet Venus," Ohio State University, AD 242-176, February, 1959.  
An excellent summary of the environmental characteristic of Venus as understood up to 1959. Regions where knowledge is lacking are defined, and various theories proposed to fill the gap have been reviewed and compared. Attempts were made to estimate the probable environment in cases where the environment could not be definitely established.
  103. J. V. Narayana, "Magnetic Fields of the Planet Venus" Kodiakanal Obs. (India) August, 1959.  
The value of the magnetic field of Venus is calculated to be about 0.4 gauss based on statistical plots of the daily equivalent planetary amplitude. The rotation is computed to be 2 to 24 days.
  104. J. E. Gibson and R. J. McEwan, "Observations of Venus at 8.6-mm Wavelength," Paris Symposium on Radio Astronomy. Stanford, Stanford University Press, 1959, p. 50.  
Observations of Venus at 8.6-mm wavelength gave a brightness temperature of  $410 \pm 160^\circ\text{K}$ .
  105. L. E. Alsop, J. A. Giordmaine, C. H. Mayer, and C. H. Townes. "Observations of Discreet Sources at 3-cm Wavelength Using a Maser," Paris Symposium on Radio Astronomy. Stanford, Stanford University Press, 1959, p. 69.  
Observations of Venus at 3.37 cm are reported giving an apparent blackbody temperature of  $575 \pm 60^\circ\text{K}$ . These observations are not significantly different from observations made with the same reflector at 3.15 cm wavelength in 1956.
  106. J. L. Raymond, "Thermodynamic Properties of the Atmosphere of Venus," Rand Corporation November, 1958.

REFERENCES (cont.)

Extensive computations and numerical analysis for the Venus atmosphere based on an assumed 100% CO<sub>2</sub> atmosphere. Mollier Chart for CO<sub>2</sub> is presented for temperatures up to 24,000°K and complete thermodynamic properties of the CO<sub>2</sub> were carefully computed including enthalpy, entropy, molecular weight, density, internal energy, and molecular composition.

107. C. H. Mayer, T. P. McCullough, and R. M. Sloanaker. "Observations of Venus at 3.15-cm Wavelength," Astrophysical Journal, Vol. 127, p. 1 (1958).

Radiation from Venus at 3.15-cm wavelength give the apparent blackbody temperature for Venus as about  $560 \pm 73^{\circ}\text{K}$ .

108. I. K. Koval, "The Absolute Photometry of Venus in Ultraviolet and Infrared Light," Soviet Astronomy AJ, Vol. 2, p. 739 (1958).\*

The diameters of the image of Venus in ultraviolet and infrared light are shown to be equal. The cloud formation was 12% brighter than a symmetrical unclouded region in ultraviolet; it was no brighter in infrared light.

109. H. C. Urey, and A. W. Brewer. "Fluorescence in Planetary Atmospheres," Proceedings of the Royal Society of London, Vol. A241, p. 37 (1957).

It is pointed out that ions and free radicals will exist in the high atmospheres of the planets and that these ions will absorb and fluoresce in the visible and near-ultraviolet radiations. With regard to the color of Venus, it is suggested that the yellow color may be due either to colored carbon compounds in the clouds or to ionized molecules, in particular CO<sup>+</sup> and CO<sub>2</sub><sup>+</sup>, or to both effects. It is suggested that the clouds cannot be composed of dust but may be composed of water.

110. Kuiper, G. P. "The Atmosphere and the Cloud Layer of Venus." The Threshold of Space, edited by M. Zelikoff. London, Pergamon Press, 1957.

A summary of some of the quantitative measurements that have been made on Venus' atmosphere is given including spectroscopic, radiometric, polarimetric, and photometric measurements. From the spectroscopic identification of CO<sub>2</sub> and the stability of the Venus polarization curve, is suggested that the Venus cloud layer may be composed of C<sub>3</sub>O<sub>2</sub> particles. It is also reported

\* Translated from Astronomical Journal (USSR), Vol. 35, p. 739 (1958).

REFERENCES (cont.)

that the near-infrared polarization curve of Venus differs markedly from the theoretically predicted curve for liquid water droplets.

111. F. Horner, "Radio Noise from Planets," Nature, Vol. 180, p. 1253 (1957).  
It has been suggested that the high-frequency radio noise reportedly received from Jupiter and Venus might originate in electrical discharges, analogous to terrestrial lightning, in their atmospheres. A comparison of the observed noise intensities with the high-frequency radiation from terrestrial lightning, with proper corrections being made, shows that the observed intensities are too large by a factor of  $10^6$  to have arisen from a single lightning flash.
112. E. J. Öpik, "The Surface Conditions on Venus," Irish Astronomical Journal, Vol. 4, p. 37 (1956).  
Since Kozyrev's measurements show that the Venus clouds are slightly yellow and absorb strongly in the near-ultraviolet region, this may indicate that the Venus clouds are not composed of water, inasmuch as terrestrial clouds are white or blue-white.
113. A. Dollfus, "Etude visuelle et photographique de l'atmosphere de Venus," L'Astronomie, Vol. 68, p. 413 (1956).  
The apparent constancy in position of dark markings on Venus may imply that the period of rotation of Venus is 225 days, equal to the period of revolution.
114. J. W. Chamberlain and G. P. Kuiper, "Rotational Temperature and Phase Variation of the Carbon Dioxide Bands of Venus," Astrophysical Journal, Vol. 124, p. 399 (1956).  
A  $\text{CO}_2$  rotational temperature of  $285 \pm 9^\circ\text{K}$  is derived. A series of low-dispersion spectra shows a marked change in the strength of  $\text{CO}_2$  versus phase angle.
115. R. S. Richardson, "Observations of Venus Made at Mount Wilson in the Winter of 1954-55," Publications of the Astronomical Society of the Pacific, Vol. 67, p. 304 (1955).  
A series of photographs of Venus in ultraviolet light was made, with particular interest in observing any markings on the disk. Markings of a banded type were always present on the disk, showing an intensity range of 25%.

REFERENCES (cont.)

116. D. H. Menzel and F. L. Whipple. "The Case for H<sub>2</sub>O Clouds on Venus," Publications of the Astronomical Society of the Pacific, Vol. 67, p. 161 (1955).  
The arguments for and against H<sub>2</sub>O clouds on Venus are discussed. Lyot's polarization measurements and requirements on particle size support the H<sub>2</sub>O hypothesis and argue against dust clouds. The objection to the H<sub>2</sub>O hypothesis on the basis of the yellowish color of Venus, in view of white (or bluish) terrestrial clouds, is deemed questionable.
117. G. P. Kuiper, "Determination of the Pole of Rotation of Venus," Astrophysical Journal, Vol. 120, p. 603 (1954).  
As the result of a series of photographs of Venus taken in infrared, red, and violet light, which showed markings consisting of several parallel bands, an identification of the pole of rotation of Venus is suggested.
118. N. A. Kozyrev, "The Emission Spectrum of the Night Sky of Venus," Publications of the Crimean Astrophysical Observatory, Vol. 12, pp. 169 and 177 (1954).  
A spectrogram taken with the 50-inch astrograph disclosed a great number of molecular bands. Fifty features are listed, of which 22 are tentatively identified as being produced by N<sub>2</sub> and N<sub>2</sub><sup>+</sup>.
119. G. P. Kuiper, "Planetary Atmospheres and Their Origin," Atmospheres of the Earth and Planets, edited by G. P. Kuiper. Chicago, Chicago University Press, 1952. p. 306.  
Observational data and theoretical suggestions are presented, with particular interest in its bearing on the origin and evolution of planetary atmospheres. Infrared spectra of Venus showing CO<sub>2</sub> absorption bands are reproduced. The main conclusions are that the intensity of the band varies systematically with phase angle, that day-to-day fluctuations in intensity of considerable magnitude occur, and that the observed distribution of CO<sub>2</sub> is often remarkably patchy over the disk.
120. J. Dunham, "Spectroscopic Observations of the Planets at Mount Wilson," Atmospheres of the Earth and Planets, edited by G. P. Kuiper, Chicago, Chicago University Press, 1952. p. 288.

REFERENCES (cont.)

The original detection and identification, in 1932, of carbon dioxide bands near 8000 A in the spectrum of Venus is described. A temperature of about  $300 \pm 50^{\circ}\text{K}$  was obtained from an analysis of the lines. Neither water-vapor lines near 8000 A nor the B band of oxygen was observed. These plates were later studied extensively by Spinrad (1962) resulting in a redefinition of the Venus atmosphere.

121. H. Spinrad, "The Anomalous Inclination of the Jovian Ammonia Lines," Jet Propulsion Laboratory. To be published in the Astrophysics Journal, late 1962.

A careful measurement of the ammonia absorption lines from plates from Mt. Wilson, and Palomar (by Dunham in 1934 and Munch in 1961) show that the ammonia rotates far more slowly than the other layers of Jupiter's atmosphere. The differential rotation was measured to be about 6 km/sec.

122. L. M. Trafton, "The Jovian Environment," Jet Propulsion Laboratory, Technical Memorandum No. 33-77, 8 March, 1962.

The quantitative knowledge in existence concerning the Jovian environment and atmosphere is summarized. Topics covered include composition and structure of the atmosphere, photometric properties of the atmosphere, period of rotation, magnetic field, and the Jovian radiofrequency spectrum. References covering the most recent works in the study of Jupiter are listed. Because of the scarcity of information available on Jupiter, many of these references are listed below for completeness:

Jeffreys, H., "Constitution of the Four Outer Planets," Royal Astronomical Society Monthly Notices, Vol. 83, pp. 350-54, 1923.

Carr, T. D., Smith, A. G., Pepple, R., and Barrow, C. H., "18-Megacycle Observations of Jupiter in 1957," Astrophysical Journal, Vol. 127, pp. 274-83, 1961.

Carr, T. D., Smith, A. G., Bollhagen, H., Six, N. F., Jr., and Chatterton, N. E., "Recent Decameter-Wave-Length Observations of Jupiter, Saturn and Venus," Astrophysical Journal, Vol. 134, pp. 105-25, 1961.

Wildt, R., "Über die Stellardissoziation des Wasserstoffmoleküls," Zeitschrift für Astrophysik, Vol. 9, pp. 176-184, 1934.

REFERENCES (cont.)

- Peck, B. M., "Physical State of Jupiter's Atmosphere," Royal Astronomical Society Monthly Notices, Vol. 97, pp. 574-82, 1937.
- Baum, W. A., and Code, A. D., "Photometric Observations of the Occultation of  $\sigma$  Arietis by Jupiter," Astronomical Journal, Vol. 58, pp. 108-12, 1953.
- Peek, B. M., The Planet Jupiter, Chapter 28, pp. 227-35. Faber and Faber, London, 1958.
- Wildt, R., "Inside the Planets," Publications of the Astronomical Society of the Pacific, Vol. 70, No. 414, pp. 237-50, 1958.
- U.S. Naval Observatory, American Ephemeris and Nautical Almanac, U.S. Government Printing Office, Washington. Published annually.
- Resse, E. J., "Possible Clue to the Rotation Period of the Solid Nucleus of Jupiter," British Astronomical Association Journal, Vol. 63, pp. 219-21, 1953.
- Peek, B. M., The Planet Jupiter, pp. 222-26, Faber and Faber, London, 1958.
- Shain, C. A., "18.3 Mc/s Radiation From Jupiter," Australian Journal of Physics, Vol. 9, pp. 61-73, 1956.
- Franklin, K. L., and Burke, B. F., "Radio Observations of the Planet Jupiter," Journal of Geophysical Research, Vol. 63, No. 4, pp. 807-24, 1958.
- Douglas, J. N., "Uniform Statistical Analysis of Jovian Decameter Radiation, 1950-1960" (abstract only), Astronomical Journal, Vol. 65, pp. 487-88, 1960.
- Gallet, R. M., "Radio Observation of Jupiter II," Solar System, Vol. 3, ed. by G. P. Kuiper and B. M. Middlehurst. Chapter 14, pp. 500-33, University of Chicago Press, Chicago, 1961.
- Harris, D. L., "Photometry and Colorimetry of Planets and Satellites," Solar System, Vol. 3, ed. by G. P. Kuiper and B. M. Middlehurst. Chapter 8, pp. 272-86, University of Chicago Press, Chicago, 1961.
- Johnson, H. L., and Morgan, W. W., "Fundamental Stellar Photometry for Standards of Spectral Type on the Revised System of the Yerkes Spectral Atlas," Astrophysical Journal, Vol. 117, No. 3, pp. 313-52, May 1953.
- Kuiper, G. P., "Survey of Planetary Atmospheres," Atmospheres of the Earth and Planets, ed. by G. P. Kuiper. Chapter 12, pp. 304-45, University of Chicago Press, Chicago, 1949.
- Borgess, A., and Dunkelmann, L., "Ultraviolet Reflectivities of Mars and Jupiter," Astrophysical Journal, Vol. 129, pp. 236-37, 1959.
- Baum, W. A., and Code, A. D., "Photometric Observations of the Occultation of  $\sigma$  Arietis by Jupiter," Astronomical Journal, Vol. 58, pp. 108-12, 1953.
- Eropkin, D. J., "Über die Extinktion des Lichtes in der Jupiteratmosphäre," Zeitschrift für Astrophysik, Vol. 3, pp. 163-70, 1931.



REFERENCES (cont.)

- Link, M. F., "Occultation et éclipses par les planètes," Bulletin Astronomique, second series - Mémoires et Variétés, Vol. 9, pp. 2270-49 1933.
- Dunham, T., "Atmospheres of Jupiter and Saturn," Publications of the Astronomical Society of the Pacific, Vol. 46, pp. 231-33, 1934.
- Zabriskie, F. R., "Hydrogen Content of Jupiter's Atmosphere," American Geophysical Union, 41st Annual Meeting, Washington, D.C., April 27-30, 1960.
- Kiess, C. C., Corliss, C. H., and Kiess, H. K., "High-Dispersion Spectra of Jupiter," Astrophysical Journal, Vol. 132, pp. 221-31, 1960.
- Herzberg, G., "Spectroscopic Evidence of Molecular Hydrogen in the Atmospheres of Uranus and Neptune," Astrophysical Journal, Vol. 115, pp. 337-45, 1952.
- Herzberg, G., "On the Possibility of Detecting Molecular Hydrogen and Nitrogen in Planetary and Stellar Atmospheres by Their Rotation-Vibration Spectra," Astrophysical Journal, Vol. 87, pp. 428-37, 1938.
- Urey, H. C., "Atmospheres of the Planets," Handbuch der Physik, Vol. 50, ed. by S. Flügge. Pp. 363-415, Springer Verlag, Vienna, 1959.
- Plaetsche, J., "Photographische Photometrie der Jupiterscheibe," Zeitschrift für Astrophysik, Vol. 19, pp. 69-115, 1939.
- Van De Hulst, H. C., "Scattering in the Atmospheres of the Earth and the Planets," Atmospheres of the Earth and Planets, ed. by G. P. Kuiper. Chapter 3, pp. 49-111, University of Chicago Press, Chicago, 1949.
- Hess, S. L., "Variations in Atmospheric Absorption Over the Disks of Jupiter and Saturn," Astrophysical Journal, Vol. 118, pp. 151-60, 1953.
- Lyot, B., "Recherches sur la polarisation de la lumière des planètes et de quelques substances terrestres," Annales de l'Observatoire de Meudon, No. 8, 1929.
- Dollfus, A., "Polarization Studies of Planets: Jupiter," Solar System, Vol. 3, ed. by G. P. Kuiper and B. M. Middlehurst. Chapter 9, Part 4.6, pp. 391-94, University of Chicago Press, Chicago, 1961.
- Menzel, D. H., Coblentz, W. W., and Lampland, C. O., "Planetary Temperatures Derived From Water-Cell Transmission," Astrophysical Journal, Vol. 63, pp. 177-87, 1926.
- Newburn, R. L., Jr., "Exploration of Mercury, the Asteroids, the Major Planets and Their Satellite Systems, and Pluto," Advances in Space Science and Technology, Vol. 3, ed. by F. I. Ordway. Pp. 196-266, Academic Press, New York, 1961.
- Smith, A. G., "Radio Spectrum of Jupiter," Science, Vol. 134, No. 3479, pp. 587-95, 1961.

REFERENCES (cont.)

- Burke, B. F., and Franklin, D. L., "Observations of a Variable Radio Source Associated With the Planet Jupiter," Journal of Geophysical Research, Vol. 60, No. 2, pp. 213-217.
- Shain, C. A., "18.3 Mc/s Radiation from Jupiter," Australian Journal of Physics, Vol. 9, pp. 61-73, 1956.
- Smith, F. G., "Search for Radiation From Jupiter at 38 Mc/s and at 81.5 Mc/s," Observatory, Vol. 75, pp. 252-54, 1955.
- Kraus, J. D., "Some Observations of the Impulsive Radio Signals From Jupiter," Astronomical Journal, Vol. 61, pp. 182-83, 1956.
- "American Astronomers' Report," Sky and Telescope, Vol. 15, pp. 358-59, 1955-1956.
- Zhelezniakov, V. V., "On the Theory of the Sporadic Radio Emission From Jupiter," Soviet Astronomy - AJ, Vol. 2, pp. 206-15, 1958.
- Franklin, K. L., and Burke, B. F., "Radio Observations of Jupiter" (abstract only), Astronomical Journal, Vol. 61, p. 177, 1956.
- Carr, T. D., "Radiofrequency Emission From the Planet Jupiter," Astronomical Journal, Vol. 64, pp. 39-41, 1959.
- Giordmaine, J. A., Alsop, L. E., Townes, C. H., and Mayer, C. H., "Observations of Jupiter and Mars at 3-cm Wave Length" (abstract only), Astronomical Journal, Vol. 64, pp. 332-33, 1959.
- Mayer, C. H., "Planetary Radiation at Centimeter Wave Lengths," Astronomical Journal, Vol. 64, pp. 43-45, 1959.
- Drake, F. D., and Ewen, H. I., "Broad-Band Microwave Source Comparison Radiometer for Advanced Research in Radio Astronomy," Proceedings of the Institute of Radio Engineers, Vol. 46, pp. 53-60, 1958.
- Sloanaker, R. M., "Apparent Temperature of Jupiter" (abstract only), Astronomical Journal, Vol. 64, p. 346, 1959.
- McClain, E. F., "Test for Non-thermal Microwave Radiation From Jupiter at a Wave Length of 21 cm" (abstract only), Astronomical Journal, Vol. 64, pp. 339-40, 1959.
- Drake, F. D., and Hvatum, S., "Non-thermal Microwave Radiation From Jupiter," Astronomical Journal, Vol. 64, pp. 329-30, 1959.
- Roberts, J. A., and Stanley, G. J., "Radio Emission From Jupiter at a Wavelength of 31 Centimeters," Publications of the Astronomical Society of the Pacific, Vol. 71, pp. 485-96, 1959.
- Mayer, C. H., "Radio Emission of the Moon and Planets," Solar System, Vol. 3, ed. by G. P. Kuiper and B. M. Middlehurst. Chapter 12, pp. 442-68, University of Chicago Press, Chicago, 1961.

REFERENCES (cont.)

Drake, F. D., "Radio Emission From the Planets," Physics Today, Vol. 14, pp. 30-34, 1961.

Field, G. B., "Source of Radiation From Jupiter at Decimeter Wavelengths," Journal of Geophysical Research, Vol. 64, pp. 1169-77, 1959.

Radhakrishnan, V., and Roberts, J. A., "Polarization and Angular Extent of the 960-Mc/sec Radiation From Jupiter," Physical Review Letters, Vol. 4, pp. 493-94, 1960.

Sloanaker, R. M., and Boland, J. W., "Observations of Jupiter at a Wave Length of 10 cm," Astrophysical Journal, Vol. 133, pp. 649-56, 1961.

Field, G. B., "Source of Radiation From Jupiter at Decimeter Wavelengths: 2 Cyclotron Radiation by Trapped Electrons," Journal of Geophysical Research, Vol. 65, pp. 1661-71, 1960.

123. F. R. Zabriskie, "Hydrogen Content of Jupiter's Atmosphere," Astronomical Journal, Vol. 67, No. 3, April 1962.

Hydrogen was definitely established by spectroscopic evidence through the work of Kiess and associates. Zabriskie has provided further analysis giving the abundance of hydrogen present.

124. Harlan Smith and James N. Douglas, "Fine Structure in Jovian Decametric Radio Noise," Yale University Observatory, Astronomical Journal, Abstr. March 1962.

This paper presents discussions of recent observations. The records show (1) there exists a radically new form of ionospheric scintillation, (2) it reflects irregularities in interplanetary plasma, and (3) much fine structure exists in the signals as they leave Jupiter.

125. G. B. Field, "Can the Jupiter Emission be Cyclotron Radiation?" Astronomical Journal, September 1961.

Recent observations of the polarization, spectrum, angular extent, and time variation of the Jovian decimeter emission are compared with a theoretical model based on cyclotron radiation by non-relativistic electrons trapped in a dipole field. Field concludes that this simple model based on cyclotron emission is inconsistent with observation and shows that synchrotron radiation by relativistic electrons provides a better model.

REFERENCES (cont.)

126. R. Hide, "Origin of Jupiter's Great Red Spot" Nature (Great Britain) Vol. 190, June 3, 1961.

A turbulent hydrodynamic model is proposed to account for the Jovian Red Spot. The spot is proposed to be a shallow "topographical feature" in the solid surface, which together with the rapid rotation of the planet, creates a turbulent regime responsible for the radio-noise bursts from this area.

127. C. H. Mayer, "The Temperature of the Planets," Scientific American, May 1961. With regard to Jupiter, photographs of radio telescope are presented and intensity data, with and without masers, and presented. The various ultra-high temperatures measured at different wavelength are discussed, and theoretical analysis regarding these extreme temperatures is briefly described.

128. J. Bolton, "Van Allen Belt Radiation on the Planet Jupiter," Electrical Engineering, Vol. 79, No. 620, July 1960.

From radio data, the existence of a magnetic field was established 200,000 miles above the surface of the planet, 85,000 miles in diameter, with an axis almost parallel to the planet's axis of rotation (as in the earth's magnetic field). The measured radiation intensity was a trillion times more than that of the earth's.

129. C. C. Kiess, C. H. Corliss, and H. K. Kiess, "High Dispersion Spectra of Jupiter," Astrophysical Journal, Vol. 132, No. 221 (1960).

The atmosphere of Jupiter has 5 km atm  $H_2$  above the cloud level. The temperature of this level is about  $170^{\circ}K$  or higher, perhaps as much as  $200^{\circ}K$ . These data are derived from the quadruple lines of  $H_2$  found in the spectrum.

130. O. Struve, B. Lynds, and H. Pillans, Elementary Astronomy, Oxford University Press, 1959.

This excellent book is well illustrated and contain appreciable data in easy reference form. The planet Jupiter is discussed only briefly while

REFERENCES (cont.)

the Jupiter satellites receive considerable attention including a listing of physical and orbital data, orbit sketches, and relative configuration alignment representations.

131. A. Borgess, and L. Dunkelman, "Ultraviolet Reflectivities of Mars and Jupiter," Astrophysical Journal, Vol. 129, p. 236 (1959).

Ultraviolet observations were made from an Aerobee rocket 140 km above the White Sand Proving Ground. A reflectivity of 0.26 at 2700 Å was measured for Jupiter.

132. G. P. Kuiper, "The Atmospheres of the Earth and the Planets," University of Chicago Press, 1952.

With regard to Jupiter (as for the other planets) orbital and physical property data are presented including information on the atmosphere, circulation, clouds, dimensions, temperature, and satellites.

133. G. Fielder, "Structure of the Moon's Surface," Pergamon Press, N.Y., (1961).
134. Z. Kopal, "The Moon, Our Nearest Celestial Neighbor," Academic Press, Inc., New York (1960).
135. Phyllis Buwalda, "The Lunar Environment," Jet Propulsion Laboratory Technical Release No. 34-159, October 28, 1960.
136. B. Elsmore, "Radio Observations of the Lunar Atmosphere," Phil. Mag., Ser. 8, Vol. 2, 1040 (1957).
137. C. H. Costain, B. Elsmore, and G. R. Whitfield, "Radio Observations of a Lunar Occultation of the Crab Nebula," M.N.R.A.S., Vol. 116, 380-385 (1956).
138. A Dollfus, "Recherche d'une Atmosphere Autour de la Lune," Ann. d'Astrophys., Vol. 19, 71-82, (1956).
139. B. Elsmore and G. R. Whitfield, "Lunar Occultation of a Radio Star and the Derivation of an Upper Limit for the Density of the Lunar Atmosphere," Nat., Vol. 176, 457-458 (1955).
140. R. Wildt, H. J. Smith, E. E. Salpeter, and H. G. W. Cameron, "The Planet Jupiter," Physics Today 16, No. 5, May 1963.

REFERENCES (cont.)

141. Francis S. Johnson, "Physics of the Atmosphere and Space," Aeronautics, 7, 11, November 1962.
142. W. G. V. Rosser, B. J. O'Brian, J. A. Van Allen, L. A. Frank and C. D. Laughlin, "Electrons in the Earth's Outer Radiation Zone," J. Geophys. Res. 67, 12, November 1962.
143. G. Pizzella, C. D. Laughlin and B. J. O'Brian, "Note on the Electron Energy Spectrum in the Inner Van Allen Belt," J. Geophys. Res. 67, 9, August 1962.
144. K. I. Gringauz, V. G. Kurtz, V. I. Moroz, and I. S. Shklovskii (1960), "The Ionized Gas and Fast Electrons in the Vicinity of the Earth and in Interplanetary Space," Doklady Acad. Nauk., 132, 1062 (transl. in Physics Express, Oct. 1960, pp. 6-9).
145. J. A. Van Allen, "The Geomagnetically Trapped Corpuscular Radiation," J. Geophys. Res. 64, 1959.
146. R. L. Arnoldy, R. A. Hoffman, and R. J. Winkler, "Observations of the Van Allen Radiation Regions During August and September 1959, Part I," J. Geophys. Res. 65, 1960.
147. A. J. Dessler (1961), Satellite Environment Handbook, (F. S. Johnson, ed.), Stanford University Press, Chapter 3.
148. S. C. Freden and R. S. White (1959), "Protons in the Earth's Magnetic Field," Physics Rev. Letters 3, p. 9-11.
149. S. C. Freden and R. S. White (1960), "Particle Fluxes in the Inner Radiation Belt," J. Geophys. Res. 65, 1377.
150. S. N. Vernov, A. E. Chudakov, P. V. Vakulov, and I. Y. Logacher (1959), "Study of Terrestrial Corpuscular Radiation and Cosmic Rays During the Flight of a Cosmic Rocket," Soviet Phys. Doklady, 4, p. 338.
151. M. L. Walt, L. F. Chase, Jr., W. L. Inhof, and D. J. Knescht (1960), Space Research, (H. Kallmann Bijl. ed.), North Holland Publishing Co., Amsterdam, p. 910.
152. T. G. Northrup and E. Teller (1960), "Stability of the Adiabatic Motion of Charged Particles in the Earth's Field," Phys. Rev. 117, 215.
153. Carl E. McIlwain, "Coordinates for Mapping the Distribution of Magnetically Trapped Particles," J. Geophys. Res. 66, 3681.
154. Explorer XII Symposium, 18 Jan. 1962, Goddard Space Flight Center, Greenbelt, Md.

REFERENCES (cont.)

155. J. E. Naugle (1961), "Space Environment," Nucleonics, 19, 4, p. 89.
156. S. H. Vernov and A. E. Chudakov (1960), "Terrestrial Corpuscular Radiation and Cosmic Rays," Space Research, (H. Kallman Bijl, ed.), North Holland Publishing Company, Amsterdam, p. 751.
157. R. A. Hoffman, R. L. Arnoldy and J. R. Winckler, "Van Allen Radiation Regions," J. Geophys. Res. 67, 12, November 1962.
158. A. Rosen and T. A. Farley (1961), "Characteristics of the Van Allen Radiation Zones as Measured by the Scintillation Counter on Explorer VI," J. Geophys. Res. 66, p. 2013.
159. Harold L. Stolov (1962), "Bifurcation of the Outer Van Allen Belt and Related Auroral Phenomena," J. Geophys. Res., 67, 404.
160. Pizzella, McIlwain and Van Allen, "Time Variation of Intensity in the Earth's Inner Radiation Zone," J. Geophys. Res. 67, 1962.
161. A. H. Armstrong, F. B. Harrison, H. H. Heckman and L. Rosen (1961), "Charged Particles in the Inner Van Allen Radiation Belt," J. Geophys. Res. 66, p. 351.
162. A. H. Kniffen and J. E. Naugle (1961), "Proton Fluxes in the Inner Van Allen Belt," Program Abstracts, Amer. Geophys. Union, (2nd Annual Meeting).
163. A. H. Kniffen and J. E. Naugle (1961), Phys. Rev. Letters, 7 p. 3.
164. D. A. Kniffen and J. E. Naugle (1961), "The Flux and Energy Spectra of the Protons in the Inner Van Allen Belt," Contributions to 1961 Kyoto Conference on Cosmic Rays and the Earth Storm, NASA.
165. J. B. Cladis, L. F. Chase, W. L. Inhoff and D. J. Knecht (1961), "Energy Spectrum and Angular Distribution of Electrons Trapped in the Geomagnetic Field," J. Geophys. Res. 66, 8, 2297.
166. M. L. Walt and W. M. MacDonald (1961), "Energy Spectra and Altitude Dependence of Electrons Trapped in the Geomagnetic Field," J. Geophys. Res. 66, p. 2047.
167. B. J. O'Brian, J. A. Van Allen, C. D. Laughlin and L. A. Frank (1962), "Absolute Electron Intensities in the Heart of the Earth's Outer Radiation Zone," J. Geophys. Res. 67, 397.
168. L. R. David, O. E. Berg and L. H. Merdith (1960), Direct Measurements of Particle Fluxes In and Near Auroras, IGY Rocket Report 6, p. 143.

REFERENCES (cont.)

169. A. M. Lenchek, S. F. Singer, and R. C. Wentworth (1961), "Geomagnetically Trapped Electrons from Cosmic Ray Albedo Neutrons," J. Geophys. Res. 66, 4027.
170. J. A. Van Allen and Wei Ching Lin (1960), "Outer Radiation Belt and Solar Proton Observation with Explorer VII During March - April 1960," J. Geophys. Res. 65, 9.
171. T. A. Farley and A. Rosen (1960), "Charged Particle Variations in the Outer Van Allen Zone During a Magnetic Storm," J. Geophys. Res. 65, 10.
172. S. E. Forbush, D. Venkatesun and C. E. McIlwain (1961), "Intensity Variations in the Outer Van Allen Radiation Belt," J. Geophys. Res. 66, 8
173. A. J. Dessler and Robert Karplus (1961), "Some Effects of Diamagnetic Ring Currents on Van Allen Radiation," J. Geophys. Res. 66, 8.
174. J. Van Allen, "Dynamics, Composition and Origin of Geomagnetic Trapped Radiation," Chap. 7, Space Science, 1963.
175. R. J. List (1951), Smithsonian Meteorological Tables, 6th ed., Washington.
176. F. Baur and H. Phillips, Gerlands Beitr. Geophys. 42, 160 (1934); Gerlands Beitr. Geophys., 45, 82 (1935).
177. V. A. Belinski (1948), Dynamic Meteorology, OGIZ, State Publishing House of Technical-Theoretical Literature, Moscow, Chapter VII.
178. R. E. Bourdeau (1961), Ionospheric Results of Sounding Rockets and the Explorer VIII Satellite, Second International Space Science Symposium, Florence, Italy, April 10-14, 1961.
179. J. W. Chamberlain (1961), "Interplanetary Gas: III, "A Hydrodynamic Model of the Corona," Astrophys. J. 133, 675.
180. S. Chapman (1959), "Interplanetary Space and the Earth's Outermost Atmosphere," Proc. Roy. Soc., A253, 462.
181. D. R. Bates (1959), Some Problems Concerning the Terrestrial Atmosphere Above About the 100-km Level, Proc. Roy. Soc., A253, 451.
182. M. Nicolet (1961), Planet Space Sci. 5, 1.
183. D. G. King-Hele and D. M. C. Walker (1961), "Density of the Upper Atmosphere Determined From Satellite Orbits and Its Variation During 1957-61," Nature 191, 114.
184. E. B. Meadows and J. W. Townsend (1960), "Rocket Measurements of Arctic Atmospheric Composition Above 100 km.," Space Science, (H. Kallmann Bijl, ed.), North Holland Publishing Company, Amsterdam, p. 175.



REFERENCES (cont.)

185. M. Nicolet (1961), "Helium, An Important Constituent in the Lower Exosphere," J. Geophys. Res., 66, 2263.
186. L. G. Jacchia (1961), The Atmospheric Drag of Artificial Satellites During the November 1960 Events, Second International Space Symposium, Florence, Italy, April 1961.
187. W. B. Hanson (1961), Satellite Environment Handbook (F. S. Johnson, ed.), Stanford University Press, Chapter 2.
188. Lewis D. Kaplan, Guido Münch and Hyron Spinrad, "An Analysis of the Spectrum of Mars," Astrophys. J. Jan. 1964.
189. G. P. Kuiper, Mem. Soc. R. Sci. Liege, 5th series, 1963.
190. A. I. Lebedinskii and G. I. Salova, Astr. J. USSR, 39, p. 494, 1962.
191. W. Sinton, J. Quant. Spectrosc. Radiat. Transfer, 3, p. 551, 1963.
192. H. Spinrad and E. H. Richardson, Icarus, 2, 49, 1963.
193. M. Rigutti and F. Frago-Chiuderi, Ann. d'Ap. 26, 253, 1963.
194. H. Spinrad, G. Münch and L. D. Kaplan, Ap. J. 137, 1319, 1963.
195. D. G. Rea, Nature, 1963.
196. N. B. Colthup, Science, 132, p. 529, 1961.
197. F. D. Drake, paper presented at the Jet Propulsion Colloquium, 1963.
198. W. M. Sinton, Science, 132, 529, 1961.
- 199a. J. H. Focas, Planetary Space Sci., 9, 371, 1962.
- 199b. J. W. Chamberlain, Astrophys. J. 1936, 582, 1962.
- 199c. C. H. Mayer, Planets and Satellites, Chap. 12, 1961.
- 199d. S. L. Hess, Advances in Space Science and Technology, Vol. 3, Academic Press, 1961.
- 199e. E. G. Opik, Progress in the Astronautical Sciences, Vol. 1, Chap. VI, 1962.
- 199f. E. Framen, "Mariner Mars - 1966, Study Report," Jet Propulsion Laboratory, E.P.D. No. 158, July 1963.
- 199g. A. Dollfus, Planets and Satellites, Chap. 9 and 15, 1961.
- 199h. H. Brown, The Atmospheres of the Earth and Planets, p. 158, ed. G. P. Kuiper University of Chicago Press, 1952.

REFERENCES (cont.)

200. G. F. Shilling, "A Note on the Atmosphere of Mars," J. Geophysical Research, March 1962.
- A concise summary of the extreme atmospheric calculations prepared previously (below) together with a listing of pertinent Martian physical properties and newer interpretation.
201. F. J. White, (editor), Flight Performance Handbook for Powered Flight Operations, prepared by Space Technology Laboratories for JPL, March 1962.
- With reference to Mars, Chapter 7, "Planetary Entry," suggests three extreme exponential atmospheres for use in entry-trajectory and aerodynamic heating calculations. These atmospheres were based on data furnished JPL. The concept of exponential atmospheres has been argued against by Kopal (Ref. 23) and others. This book is, however, primarily for flight calculations and therefore does not consider in detail the Martian environments.
202. C. Sagan, Is the Martian Blue Haze Produced by Solar Protons?, Rand Corporation RM-2832-JPL, November 1961.
- If the Blue Haze were produced by solar protons, proton energies in excess of 2 Mev, fluxes of  $10^{11} \text{ cm}^{-2} \text{ sec}^{-1}$ , and interplanetary field strengths of  $10^{-8}$  gauss would be required. Sagan shows these values not probable and suggests rejecting the solar proton hypothesis.
203. Carl Sagan and W. W. Kellogg, The Atmospheres of Mars and Venus, National Academy of Sciences, Washington, D.C., Publication 944, 1961.
- An unusually well-written technical discussion presenting a good summary of recent work, including certain unpublished information. No doubt one of the most comprehensive studies available.
204. L. Hobbs, An Annotated Bibliography of Articles on the Atmospheres of Mars and Venus, General Electric Co., R61SD175, November 1961.
- With reference to Mars, this report covers work prior to and during 1960. The recent extensive work at Rand and Ohio State is not covered. It is, however, an excellent and complete bibliography going back to early 1924 work, with many interesting comments by the author. The abstracts are comprehensive and well written; certain of these were incorporated in this work.
205. D. L. Lamar, "The Optical Ellipticity and Internal Structure of Mars," Rand Corporation Memorandum RM-2900-JPL, September 1961.
- The ellipticity measurements of Mars are examined. After considerable mathematical analysis, it is concluded that Mars may have a core similar to that of the earth.

REFERENCES (cont.)

206. G. F. Shilling, "On the Consequences of a Possible Ozonosphere on Mars," Rand P-2387, 28 July, 1961.
- The presence of ozone at high altitudes on Mars is shown to be reasonable on the basis of current knowledge. Further, the existence of the ozonosphere with the higher temperatures helps to explain a number of meteorological features which are not yet fully understood.
207. J. H. Shaw and N. T. Bobrovnikoff, Preliminary Investigation of Interplanetary, Lunar and Near Planet Environments and Methods of Simulation, Ohio State University, ASD Technical Report 61-267, July 1961.
- This report contains a summary of the individual studies carried out at Ohio State including a condensation of the Mars work (Ref. 208 below). Despite the rather recent publication date, the Mars references are all pre-1958 and do not include the Rand studies. The information presented here is, however, concise and represents generally accepted values for physical and orbital data. No model atmospheres are proposed.
208. G. F. Shilling, "Parametric Comparison of Model Atmospheres of Earth and Mars," Rand, RM-2817-JPL, 30 June, 1961.
- The various extreme model atmospheres are compared with the ARDC 1959 earth atmosphere. The predicted Martian atmosphere has such a wide range of predicted densities for the various models that at least for altitudes above 20 km, the range of predicted Martian densities includes the earth values. A discussion of probable Mars surface meteorology and favorable comparison with the conditions in the Chang Tan desert in Tibet is included.
209. B. Haurwitz, "Effect of Errors in Surface Temperature and Temperature Lapse Rate on the Vertical Distribution of Pressure and Density in the Mars Atmosphere." RM-2817-JPL, Rand Corporation, 30 June, 1961.
- The surface pressure is shown to be the most important parameter to determine accurately. Error calculations for the atmosphere are carried out systematically assuming errors in surface, pressure, temperature, and lapse rate.
210. M. H. Davis, "Estimates of the Specific Heats of the Martian Atmosphere," RM-2817-JPL, Rand Corporation, 30 June, 1961.

REFERENCES (cont.)

The specific heats are calculated using classical kinetic theory assuming an atmosphere of  $N_2$  (87-99%),  $CO_2$  (0-17%), and A (0-6%). The values of  $C_p$  vary from 0.94 to -0.038 joules/g  $^{\circ}C$  for volume concentrations of  $CO_2$  from 0-10% and argon concentration from 0-10%.

211. G. F. Shilling, "Extreme Model Atmospheres of Mars," RM-2782-JPL, Rand Corporation, 22 June, 1961.

An extensive analysis of three proposed model atmospheres: (1) assuming convective equilibrium throughout, (2) convective equilibrium to assumed tropopause and conductive equilibrium above, and (3) a conjectural model assuming an appreciable amount of ozone exists in the upper atmosphere. The resulting density, temperature, and pressure gradients are calculated and discussed.

212. M. H. Davis, "Properties of the Martian Atmosphere," RM-2817-JPL, Rand Corporation, May 1961.

Suggested means, as well as extreme values, are presented for the total atmospheric mass, surface acceleration of gravity, surface pressures, mean surface temperature, atmospheric composition, mean molecular weight, dry adiabatic lapse rate, and temperature of the stratosphere (above the tropopause).

213. G. F. Shilling, "Preliminary Remarks on a Permissible Model of the Lower Atmosphere of Mars," RM-2769-JPL, Rand Corporation, April 1961.

A discussion of the general features of a probable Martian atmosphere pointing out that the Martian atmosphere could resemble the earth's atmosphere on a high plateau. At this time, Shilling felt that the existence of ozone was improbable in significant quantities, a thesis which he later revised (see Ref. 211 above).

214. D. S. Kirby, "The Surface Gravity of Mars," (incl. in) RM-2769-JPL, Rand Corporation, 28 April, 1961.

The surface gravity is computed considering uncertainties in planet mass, radius, oblateness, and rotation. The values of the relative surface gravity, based on earth units, vary between 0.368 and 0.509 for the most extreme cases.

REFERENCES (cont.)

215. D. Deirmendjian, "Note on the Surface Pressure Estimates of the Martian Atmosphere," (incl. in) RM-2769-JPL, Rand Corporation, 28 April, 1961.  
The viewpoint is given that the methods of De Vaucouleurs (1960), Dollfus (1957), and Āpik (1960) are not very reliable in predicting surface pressures (i.e., the values of 220, 230, and 300 g/cm<sup>2</sup> respectively). It is suggested that since all the quoted methods may be affected by the same systematic errors, their consistency does not imply accuracy of the final result. It is suggested that value of 250  $\pm$  100 g/cm<sup>2</sup> is a reasonable estimate which reflects the uncertainty existing at this time.
216. Y. Mintz, "A Note on the Temperature of the Equatorial Troposphere of Mars," (incl. in) RM-2769-JPL, Rand Corporation, 28 April, 1961.  
A careful analysis is made of the Sinto and Strong (1960) radiometric data, with considerable effort to correct for the Mars surface emissivity. After the measured temperatures are reduced, an empirical troposphere temperature model is calculated using the calculated adiabatic temperature lapse rate for the equatorial troposphere and "anchoring" this to the temperature curve near surface at the time of the temperature maximum (as suggested by Hess, 1961). This model indirectly predicts a very low upper limit for the amount of water vapor present.
217. Carl Sagan, "The Abundance of Water Vapor on Mars," Astronomical Journal, March 1961.  
The upper limit for water vapor abundance on Mars is  $3.5 \times 10^{-2}$  g/cm<sup>-2</sup>. This value is shown to be consistent with spectroscopic tolerance, the assumed greenhouse effect temperatures and the fluctuation of the polar caps.
218. W. M. Sinton and J. Strong, "Radiometric Observations of Mars," Astrophysical Journal, Vol. 131, p. 459 (1960).  
Radiometric temperature measurements of Mars were made in the 8-13 $\mu$  range. The temperature of Mars at the center of the disk was found to be 288°K. The temperature of a yellow cloud was 248°K. Dark areas were a few degrees warmer than adjacent bright regions.

REFERENCES (cont.)

219. E. J. Öpik, "The Atmosphere and Haze of Mars," Journal of Geophysical Research, Vol. 65, No. 10, p. 3057 (1960).  
The blue haze is an absorbing smoke, grey and dark as soot in reflection, red in transmission. Its explanation by pure scattering is untenable. The limb darkening of Mars is mainly the result of absorption by the smoke. The opacity of the Martian atmosphere increases from the red toward the violet. In all wavelengths, the extension by the Martian atmosphere is greater than that of the terrestrial. Only about 30% of the Martian extinction is due to scattering. The atmospheric pressure, based on Dollfus' polarization estimate corrected for self-absorption, is 87 mm Hg. The photochemical breakup of CO<sub>2</sub> and the escape of O must lead to considerable concentrations of CO in the Martian atmosphere. (Taken from Physics Abstracts, Vol. 24, No. 768, December 1961).
220. D. S. Kirby, Summary of Orbital and Physical Data for the Planet Mars, Research Memorandum RM-2567, Rand Corporation, 1960.  
An unusually complete discussion and set of tabulated values of physical constants and uncertainties in these constants is presented. Starting with the two observable quantities, mass and radius, the author derives other related physical quantities. To these are added photometric, spectroscopic, and radiometric data, and a discussion of orbital elements. The excellent bibliography contains 121 referenced works.
221. Zdenek Kopal, "Aerodynamic Effects of Planetary Atmospheres," Aerospace Engineering, December 1960.  
A brief survey of the principal physical and chemical characteristics of Mars and Venus atmospheres is presented. The fallacy of using an exponential atmosphere model is discussed. The possibility of a significant magnetic field on Mars is rejected although in more recent work (1962 from JPL) Kopal reconsidered this possibility.
222. G. De Vaucouleurs, "The Physical Environment on Mars," Physics and Medicine of the Atmosphere and Space, edited by O. O. Benson and H. Strughold, New York, Wiley & Sons, 1960. Also, "Remarks on Venus and Mars," The Exploration of Space, edited by R. Jastrow, The MacMillan Company, 1960.

REFERENCES (cont.)

- A knowledgeable discussion together with pertinent data on the Mars environment. The first article includes an extensive bibliography covering pertinent work from 1954 through 1959, bringing up to date DeVaucouleurs' previous comprehensive bibliography (see Ref. 45).
223. H. C. Urey, "The Atmospheres of the Planets," Handbrich der Physik., Berlin, Springer-Verlag, Vol. 52, p. 363 (1959).  
Total pressure, chemical composition, temperature, clouds, violet layer, structure, and evolution of the Mars atmosphere is discussed. A review of important quantitative measurements and an extensive bibliography are included.
224. R. S. Richardson and P. E. Roques, "An Example of the Blue Clearing Observed 74 Days Before Opposition," Publications of the Astronomical Society of the Pacific, Vol. 71, p. 321 (1959).  
A summary of notable instances of blue clearing and the associated opposition dates for Mars is presented. A series of photographs taken in 1958 is presented. It is concluded that the alignment of the sun, earth, and Mars is not a critical factor in the production of blue clearings.
225. A. Boggess and L. Dunkelmann, "Ultraviolet Reflectivities of Jupiter and Mars," Astrophysical Journal, Vol. 129, p. 236 (1959).  
Ultraviolet observations of Mars and Jupiter were made from an Aerobee rocket approximately 140 km above the White Sands missile range. Very marginal data in the 2700 Å range was obtained. The computed reflectivity of Mars, 0.24, is not consistent with other observations.
226. J. H. Shaw, "The Natural Environment of the Planet Mars," Ohio State Univ. AD-242-175, February 1959.  
A concise summary of important physical constants of both the planet and the planetary atmosphere is presented. Although less detailed than the more recent Rand work, the values quoted are in good agreement with recent predictions.
227. N. P. Barabashov, "Basic Results of Observations of Mars\* During the Favorable Opposition of 1956," Soviet Astronomy AJ, Vol. 2, p. 814, 1958.

---

\* Translated from Astronomical Journal (USSR), Vol. 35, p. 827, 1958.

REFERENCES (cont.)

The results of photographic and visual observations are presented as well as those of photoelectric and spectrographic observations. Conclusions are drawn on the structure of the continent, sea, and polarcap areas of Mars and on the absorbing and scattering properties of its atmosphere.

228. C. H. Mayer, J. P. McCullough, and R. M. Sloanaker, "Radiation from Mars and Jupiter at 3.15 cm Wavelength," Astrophysical Journal, Vol. 127, p. 11, 1958.

A number of observations of Mars were made at the Naval Research Laboratory at a 3.15 cm wavelength. The resulting black-body temperature was found to be  $218 \pm 76^{\circ}\text{K}$ .

229. G. DeVaucouleurs, "Observations of Mars in 1958," Air Force CRC TN 59-476, 15 September 1959. AD 226514.\*

Visual and photoelectric observations of Mars in 1958 from the Lowell Observatory are presented. Monochromatic magnitudes and albedos are given at 3300, 3600, 4550, 5500, and 6900 Å. Main visual cloud phenomena and surface features are illustrated. Several surface changes and an outstanding moving cloud system are discussed.

230. H. C. Urey, "The Blue Haze of Mars," Astrophysical Journal, Vol. 128, p. 736 (1958).

Objections to the concept of a condensable substance as the origin of the blue haze on Mars are discussed.

231. S. L. Hess, "Blue Haze and the Vertical Structure of the Martian Atmosphere," Astrophysical Journal, Vol. 127, p. 743 (1958).

The Martian blue haze may be a condensate rather than a dust because it can clear away rapidly.  $\text{CO}_2$  and  $\text{H}_2\text{O}$  are both present in the atmosphere, and condensation of each into the solid phase has been suggested to explain the blue haze. It is shown that  $\text{CO}_2$  ice clouds are far too opaque to be the cause of the blue haze.

---

\* Air Force, Cambridge Research Center. Technical Note 59-476. 15 September, 1959. ASTIA Document 226514.



REFERENCES (cont.)

232. C. C. Kiess, C. H. Corliss, H. K. Kiess, and R. L. Corliss. "High Dispersion Spectra of Mars," Astrophysical Journal, Vol. 126, p. 579 (1957). These experiments were designed to detect  $H_2O$  and  $O_2$  in the Martian atmosphere. The resulting spectrograms taken at both the Slope Observatory, Hawaii, and at Georgetown College Observatory gave negative results.
233. R. S. Richardson, "Preliminary Report on Observations of Mars Made at Mount Wilson in 1956," Publications of the Astronomical Society of the Pacific, Vol. 69, p. 23 (1957).  
Direct photographs show a great dust storm, clouds, and some "canals." Spectrograms failed to identify the 7820 A band of  $CO_2$ , but infrared spectra show the A band of  $O_2$  at 7600 A as well as water vapor lines from about 7900 to 8400 A. Significant variations in the intensity of the  $H_2O$  lines over the disk, which might indicate presence of water vapor in the atmosphere over the polar caps, could not be detected.
234. H. C. Urey and A. W. Brewer, "Fluorescence in Planetary Atmospheres," Proceedings of the Royal Society of London, Vol. A241, p. 37 (1957).  
It is suggested that the blue haze of Mars arises from fluorescence by  $CO^+$ ,  $CO_2^+$ , and  $N_2^+$ . The blue clearings which occur at opposition, may be caused by deflection of the solar corpuscular radiation, which excites the fluorescence, by the earth's magnetic field. This thesis was later rejected by Sagan (1961, Ref. 2), above.
235. V. V. Sharanov, "On the Role of True Absorption in the Martian Atmosphere," Soviet Astronomy AJ, Vol. 1, p. 547 (1957).  
It is suggested that the blue-diameter-excess in photographs of Mars is a photographic effect, and that there are no definite proofs for or against the existence of a special high-altitude scattering layer in the Martian atmosphere at the present time.
236. R. M. Goody, "The Atmosphere of Mars," Journal of the British Interplanetary Society, Vol. 16, p. 69 (1957).  
A summary of the important observational facts and their interpretations is first presented. A model atmosphere is suggested, which is taken to be isothermal at an equilibrium temperature of  $217^{\circ}K$  throughout the statosphere.

REFERENCES (cont.)

In the suggested troposphere, the lapse rate is  $3.7^{\circ}\text{K}/\text{km}$ , the surface temperature is  $270^{\circ}\text{K}$ , and the surface pressure is 85 mb. The importance of absorption processes in the blue layer in view of its small albedo of 0.05, is emphasized, and both  $\text{CO}_2$  and  $\text{H}_2\text{O}$  crystals are rejected as blue-layer constituents.

237. H. C. Urey, "On the Escape of Water Vapor From Mars," Publications of the Astronomical Society of the Pacific, Vol. 68, p. 220 (1956).

A discussion of the origin, evolution, and production of water and oxygen on Mars is presented.

238. G. DeVaucouleurs, "Photographic Observations in 1956 of the Blue Clearing on Mars," Publications of the Astronomical Society of the Pacific, Vol. 69, p. 530 (1957).

A short series of photographic observations of Mars near opposition in 1956 are presented. An extensive blue clearing was recorded which reached its maximum 12 days before opposition.

239. F. Gifford, "The Surface Temperature Climate of Mars," Astrophysical Journal, Vol. 123, p. 154 (1956).

The Lowell Observatory radiometric measurements of Martian surface temperatures are analyzed, and surface-temperature climatological properties of Mars are obtained. Annual and diurnal temperature variations and seasonal isotherm maps are displayed and discussed.

240. J. Grandjean, and R. M. Goody, "The Concentration of Carbon Dioxide in the Atmosphere of Mars," Astrophysical Journal, Vol. 121, p. 548 (1955).

From observations of carbon dioxide bands in the spectrum of Mars by G. P. Kuiper, the fraction by volume of  $\text{CO}_2$  in the planet's atmosphere is determined taking into account the fine structure of the band and the shape of the rotation lines. If the ground-level pressure of Mars is 100 mb, the fraction by volume of  $\text{CO}_2$  is 50 times greater than in the earth's atmosphere.

241. E. P. Martz, "Variation in Atmospheric Transparency of Mars in 1939," Publications of the Astronomical Society of the Pacific, Vol. 66, p. 45 (1954).

Discussion and photographs of the blue clearing on Mars near opposition in 1939 are presented. Short-time-scale variations in transparency are emphasized. A review of suggestions as to the nature of the blue haze is included.

REFERENCES (cont.)

242. E. C. Slipher and A. G. Wilson, "On Blue Clearings of Mars," Astronomical Society of the Pacific, Leaflet No. 301, p. 7 (1954).  
A study of available photographic records shows that the time of a blue clearing is always within a few days of opposition although the blue clearing does not occur at every opposition. Whenever Mars lies very far above or below the ecliptic at opposition, the blue clearing is not observed. This suggests that perhaps the earth is somehow affecting solar radiations received on Mars and that the blue layer on Mars is associated with solar radiation.
243. G. De Vaucouleurs, Physics of the Planet Mars, London, Faber and Faber, 1954.  
This paper was one of the first complete collective descriptions of the atmosphere of Mars. Important contributions up through 1953 are summarized. A bibliography of 115 references is included.
244. E. P. Martz, "Heterochromatic Photography and Photometry of Mars in 1937 and 1939," Astronomical Journal, Vol. 58, p. 221 (1953).  
An analysis of an extensive series of photographs of Mars secured during the close approaches of 1937 and 1939 is presented. A number of conclusions are reached, most of them confirming previous results obtained by others. A maximum of approximately 5% excess of blue-violet diameter over red diameter is reported.
245. G. P. Kuiper, "Planetary Atmospheres and Their Origin," The Atmospheres of the Earth and Planets, edited by G. P. Kuiper. Chicago, Chicago University Press, 1952, p. 306.  
A comprehensive review of observational data and theoretical suggestion are presented, with particular interest in their bearing on the origin and evolution of planetary atmospheres. Extensive consideration is given to the atmosphere of Mars.
246. A. Dollfus, "La Lumiere de la planete Mars," Comptes Rendus de l'Academie des Sciences, Vol. 235, p. 1479 (1952).

REFERENCES (cont.)

Visual measurements of the diameter of Mars are reported. The measured polar diameter, reduced at unit distance, was  $9''25 \pm 0''03$  in yellow light and  $9''40$  in blue light. On this basis, the altitude of the violet clouds was calculated to be about 120 km.

247. J. Dunham, "Spectroscopic Observations of the Planets at Mount Wilson," The Atmospheres of the Earth and Planets, edited by G. P. Kuiper. Chicago, Chicago University Press, 1952, p. 288.  
A detailed discussion of the abundances of oxygen and water vapor in the atmosphere of Mars is given. The final conclusion is that the upper limit for the ratio of both oxygen and water vapor in the Mars atmosphere to that in the terrestrial atmosphere is 0.0015.
248. Gerard P. Kuiper, The Atmospheres of the Earth and Planets, University of Chicago Press, Chicago, 1952.
249. Krafft A Ehricke, Space Flight: I - Environment and Celestial Mechanics, Van Nostrand, New York - London, 1960.
250. H. J. Goett, The Scientific Exploration of Space, Goddard Space Flight Center, Greenbelt, Maryland, Report X-100-62-56, May 25, 1962.
251. M. Neugebauer and C. Snyder, Preliminary Results from MARINER II Solar Plasma Experiment, JPL Tech Note No. 33-111, Nov. 15, 1962.
252. F. S. Johnson, "Physics of the Atmosphere and Space," Astronautics, November, 1962.
253. F. L. Whipple, "On Meteoroids and Penetration," American Astronautical Society, Jan. 1963.
254. G. S. Hawkins and E.K.L. Upton, "The Influx Rate of Meteors in the Earth's Atmosphere," Astrophys. J. 128, p. 727-735, 1958.
255. G. S. Warwick, "Solar Particles and Interplanetary Fields," American Astronautical Society, Jan. 1963.
256. F. S. Johnson, Satellite Environment Handbook, Ed., F. S. Johnson, Stanford University Press, Chapter 4, 1961.
257. R. Tousey, "The Solar Spectrum in Space," Astronautics, p. 32, July 1961.
258. H. E. Hinteregger, Astrophys. J., Vol. 132, 801, 1960.

REFERENCES (cont.)

259. H. E. Hinteregger, "Solar Extreme Ultraviolet Radiation," J. Geophys. Res., Vol. 66, (8), 2367, (1961).
260. F. S. Johnson, J. Meteorol., Vol. 11, p. 431, 1954.
261. H. Friedman, Space Astrophysics (W. Tiller, Ed.), McGraw-Hill, 1961, p. 107.
262. C. G. Little, and H. Leinbach, Proc. Inst. Radio Engineers, Vol. 46, 334 (1958).
263. H. Leinbach, and C. C. Reid, Phys. Rev. Letters, Vol. 2, 61 (1959).
264. C. G. Little, and H. Leinbach, Proc. Ins. Radio Engrs., Vol. 47, 315 (1959).
265. J. A. Simpson, Science in Space, Editors: L. V. Berkner and H. Odishaw, McGraw-Hill Book Co. Inc., Chapter 13 (1961).
266. A. D. Goedeke, Engineering Paper No. 1103, Douglas Aircraft Company, Inc., Santa Monica, Calif., 1961.
267. A. J. Dessler, "Satellite Environment Handbook," Ed: F. S. Johnson; Stanford University Press (1961); Chapter 3, 1961.
268. T. Obayaski, and Y. Hakura "Enhanced Ionization in the Polar Ionosphere," Space Research, Ed: H. Kallmann Bijl, North Holland Publishing Company, Amsterdam, pp. 665-694 (1960).
269. S. Chapman, "Note on the Solar Corona and the Terrestrial Ionosphere," Smithsonian Contribution Astrophys. Vol. 2, No. 1 (1957).
270. H. Siedentopf, A. Behr, and H. Elsasser, "Photoelectric Observation of the Zodiacal Light," Nature, Vol. 171, No. 1066 (1953).
271. P. Meyer, E. N. Parker, and J. A. Simpson, "Solar Cosmic Rays of February 23, 1956, and Their Propagation Through Interplanetary Space," Phys. Rev., Vol. 108, No. 1563 (1957).
272. J. A. Van Allen and S. F. Singer, "On the Primary Cosmic Ray Spectrum," Phys. Rev., Vol. 78, No. 819 (1950).
273. D. K. Bailey, "Abnormal Ionization in the Lower Ionosphere," Proc. Inst. Radio Eng., Vol. 47, No. 255 (1959).
274. J. A. Van Allen and J. R. Winckler, "Spectrum of Low Rigidity Cosmic Rays During the Solar Flare of Feb. 23, 1956," Phys. Rev., Vol. 106, No. 1072 (1957).

REFERENCES (cont.)

275. P. Rothwell and C. McIlwain, "Satellite Observation of Solar Cosmic Rays," Nature, Vol. 184, No. 138 (1959).
276. K. A. Anderson, R. Arnoldy, R. Hoffman, L. Peterson, and J. R. Winckler, "Observations of Low Energy Solar Cosmic Rays from the Flare of 22 Aug. 1958," J. Geophys. Res., Vol. 64, No. 1133 (1959).
277. J. W. Chamberlain, "The Excitation of Hydrogen in Aurorae," Astrophys. J., Vol. 120, No. 360 (1954).
278. J. A. Van Allen, "Rocket Measurement of Soft Radiation," IGY Rocket Report Series, No. 1, p. 159 (1958).
279. L. H. Meredith, L. R. Davis, J. P. Heppner, and O. E. Berg, "Rocket Auroral Investigations," IGY Rocket Report Series, No. 1, p. 169 (1958).
280. V. C. A. Ferraro, "On the Theory of the First Phase of a Geomagnetic Storm," J. Geophys. Res., Vol. 57, No. 15 (1952).
281. K. A. Anderson and D. C. Enemark, "Observations of Solar Cosmic Rays Near the North Magnetic Pole," J. Geophys. Res., Vol. 65, No. 2657 (1960).
282. J. A. Van Allen, "Explorer VII Observations of Solar Cosmic Rays, Nov. 12-23, 1960," Bull. Am. Phys. Soc., II, 6, 276 (1961).
283. John T. Wasson, "Radioactivity Produced in Discoverer XVII by Nov. 12, 1960, Solar Protons," J. Geophys. Res., Vol. 66, No. 9 (1961).
284. J. R. Winckler, P. S. Bhavsar, and L. Peterson, "The Time Variations of Solar Cosmic Rays During July 1959 at Minneapolis," J. Geophys. Res., Vol. 66, No. 995 (1961).
285. D. H. Robey, "Solar Corpuscular and Radio Emission," American Astronautical Society, San Francisco, California, Aug. 1-3, 1961, Preprint No. 61-85 (1961).
286. K. A. Anderson and Carl E. Fichtell, "Discussions of Solar Proton Events and Manned Space Flight," NASA-TN-D-671 (1961).
287. W. S. Forsythe, Smithsonian Physical Tables, Wash., Sm. Inst. (1954).
288. S. F. Singer, "The Primary Cosmic Radiation and Its Time Variations," Progress in Cosmic Ray and Elementary Particle Physics, Vol. IV, p. 205, Interscience, New York (1958).
289. J. H. Noon, A. J. Hertz, and B. J. O'Brien, Nature, Vol. 179, p. 91 (1957).

REFERENCES (cont.)

290. F. B. McDonald and W. R. Webber, Space Research, H. Kallmann Bijl (ed), North Holland Publishing Co., Amsterdam, p. 968 (1960).
291. G. S. Hawkins, "Relation Between Asteroids, Fireballs, and Meteorites," Astronom. J., 64, No. 450 (1959).
292. H. Brown "Density and Mass Distribution of Meteoritic Bodies in the Neighborhood of the Earth's Orbit," J. Geophys. Res., 66, No. 1316 (1961).
293. F. L. Whipple and R. F. Hughes, "Velocities and Orbits of Meteors, Fireballs, and Meteorites."
294. Verniani, "On the Density of Meteors," Second International Space Science Symposium, Florence, Italy, April 10-14, 1961 (1961).
295. F. F. Whipple, "Dust and Meteorites," Space Flight Report to the Nation, October 9-15, 1961, ARS Paper 2253 (1961).
296. Micrometeorite Collection from A Recoverable Sounding Rocket, (R. K. Soberman, ed), GRD Research Note 71, November 1961.
297. D. B. Beard, "Interplanetary Dust Distribution," Astrophys. J., 129, No. 496 (1959).
298. C. Jager, "Capture of Zodiacal Dust by the Earth," Memoirs Soc. Roy. Sci., Liège, 15, No. 174 (1955).
299. F. L. Whipple, "The Dust Cloud About the Earth," Nature, 189, 127 (1961) Jan. 14.
300. A. R. Hibbs, "The Distribution of Micrometeorites Near the Earth," J. Geophys. Res., 66, No. 371 (1961).
301. D. W. Parkin and W. Hunter, "Meteorites and Cosmic Dust," Advances in Astronomy and Astrophysics, 1, Academic Press, New York (1962).
302. Staff, Jet Propulsion Laboratory, Mariner Mission to Venus, McGraw Hill Book Co., Inc., New York (1963).
303. F. L. Whipple, "The Meteoric Risk to Space Vehicles," Vistas in Astronautics (M. Alperin and M. Stern, ed.), Pergamon Press, London, p. 115 (1958).
304. J. F. Vedder, Satellite Environment Handbook (F. S. Johnson, ed.), Stanford University Press, Chapter 5 (1961).
305. C. W. McCracken and W. M. Alexander (1961), "The Distribution of Small Interplanetary Dust Particles in the Vicinity of the Earth," Presented at the International Symposium on the Astronomy and Physics of Meteors, Cambridge Mass., 28 Aug. - 1 Sept., 1961. (Also published in the Smithsonian Contributions to Astrophysics.)

REFERENCES (cont.)

306. T. N. Nazarova and V. I. Moroz, "The Research of Micrometeorites with the Help of Rockets and Satellites," Second International Space Science Symposium, Florence, Italy, April 7-18, 1961 (1961).
307. R. L. Bjork, "Meteoroids vs Space Vehicles," ARS, 31, 803 (1961).
308. R. E. McCrosky and R. K. Soberman, Results from an Artificial Iron Meteoroid at 10 km/sec, AFCRL, Res. Note 62-803, July 1962.
309. A. F. Cook, L. G. Jacchia, and R. E. McCrosky, "Luminous Efficiency of Iron and Stone Asteroidal Meteors," Smithsonian Contributions to Astrophysics (in press).
310. A. C. B. Lovell, "Geophysical Aspects of Meteors," Handbook of Physics, Bd XLVIII, Geophysics II, Springer-Verlag (Berlin), 1957, pp. 427-454.
311. "New Data Pinpoints Micrometeorite Size," Aviation Week and Space Technology, April 29, 1963.
312. R. K. Soberman and L. Della Lucca, Micrometeorite Measurements from the Midas II Satellite, AFCRL Report 1053, Nov. 1961.
313. T. N. Nazarova, "The Investigation of Meteoric Dust by Means of Rockets and Artificial Earth Satellites" (translated by R. E. Daisley from Iskusstvennye Sputniki Zemli), Planetary and Space Science, March 1963.
314. Earl C. Hastings, Jr., The Explorer XVI Micrometeoroid Satellite: Description and Preliminary Results for the Period December 16, 1962 to January 13, 1963, NASA - Langley Research Center, TM X-810, Feb. 1963.
315. Earl C. Hastings, Jr., The Explorer XVI Micrometeoroid Satellite: Preliminary Results for the Period January 14, 1963 through March 2, 1963, TM X-824, April 1963.
316. D. E. Blackwell, "The Zodiacal Light and Its Interpretation," Endeavour, 19, 14-19 (1960) January.
317. F. L. Whipple, "A Comet Model III - The Zodiacal Light," Astrophys. J. 121, 750-770 (1955) May.
318. H. P. Robertson, "Dynamical Effects of Radiation in the Solar System," Roy. Astronomical Soc. Monthly Notices, 97, 423-438 (1937) April.
319. Sydney Chapman, "The Earth in the Sun's Atmosphere," Sci. Am., 201, 4, 64-71 (1959) October.
320. J. G. Davies, "Radio Observation of Meteors," Advances in Electronics and Electron Physics, Academic Press, New York, 1957.



REFERENCES (cont.)

321. R. F. Mlondnosky, V. R. Eshleman, and L. A. Manning, On the Velocity Distribution of Sporadic Meteors, Stanford Electronics Laboratories, Scientific Report No. 5, April 1962.

References Cited in Tables 15 and 16

- Ditchburn, R. W. and Heddle, D. W. D., Proc. Roy. Soc., A220, 61, 1953.
- Friedman, H., Space Astrophysics (W. Liller, ed.), McGraw-Hill, 1961, p. 107.
- Hinteregger, H. E., Astrophys. J., Vol. 132, No. 801, 1960.
- Hinteregger, H. E., Tenth International Astrophysical Symposium, Liège (1960).
- Kreplin, R. W., International Aeronomy Symposium, Copenhagen (to be published).
- Purcell, J. D., Packer, D. M., and Tossey, R., Proc. First Intern. Space Sci. Symposium, North Holland Publishing Co., Amsterdam, p. 581 (1960).
- Rense, W. A., Phys. Rev., 91, No. 229 (1953).
- Tousey, R., Space Astrophysics (W. Liller, ed.), McGraw-Hill, p. 1 (1961).
- Violet, T., and Rense, W. A., Astrophys. J., 130, No. 954 (1959).
- Watanabe, K., Advances in Geophys., 5, No. 153 (1958).
- Young, P. A., Unpublished Thesis, Reading University, 1960.

TABLE 1

## THE PLANETS—ORBITAL DATA\*

Planet	Symbol	No. of Satellites	Major Semi-axis (A.U.) [a]	Eccentricity [e]	Perihelion (A.U.) [R <sub>p</sub> ]	Aphelion (A.U.) [R <sub>a</sub> ]	Mean longitude			Inclination		Sidereal Mean Daily Motion (Sec) [μ]	Mean Orbital Velocity (Θ=1) V <sub>c</sub>	Period of Revolution	
							Of Ascending Node [Ω]	Of Perihelion [ω]	Of Planet at Epoch Jan. 1, 1963 [L]	Orbital to Ecciptic [i]	Equatorial to Orbit [i]			In Earth Years	y d h
1	2	3	4	5	6	7	8	9	10	11	12	13	14	15	16
Mercury	☿		0.387099	0.2056259	0.307501	0.466697	47 49 17.6	76 47 11.1	17.7	7 0 14.2	—	14,732.420	1.607271	-0.2411	0 88
Venus	♀		0.723332	0.0067935	0.718418	0.728246	76 17 33.7	130 57 57.9	128.3	3 23 39.1	—	5767.670	1.175794	0.6156	0 224 17
Earth	⊕	1	1.000000	0.0167272	0.983273	1.016727	—	102 12 3.2	99.9	—	23 26 59	3548.193	1.0	1.0	1 0 0
Mars	♂	2	1.523691	0.0933654	1.381431	1.665951	49 13 33.2	335 16 2.9	113.0	1 50 50.8	25 12	1886.519	0.8068546	1.8822	1 322 0
Jupiter	♃	12	5.202803	0.0484305	4.950829	5.454777	100 0 50.7	13 37 47.5	350.7	1 18 19.9	3 6.9	299.128	0.4384109	11.86	11 313 21
Saturn	♄	9	9.538843	0.0556922	9.007604	10.070082	113 16 52.6	92 12 20.4	317.0	2 29 42.2	26 44.7	120.455	0.3237816	29.46	29 167 22
Uranus	♅	5	19.181973	0.0472012	18.276561	20.087385	73 43 51.4	169 57 44	154.0	0 46 22.9	97 59	42.235	0.2283249	84.0	84 0 0
Neptune	♆	3	30.057707	0.0085724	29.800040	30.315374	131 18 24.2	44 14 51.9	223.4	1 46 26.5	29	21.532	0.1823988	164.8	164 292 0
Pluto	♇		39.51774	0.2486438	29.691899	49.343581	109 38 0.2	223 10 30.2	116.2	17 8 38.4	—	14.283	0.7590757	247.7	247 255 12

Cols. 4, 5, 8, 9, 11 and 13 The American Ephemeris and Nautical Almanac, 1957. The mean distance is equal to the major axis of the planet's orbit.

Cols. 6 and 7 computed from 4 and 5 in "Principles of Guided Missile Design" by K. Ziercke.

Col. 12 Russell, Dugan and Stewart, *Astronomy*, Vol. 1 (1945).

Col. 10, R. Nadile, Space General Corp.

Col. 14, V<sub>c</sub> for Θ = 29.77 km/sec.

Col. 4, A.R. = 149.4 × 10<sup>6</sup> km.

\* From *Enrike's Space Flight* copyright 1960, D. Van Nostrand Company, Inc., Princeton, N. J.

TABLE 2

THE PLANETS - PHYSICAL DATA

\*

Planet	Radius (Equator)		Ob- late- ness [ $\epsilon$ ]	Density		Volume $\oplus = 1$	Mass		Mass Gravitational Acceleration at 45° Latitude				Mean Surface Gravity $\oplus = 1$	Escape Velocity  $\frac{\text{km}}{\text{sec}}$	Activity Sphere (A.U.)	Period of Rotation, $\omega$	
	n. mi.	km		$\oplus = 1$	Water $= 1$		$\frac{M_{\odot}}{M_{\text{planet}}}$	$\oplus = 1$	$g_{\oplus}$ units	cm/sec <sup>2</sup>	ft/sec <sup>2</sup>	h.				m.	rad/sec
1	2 /	3	4	5	6	7	8	9	10	11	12	13	14	15	16	17	
(Sun)	375,557	696,000	—	0.2554	1.41	$1.302 \times 10^6$	1.0	$3.3253 \times 10^5$	—	—	—	27.89	617.0	—	244.2 (Equ.) 334.5 (75° $\lambda$ )	—	
Mercury	1350	2500	0	0.9058	5.00	0.06	$6.12 \times 10^4$ $\pm 43,000$	0.0543	0.35238	346.3904	11.36449	0.27	3.9	0.000746	—	$1.98333 \times 10^{-4}$	
Venus	3348	6200	0	0.8877	4.90	0.92	$4.08645 \times 10^4$ $\pm 208$	.8148	0.85805	843.4703	27.67285	0.85	10.3	0.00412	$230^{\text{d}} \pm 50^{\text{d}}$	$7.93013 \times 10^{-4}$	
Earth	3440	6378.39	$\frac{1}{297}$	1.0	5.52	1.0	$3.32488 \times 10^4$	1.0	1.00000	983.008	32.25085	1.00	11.2	0.00618	23 56.068	$7.31958 \times 10^{-4}$	
Mars	1787	3310	$\frac{1}{163}$	0.7609	4.20	0.153	$3.0880 \times 10^4$ $\pm 3000$	0.1077	0.40894	401.9938	13.18875	0.38	5.1	0.00378	24 37.38	$7.08821 \times 10^{-4}$	
Jupiter	37,732	69,880	$\frac{1}{16.4}$	0.2409	1.33	1318	$1.0474 \times 10^3$ $\pm 0.03$	318.35	2.81509	2767.252	90.78892	2.64	60.2	0.3216	9 50.5	$1.77341 \times 10^{-4}$	
Saturn	31,075	57,550	$\frac{1}{9.5}$	0.1286	0.71	736	$3.49764 \times 10^3$ $\pm 0.27$	95.3	1.29640	1274.368	41.80986	1.17	36.3	0.3246	10 2	$1.73953 \times 10^{-4}$	
Uranus	13,769	25,500	$\frac{1}{4}$	0.2283	1.26	64	$2.2869 \times 10^4$ $\pm 300$	14.58	0.97479	958.2298	31.43792	0.92	22.0	0.346	10 48	$1.61605 \times 10^{-4}$	
Neptune	13,499	25,000	$\frac{1}{4.6}$	0.2917	1.61	60	$1.9314 \times 10^4$ $\pm 300$	17.26	1.14183	1122.431	36.82509	1.12	25.1	0.5805	15 48	$1.10464 \times 10^{-4}$	
Pluto	—	—	—	—	—	1.0(?)	$4.0 \times 10^5$ $\pm 30,000$	0.8312	0.40096	394.151	12.93144	?	?	0.2366	—	—	

Cols. 3, 5 and 6, H. C. Urey, The Planets (1952), **except for Sun.**  
Cols. 6 and 7, Russell, Dugan and Stewart, Astronomy I (1945)  
Col. 8, W. Rabe, Astronautical Journal, Vol. 55, pp. 112-126, May 1950  
Col. 15, The activity sphere describes the space in which the planet, rather than the sun should be regarded as center body in the perturbation analysis of hyperbolic encounter between the planet and a particle of negligible mass. The activity sphere, therefore, may be used to define the circumplanetary space (e.g. circumterrestrial space). Values computed by K. Ehrike, "Principles of Guided Missile Design."

\* From Ehrike's Space Flight Copyright 1960, D. Van Nostrand Company Inc., Princeton, N.J.

TABLE 3

## THE PLANETS—SURFACE DATA

Planet	Circular Velocity at Equat. Radius Distance			Condition of Visible Surface	Albedo	Temperature (°K)			Atmosphere	
	km/sec	ft/sec	A.U./sec			Black Spher.	Max. (Day- side)	Av. Temp.	Composition	Abund- ance N.P.T. (cm)
1	2	3	4	5	6	7	8	9	10	11
Mercury	2.94276	$9.6547 \times 10^4$	$1.57737 \times 10^{-10}$	S	0.058	450	625	—	Traces of A <sup>40</sup> , Kr, X(?)	—
Venus	7.231538	$2.37258 \times 10^4$	$3.15795 \times 10^{-10}$	C	0.76- .80	329	700	700	CO, CO, N <sub>2</sub> O CH <sub>4</sub> , C <sub>2</sub> H <sub>4</sub> , C <sub>2</sub> H <sub>6</sub> , NH <sub>3</sub> , N <sub>2</sub>	100,000 <100 <100 <20 <3 <1 <4 (abundant)
Earth	7.90959	$2.59497 \times 10^4$	$3.45381 \times 10^{-10}$	S	0.39	279	349	246	N, O, CO, CH <sub>4</sub> , N <sub>2</sub> O O <sub>3</sub>	625,000 168,000 220 1.2 0.4 0.3
Mars	3.60036	$1.18122 \times 10^4$	$1.57143 \times 10^{-10}$	S	0.148	225	307	217	CO, SO, O, N <sub>2</sub> O CH <sub>4</sub> , C <sub>2</sub> H <sub>4</sub> , C <sub>2</sub> H <sub>6</sub> , NH <sub>3</sub> , N <sub>2</sub> , A(2200?)	440 <0.003 <0.05 <200 <10 <2 <1 <2
Jupiter	42.5467	$1.395886 \times 10^4$	$1.54755 \times 10^{-9}$	C	0.51	122	145	102	CH <sub>4</sub> , NH <sub>3</sub> , H <sub>2</sub>	15,000 700 large amt.
Saturn	25.6560	$8.41733 \times 10^4$	$1.12049 \times 10^{-9}$	C	0.50	90	107	76	CH <sub>4</sub> , NH <sub>3</sub> , O, SO <sub>2</sub> , H <sub>2</sub>	35,000 <250 <0.1 <0.01 LARGE AMT.
Uranus	15.0733	$5.14215 \times 10^4$	$6.58391 \times 10^{-10}$	C	0.66	64	69	49	CH <sub>4</sub> , O, SO <sub>2</sub>	220,000 <0.1 <0.01
Neptune	16.5651	$5.4347 \times 10^4$	$2.2946 \times 10^{-9}$	C	0.62	51	56	40	CH <sub>4</sub> , H <sub>2</sub>	370,000 LARGE AMT.
Pluto	7.43214	$2.43836 \times 10^4$	$5.0307 \times 10^{-9}$	?	0.16	45	60	42	—	—

Col. 7 : Perfect conductor.

Cols. 6, 8, 11 : G. P. Kuiper, *The Atmospheres of the Earth and the Planets* (1952) Chapter XII, Table 1 and Table 9. N.P.T. (cm): equivalent height of atmosphere component at normal pressure and temperature. The Earth's atmosphere is equivalent to about 800,000 cm (N.P.T.).

Col. 5 : S=solid, C=clouds.

\* From Ehrike's *Space Flight* Copyright 1960, D. Van Nostrand Company, Inc., Princeton, N.J.

Table 4

THE SATELLITES OF THE SOLAR SYSTEM \*

Planet	Satellite	Stellar Magnitude	App. Distance from $\odot$ (Sec. of Arc)	Distance from Planet		Period of Revolution		Eccentricity, (e)	Inclination				Direction of Rotation	Dia- meter (km)	Mass		Escape Velocity		Surface $\phi = 1$	Atmosphere Component (gm) N.P.T.
				Planet Radius = 1	km	d	h		m	Days	Satellite Orbit to its Proper Plane (or the Planet's Equator)	Mean inc. of Proper Plane to Planet's Orbit			Mean inc. of Satellite's Orbit to Planet's Orbit	Longitude of Ascending Node	$\bar{q} = 1$	$\bar{C} = 1$		
1	2	3	4	5	6	7	8	9	10	11	12	13	14	15	16	17	18	19	20	21
Earth	Moon	-12.5	529.75	60.267	384,400	27 7 43.19	27.321661	0.05490	28° 35' to 18° 19'	5° 8.55'			Direct	3476	0.2259	1	2.372	7873	0.1650	SO <sub>2</sub> (<0.0003) O <sub>2</sub> (<0.0005) Kr (?)
Mars	Phobos	11.5	8.46	2.79	9350	0 7 39.23	0.3189103	0.021	1 8	25° 11'	26° 19'		Direct	~15						
	Deimos	13	21.25	6.93	23,500	1 6 17.92	1.2631354	0.003	1 46	24 16	26 2		Direct	~8						
Jupiter	V	13	48.06	2.540	181,500	0 11 57.38	0.49817938	0.0028	27.3	3 6.9	3 34.2		Direct	75-150						
	I 10	5.5	111.78	5.905	422,000	1 18 27.56	1.76913783	0.0	1.6	3 6.7	3 8.3		Direct	3730	0.2236	0.99	2.279	7476	0.1337	CH <sub>4</sub> (<200) NH <sub>3</sub> (<40)
	II Europa	5.7	177.86	9.401	671,400	3 13 13.70	3.55188113	0.0003	28.1	3 5.8	3 33.9		Direct	3150	0.1446	0.64	1.994	6541	0.1286	CH <sub>4</sub> (<200) NH <sub>3</sub> (<40)
	III Ganymede	5.1	283.7	14.995	1,071,000	7 3 42.56	7.15455265	0.0015	11.0	3 2.3	3 13.3		Direct	5150	0.4766	2.11	2.831	9288	0.1586	CH <sub>4</sub> (<200) NH <sub>3</sub> (<40)
	IV Callisto	6.3	498.99	26.379	1,884,000	16 16 32.19	16.68901862	0.0075	15.2	3 42.7	3 57.9		Direct	5180	0.2982	1.32	2.233	7325	0.0981	CH <sub>4</sub> (<200) NH <sub>3</sub> (<40)
	VI	13.7	3037	161	11,500,000	240.7	250.7	0.155			28 45	181°	Direct	120?						
	VII	16	3113	165	11,750,000	260	260	0.207			27 58	243	Direct	50?						
	X	17.8	3116	165	11,750,000	260	260	0.08			28	82	Direct	20?						
	XI	16	5990	315	22,500,000	692	692	0.21			148 1	208	Retrograde	25?						
	VIII	17.6	6240	330	23,500,000	739	713-768	0.29-0.45			157	61	Retrograde	50?						
	IX	17.4	6360	332	23,700,000	758	758	0.1-0.4			163	232	Retrograde	22?						
	XII				23,700,000															
Saturn	Mimas	12.1	26.83	3.11	185,700	0 22 37.09	0.9424219	0.019	1 31	26 44.7	26 25.4		Direct	450?	0.000117	0.000516	0.1498	491	0.00508	
	Enceladus	11.6	34.42	3.99	238,200	1 8 53.11	1.3702178	0.0001	1.4	26 44.7	27 2.4		Direct	500?	0.000264	0.00117	0.2139	702	0.00933	
	Tethys	10.5	42.6	4.94	294,800	1 21 18.44	1.8878025	0.0	1 5.6	26 44.7	30 9.9		Direct	1100?	0.00206	0.0088	0.3956	1298	0.01450	
	Dione	10.7	54.57	6.33	337,700	2 17 41.16	2.7369159	0.002	0 0	26 44.7	26 44.7		Direct	1100?	0.00316	0.014	0.4990	1637	0.02306	
	Rhea	10	76.20	8.84	527,500	4 12 25.20	4.5175026	0.0009	20.5	26 41.9	27 50.3		Direct	1600?	0.00678	0.03?	0.6055	1987	0.02335	
	Titan	8.3	176.67	20.48	1,223,000	15 22 41.41	15.9454201	0.0289	18.3	26 7.1	26 46.1		Direct	4200	0.4337	1.92	2.990	9811	0.21694	CN <sub>2</sub> (20,000) NH <sub>3</sub> (<300)
	Hyperion	13	214.13	24.82	1,484,000	21 6 38.40	21.2766667	0.1043	1 31	26 44.7	28 15.7		Direct	400?	<0.000136	<6 × 10 <sup>-4</sup>	<0.1713	<562	<0.0075	
	Japetus	10.1 to 11.9	514.73	59.68	3,563,000	79 7 55.54	79.330234	0.0284	13 51.8	16 18.1	26 17 to 26 56		Direct	1300?	0.00429	0.019	0.5325	1747	0.0223	
Uranus	Phoebe	14.5	1870.4	216.8	12,950,000	550 10.6	550.4416	0.1659	(148.9)	(174.7)	175 18.7		Retrograde	300?						
	Ariel	15.2	13.78	7.35	191,800	2 12 29.35	2.5203796	0.007	(0)	—	97 59		Retrograde	500?						
	Umbriel	15.8	19.2	10.2	267,300	4 3 27.61	4.1441748	0.008	(0)	—	97 59		Retrograde	400?						
	Titania	14	31.5	16.8	438,700	8 16 56.45	8.705865	0.023	(0)	—	97 59		Retrograde	1000?						
	Oberon	14.2	42.12	22.4	586,600	13 11 7.06	13.463235	0.01	(0)	—	97 59		Retrograde	900?						
	Miranda				130,100															
Neptune	Triton	13.6	16.23	14.2	354,000	5 21 2.66	5.8768437	0.0	(160)		140 (1900)		Retrograde	4500?	0.4066	1.8	2.7972	9177	0.1772	
	Nereid				6,000,000															

Cols. 3-8, 9, 10-13, 15 and 17, Russell, Dugan and Stewart, *Astronomy* 1 (1945)

Col. 9, 14-20, K. Ehrike, *Principles of Guided Missile Design*

\* From Ehrike's *Space Flight* Copyright 1960, D. Van Nostrand Company, Inc., Princeton, N. J.

Col. 16, Computed from  $m_0/m_c = 4.427$

Col. 23, G. Kuiper, *The Atmosphere of the Earth and the Planets* (1952), P. 308

TABLE 6  
SELECTED PERIODIC COMETS

<u>Family</u>	<u>Name</u>	<u>Discovery</u>	<u>Perihelion Distance A.U.</u>	<u>Aphelion Distance A.U.</u>	<u>Orbital Inclination deg</u>	<u>Period yrs</u>
JUPITER						
	Encke	1818	0.3	4.1	12.5	3.3
	Biela	1826	0.9	6.2	12.6	6.6
	Faye	1843	1.6	5.9	10.6	7.3
	Brorsen I	1846	0.6	5.6	29.4	5.5
	d'Arrest	1851	1.4	5.7	18.1	6.6
	Tempel I	1867	1.8	4.8	9.8	6.0
	Tempel II	1873	1.3	4.7	12.8	5.2
	Wolf I	1884	2.4	5.8	27.3	8.3
	Finlay	1886	1.1	6.2	3.4	6.9
	Brooks II	1889	1.9	5.4	5.6	6.9
	Holmes	1892	2.1	5.1	20.8	6.9
	Perrine I	1896	1.2	5.8	15.7	6.5
	Zinner	1900	1.0	6.0	30.7	6.6
	Borelli	1905	1.4	5.8	30.5	6.9
	Schaumasse	1911	1.2	6.8	14.7	8.0
	Neujmin II	1916	1.3	4.8	10.6	5.4
SATURN						
	Tuttle I	1858	1.0	10.3	55.0	13.5
	Neujmin I	1913	1.5	12.0	15.2	17.7
URANUS						
	Pons-Forbes	1818	0.7	18.0	28.9	28.7
NEPTUNE						
	Pons-Brooks	1812	0.8	33.7	74.0	71.6
	Olbers	1815	1.2	33.6	44.6	72.7
	Westphal	1852	1.3	30.0	40.9	61.7
	Halley	unknown	0.6	35.5	102.2	75.0

TABLE 5

## THE MAJOR ASTEROIDS \*

No.	Name	EPOCH $t_0$	Longitude PERMELION $\omega$	Longitude ASCENDING NODE $\Omega$	Inclination of orbital plane to ecliptic, $i$	Eccentricity $e$	Mean daily motion sec	Major semi-axis A.U.	Perihelion $R_p$ A.U.	aphelion $R_a$ A.U.	Closest Approach to Earth A.U.	Diameter Miles	Period of Rotation h m	Albedo
1	Ceres	1957 June 11	71.853	80.514	10.607	0.0759	770.695	2.7675	2.5574	2.9776		480		0.06
2	Pallas	1957 June 11	309.759	172.975	34.798	0.2340	768.884	2.7718	2.1232	3.4204		304		0.07
3	Juno	1957 June 11	246.133	170.438	12.993	0.2585	814.046	2.6683	1.9785	3.3581		120		0.12
4	Vesta	1957 June 11	149.134	104.102	7.132	0.0889	977.646	2.3617	2.1517	2.5717		240		0.26
7	Iris	1949 Mar. 25	144.093	259.829	5.509	0.2315	963.378	2.3849	1.8328	2.9370			6 12	
15	Eunomia	1900 Jan.	94.98	294.42	11.76	0.1870	825.347	2.6439	2.1495	3.1383			3 2	
116	Sirona	1929 Apr. 22	91.551	64.842	3.580	0.1404	770.820	2.7672	2.3787	3.1557			9 40	
345	Tercidina	1925 Jan. 1	228.308	213.246	9.728	0.0613	1000.550	2.3255	2.1829	2.4681			8 47	
433	Eros	1931 Jan. 18	177.930	304.071	10.831	0.2398	2015.293	1.4581	1.1084	1.8078	0.1742 (1931)	15	5 16	
434	Hungaria	1925 Jan. 1	123.100	175.196	22.504	0.0737	1308.770	1.9443	1.8010	2.0876				
719	Albert	1911 Oct. 2	151.940	186.094	10.825	0.5406	853.665	2.5852	1.1876	3.9828		2-3		
887	Alinda	1942 Jan. 31	348.119	111.029	9.024	0.5398	886.351	2.5212	1.1602	3.8822				
944	Hidalgo	1948 Feb. 29	57.506	21.273	42.529	0.6557	254.384	5.7944	1.9950	9.5938				
1019	Strackea	1924 Mar. 14	121.198	144.244	26.972	0.0716	1342.468	1.9116	1.7747	2.0485		15-30		
1025	Riema	1943 Dec. 22	347.568	163.100	26.871	0.0389	1274.509	1.9790	1.9020	2.0560				
1139	Atami	1941 June 19	205.517	213.215	13.102	0.2552	1305.814	1.9472	1.4503	2.4441				
1172	Aneas	1948 Aug. 7	45.617	246.784	16.687	0.1029	300.254	5.1881	4.6542	5.7220				
1173	Anchises	1948 Aug. 7	30.710	284.132	6.980	0.1376	308.455	5.0958	4.3946	5.7970				
1208	Troilus	1948 Aug. 7	292.565	47.985	33.694	0.0924	302.757	5.1595	4.6828	5.6362				
1221	Amor	1948 June 3	25.549	171.202	11.924	0.4346	1334.746	1.9190	1.0850	2.7530	0.1075 (1932)			
1235	Schorria	1931 Dec. 8	43.005	12.767	25.020	0.1537	1343.831	1.9103	1.6167	2.2039				
1404	Ajax	1948 Aug. 7	57.197	332.320	18.132	0.1118	302.437	5.1631	4.5859	5.7403				
1437	Diomedes	1948 Aug. 7	126.771	315.330	20.563	0.0436	304.209	5.1431	4.9189	5.3673				
1509	Esclangona	1939 Jan. 1	267.061	283.286	22.320	0.0329	1391.117	1.8668	1.8054	1.9282				
1566	Icarus	1950 Aug. 7	30.912	87.746	22.979	0.8266	3171.432	1.0777	0.1869	1.9685	0.038 (1968)			
1580	Betulia	1952 Dec. 14	158.888	61.874	52.037	0.4928	1090.753	2.1954	1.1135	3.2773				
1583	Antiochus	1950 Nov. 15	186.229	221.067	28.303	0.0542	292.703	5.2770	4.9910	5.5630				
1600	1947 UC	1948 Feb. 19	49.765	60.314	21.177	0.0376	1411.228	1.8490	1.7795	1.9185				
1620	Geographos	1954 Dec. 24	276.211	336.999	13.325	0.3352	42.612	1.2441	0.8271	1.6611	0.032 (1969)	1		
	1948 Oa	1948 Oct. 7	126.314	274.191	9.397	0.4360	36.960	1.3679	0.7715	1.9643				
	Apollo	1932 Apr. 25	284.878	36.077	6.422	0.5663	1958.60	1.4861	0.6445	2.3277	0.0699 (1932)	1-2		
	Adonis	1936 Feb. 25	39.537	352.538	1.480	0.7792	1284.03	1.9692	0.4348	3.5036	0.0161 (1936)	1-2		
	Hermes	1937 Nov. 7	90.687	35.367	4.685	0.4746	2420.68	1.2904	0.6780	1.9028	0.0052 (1937)	<1		

\* Ref. Ephemerides of minor planets by the Institute of Theoretical Astronomy at Leningrad except for Geographos and 1948 Oa where elements were computed by Prof. S. Herrick, University of California; taken from K. Ehrke, Principles of Guided Missile Design.  
\* From Ehrke's Space Flight Copyright 1960, D. Van Nostrand Company, Inc., Princeton, N. J.

TABLE 7

## MODEL VENUSIAN ATMOSPHERE

Height km	Pressure atm	Temperature °K	Density gm/cu cm
0	10	700	$5.09 \times 10^{-3}$
10	6.27	651.7	$3.43 \times 10^{-3}$
20	3.79	603.3	$2.24 \times 10^{-3}$
30	2.20	555.0	$1.41 \times 10^{-3}$
40	1.21	506.6	$8.52 \times 10^{-4}$
50	$6.30 \times 10^{-1}$	458.3	$4.90 \times 10^{-4}$
60	$3.04 \times 10^{-1}$	409.9	$2.64 \times 10^{-4}$
70	$1.34 \times 10^{-1}$	361.6	$1.32 \times 10^{-4}$
80	$5.25 \times 10^{-2}$	313.2	$5.97 \times 10^{-5}$
90	$1.76 \times 10^{-2}$	264.9	$2.36 \times 10^{-5}$
97.21	$7 \times 10^{-3}$	230	$1.08 \times 10^{-5}$
100	$4.81 \times 10^{-3}$	228.5	$7.50 \times 10^{-6}$
110	$1.23 \times 10^{-3}$	222.9	$1.97 \times 10^{-6}$
120	$3.04 \times 10^{-4}$	217.4	$4.98 \times 10^{-7}$
130	$7.23 \times 10^{-5}$	211.8	$1.22 \times 10^{-7}$
140	$1.66 \times 10^{-5}$	206.3	$2.86 \times 10^{-8}$
150	$3.65 \times 10^{-6}$	200.7	$6.48 \times 10^{-9}$
151.28	$3 \times 10^{-6}$	200	$5.34 \times 10^{-9}$
160	$8.85 \times 10^{-7}$	215.4	$1.40 \times 10^{-9}$
168.29	$3 \times 10^{-7}$	230	$4.22 \times 10^{-10}$
170	$2.45 \times 10^{-7}$	236.9	$3.35 \times 10^{-10}$
178.24	$10^{-7}$	270	$1.20 \times 10^{-10}$

Note: Table refers to the standard atmosphere.



TABLE 8

## SOME LUNAR CONSTANTS

Mean Diameter-----	3476km (0.273 earth's diameter)
Mass-----	0.0123 (1/81.3 earth's mass)
Mean Density-----	3.34
Surface Gravity-----	0.16 earth's gravity
Escape Velocity-----	2.4 km/sec
Mean Distance from Earth-----	$3.844 \times 10^5$ km
Eccentricity of Orbit-----	0.0549
Average Inclination of Orbit to Ecliptic--	$5.1^\circ$
Orbital Velocity-----	1.03 km/sec
Period of Rotation-----	27.32 days
Albedo-----	0.07
Surface-----	41% never visible from earth

TABLE 9

## VAN ALLEN'S ESTIMATE OF PARTICLE FLUX

<u>Particles</u>	<u>Energy</u>	<u>Intensity</u>
<u>Heart of Inner Zone</u>		
Electrons	20 Kev	$2 \times 10^9/\text{cm}^2/\text{sec}/\text{ster}$
Electrons	600 Kev	$10^7/\text{cm}^2/\text{sec}/\text{ster}$
Protons	40 Mev	$2 \times 10^4/\text{cm}^2/\text{sec}$
<u>Heart of Outer Zone</u>		
Electrons	20 Kev	$10^{11}/\text{cm}^2/\text{sec}$
Electrons	200 Kev	$10^8/\text{cm}^2/\text{sec}$
Protons	60 Mev	$10^2/\text{cm}^2/\text{sec}$
Protons	30 Mev	No information

TABLE 10  
ATMOSPHERIC PARAMETERS AS A FUNCTION OF  
ALTITUDE NEAR SOLAR MAXIMUM

$h$ (km)	$T$ (°K)	$M$	$n$ (particles/cm <sup>3</sup> )	$\rho$ (g/cm <sup>3</sup> )	$p$ (dyne/cm <sup>2</sup> )	$H$ (km)
0	288	29.0	$2.5 \times 10^{19}$	$1.22 \times 10^{-3}$	$1.01 \times 10^6$	8.43
10	223	29.0	$8.6 \times 10^{18}$	$4.1 \times 10^{-4}$	$2.65 \times 10^5$	6.56
20	217	29.0	$1.85 \times 10^{18}$	$8.9 \times 10^{-5}$	$5.5 \times 10^4$	6.38
30	231	29.0	$3.7 \times 10^{17}$	$1.79 \times 10^{-5}$	$1.19 \times 10^4$	6.83
40	261	29.0	$8.3 \times 10^{16}$	$4.0 \times 10^{-6}$	$3.0 \times 10^3$	8.40
50	283	29.0	$2.3 \times 10^{16}$	$1.08 \times 10^{-6}$	$9.0 \times 10^2$	8.11
60	245	29.0	$7.53 \times 10^{15}$	$3.7 \times 10^{-7}$	$2.55 \times 10^2$	7.35
70	173	29.0	$1.96 \times 10^{15}$	$9.4 \times 10^{-8}$	$4.7 \times 10^1$	5.21
80	168	29.0	$2.84 \times 10^{14}$	$1.36 \times 10^{-8}$	$6.6 \times 10^0$	5.08
90	176	28.8	$3.9 \times 10^{13}$	$1.88 \times 10^{-9}$	$9.5 \times 10^{-1}$	5.35
100	208	27.8	$6.0 \times 10^{12}$	$2.8 \times 10^{-10}$	$1.74 \times 10^{-1}$	6.54
120	390	26.1	$6.3 \times 10^{11}$	$2.9 \times 10^{-11}$	$3.4 \times 10^{-2}$	13.1
140	662	24.5	$1.07 \times 10^{11}$	$4.7 \times 10^{-12}$	$1.04 \times 10^{-2}$	24.0
160	926	23.7	$4.0 \times 10^{10}$	$1.52 \times 10^{-12}$	$5.1 \times 10^{-3}$	34.8
180	1115	22.8	$2.0 \times 10^{10}$	$7.7 \times 10^{-13}$	$3.1 \times 10^{-3}$	43.6
200	1230	22.0	$1.07 \times 10^{10}$	$4.2 \times 10^{-13}$	$1.95 \times 10^{-3}$	50.2
220	1305	21.2	$6.6 \times 10^9$	$2.7 \times 10^{-13}$	$1.20 \times 10^{-3}$	55.3
240	1356	20.6	$4.6 \times 10^9$	$1.70 \times 10^{-13}$	$8.5 \times 10^{-4}$	60.0
260	1400	20.0	$3.3 \times 10^9$	$1.12 \times 10^{-13}$	$6.4 \times 10^{-4}$	63.8
280	1430	19.5	$2.35 \times 10^9$	$7.9 \times 10^{-14}$	$4.7 \times 10^{-4}$	67.0
300	1455	19.1	$1.82 \times 10^9$	$5.7 \times 10^{-14}$	$3.6 \times 10^{-4}$	70.6
320	1472	18.7	$1.32 \times 10^9$	$4.3 \times 10^{-14}$	$2.7 \times 10^{-4}$	73.0
340	1485	18.4	$1.00 \times 10^9$	$3.1 \times 10^{-14}$	$2.04 \times 10^{-4}$	75.6
360	1491	18.0	$7.6 \times 10^8$	$2.3 \times 10^{-14}$	$1.54 \times 10^{-4}$	77.8
380	1496	17.8	$5.9 \times 10^8$	$1.78 \times 10^{-14}$	$1.23 \times 10^{-4}$	79.9
400	1500	17.5	$4.7 \times 10^8$	$1.38 \times 10^{-14}$	$9.8 \times 10^{-5}$	81.8
450	1500	17.0	$2.5 \times 10^8$	$7.2 \times 10^{-15}$	$5.2 \times 10^{-5}$	85.7
500	1500	16.6	$1.44 \times 10^8$	$4.1 \times 10^{-15}$	$2.9 \times 10^{-5}$	88.6
600	1500	16.3	$4.8 \times 10^7$	$1.32 \times 10^{-15}$	$1.00 \times 10^{-5}$	93.1
700	1500	16.1	$1.70 \times 10^7$	$4.6 \times 10^{-16}$	$3.5 \times 10^{-6}$	97.0
800	1500	16.0	$6.3 \times 10^6$	$1.66 \times 10^{-16}$	$1.32 \times 10^{-6}$	101
900	1500	15.8	$2.35 \times 10^6$	$6.0 \times 10^{-17}$	$4.9 \times 10^{-7}$	105
1000	1500	15.7	$9.1 \times 10^5$	$2.4 \times 10^{-17}$	$1.90 \times 10^{-7}$	108
1200	1500	15.2	$1.52 \times 10^5$	$3.8 \times 10^{-18}$	$3.2 \times 10^{-8}$	118
1400	1500	13.0	$3.2 \times 10^4$	$6.6 \times 10^{-19}$	$6.7 \times 10^{-9}$	145
1600	1500	8.3	$1.00 \times 10^4$	$1.35 \times 10^{-19}$	$2.1 \times 10^{-9}$	239
1800	1500	3.5	$5.7 \times 10^3$	$3.5 \times 10^{-20}$	$1.14 \times 10^{-9}$	836
2000	1500	1.8	$4.6 \times 10^3$	$1.44 \times 10^{-20}$	$9.5 \times 10^{-10}$	1167
2500	1500	1.0	$3.47 \times 10^3$	$6.0 \times 10^{-21}$	$7.2 \times 10^{-10}$	2095

The temperature  $T$ , molecular weight  $M$ , number concentration  $n$ , density  $\rho$ , pressure  $p$ , and scale height  $H$  are given as functions of altitude  $h$ .

TABLE 11

ATMOSPHERIC PARAMETERS AS A FUNCTION OF  
ALTITUDE NEAR SOLAR MINIMUM

$h$ (km)	$T$ (°K)	$M$	$n$ (particles/cm <sup>3</sup> )	$\rho$ (g/cm <sup>3</sup> )	$p$ (dyne/cm <sup>2</sup> )	$H$ (km)
100	208	27.8	$6.0 \times 10^{12}$	$2.8 \times 10^{-10}$	$1.74 \times 10^{-1}$	6.54
120	340	26.1	$4.5 \times 10^{11}$	$1.94 \times 10^{-11}$	$2.1 \times 10^{-2}$	11.38
140	500	24.3	$6.6 \times 10^{10}$	$2.9 \times 10^{-12}$	$4.6 \times 10^{-3}$	18.1
160	628	22.9	$2.15 \times 10^{10}$	$7.7 \times 10^{-13}$	$1.86 \times 10^{-3}$	23.8
180	732	21.5	$9.1 \times 10^9$	$3.0 \times 10^{-13}$	$9.1 \times 10^{-4}$	29.5
200	807	20.5	$4.5 \times 10^9$	$1.48 \times 10^{-13}$	$5.0 \times 10^{-4}$	35.2
220	865	19.5	$2.35 \times 10^9$	$7.7 \times 10^{-14}$	$2.8 \times 10^{-4}$	39.6
240	906	18.9	$1.42 \times 10^9$	$4.3 \times 10^{-14}$	$1.77 \times 10^{-4}$	44.1
260	937	18.3	$8.9 \times 10^8$	$2.6 \times 10^{-14}$	$1.14 \times 10^{-4}$	47.2
280	959	17.9	$5.8 \times 10^8$	$1.62 \times 10^{-14}$	$7.6 \times 10^{-5}$	49.9
300	973	17.5	$3.8 \times 10^8$	$1.04 \times 10^{-14}$	$5.1 \times 10^{-5}$	51.9
320	984	17.2	$2.6 \times 10^8$	$6.9 \times 10^{-15}$	$3.5 \times 10^{-5}$	53.3
340	991	16.9	$1.70 \times 10^8$	$4.8 \times 10^{-15}$	$2.34 \times 10^{-5}$	54.9
360	996	16.7	$1.20 \times 10^8$	$3.3 \times 10^{-15}$	$1.66 \times 10^{-5}$	56.0
380	998	16.5	$8.3 \times 10^7$	$2.2 \times 10^{-15}$	$1.14 \times 10^{-5}$	57.1
400	1000	16.3	$6.0 \times 10^7$	$1.58 \times 10^{-15}$	$8.3 \times 10^{-6}$	58.4
450	1000	16.0	$2.6 \times 10^7$	$6.8 \times 10^{-16}$	$3.6 \times 10^{-6}$	60.1
500	1000	15.9	$1.20 \times 10^7$	$3.1 \times 10^{-16}$	$1.66 \times 10^{-6}$	61.6
600	1000	15.6	$2.45 \times 10^6$	$6.3 \times 10^{-17}$	$3.4 \times 10^{-7}$	66.0
700	1000	14.7	$5.8 \times 10^5$	$1.28 \times 10^{-17}$	$7.9 \times 10^{-8}$	76.0
800	1000	10.2	$1.74 \times 10^5$	$2.9 \times 10^{-18}$	$2.4 \times 10^{-8}$	157
900	1000	5.1	$9.1 \times 10^4$	$7.2 \times 10^{-19}$	$1.26 \times 10^{-8}$	312
1000	1000	2.3	$7.1 \times 10^4$	$2.7 \times 10^{-19}$	$9.8 \times 10^{-9}$	487
1200	1000	1.3	$5.3 \times 10^4$	$1.07 \times 10^{-19}$	$7.2 \times 10^{-9}$	915
1400	1000	1.0	$4.5 \times 10^4$	$7.6 \times 10^{-20}$	$6.2 \times 10^{-9}$	1220
1600	1000	1.0	$3.7 \times 10^4$	$6.3 \times 10^{-20}$	$5.1 \times 10^{-9}$	1319
1800	1000	1.0	$3.1 \times 10^4$	$5.6 \times 10^{-20}$	$4.3 \times 10^{-9}$	1390
2000	1000	1.0	$2.7 \times 10^4$	$4.8 \times 10^{-20}$	$3.8 \times 10^{-9}$	1456
2500	1000	1.0	$2.0 \times 10^4$	$3.4 \times 10^{-20}$	$2.8 \times 10^{-9}$	1634

The temperature  $T$ , molecular weight  $M$ , number concentration  $n$ , density  $\rho$ , pressure  $p$ , and scale height  $H$  are given as functions of altitude  $h$ .

TABLE 12

## MARS MODEL ATMOSPHERES WITH 13.0 mb ARGON

Property	Symbol	Dimensions	G	H	I	J	K
Surface pressure	$P_o$	mb lb/ft <sup>2</sup>	11 23.0	11 23.0	15 31.3	30 62.6	30 62.6
Stratosphere temperature	$T_s$	<sup>o</sup> K <sup>o</sup> R	130 234	230 414	180 324	130 234	230 414
Surface temperature	$T_o$	<sup>o</sup> K <sup>o</sup> R	260 468	260 468	230 414	210 378	230 414
Acceleration of gravity at surface	$g$	cm/sec <sup>2</sup> ft/sec <sup>2</sup>	375 12.3	375 12.3	375 12.3	375 12.3	375 12.3
Composition (volume)		%					
CO <sub>2</sub>			64.8	64.8	43.3	10.5	10.5
A <sub>2</sub>			35.2	35.2	32.2	13.0	13.0
N <sub>2</sub>			0	0	24.5	76.5	76.5
Molecular weight	$M$	mol <sup>-1</sup>	42.6	42.6	38.8	31.3	31.3
Specific heat ratio	$\gamma$		1.37	1.37	1.39	1.40	1.40
Adiabatic temp. lapse rate	$\Gamma$	<sup>o</sup> K/km <sup>o</sup> R/ft x 10 <sup>3</sup>	5.18 2.84	5.18 2.84	4.91 2.69	4.05 2.22	0
Tropopause altitude	$h_T$	km ft	25.09 82,300	5.79 19,000	10.19 33,400	19.75 64,800	0
Inverse scale height (stratosphere)	$\beta$	km <sup>-1</sup> ft <sup>-1</sup> x 10 <sup>5</sup>	0.1478 4.506	0.0835 2.546	0.0972 2.963	0.1085 3.308	0.0613 1.869
Surface density	$\rho_o$	(g/cm <sup>3</sup> )10 <sup>5</sup> (sl/ft <sup>3</sup> )10 <sup>5</sup>	2.17 4.21	2.17 4.21	3.04 5.90	5.37 10.42	4.91 9.54
Artificial surface density	$\rho_o'$	(g/cm <sup>3</sup> )10 <sup>5</sup> (sl/ft <sup>3</sup> )10 <sup>5</sup>	13.60 26.40	2.52 4.89	4.35 8.44	14.20 27.55	4.91 9.54
Density at tropopause	$\rho_T$	(g/cm <sup>3</sup> )10 <sup>5</sup> (sl/ft <sup>3</sup> )10 <sup>5</sup>	0.332 0.643	1.55 3.02	1.62 3.14	1.66 3.23	4.91 9.54

Table 12

TABLE 13

## MARS MODEL ATMOSPHERES WITH NO ARGON

Property	Symbol	Dimensions	L	M	N	O	P
Surface pressure	$P_o$	mb lb/ft <sup>2</sup>	11 23.0	11 23.0	15 31.3	30 62.6	30 62.6
Stratosphere temperature	$T_s$	$^{\circ}\text{K}$ $^{\circ}\text{R}$	130 234	230 414	180 324	130 234	230 414
Surface temperature	$T_o$	$^{\circ}\text{K}$ $^{\circ}\text{R}$	260 468	260 468	230 414	210 378	230 414
Acceleration of gravity at surface	$g$	cm/sec <sup>2</sup> ft/sec <sup>2</sup>	375 12.3	375 12.3	375 12.3	375 12.3	375 12.3
Composition (volume)		%					
CO <sub>2</sub>			100.0	100.0	38.3	11.8	11.8
N <sub>2</sub>			0	0	61.7	88.2	88.2
Molecular weight	$M$	mol <sup>-1</sup>	44.0	44.0	34.2	29.9	29.9
Specific heat ratio	$\gamma$		1.30	1.30	1.35	1.38	1.38
Lapse rate (adiabatic temp)	$\Gamma$	$^{\circ}\text{K/km}$ $^{\circ}\text{R}/10^3\text{ft}$	4.60 2.52	4.60 2.52	4.02 2.20	3.72 2.04	3.72 2.04
Tropopause altitude	$h_T$	km ft	28.25 92,600	6.52 21,400	12.44 40,800	21.50 70,500	0 0
Inverse scale height (stratosphere)	$\beta$	km <sup>-1</sup> ft <sup>-1</sup> x 10 <sup>5</sup>	0.1528 4.66	0.0863 2.63	0.0858 2.61	0.1038 3.16	0.0586 1.79
Surface density	$\rho_o$	g/cm <sup>3</sup> x 10 <sup>5</sup> sl/ft <sup>3</sup> x 10 <sup>5</sup>	2.24 4.35	2.24 4.35	2.68 5.20	5.14 9.97	4.69 9.10
Artificial surface density	$\rho_o'$	g/cm <sup>3</sup> x 10 <sup>5</sup> sl/ft <sup>3</sup> x 10 <sup>5</sup>	16.94 32.9	2.62 5.09	3.89 7.55	13.50 26.20	4.69 9.10
Density at tropopause	$\rho_T$	g/cm <sup>3</sup> x 10 <sup>5</sup> sl/ft <sup>3</sup> x 10 <sup>5</sup>	0.226 0.439	1.492 2.90	1.337 2.59	1.452 2.82	4.690 9.10

Table 13

TABLE 14

## SOLAR-SPECTRAL-IRRADIANCE DATA — 0.22 TO 7.0 MICRONS

Reproduced by permission of the Stanford University Press from *Satellite Environment Handbook*, ed. Francis S. Johnson, copyright 1961 by Lockheed Aircraft Corp.

$\lambda^a$ ( $\mu$ )	$H_\lambda$ ( $w/cm^2\mu$ )	$P_\lambda$ (%)	$\lambda$ ( $\mu$ )	$H_\lambda$ ( $w/cm^2\mu$ )	$P_\lambda$ (%)	$\lambda$ ( $\mu$ )	$H_\lambda$ ( $w/cm^2\mu$ )	$P_\lambda$ (%)	$\lambda$ ( $\mu$ )	$H_\lambda$ ( $w/cm^2\mu$ )	$P_\lambda$ (%)
0.22	0.0030	0.02	0.395	0.120	3.54	0.57	0.187	33.2	1.9	0.01274	93.02
0.225	0.0042	0.03	0.40	0.154	9.03	0.575	0.187	33.9	2.0	0.01079	93.87
0.23	0.0052	0.05	0.405	0.188	9.65	0.58	0.187	34.5	2.1	0.00917	94.58
0.235	0.0054	0.07	0.41	0.194	10.3	0.585	0.185	35.2	2.2	0.00785	95.20
0.24	0.0058	0.09	0.415	0.192	11.0	0.59	0.184	35.9	2.3	0.00676	95.71
0.245	0.0064	0.11	0.42	0.192	11.7	0.595	0.183	36.5	2.4	0.00585	96.18
0.25	0.0064	0.13	0.425	0.189	12.4	0.60	0.181	37.2	2.5	0.00509	96.57
0.255	0.010	0.16	0.43	0.178	13.0	0.61	0.177	38.4	2.6	0.00445	96.90
0.26	0.013	0.20	0.435	0.182	13.7	0.62	0.174	39.7	2.7	0.00390	97.21
0.265	0.020	0.27	0.44	0.203	14.4	0.63	0.170	40.9	2.8	0.00343	97.47
0.27	0.025	0.34	0.445	0.215	15.1	0.64	0.166	42.1	2.9	0.00303	97.72
0.275	0.022	0.43	0.45	0.220	15.9	0.65	0.162	43.3	3.0	0.00268	97.90
0.28	0.024	0.51	0.455	0.219	16.7	0.66	0.159	44.5	3.1	0.00230	98.08
0.285	0.034	0.62	0.46	0.216	17.5	0.67	0.155	45.6	3.2	0.00214	98.24
0.29	0.052	0.77	0.465	0.215	18.2	0.68	0.151	46.7	3.3	0.00191	98.39
0.295	0.063	0.98	0.47	0.217	19.0	0.69	0.148	47.8	3.4	0.00171	98.52
0.30	0.061	1.23	0.475	0.220	19.8	0.70	0.144	48.8	3.5	0.00153	98.63
0.305	0.067	1.43	0.48	0.216	20.6	0.71	0.141	49.8	3.6	0.00139	98.74
0.31	0.076	1.69	0.485	0.203	21.3	0.72	0.137	50.8	3.7	0.00125	98.83
0.315	0.082	1.97	0.49	0.199	22.0	0.73	0.134	51.8	3.8	0.00114	98.91
0.32	0.085	2.26	0.495	0.204	22.8	0.74	0.130	52.7	3.9	0.00103	98.99
0.325	0.102	2.60	0.50	0.198	23.5	0.75	0.127	53.7	4.0	0.00095	99.05
0.33	0.115	3.02	0.505	0.197	24.2	0.80	0.1127	57.9	4.1	0.00087	99.13
0.335	0.111	3.40	0.51	0.196	24.9	0.85	0.1003	61.7	4.2	0.00080	99.18
0.34	0.111	3.80	0.515	0.189	25.6	0.90	0.895	65.1	4.3	0.00073	99.23
0.345	0.117	4.21	0.52	0.187	26.3	0.95	0.0803	68.1	4.4	0.00067	99.29
0.35	0.118	4.63	0.525	0.192	26.9	1.0	0.0725	70.9	4.5	0.00061	99.33
0.355	0.116	5.04	0.53	0.195	27.6	1.1	0.0606	75.7	4.6	0.00056	99.38
0.36	0.116	5.47	0.535	0.197	28.3	1.2	0.0501	79.6	4.7	0.00051	99.41
0.365	0.129	5.89	0.54	0.198	29.0	1.3	0.0406	82.9	4.8	0.00048	99.45
0.37	0.133	6.36	0.545	0.198	29.8	1.4	0.0328	85.5	4.9	0.00044	99.48
0.375	0.132	6.84	0.55	0.195	30.5	1.5	0.0267	87.6	5.0	0.00042	99.51
0.38	0.123	7.29	0.555	0.192	31.2	1.6	0.0220	89.4	6.0	0.00021	99.74
0.385	0.115	7.72	0.56	0.190	31.8	1.7	0.0182	90.83	7.0	0.00012	99.86
0.39	0.112	8.13	0.565	0.189	32.5	1.8	0.0152	92.03			

<sup>a</sup>  $\lambda$  is wavelength;  $H_\lambda$  is spectral irradiance; and  $P_\lambda$  is the percentage of the solar constant associated with wavelengths shorter than  $\lambda$ .

TABLE 15  
CHARACTERISTICS OF EXTREME ULTRAVIOLET  
RADIATION (3000 TO 1300 Å)

Note:  $h^*$  data for overhead sun ( $Z \sim 0^\circ$ ).  $a \times 10^b \equiv a^b$  in  $\Phi_0$ ,  $I_0$ , data.

$\lambda$ or $\lambda_1/\lambda_2$ , Å	$h\nu$ , ev	Top of Atmosphere		$h^*$ $\Phi(h^*) \equiv \Phi_0/e$ (approx.), km	$\sigma(M)$ , Absolute Absorption Cross Section for Species M, $\text{cm}^2$	Remarks
		$\Phi_0$ , $\text{ph}/\text{cm}^2 \text{ sec}$	$I_0$ , $\text{erg}/\text{cm}^2 \text{ sec}$			
3000/ 2800	4.3	$1.5^{15}$	$1.0^4$	30-40	$\sigma(\text{N}_2, \text{O}_3, \text{O}, \text{N})$ are negligible	Below 3000 Å: Strong absorption by ozone.
2800/ 2600	4.6	$6.8^{14}$	$5.0^3$	30-40		
2600/ 2400	5.0	$2.5^{11}$	$2.0^3$	35-45	$\sigma(\text{O}_2) = 1.2 \times 10^{-17}$	2550 Å: Spectral peak of ozone absorption. Below 2420 Å: Weak photodissociation of oxygen ( $\text{O}_2$ - Herz- berg continuum).
2400/ 2200	5.4	$1.3^{14}$	$1.1^3$	40	$(\text{O}_2) = 5 \times 10^{-24}$ [Young, 1960]	
2400/ 2000	5.9	$5.3^{13}$	500			
3000/ 2000	5	$2.6^{15}$	$1.9^4$	30-45		Mainly absorbed by $\text{O}_3$ above 2300 Å; ab- sorbed by both $\text{O}_3$ and $\text{O}_2$ below 2300 Å.
2000/ 1900	6.4	$1.3^{13}$	130	30-50	$\sigma(\text{O}_2) < 6 \times 10^{-21}$	$\text{O}_2$ bands. $\text{O}_2$ Herzberg conti- uum [Young, 1960]. Below 1750 Å: Strong photodissociation of $\text{O}_2$ (Schumann continuum).
1900/ 1800	6.7	$5.6^{12}$	60	75	$\sigma(\text{O}_2) \sim 10^{-18}$ $\sigma(\text{O}_2) \sim 3 \times 10^{-20}$ $\sigma(\text{O}_2) \sim 1.5 \times 10^{-22}$	
1800/ 1700	7.1	$3.5^{12}$	40	85-100	$\sigma(\text{O}_2) = 10^{-19}$ $- 8 \times 10^{-19}$	
1700/ 1600	7.5	$1.6^{12}$	20	$\sim 105$	$8 \times 10^{-19}$ $- 4 \times 10^{-18}(\text{O}_2)$	Spectral peak of $\text{O}_2$ dissociation.
1600/ 1500	8.0	$7^{11}$	9	$\sim 115$	$4 \times 10^{-18}$ $- 1.1 \times 10^{-17}(\text{O}_2)$	
1500/ 1400	8.5	$2.6^{11}$	3.5	$\sim 125$	$1.5 \times 10^{-17}(\text{O}_2)$ [Watanabe, 1958] $1.8 \times 10^{-17}(\text{O}_2)$ [Ditchburn and Heddle, 1953]	
1400/ 1300	9.2	$8^{10}$ (continuum)	1.2	95-125	$1.4 \times 10^{-17}$ $- 4 \times 10^{-19}(\text{O}_2)$	
1403/ 1394	8.8	$5^9$ (Si IV)	0.07	$\sim 125$	$1.4 \times 10^{-17}(\text{O}_2)$	
1336/ 1334	9.3	$1^{10}$ (C II, Si II)	0.15	$\sim 110$	$2.2 \times 10^{-18}(\text{O}_2)$	
1309/ 1302	9.5	$1^{10}$ (Si II, O I)	0.15	$\sim 95$	$5 \times 10^{-19}(\text{O}_2)$	
1400/ 1300	9.5	$1.1^{11}$ (total)	1.5	95-125	$4 \times 10^{-19}$ $- 1.4 \times 10^{-17}(\text{O}_2)$	
2000/ 1300	6.2/ 9.5	$2.5^{13}$ (total)	260	50-125		Mainly absorbed by molecular oxygen; no ionization.
3000/ 1300	4.2/ 9.5	$2.6^{15}$ (total)	$1 \times 10^4$	25-125		Mainly absorbed by ozone and molecular oxygen; no ionization.



TABLE 16

## CHARACTERISTICS OF THE SOLAR SPECTRUM BELOW 1300 Å

Note:  $h^*$  data estimated for summer day 1960, near noon, temperate latitudes.

$\lambda$ or $\lambda_1/\lambda_2$ , Å	$h\nu$ , ev	$\Phi$ 235 km, $\cos Z \approx 0.8$ , 8/23/60, New Mexico, ph/cm <sup>2</sup> sec	Estimated for Top of Atmosphere August 1960		Estimated, $\Phi^* \equiv \Phi_0/e$ , $\cos Z = 1$ , km	$\sigma_0(M)$ or $\sigma_i(M)$ Absolute Cross Sections Total Absorp- tion —, or Ionization; Species M, $10^{-18}$ cm <sup>2</sup>	Remarks
			$\Phi_0$ , ph/cm <sup>2</sup> sec	$I_0$ , erg/cm <sup>2</sup> sec			
1300-1200 Å							
1300/1200	10.0	$\sim 5^a$	$5^a$ (continuum)	0.08	70-135	0.01-40 <sub>a</sub> (O <sub>2</sub> )	Notation for $\Phi$ : $a^b$ means $a \times 10^b$ throughout tables.
1265/1259	9.9	$2.5^a$	$2.5^a$ (lines, Si II)	0.04	$\sim 100$	Rapidly variable with $\lambda$ $0.5_a(O_2)$	
1248/1239	10.0	$\sim 1^a$	$\sim 1^a$ (lines, N V)	$\sim 0.01$	$\sim 105$	$0.5_a(O_2)$	
1216	10.2	$2^{11}$ (3.7 <sup>11</sup> ) 210 km	$2^{11}$ (H Ly $\alpha$ ) (3.7 <sup>11</sup> ) $3.7^{11}$	3.3 (6.0) 6.0	$\sim 75$ (GRD 1/19/60 estimated max. error 20%)	0.01 <sub>a</sub> (O <sub>2</sub> ), 0.000 <sub>a</sub> (N <sub>2</sub> ), 2.4 <sub>a</sub> (NO), 2.0 <sub>a</sub> (NO)	H Ly $\alpha$ : Considered as main source of normal D-region ion- ization (quiet sun).
For spectral shape of H Ly- $\alpha$ line see Tousey [1961]				$\sim 0.1$	Preferred value from many ion-chamber measurements by Friedman and collaborators, NRL, up to spring 1960 (estimated experimental error 10-20%). Lowest values from earlier NRL experiments found closer to minimum of solar cycle; low value, however, possibly attributed to instrumental error. Extreme excursion believed to be possible; actual variation probably within a factor of 10 and quite possibly less, even under conditions of major flares [Fried- man, 1961]; H Ly- $\alpha$ first detected photographically at University of Colorado [Rense, 1953].		
				0.1-10			
1206	10.2	$4^a$	$4^a$ (line, Si III)	0.07	$\sim 115$	15 <sub>a</sub> (O <sub>2</sub> )	
1300/1200	10.0	$2.1^{11}$ (all lines + continuum)	$2.1^{11}$	3.5	70-135 see Ly- $\alpha$	0.01 <sub>a</sub> -40 <sub>a</sub> (O <sub>2</sub> ) rapid vari- ation with $\lambda$ 2 <sub>a</sub> (NO) for H Ly- $\alpha$	Mostly absorbed by O <sub>2</sub> ; the dominant line, H Ly- $\alpha$ , is be- lieved to be partly absorbed by NO, causing the normal D- region ionization.
1200-990 Å							
1200/1100	$\sim 10.8$	$\sim 3^a$	$\sim 3^a$ (continuum estimated)	$\sim 0.05$	70-120	0.01 <sub>a</sub> -6 <sub>a</sub> (O <sub>2</sub> )	
1176	10.6	$\sim 2^a$	$\sim 2^a$ (C III)	$\sim 0.03$	$\sim 100$	1.3 <sub>a</sub> (O <sub>2</sub> )	
1200/1100	$\sim 10.8$	$\sim 2^a$	$\sim 2^a$ (other lines)	$\sim 0.03$	70-120		
1200/1100	$\sim 10.8$	$\sim 7^a$	$\sim 7^a$ (all lines + continuum)	$\sim 0.10$	70-120	$\sigma_0(O_2)$ rapidly variable with $\lambda$	Absorbed by O <sub>2</sub> ; contribution of $\leq 5\%$ to Friedman's Ly- $\alpha$ de- tectors (NO chamber with LiF window).
1100/1000	$\sim 11.8$	$\sim 2^a$	$\sim 2^a$ (continuum estimated)	0.03	80-120	0.05-6 <sub>a</sub> (O <sub>2</sub> )	
1038/1031	11.9	$3^a$	$3^a$ (lines, O VI)	0.06	$\sim 100$	1.0 <sub>a</sub> (O <sub>2</sub> ); $\sigma_i = 0$	Contribution $\leq 2\%$ NO ion chamber signals.
1026	12.0	$2.2^a$	$2.2^a$ (H Ly- $\beta$ )	0.03	$\sim 105$	1.7(O <sub>2</sub> ), 0.9 <sub>a</sub> (O <sub>2</sub> )	Below 1030 Å: photoioniza- tion of molecular oxygen H Ly- $\beta$ causes much of the ionization in lower E region.
1006	12.2	$7^a$	$7^a$ (N III)	0.01	$\sim 105$	2.0 <sub>a</sub> (O <sub>2</sub> ), 1.5 <sub>a</sub> (O <sub>2</sub> )	
1100/1000	11.8	$8^a$	$3^a$ (all lines + continuum)	0.13	80-120	0.05 <sub>a</sub> -6.0 <sub>a</sub> (O <sub>2</sub> ); 0 <sub>a</sub> -1.5 <sub>a</sub> (O <sub>2</sub> )	See note above; absorbed mostly by O <sub>2</sub> .
1000/900	$\sim 13.0$	$2^a$	$\leq 2^a$ (continuum estimated excluding Ly continuum)	$\leq 0.03$	110-250?	1.5 <sub>a</sub> -54 <sub>a</sub> (O <sub>2</sub> ); 1.3 <sub>a</sub> -3.8 <sub>a</sub> (O <sub>2</sub> ); 0.01-300 <sub>a</sub> (N <sub>2</sub> )	Sharp N <sub>2</sub> -absorption bands (see $\sigma_0(N_2)$ ). Mostly absorbed by O <sub>2</sub> .
993/990	12.5	$3^a$	$3^a$ (Si II, N III, O I)	0.006	115	1.6 <sub>a</sub> -20 <sub>a</sub> (O <sub>2</sub> ); 1.4 <sub>a</sub> -10 <sub>a</sub> (O <sub>2</sub> ); $\sim 0.5_a(N_2)$	
976-800 Å							
976	12.7	$4^a$	$4^a$ (C III line)	0.08	$\sim 115$	8.5 <sub>a</sub> , 8.0 <sub>a</sub> (O <sub>2</sub> ); 3 <sub>a</sub> (N <sub>2</sub> )	Significant contribution to E- region ionization. H Ly- $\gamma$ may contribute to up per atmosphere heating (Nicolet, private communication). This line, 'missing' in all photographic spectra until recently discovered in exposure at 220 km [Purcell, Packer, and Tousey, 1960]. N <sub>2</sub> absorption spectrum is extremely complex. $\sigma(\lambda)$ varies over many orders of magnitude and is not accurately known.
972	12.7	$3^a(?)$	$1^a(?)$ (H Ly- $\gamma$ )	0.02(?)	250-300	$\leq 300_a(N_2)$ , 'effective' cross section very uncertain (?)	
949	13.0	$3.5^a$	$3.5^a$ (H Ly- $\delta$ )	0.006	$\sim 130$	4 <sub>a</sub> (O <sub>2</sub> ), 3 <sub>a</sub> (O <sub>2</sub> ); 0.2 <sub>a</sub> -2.0 <sub>a</sub> (N <sub>2</sub> )	
937/912	$\sim 13.7$	$\sim 1^a$	$\sim 1^a$ (rest of Ly series)	$\sim 0.02$	115-160	4 <sub>a</sub> -20 <sub>a</sub> (O <sub>2</sub> ); 3 <sub>a</sub> -15 <sub>a</sub> (O <sub>2</sub> ); 0.2 <sub>a</sub> -10 <sub>a</sub> (N <sub>2</sub> )(?)	
1000/911	$\sim 12.8$	$8^a$	$3^a$ (all lines + continuum)	0.16	110-160 (300?)	1.5 <sub>a</sub> -50 <sub>a</sub> (O <sub>2</sub> ); 1.3 <sub>a</sub> -38 <sub>a</sub> (O <sub>2</sub> ); 0.01 <sub>a</sub> -300 <sub>a</sub> (N <sub>2</sub> )	
912/900	13.7	$3^a$	$3^a$ (H Ly continuum)	0.07	$\sim 135$	4 <sub>a</sub> -14 <sub>a</sub> (O <sub>2</sub> ); 3.5 <sub>a</sub> -9.7 <sub>a</sub> (O <sub>2</sub> ); $< 0.1_a-150_a(N_2)$ ; 7 <sub>a</sub> (H)	Below 911 Å: photoionization of atomic oxygen (also H) H Ly continuum: dominating cause of ionization and heating of E re- gion, contributing source of F <sub>1</sub> region and highest F <sub>2</sub> .
900/840	$\sim 14.1$	$5^a$	$5^a$ (H Ly continuum)	0.11	$\sim 140$	2.6 <sub>a</sub> -3.0 <sub>a</sub> (O)	
835/833	14.9	$7^a$	$7^a$ (lines, C II, III)	0.017	$\sim 140$	14.5 <sub>a</sub> (O <sub>2</sub> ); 4.7 <sub>a</sub> (O <sub>2</sub> ); 10 <sub>a</sub> (N); 3.0 <sub>a</sub> (O); $\sigma_0(N_2) = ?$	Below 850 Å: photoionization of atomic nitrogen.
911/800	13.6/ 15.6	$9^a$	$9^a$ (all lines and continua)	0.20	$\sim 135$	4.5 <sub>a</sub> -30 <sub>a</sub> (O <sub>2</sub> ); 3.8 <sub>a</sub> -9 <sub>a</sub> (O <sub>2</sub> ); $\sigma_0(N_2) = ?$	Ionization and heating in E and F <sub>1</sub> regions; see notes above.
800-500 Å							
790/888	15.7	$5^a$	$7^a$ (lines, C II, III)	0.018	$\sim 185$	30 <sub>a</sub> (O <sub>2</sub> ); 13 <sub>a</sub> (O <sub>2</sub> ); 8 <sub>a</sub> (N <sub>2</sub> ); 3 <sub>a</sub> (O); 10 <sub>a</sub> (N)	Below 797 Å: photoionization of molecular nitrogen; $\sigma_0(N) =$ $\sigma_i(N)$ and $\sigma_0(O) = \sigma_i(O)$ (val- ues taken close to those calcu- lated by Dalgarno, private communication).
780/770	16.0	$4.5^a$	$6^a$ (lines, Ne VIII)	0.015	$\sim 175$	10 <sub>a</sub> (N <sub>2</sub> ); 22 <sub>a</sub> , 11 <sub>a</sub> (O <sub>2</sub> ); 10 <sub>a</sub> (N); 3.4 <sub>a</sub> (O)	
704/702	17.6	$2.8^a$	$6^a$ (lines, O II)	0.016	$\sim 220$	20 <sub>a</sub> (N <sub>2</sub> ); 25 <sub>a</sub> (O <sub>2</sub> ); 10 <sub>a</sub> (N); 7 <sub>a</sub> (N)	
800/700	17.6/ 20.7	$1.2^a$	$1.4^a-3^a$ (all lines + continuum)	0.04-0.10	$\sim 180$ mostly	See above.	Apparently modest contribu- tion to ionization and heating of F <sub>1</sub> and F <sub>2</sub> region.
630/625	20.0	$9^a$	$2^a$ (lines, O V, Mg X)	0.064	$\sim 250$	20 <sub>a</sub> (N <sub>2</sub> ); 23 <sub>a</sub> (O <sub>2</sub> ); 11 <sub>a</sub> (N); 12 <sub>a</sub> (O)	Probably strongest monochro- matic flux dissipated in F <sub>2</sub> region.
610	20.3	$6^a$	$1.5^a$ (line, Mg X)	0.05	$\sim 250$	22 <sub>a</sub> (N <sub>2</sub> ); 25 <sub>a</sub> (O <sub>2</sub> ); 10 <sub>a</sub> (N); 12 <sub>a</sub> (O)	
584	21.2	$8^a$	$3^a$ (He I res. line)	0.10	$\sim 250$	22 <sub>a</sub> (N <sub>2</sub> ); 25 <sub>a</sub> (O <sub>2</sub> ); 12 <sub>a</sub> (N); 13 <sub>a</sub> (O)	
555/521/ 500	22.5/ 23.7/ 24.7	$5^a$	$1.3^a$ (lines, O II, IV; Si XII, C III)	0.05	$\sim 250$		Dominant cause of ionization and heating in F <sub>2</sub> region.
700/500	17.6/ 24.7	$2.8^a$	$7.8^a$ (all lines + continuum)	0.26	$\sim 250$	12 <sub>a</sub> (O), 22 <sub>a</sub> (N <sub>2</sub> ), 11 <sub>a</sub> (N), 12 <sub>a</sub> (O <sub>2</sub> )	
500-260 Å							
500/400	24.8/ 29.5	$7^a$	$1.5^a$ (all lines + continuum)	0.07	220	12 <sub>a</sub> (O), 15 <sub>a</sub> (N <sub>2</sub> ), 5 <sub>a</sub> (N); 20 <sub>a</sub> (O <sub>2</sub> )	Apparently modest contribu- tion to F-region ionization and heating. $\Phi_0(500/300)$ Å data un- certain by a factor of about 2.
370	33.5	$3^a$	$4.5^a$ (line, C III)	0.024	190	10 <sub>a</sub> (O), 13 <sub>a</sub> (N <sub>2</sub> ), 20 <sub>a</sub> (O <sub>2</sub> ), 2.6 <sub>a</sub> (N)	(Identification of specific solar emission lines as shown is tenta- tive except for He <sup>+</sup> Ly- $\alpha$ .)
360	34.5	$3^a$	$4.5^a$ (C III, N II, Ne II)	0.025	190	10 <sub>a</sub> (O), 12 <sub>a</sub> (N <sub>2</sub> ), 20 <sub>a</sub> (O <sub>2</sub> ), 5.7 <sub>a</sub> (N)	
335	37.0	$4.3^a$	$8^a$ (line, N IV?)	0.047	190	8.5 <sub>a</sub> (O), 10 <sub>a</sub> (N <sub>2</sub> ), 17 <sub>a</sub> (O <sub>2</sub> ), 4.3 <sub>a</sub> (N)	
323/310	39.5	$2^a$	$4^a$	0.026	180	7.8 <sub>a</sub> (O), 6 <sub>a</sub> (N <sub>2</sub> ), 15 <sub>a</sub> (O <sub>2</sub> ), 3.5 <sub>a</sub> (N)	
304	41.0	$2.1^a$	$4^a$ (He <sup>+</sup> Ly- $\alpha$ )	0.25	180	10 <sub>a</sub> (O), 4 <sub>a</sub> (N <sub>2</sub> ), 20 <sub>a</sub> (O <sub>2</sub> ), 2.9 <sub>a</sub> (N)	First detected photographi- cally in 1958 [Violet and Rense, 1959] and photoelectrically in 1959 [Hinteregger, 1960a, b].
285/282	43.5	$5^a$	$8^a$ (lines, N IV, Ne III?)	0.05	160	8.5 <sub>a</sub> (O), 5 <sub>a</sub> (N <sub>2</sub> ), 17 <sub>a</sub> (O <sub>2</sub> ), 2.3 <sub>a</sub> (N)	Major source of heating and ionization in F <sub>1</sub> region.
280/260	45.0/ 47.5	$5^a$	$7.5^a$ (lines, O II, III, IV; N V; C IV)	0.045	155	7.5 <sub>a</sub> -8.0 <sub>a</sub> (O); 6 <sub>a</sub> -7 <sub>a</sub> (N <sub>2</sub> ); 15 <sub>a</sub> -16 <sub>a</sub> (O <sub>2</sub> ); 1.9 <sub>a</sub> -2.2 <sub>a</sub> (N)	
400/260		$4.3^a$	$7.7^a$ (all lines + continuum estimated)	0.467			
260-60 Å							
259/228	47.5/ 54.5		$1.5^a$ (lines, including He I Ly- $\beta$ + continuum)	0.12	$\sim 150$	5 <sub>a</sub> (N <sub>2</sub> ); 15 <sub>a</sub> (O <sub>2</sub> ); 7.5 <sub>a</sub> (O)	Estimated error of a factor of 3.
228/166	54.5/ 74.0		$5^a$ (lines + continuum)	0.5	$\sim 140$	1 <sub>a</sub> -5 <sub>a</sub> (N <sub>2</sub> ); 5 <sub>a</sub> -10 <sub>a</sub> (O <sub>2</sub> )	Same source of data; esti- mated error of a factor of 4.
260/166	47.5/ 74.0		$\sim 6.5^a$ (lines + continuum)	0.65	140-150	(Probably more than one ion-electron pair per ab- sorbed photon)	Important source of E- and F <sub>1</sub> -region ionization; may be in error by as much as a factor of 4 (listed values are more likely to be too high than too low).
166/105	74/ 120		$\sim 5^a?$	$\sim 0.07?$	$\sim 135$	0.3 <sub>a</sub> -1 <sub>a</sub> (N <sub>2</sub> ); 2 <sub>a</sub> -5 <sub>a</sub> (O <sub>2</sub> )	Least accurate estimate from 1/29/60 GRD experiment (fac- tor of 10).
105/60	120/ 205		$\sim 1.5^a$	$\sim 0.35$	$\sim 110$	Probably up to about 6 ion pairs per absorbed photon	Important source of E-region ionization; error in $\Phi_0$ (from GRD data) estimated as high as factor of 5.

Note: All flux data in the section of the table between double rules are based on extrapolated assumed calibration factors ( $\lambda < 300$  Å) for GRD rocket monochromator flown on January 29, 1960, near noon from White Sands, New Mexico. Therefore the experimental accuracy of these data remains undetermined. The experiment was performed under normal solar conditions (compare with summary that follows).

Summary Reference for  $\lambda < 200$  Å

$\lambda$ or $\lambda_1/\lambda_2$ , Å	$h\nu$ , ev	Estimated for Top of Atmosphere August 1960		$h^*$ Estimated, $\Phi^* = \Phi_0/e$ , $\cos Z = 1$ , km	Number of Ion Pairs per Absorbed Photon	Solar Activity	Remarks
		$\Phi_0$ , ph/cm <sup>2</sup> sec	$I_0$ , erg/cm <sup>2</sup> sec				
200/44	61/280	$5^a-5^a$ up to $5^a$	0.1-1 up to 9	$< 140$	$\sim 2$ to 10	Normal Flares (class 2+)	From NRL photoionization mea- surements with different fillers and assum- ing gray body radiation of $T \sim 5-7 \times 10^4$ deg K [Kreplin].
60/44	205/280	$5^a-5^a$ up to $5^a$	0.02-0.17 up to 1.7	$< 100$	$\sim 6$ to 10	Normal Flares	Same source of data; $T \sim 5 \times 10^4$ deg K.
105/60	120/205	$\sim 1.5^a$	$\sim 0.35$	$\sim 110$	$\sim 4$ to 6	Normal	GRD 1/29/60 experiment (see above).
20-8	620/520	$4^a-2^a$ up to $1^a$	$4^a-2^a$ up to $> 0.9$	85-105	$\sim 20$ to 50	Normal Flares	NRL data with $T \sim 2 \times 10^4$ deg K [Kreplin].
$< 8$	$> 1500$	$< 1^a$ up to $> 2^a$	$\sim 1^a$ up to $> 0.2$	$< 90$	$> 50$	Normal Flares	NRL data 1949/60 (enhances D- region ionization during flares).

TABLE 17

## COMPOSITION AND ENERGY SPECTRUM OF COSMIC RAYS

Charge (Z)	Range of Validity ( $E_t$ in Bev per nucleon)	Integral Spectrum (particles/sq meter-sec-ster)	
		Best Value	Extreme Limits of Exponent
1	2 - 20	$4000E_t - 1.15$	$1.05 - 1.25^*$
2	1.5 - 8	$450E_t - 1.6$	$1.3 - 1.7$
3, 4, 5	---	$\approx 50\%$ of C, N, O, F flux	
6, 7, 8, 9	3 - 8	$24E_t - 1.6$	$1.45 - 1.75$
$\geq 10$	3 - 8	$16E_t - 2.0$	$1.85 - 2.25$

\* Slope increases up to 1.8 at higher energies

$$P(> E_t) = CE_t^{-1.5} / \text{sq meter-sec-ster} \quad (\text{Low energies})$$

protons	$C = 3800$
alpha	370
Li, Be, B	$\leq 14$
C, N, O, F	21
$Z \geq 10$	10

TABLE 18  
METEOR STREAMS

Shower	Date of Maximum	Limits	Radiant		Ve- locity (km/sec)	Maximum Hourly Radar Echo Rate
			R.A. (°)	Dec. (°)		
Quadrantids	Jan 3	Jan 1-Jan 4	230	+48	42.7	95
Virginids	Mar 13	Mar 5-Mar 21	183	+ 4	30.8	<5
Lyrids	Apr 21	Apr 20-Apr 23	270	+33	48.4	11
$\eta$ Aquarids	May 4	May 2-May 6	336	+ 0	64	15
Daytime Arietids	June 8	May 29-June 18	44	+23	39	66
Daytime $\xi$ Perseids	June 9	June 1-June 16	62	+23	29	42
Sagittarids	June 11		304	-35		30
Daytime $\beta$ Taurids	June 30	June 24-July 6	86	+19	32	27
Phoenicids	July 14		32	-48		30
Southern $\delta$ Aquarids	July 30	July 21-Aug 15	339	-17	43.0}	34
Northern $\delta$ Aquarids		July 14-Aug 19	339*	- 5	42.3}	
Southern $\iota$ Aquarids		July 16-Aug. 25	338	-14	35.8	
Northern $\iota$ Aquarids		July 16-Aug 25	331	- 5	31.2	
$\alpha$ Capricornids	Aug 1	July 17-Aug 21	309	-10	25.5	10
Perseids	Aug 12	July 29-Aug 17	46	+58	60.4	49
$\kappa$ Cygnids		Aug 19-Aug 22	289	+56	26.6	<5
Draconids	Oct 10	Oct 10	264	+54	23.1	Periodic
Orionids	Oct 22	Oct 18-Oct 26	94	+16	66.5	18
Southern Taurids	Nov 1	Sept. 15-Dec 15	51	+14	30.2}	<15
Northern Taurids	Nov 1	Oct 17-Dec 2	52	+21	31.3}	
Andromedids	Nov 7	Nov 7	22	+27	21.3	<5
Leonids	Nov 17	Nov 14-Nov 20	152	+22	72.0	<10
Puppids/Velids	Dec 6	Dec 1-Dec 9	140	-50		50
Geminids	Dec 14	Dec 7-Dec 15	113	+32	36.5	80
$\chi$ Orionids		Dec 9-Dec 14	87	+21	30.6	
Monocerotids		Dec 13-Dec 15	103	+ 8	44.0	
Ursids	Dec 22	Dec 17-Dec 24	206	+80	35.2	13

TABLE 19

## PARAMETERS OF MICROMETEORIDS

Visual Magni- tude	Mass (g)	Radius ( $\mu$ )	Ve- locity (km/sec)	Kinetic Energy (ergs)	No. Striking 3-m Sphere per Day	Flux (particle/ cm <sup>2</sup> -sec)
0	25.0	49,200	28	$1.0 \times 10^{14}$		
1	9.95	36,200	28	$3.98 \times 10^{13}$		
2	3.96	26,600	28	$1.58 \times 10^{13}$		
3	1.58	19,600	28	$6.31 \times 10^{12}$		
4	0.628	14,400	28	$2.51 \times 10^{12}$		
5	0.250	10,600	28	$1.00 \times 10^{12}$	$2.22 \times 10^{-5}$	$1.83 \times 10^{-15}$
6	$9.95 \times 10^{-2}$	7,800	28	$3.98 \times 10^{11}$	$6.48 \times 10^{-5}$	$5.34 \times 10^{-15}$
7	$3.96 \times 10^{-2}$	5,740	28	$1.58 \times 10^{11}$	$1.63 \times 10^{-4}$	$1.34 \times 10^{-14}$
8	$1.58 \times 10^{-2}$	4,220	27	$5.87 \times 10^{10}$	$4.09 \times 10^{-4}$	$3.36 \times 10^{-14}$
9	$6.28 \times 10^{-3}$	3,110	26	$2.17 \times 10^{10}$	$1.03 \times 10^{-3}$	$8.49 \times 10^{-14}$
10	$2.50 \times 10^{-3}$	2,290	25	$7.97 \times 10^9$	$2.58 \times 10^{-3}$	$2.12 \times 10^{-13}$
11	$9.95 \times 10^{-4}$	1,680	24	$2.93 \times 10^9$	$6.48 \times 10^{-3}$	$5.34 \times 10^{-13}$
12	$3.96 \times 10^{-4}$	1,240	23	$1.07 \times 10^9$	$1.63 \times 10^{-2}$	$1.34 \times 10^{-12}$
13	$1.58 \times 10^{-4}$	910	22	$3.89 \times 10^8$	$4.09 \times 10^{-2}$	$3.36 \times 10^{-12}$
14	$6.28 \times 10^{-5}$	669	21	$1.41 \times 10^8$	$1.03 \times 10^{-1}$	$8.49 \times 10^{-12}$
15	$2.50 \times 10^{-5}$	492	20	$5.10 \times 10^7$	$2.58 \times 10^{-1}$	$2.12 \times 10^{-11}$
16	$9.95 \times 10^{-6}$	362	19	$1.83 \times 10^7$	$6.48 \times 10^{-1}$	$5.34 \times 10^{-11}$
17	$3.96 \times 10^{-6}$	266	18	$6.55 \times 10^6$	1.63	$1.34 \times 10^{-10}$
18	$1.58 \times 10^{-6}$	196	17	$2.33 \times 10^6$	4.09	$3.36 \times 10^{-10}$
19	$6.28 \times 10^{-7}$	144	16	$8.20 \times 10^5$	$1.03 \times 10$	$8.49 \times 10^{-10}$
20	$2.50 \times 10^{-7}$	106	15	$2.87 \times 10^5$	$2.58 \times 10$	$2.12 \times 10^{-9}$
21	$9.95 \times 10^{-8}$	78.0	15	$1.14 \times 10^5$	$6.48 \times 10$	$5.34 \times 10^{-9}$
22	$3.96 \times 10^{-8}$	57.4	15	$4.55 \times 10^4$	$1.63 \times 10^2$	$1.34 \times 10^{-8}$
23	$1.58 \times 10^{-8}$	39.8 <sup>a</sup>	15	$1.81 \times 10^4$	$4.09 \times 10^2$	$3.36 \times 10^{-8}$
24	$6.28 \times 10^{-9}$	25.1 <sup>a</sup>	15	$7.21 \times 10^3$	$1.03 \times 10^3$	$8.49 \times 10^{-8}$
25	$2.50 \times 10^{-9}$	15.8 <sup>a</sup>	15	$2.87 \times 10^3$	$2.58 \times 10^3$	$2.12 \times 10^{-7}$
26	$9.95 \times 10^{-10}$	10.0 <sup>a</sup>	15	$1.14 \times 10^3$	$6.48 \times 10^3$	$5.34 \times 10^{-7}$
27	$3.96 \times 10^{-10}$	6.30 <sup>a</sup>	15	$4.55 \times 10^2$	$1.63 \times 10^4$	$1.34 \times 10^{-6}$
28	$1.58 \times 10^{-10}$	3.98 <sup>a</sup>	15	$1.81 \times 10^2$	$4.09 \times 10^4$	$3.35 \times 10^{-6}$
29	$6.28 \times 10^{-11}$	2.51 <sup>a</sup>	15	$7.21 \times 10$	$1.03 \times 10^5$	$8.49 \times 10^{-6}$
30	$2.50 \times 10^{-11}$	1.58 <sup>a</sup>	15	$2.87 \times 10$	$2.58 \times 10^5$	$2.12 \times 10^{-5}$
31	$9.95 \times 10^{-12}$	1.00 <sup>a</sup>	15	$1.14 \times 10$	$6.48 \times 10^5$	$5.34 \times 10^{-5}$

<sup>a</sup> Maximum radius permitted by solar light pressure.

TABLE 20

Direct Measurements Obtained with Microphone Systems on the U. S. Satellites and Space Probes

Spacecraft	Momentum Sensitivity (dyne seconds)	Mass Sensitivity (grams)	Effective Area (meter <sup>2</sup> )	Exposure Time (seconds)	Exposure (m <sup>2</sup> sec)	Number of Particles	Cumulative Influx Rate (particles/m <sup>2</sup> /sec)	
							Observed	Corrected for Earth Shielding
EXPLORER I	$> 2.5 \times 10^{-3}$	$8.3 \times 10^{-10}$	$2.3 \times 10^{-1}$	$7.9 \times 10^4$	$1.8 \times 10^4$	145	$8.4 \times 10^{-3}$	$1.7 \times 10^{-2}$
PIONEER I	$> 1.5 \times 10^{-4}$	$5.0 \times 10^{-11}$	$3.9 \times 10^{-2}$	$1.1 \times 10^5$	$4.2 \times 10^3$	25 (18)	$4.3 \times 10^{-3}$	$4.3 \times 10^{-3}$
VANGUARD III	$> 1.0 \times 10^{-2}$	$3.3 \times 10^{-9}$	$4.0 \times 10^{-1}$	$\sim 6 \times 10^6$	$2.4 \times 10^6$	$\sim 3500$	$1.3 \times 10^{-3}$	$2.0 \times 10^{-3}$

TABLE 21

Direct Measurements Obtained with Microphone Systems on the Soviet Satellites and Space Probes

Spacecraft	Mass Sensitivity (grams)		Effective Area (meter <sup>2</sup> )	Exposure Time (seconds)	Exposure (m <sup>2</sup> sec)	Number of Particles	Cumulative Influx Rate (particles/m <sup>2</sup> /sec)
	$\bar{V}_C = 40 \text{ Km/sec}$	$\bar{V}_C = 30 \text{ Km/sec}$					
SPUTNIK III	$8.0 \times 10^{-9} - 2.7 \times 10^{-8}$ $2.7 \times 10^{-8} - 1.5 \times 10^{-7}$ $1.5 \times 10^{-7} - 5.6 \times 10^{-6}$ $> 5.6 \times 10^{-6}$	$1.4 \times 10^{-8} - 4.8 \times 10^{-8}$ $4.8 \times 10^{-8} - 2.7 \times 10^{-7}$ $2.7 \times 10^{-7} - 1.0 \times 10^{-5}$ $> 1.0 \times 10^{-5}$	0.34	$\sim 8 \times 10^5$	$\sim 3 \times 10^5$	?	$< 1 \times 10^{-4}$
SPACE ROCKET I	$2.5 \times 10^{-9} - 1.5 \times 10^{-8}$ $1.5 \times 10^{-8} - 2.0 \times 10^{-7}$ $> 2.0 \times 10^{-7}$	$4.4 \times 10^{-9} - 2.7 \times 10^{-8}$ $2.7 \times 10^{-8} - 3.6 \times 10^{-7}$ $> 3.6 \times 10^{-7}$	0.2	$3.6 \times 10^4$	$7.2 \times 10^3$	$< 16$ $< 4$ $< 1$	$< 2.9 \times 10^{-3}$ $< 7.0 \times 10^{-4}$ $< 1.4 \times 10^{-4}$
SPACE ROCKET II	$2.0 \times 10^{-9} - 6.0 \times 10^{-9}$ $6.0 \times 10^{-9} - 1.5 \times 10^{-8}$ $> 1.5 \times 10^{-8}$	$3.6 \times 10^{-9} - 1.1 \times 10^{-8}$ $1.1 \times 10^{-8} - 2.7 \times 10^{-8}$ $> 2.7 \times 10^{-8}$	0.2	$1.1 \times 10^5$	$2.2 \times 10^4$	0 0 2	$9.1 \times 10^{-5}$
INTERPLANETARY STATION	$1.0 \times 10^{-9} - 3.0 \times 10^{-9}$ $3.0 \times 10^{-9} - 8.0 \times 10^{-9}$ $> 8.0 \times 10^{-9}$	$1.8 \times 10^{-9} - 5.3 \times 10^{-9}$ $5.3 \times 10^{-9} - 1.4 \times 10^{-8}$ $> 1.4 \times 10^{-8}$	0.1	$2.3 \times 10^4$	$2.3 \times 10^3$	1 5 1	$3.0 \times 10^{-3}$ $2.6 \times 10^{-3}$ $4.3 \times 10^{-4}$

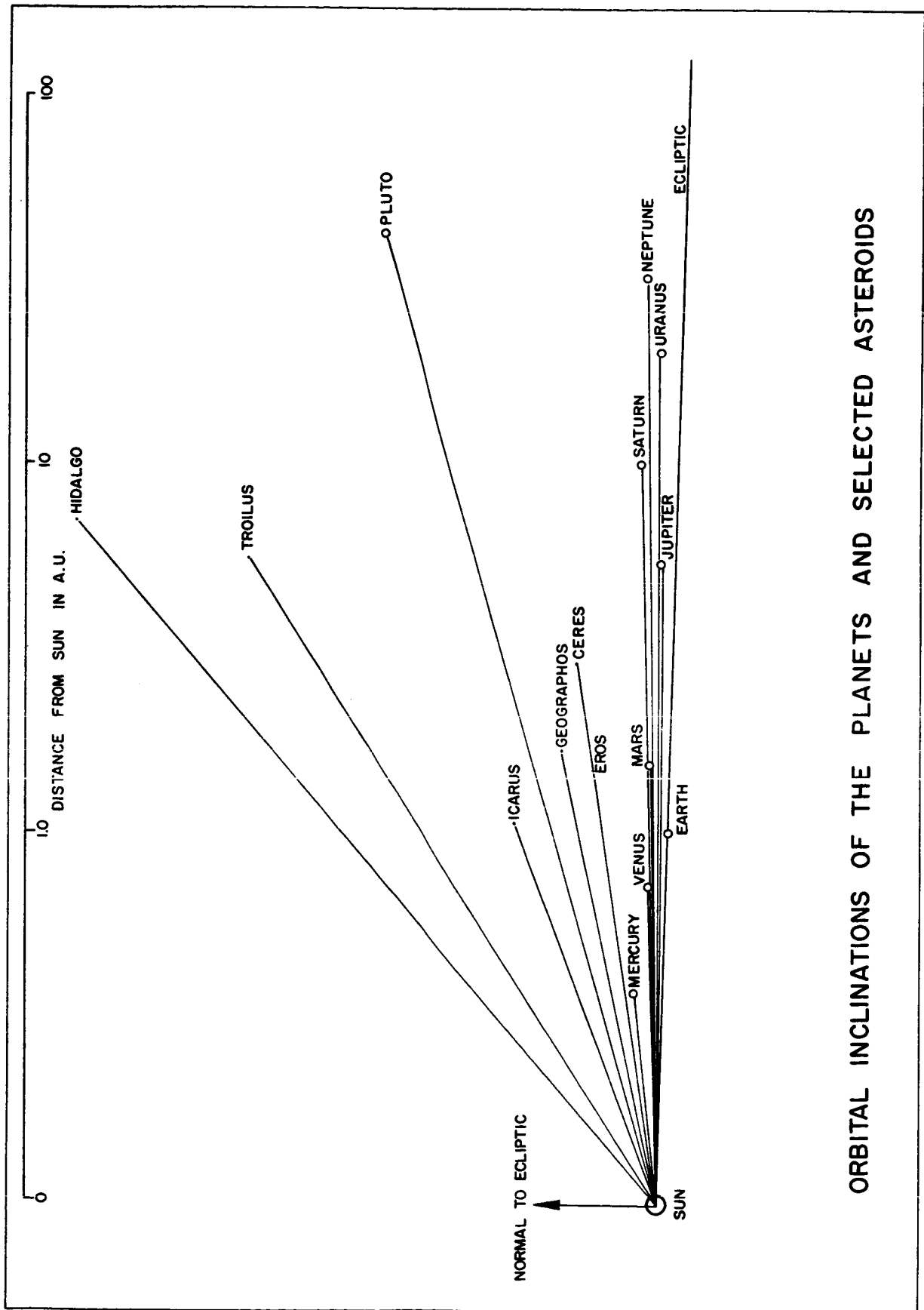


Figure 1

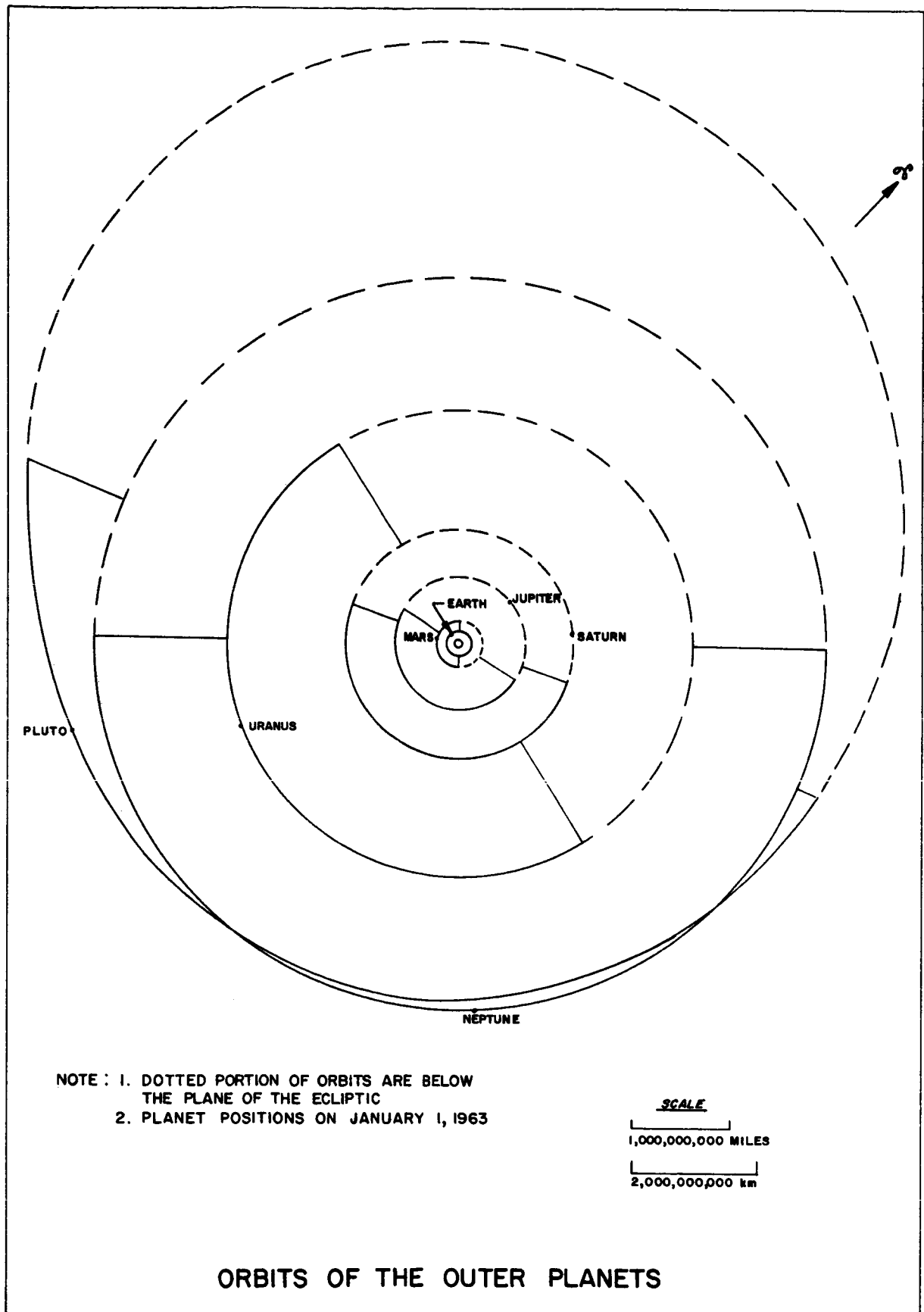


Figure 2

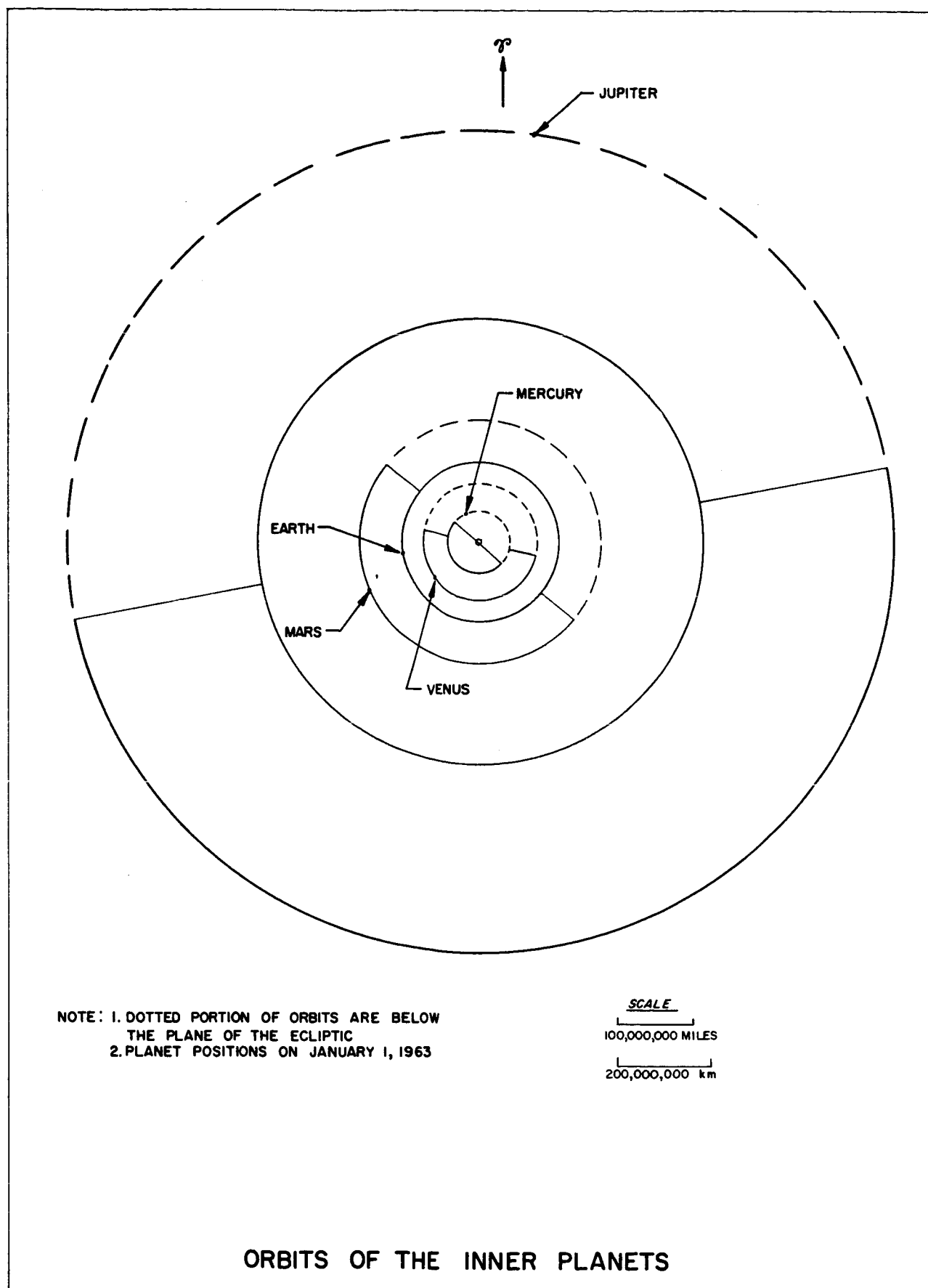


Figure 3

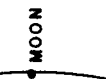


PLANET

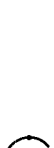
NEAR SATELLITES

FAR SATELLITES

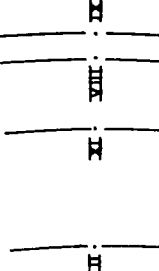
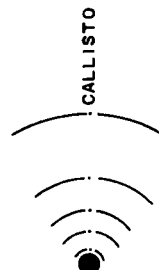
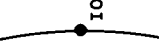
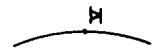
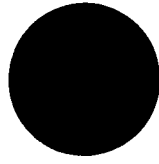
EARTH



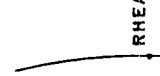
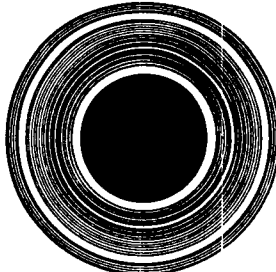
MARS



JUPITER



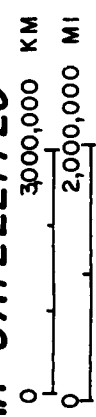
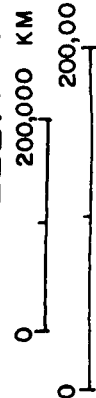
SATURN



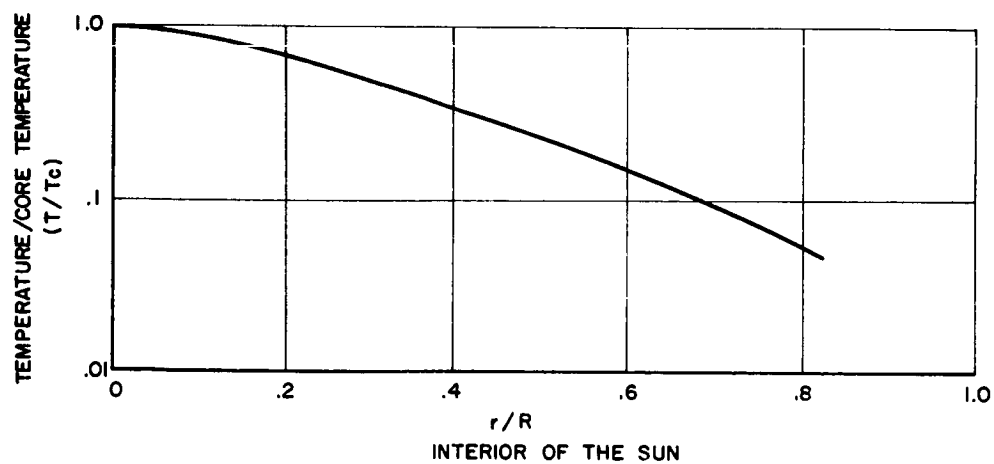
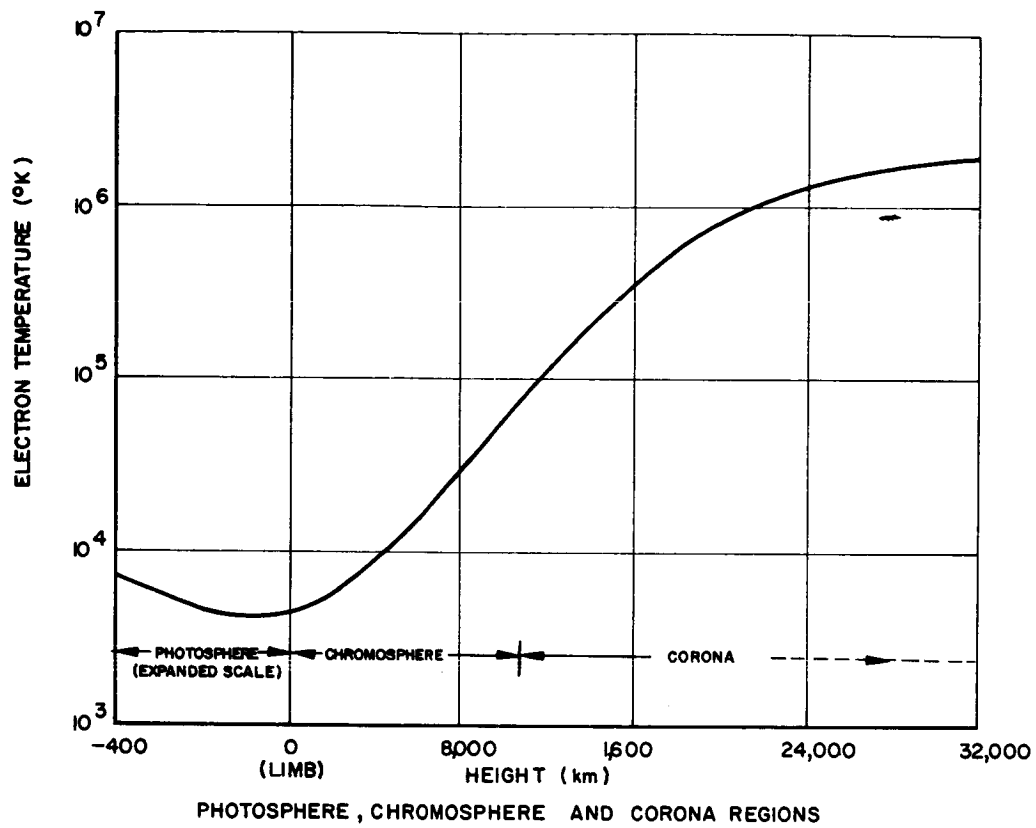
URANUS



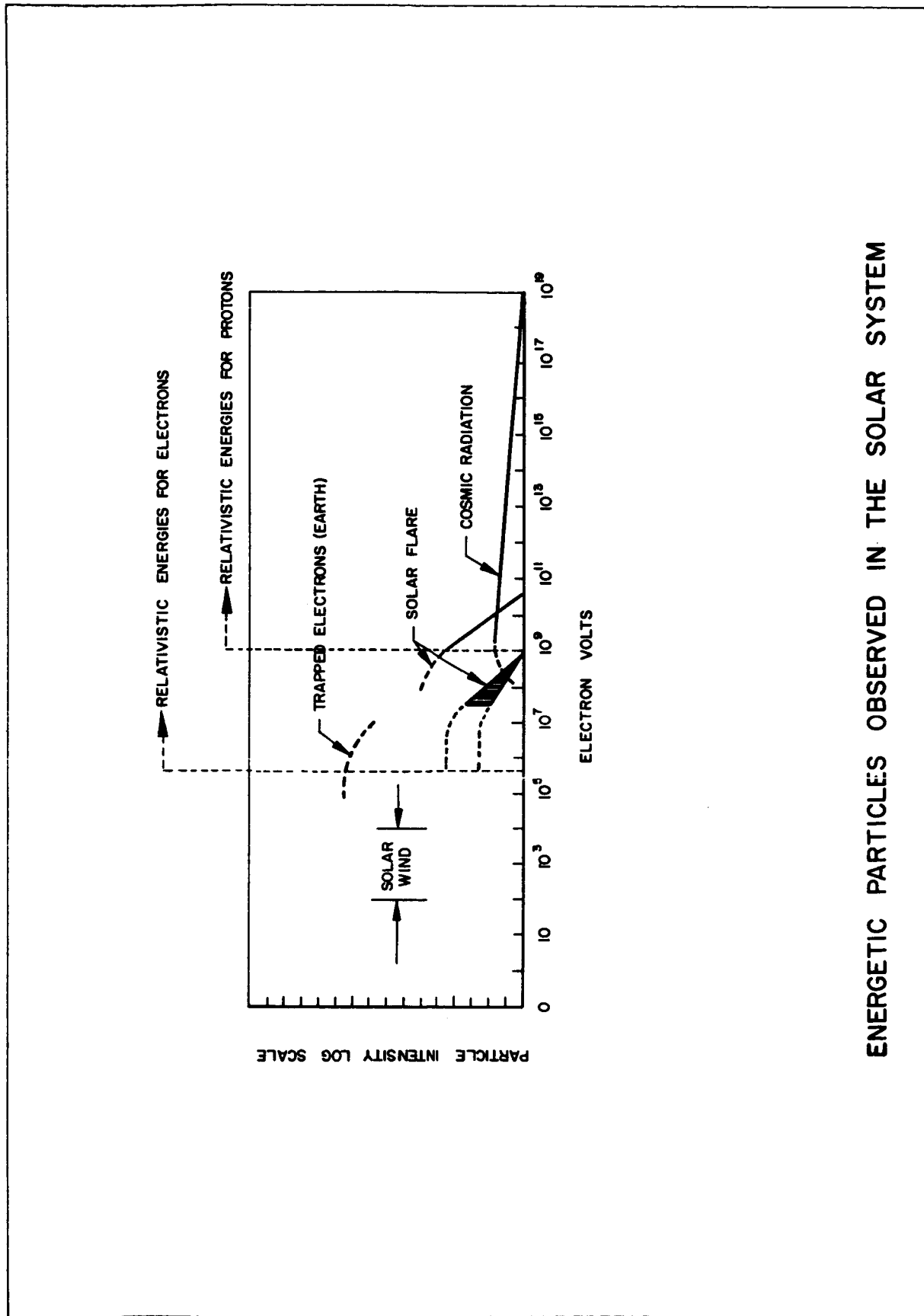
NEPTUNE



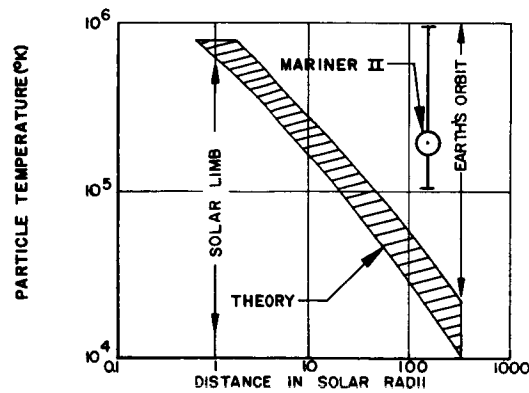
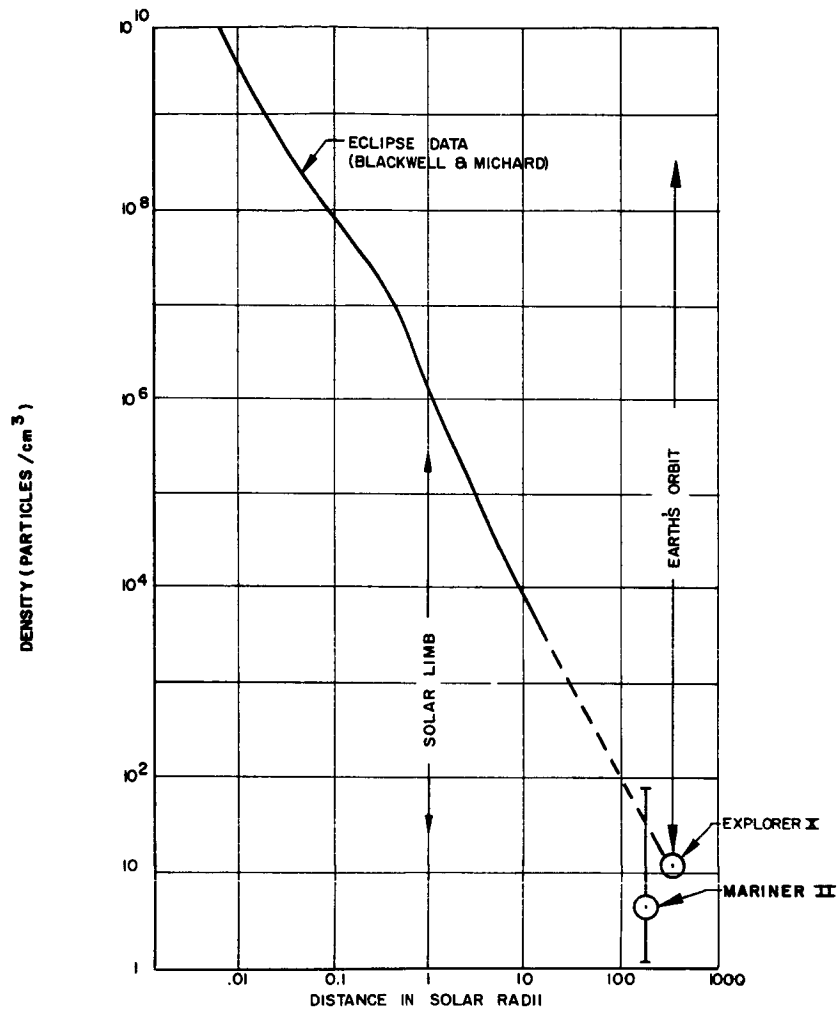
PLANETARY SATELLITES



SOLAR TEMPERATURE DISTRIBUTION



ENERGETIC PARTICLES OBSERVED IN THE SOLAR SYSTEM



ELECTRON DENSITY AND TEMPERATURE IN SPACE

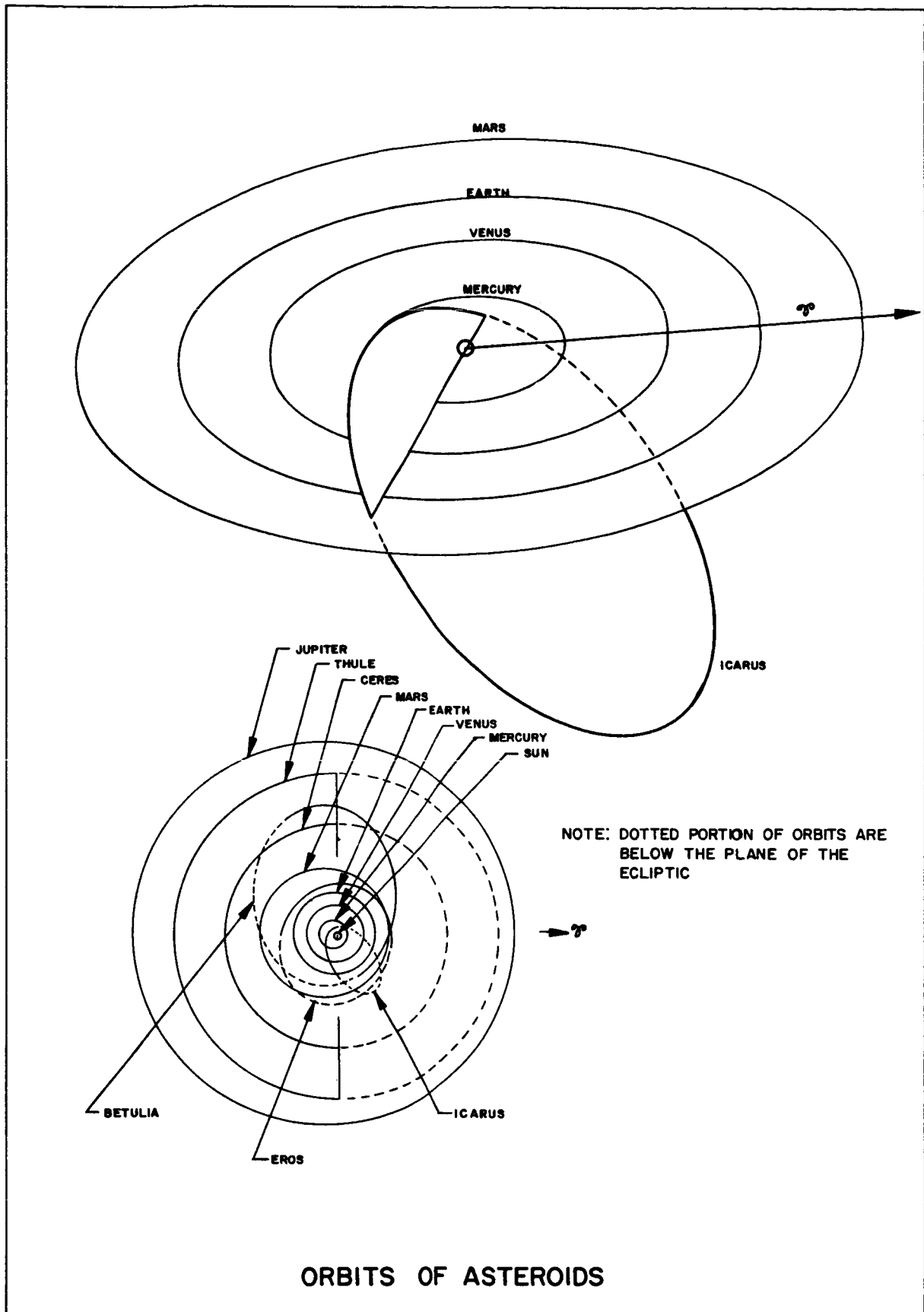


Figure 8

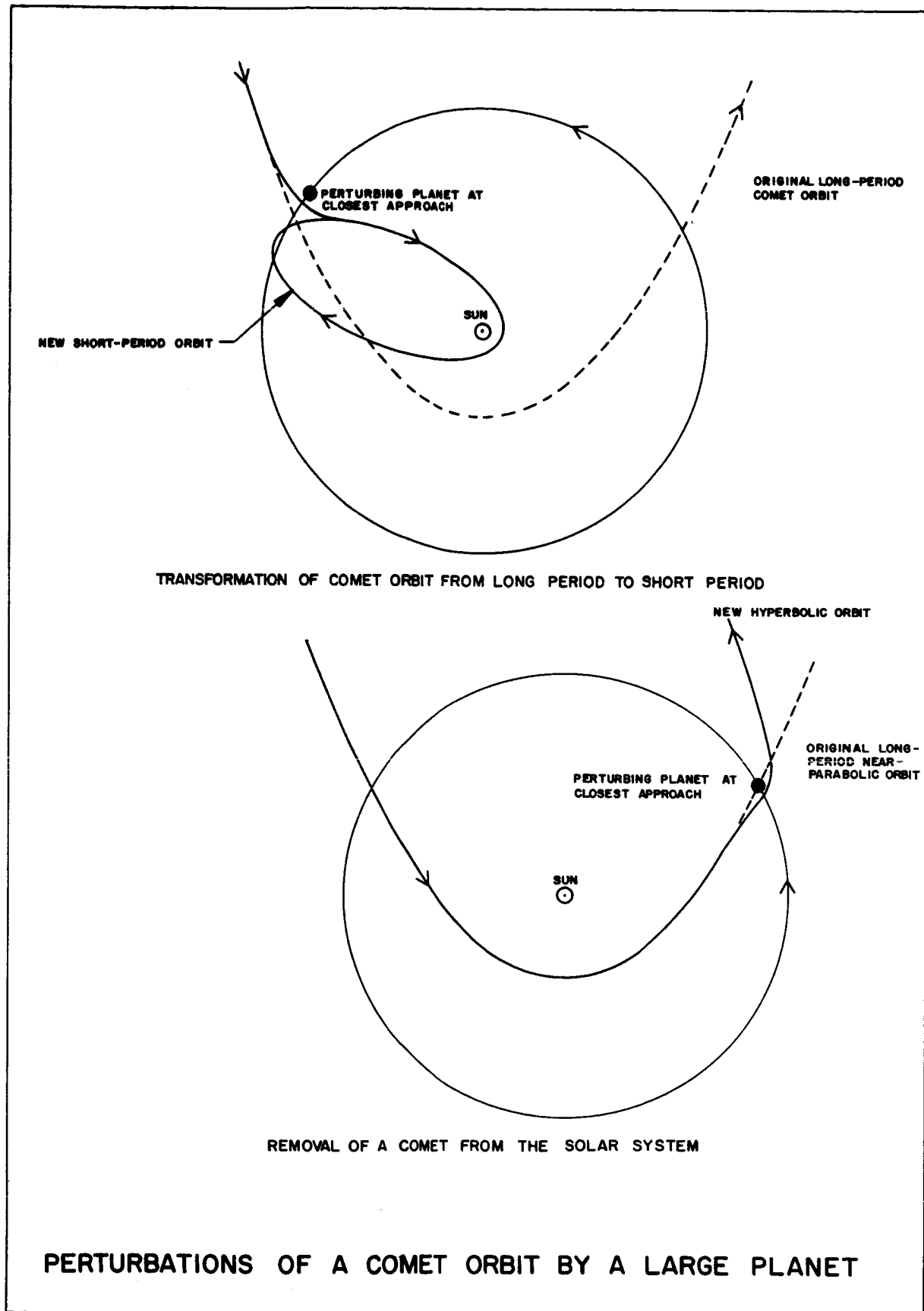
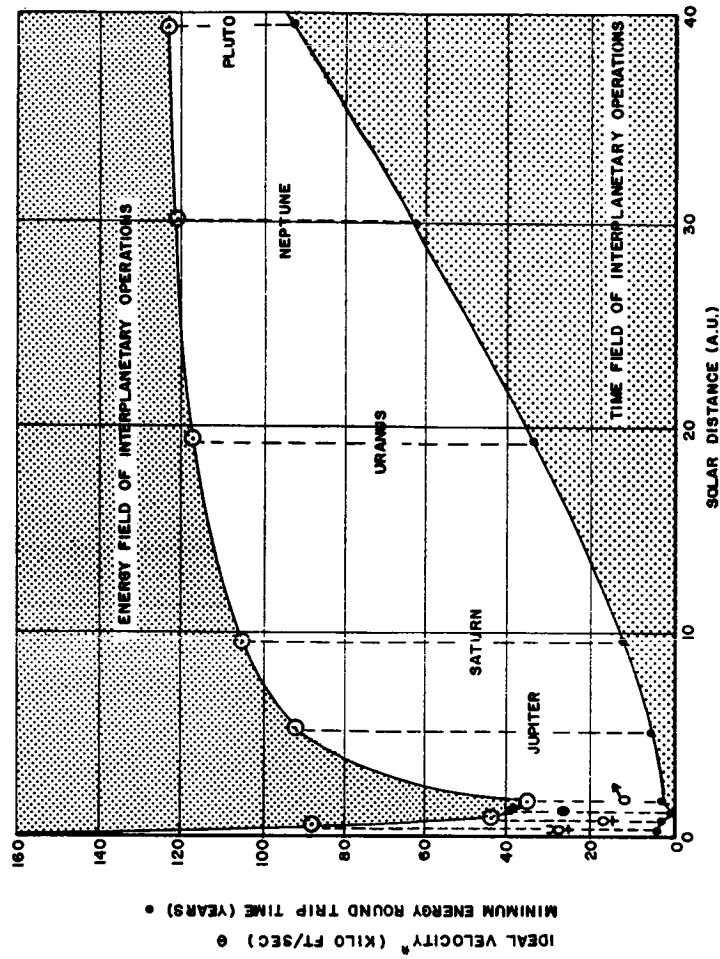


Figure 9

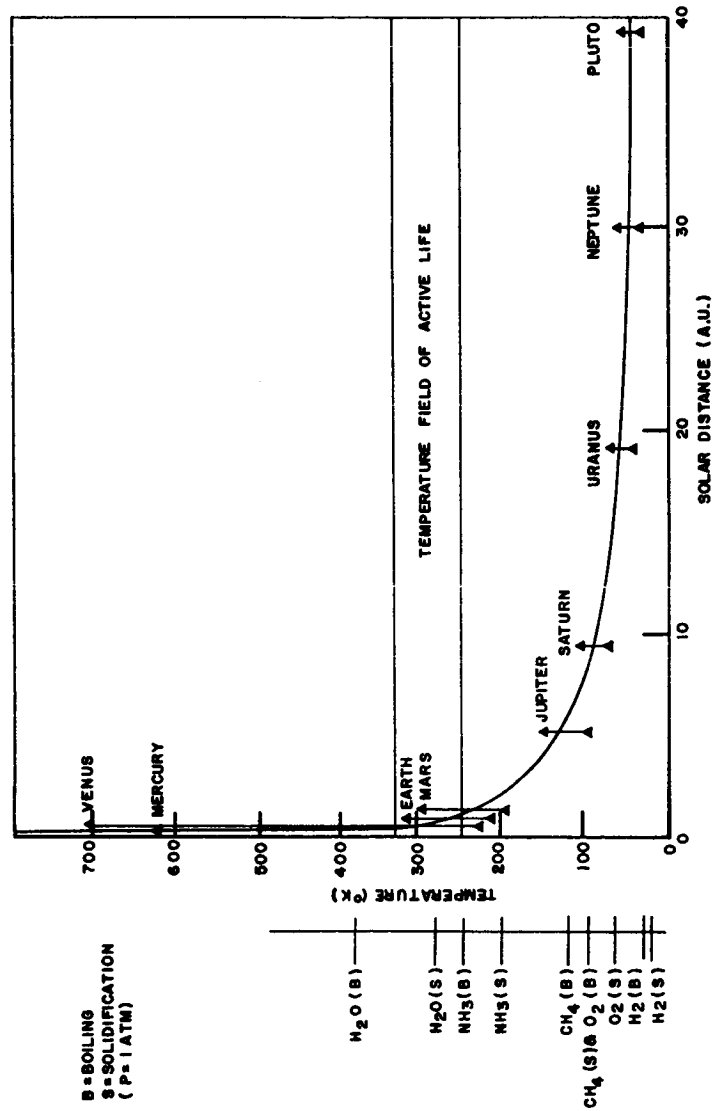


\* THE VELOCITY WHICH BURN-OUT STAGE WOULD ATTAIN IF IT USED UP ALL ENERGY REQUIRED FOR THE ROUND TRIP IN ONE IMPULSE BURST

LEGEND  
 MERCURY  
 VENUS  
 EARTH  
 MARS

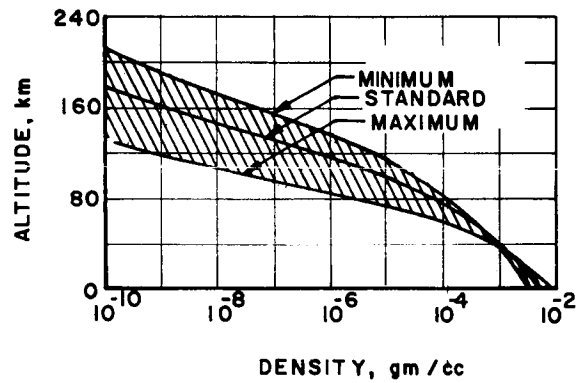
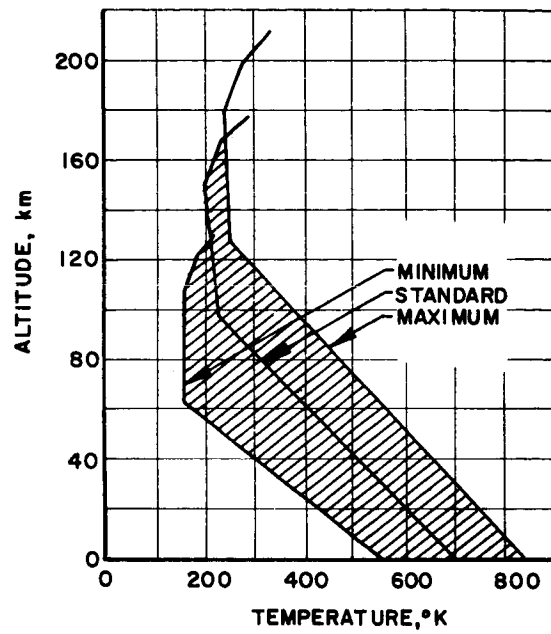
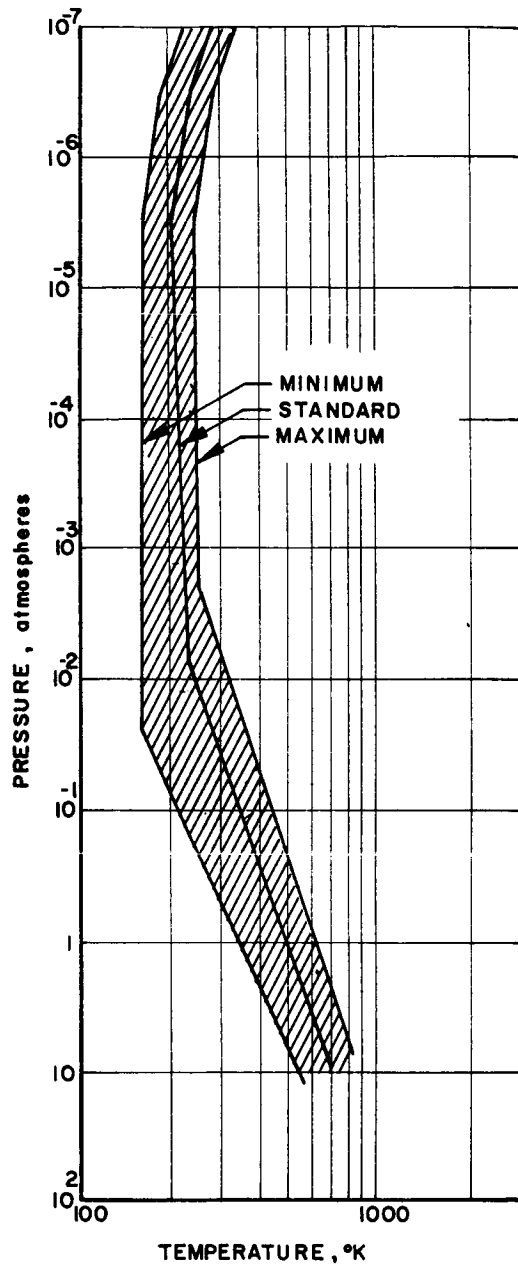
## TIME AND VELOCITY REQUIRED FOR SPACE MISSIONS

Figure 10



PLANETARY TEMPERATURES





VENUSIAN MODEL ATMOSPHERE

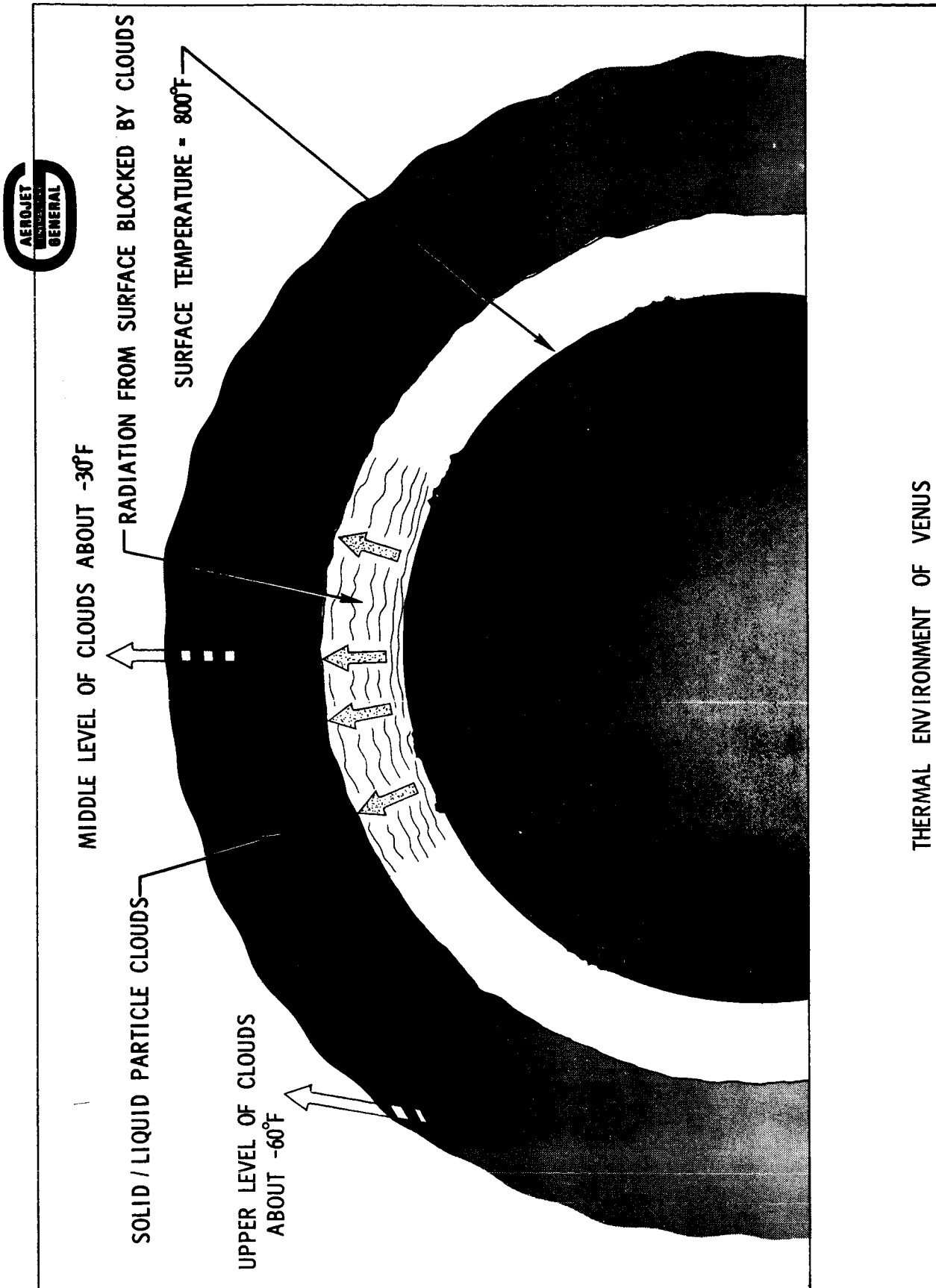


Figure 13

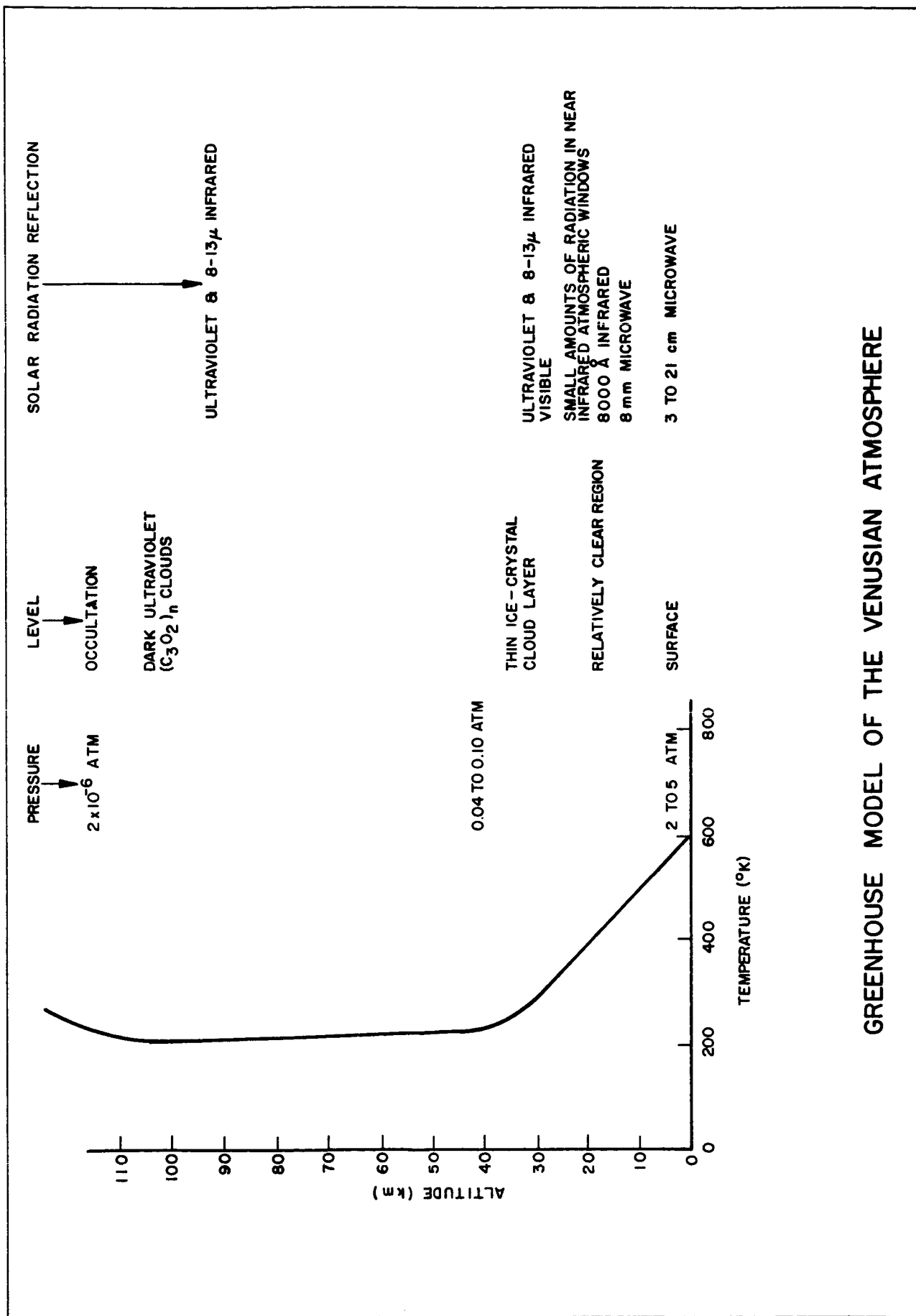
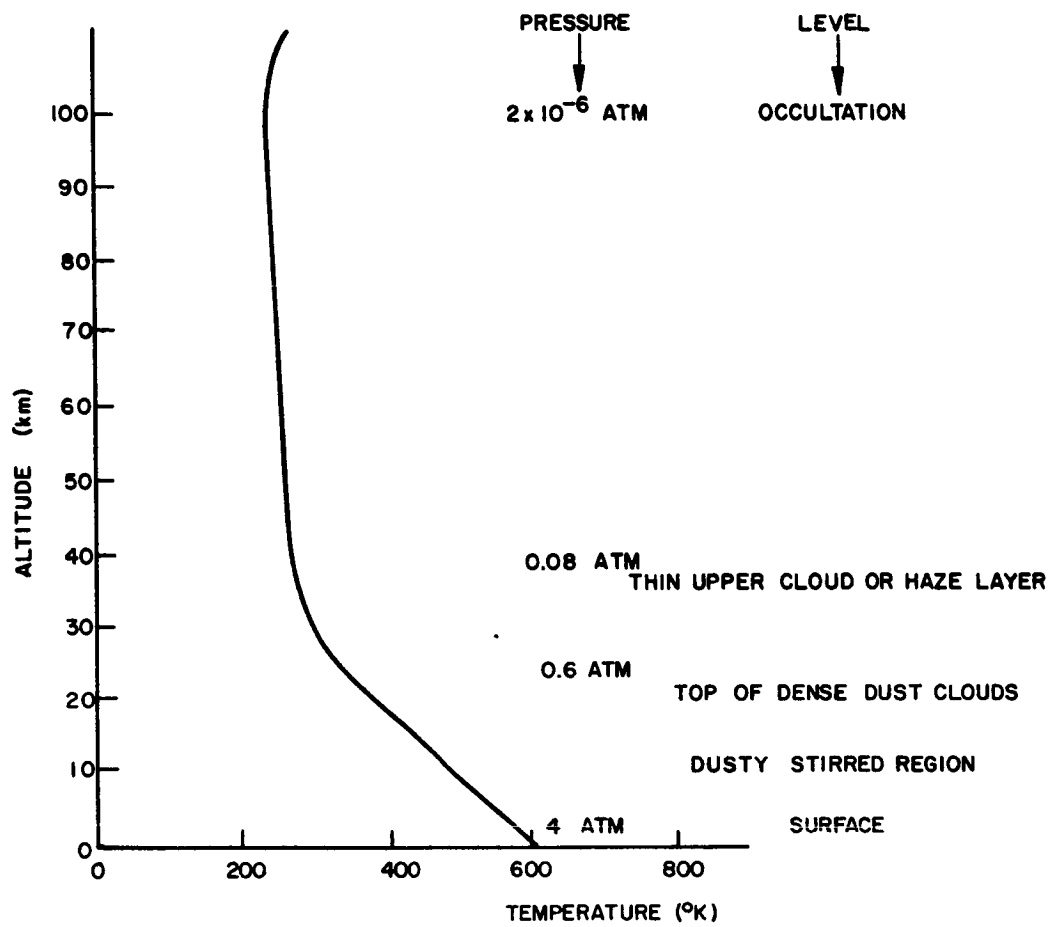
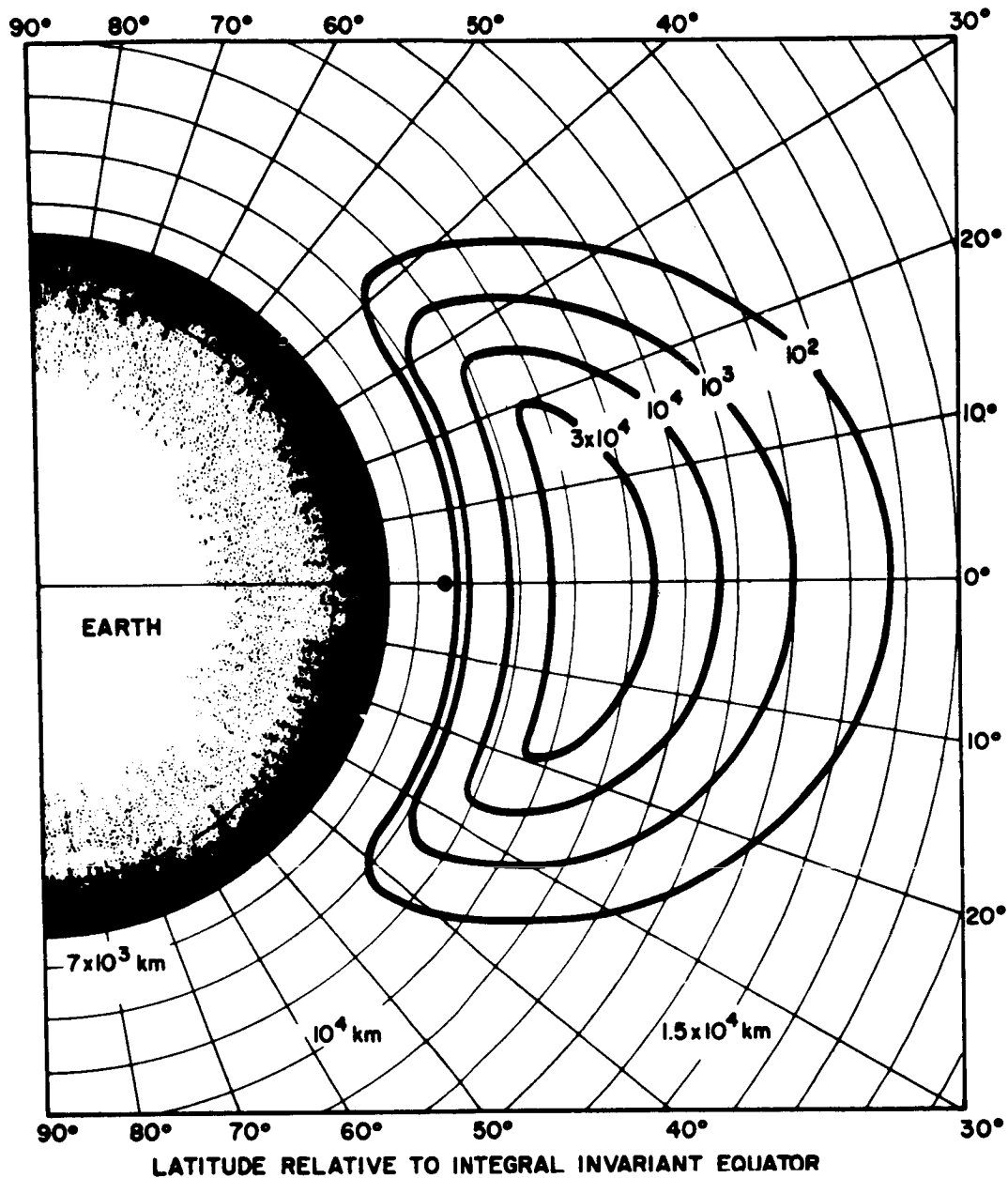


Figure 14



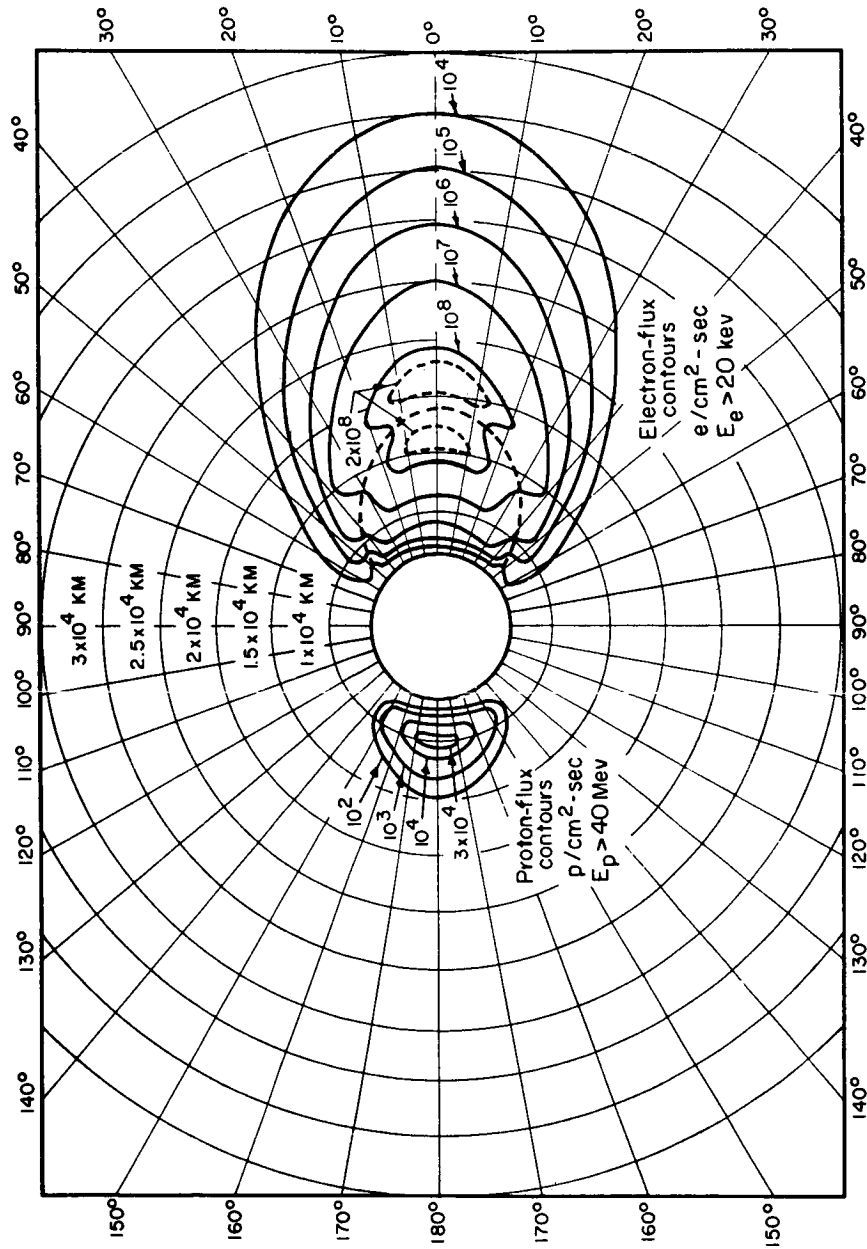
# AEOLOSHERE MODEL OF THE VENUSIAN ATMOSPHERE



PROTON BELT (INNER ZONE) OF THE VAN ALLEN RADIATION

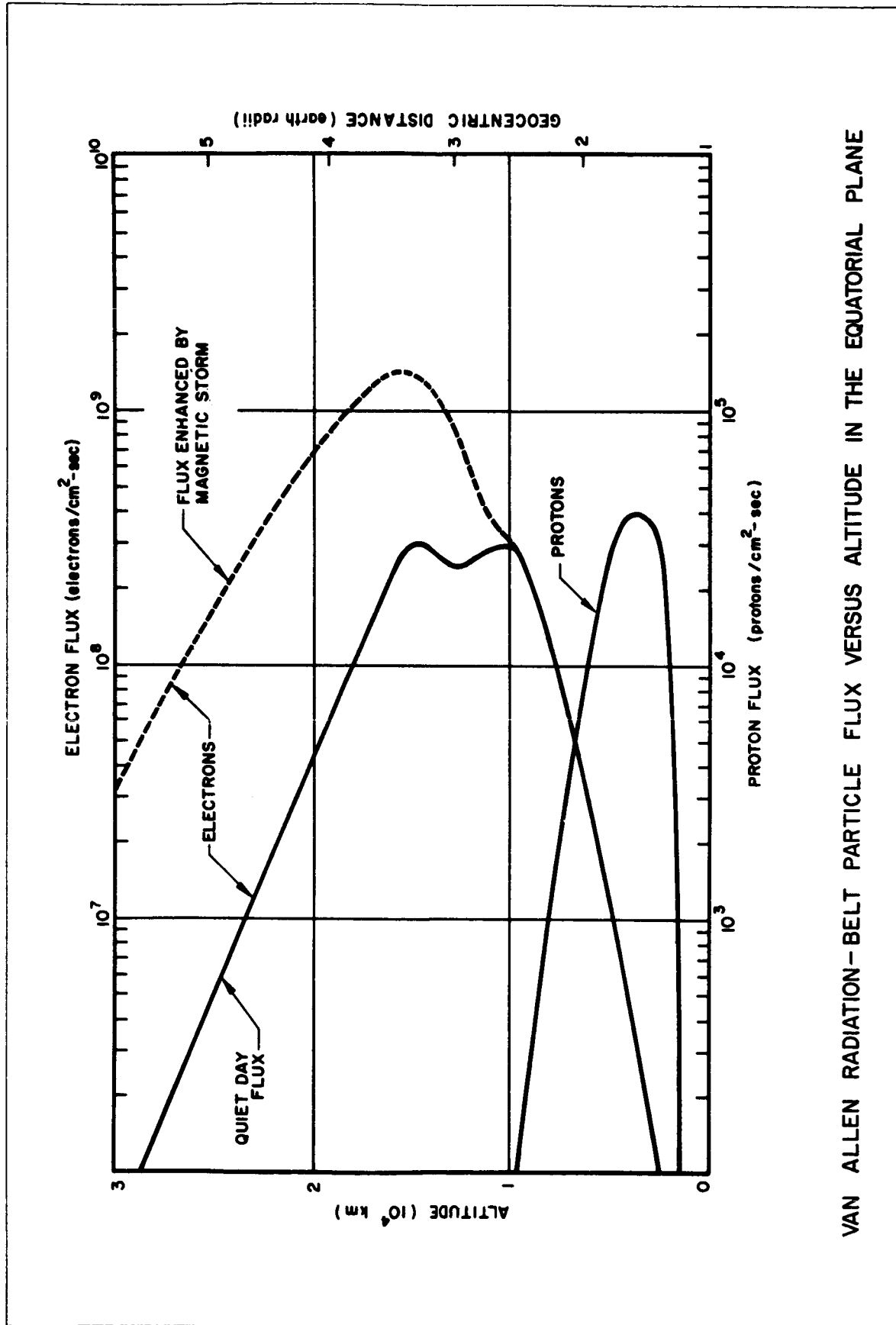
The numbers identify flux contours of protons with energies greater than 40 Mev in protons/cm<sup>2</sup>-sec. The dot at the lower edge of the belt is to be put at the altitudes indicated in Fig. 22a to take into account the variations in the altitude and latitude of the belt as a function of longitude. As shown, the altitude of the belt is appropriate for 210° E longitude.

Reproduced by permission of the Stanford University Press from Satellite Environment Handbook, ed. Francis S. Johnson, copyright 1961 by Lockheed Aircraft Corp.

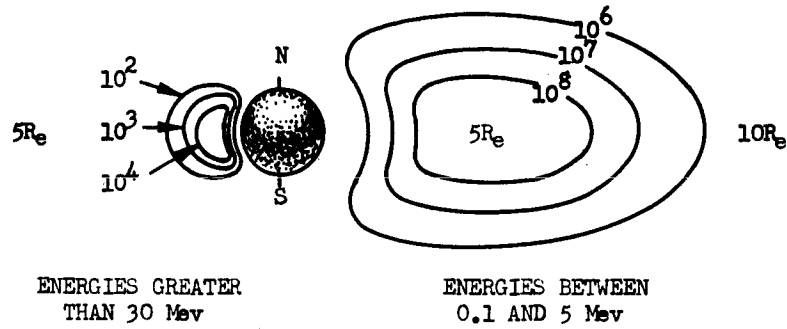


QUIET - DAY ELECTRON FLUXES AS A FUNCTION OF DISTANCE FROM THE CENTER OF THE EARTH & LATITUDE

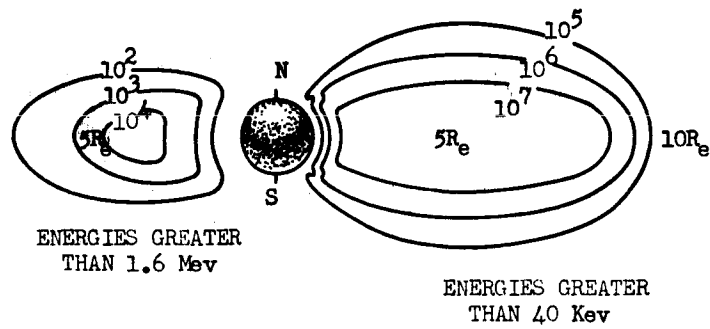
Reproduced by permission of the Stanford University Press from Satellite: Environment Handbook, ed. Francis S. Johnson, copyright 1961 by Lockheed Aircraft Corp.



VAN ALLEN RADIATION-BELT PARTICLE FLUX VERSUS ALTITUDE IN THE EQUATORIAL PLANE



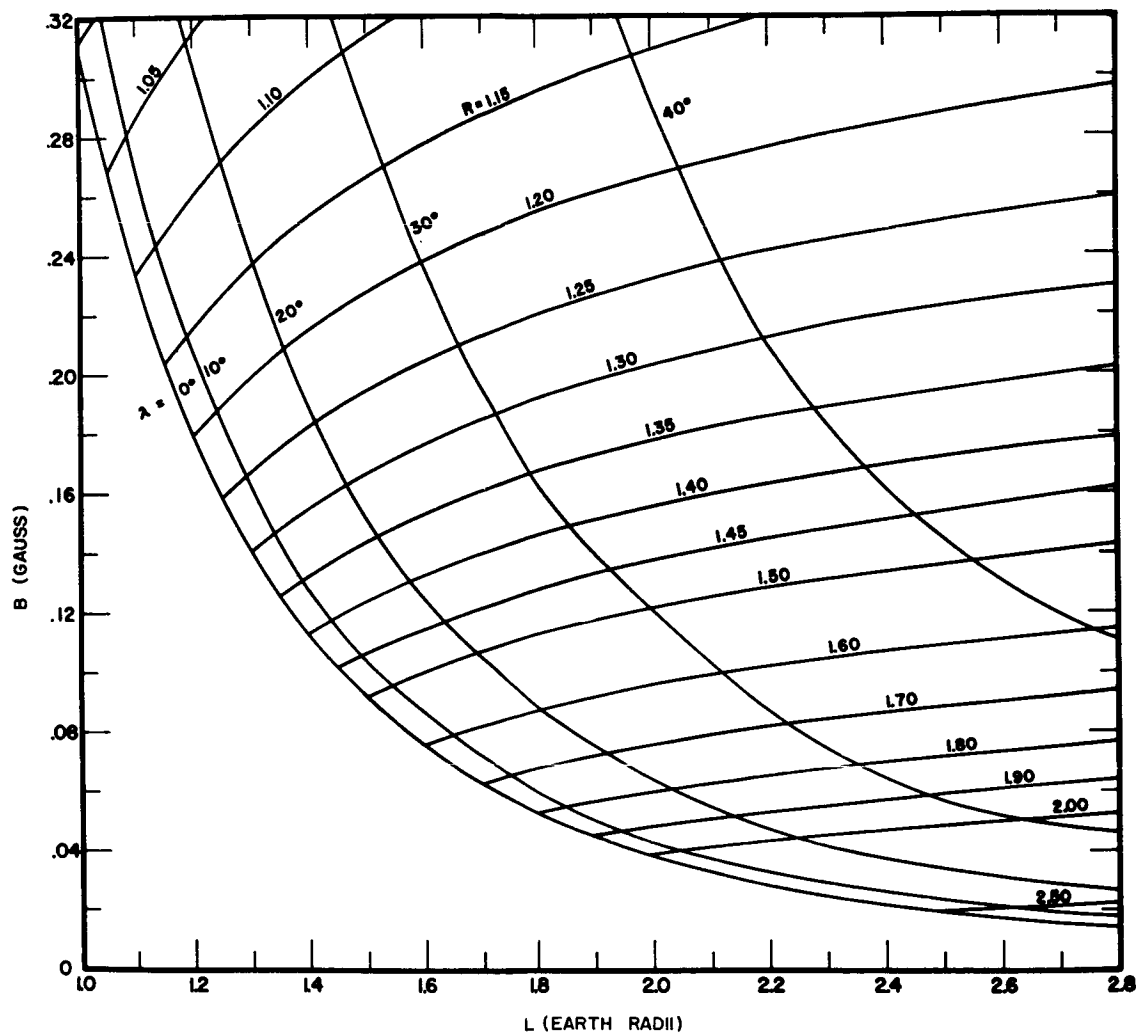
PROTONS



ELECTRONS

# THE VAN ALLEN BELTS





RELATIONSHIP BETWEEN POLAR-COORDINATE  
AND MAGNETIC-SHELL REFERENCE SYSTEMS FOR A DIPOLE FIELD

Reproduced by permission of the Stanford University Press from Satellite Environment Handbook, ed. Francis S. Johnson, copyright 1961 by Lockheed Aircraft Corp.

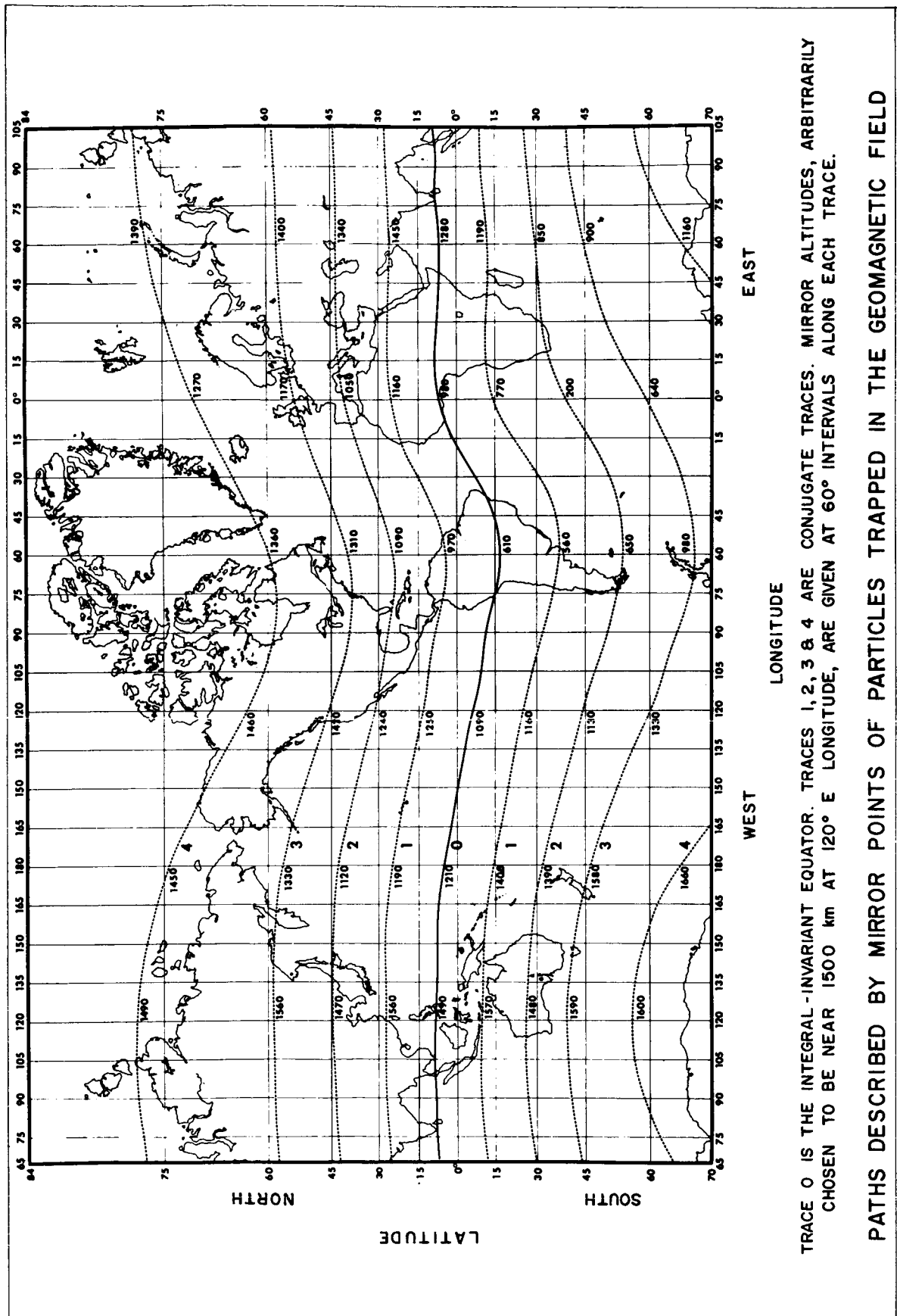
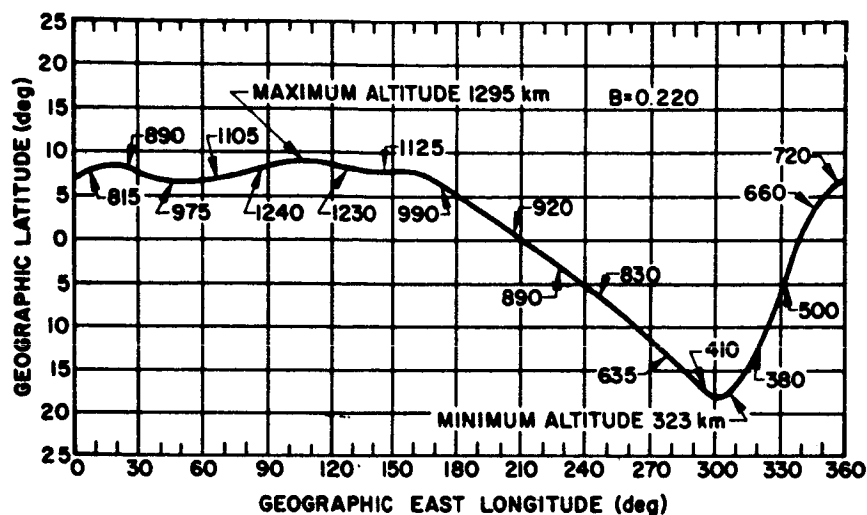
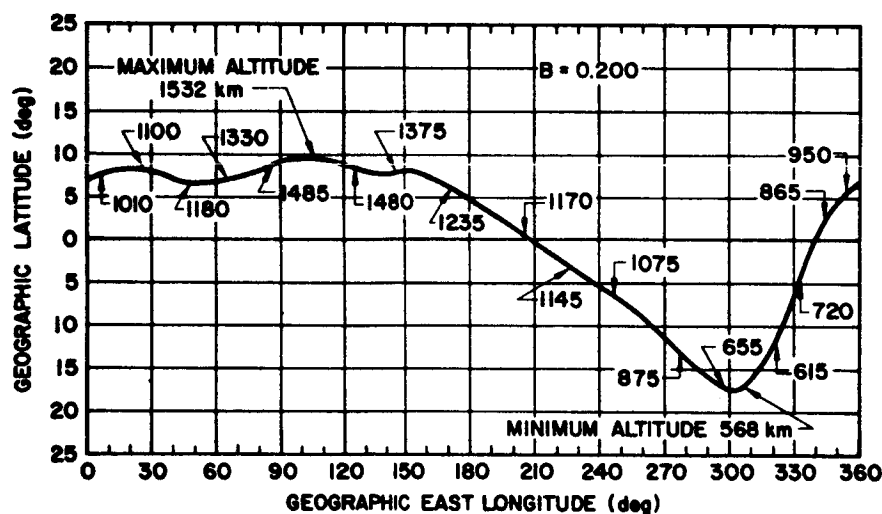


Figure 21

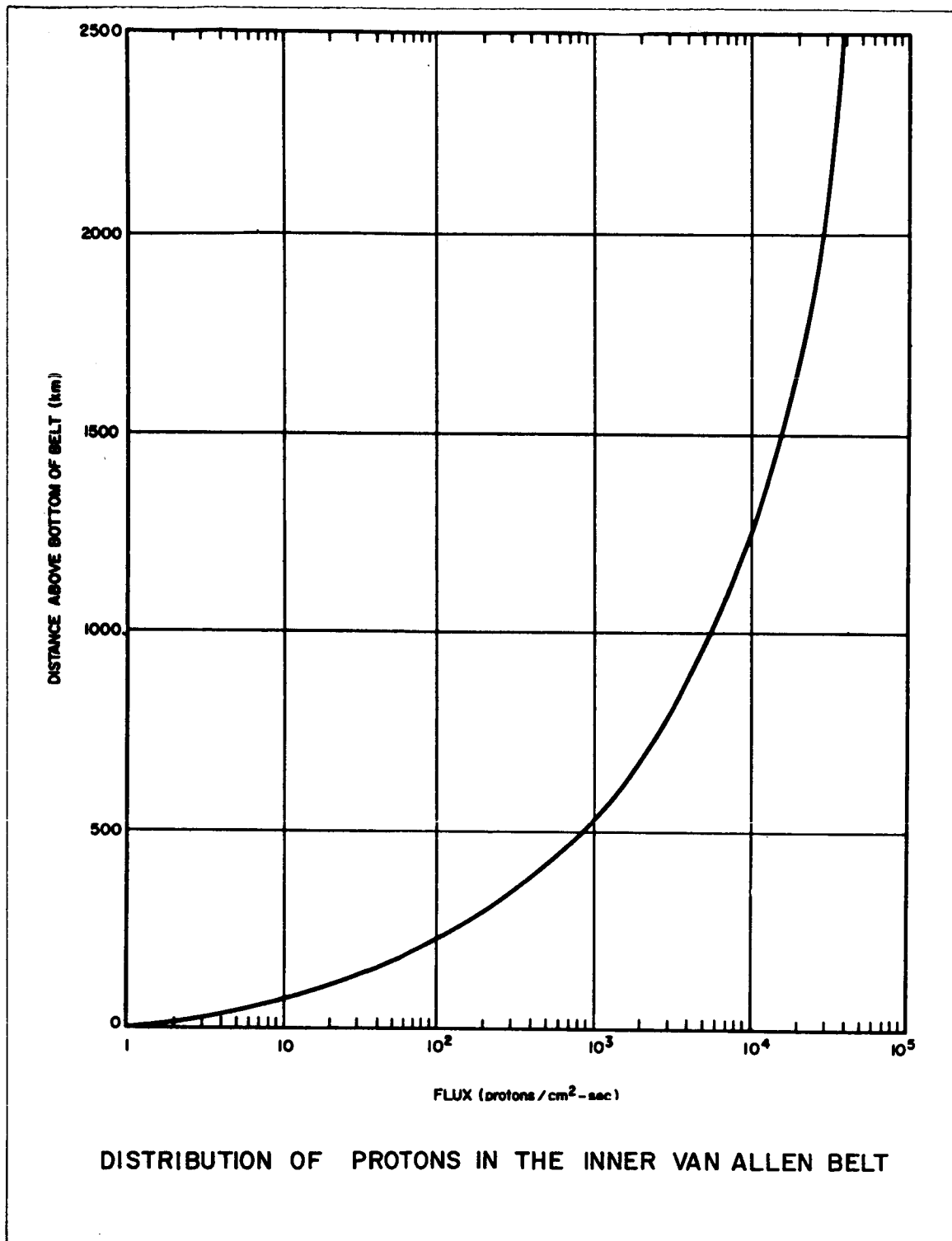


a. Field strength of 0.220 gauss. The numbers are the altitudes in kilometers where the proton flux is barely detectable above cosmic-ray background.



b. Field strength of 0.200 gauss. The numbers are the altitudes in kilometers where the flux is  $10^2$  protons/cm<sup>2</sup>-sec above 40 Mev.

### LOCATION AND ALTITUDE OF THE INTEGRAL-INVARIANT EQUATOR WITH RESPECT TO GEOGRAPHIC COORDINATES



Distribution of protons, with energies greater than 40 Mev, above the bottom of the radiation belt near the integral-invariant equator. To obtain the altitude at which a given flux occurs at a given longitude, add the altitude indicated here to that shown in Fig. 22a. Flux values shown on this graph should be correct to within a factor of 2.

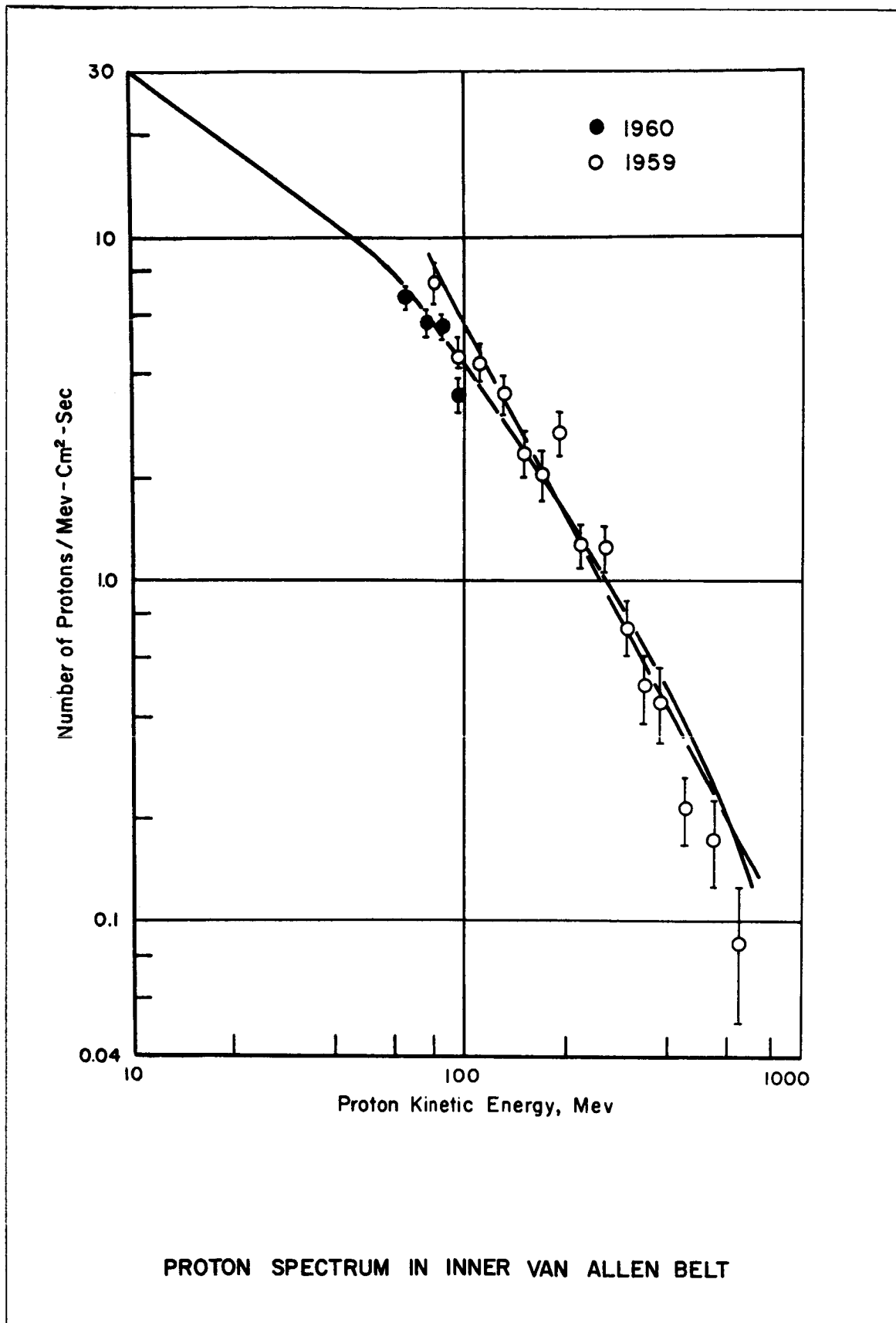
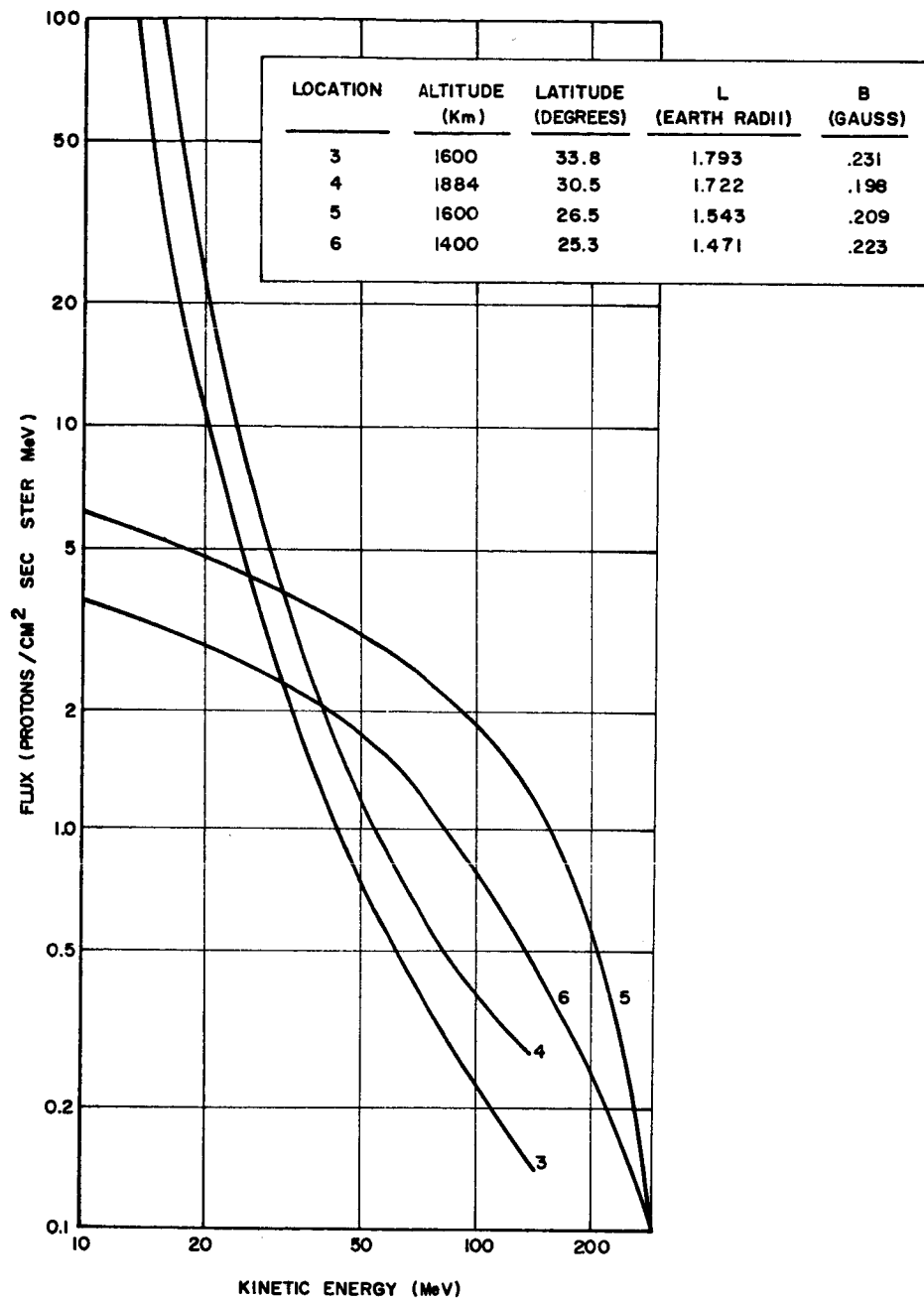
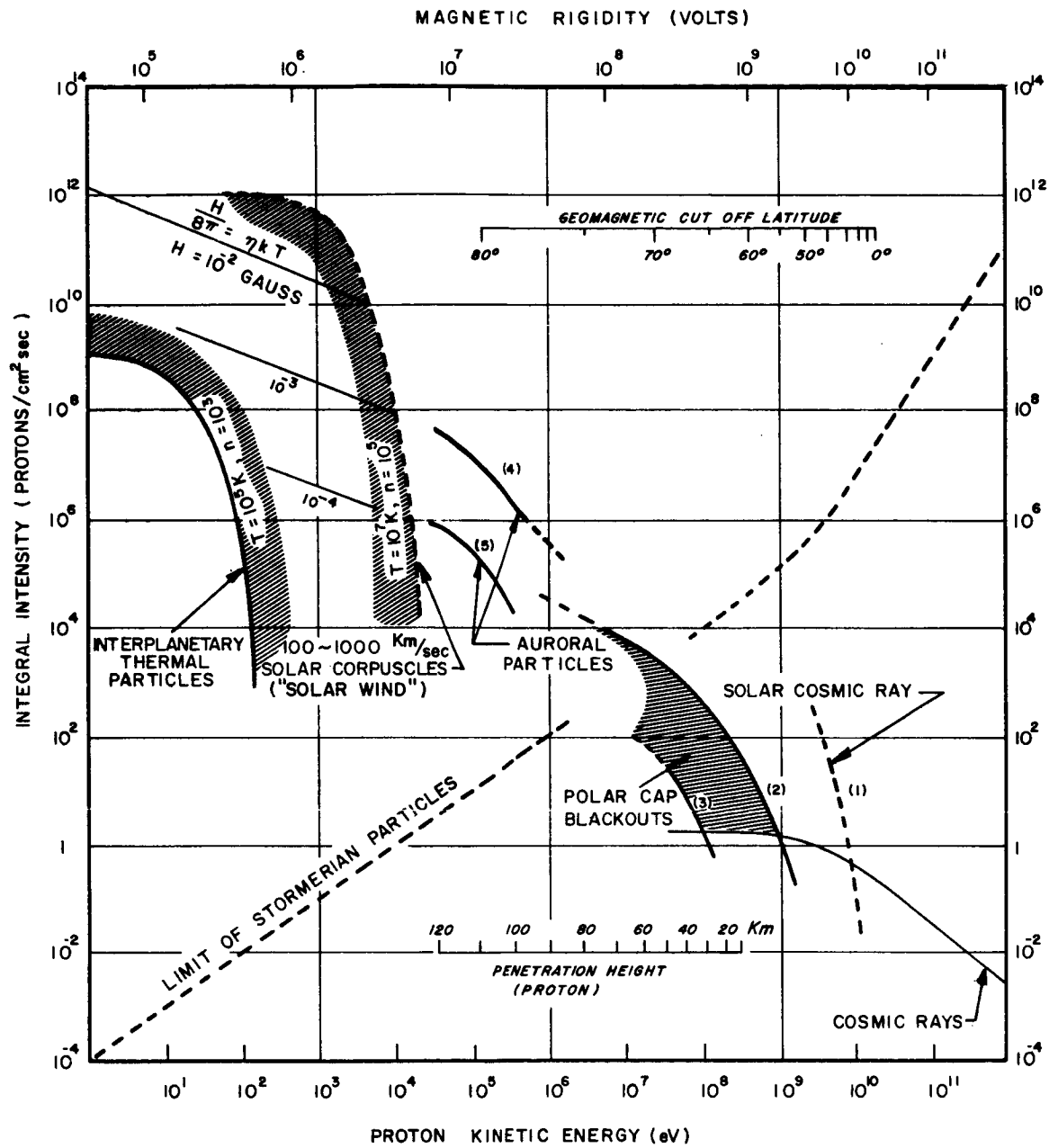


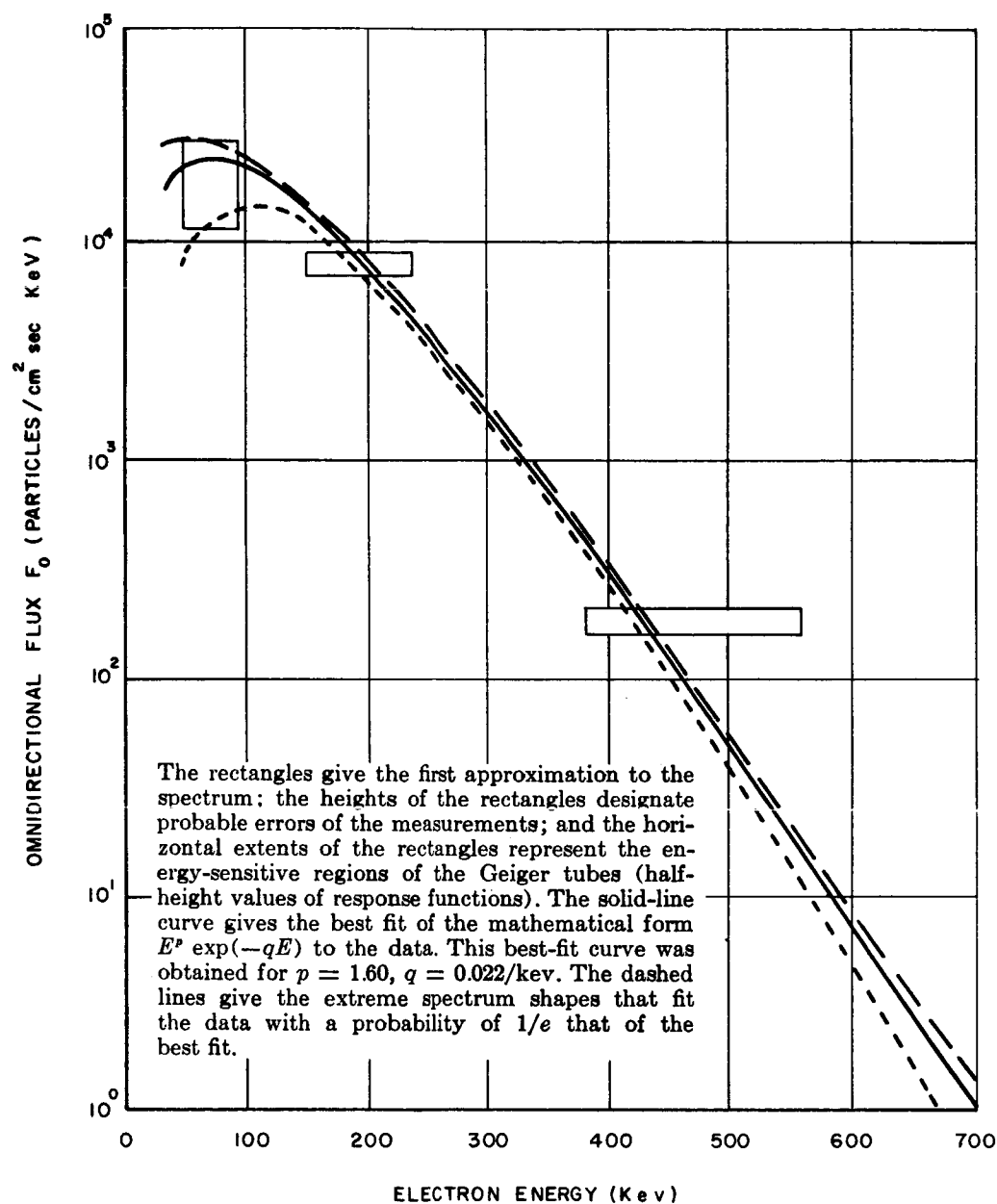
Figure 24



DIFFERENTIAL ENERGY SPECTRA AT  
FOUR POSITIONS IN THE INNER VAN ALLEN BELT



THE INTEGRAL ENERGY SPECTRUM OF SOLAR PARTICLES



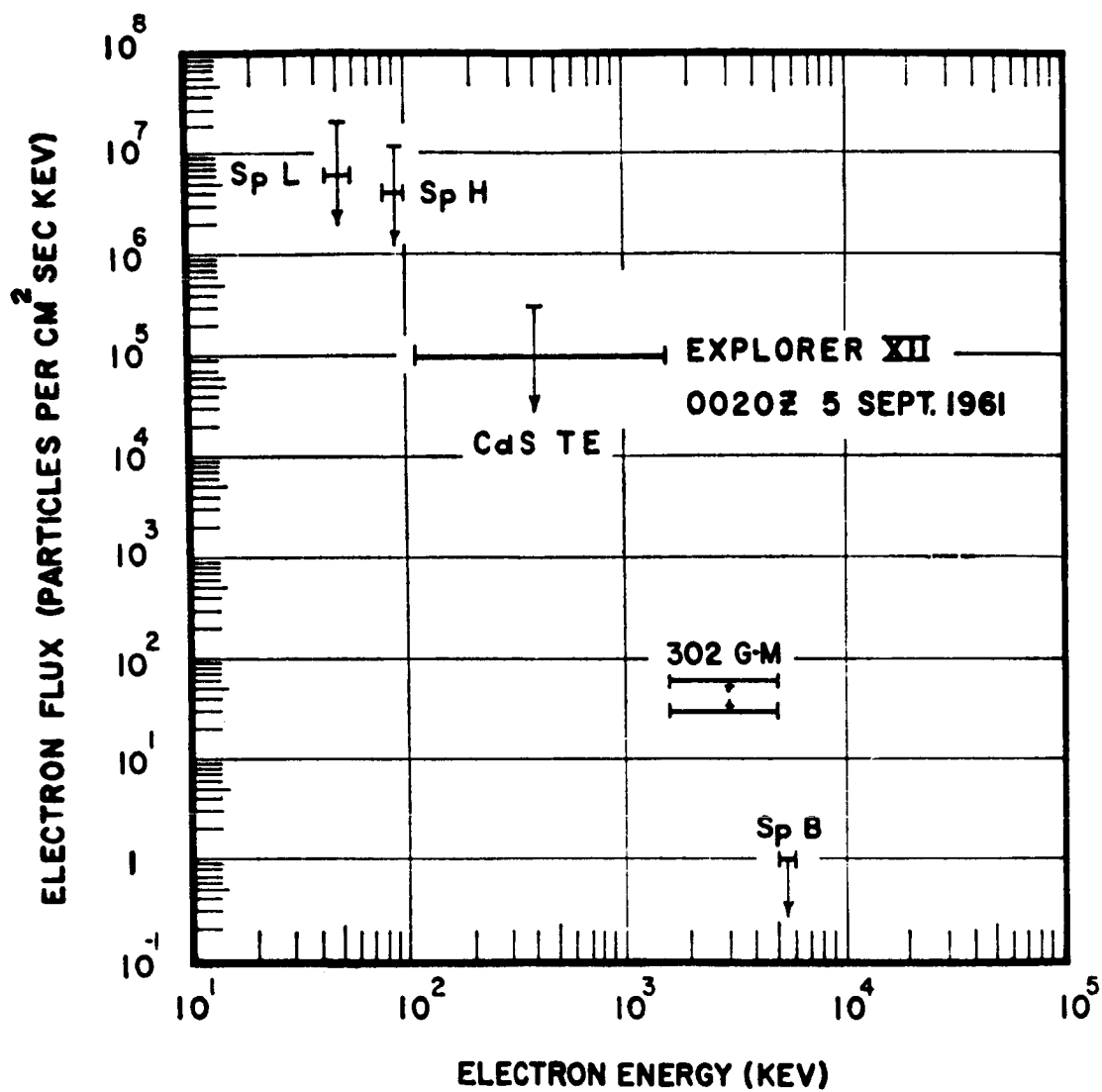
$$F_0(E) \sim E^p \exp(-qE)$$

- $p = 1.16$ ,  $q = 0.020/\text{Kev}$
- $p = 1.60$ ,  $q = 0.022/\text{Kev}$
- $p = 2.34$ ,  $q = 0.024/\text{Kev}$

OMNIDIRECTIONAL ELECTRON FLUX AT 920 KM

Figure 27





ABSOLUTE DIFFERENTIAL ENERGY SPECTRUM  
FOR THE OMNIDIRECTIONAL ELECTRON INTENSITY  
IN THE HEART OF THE ELECTRON BELT

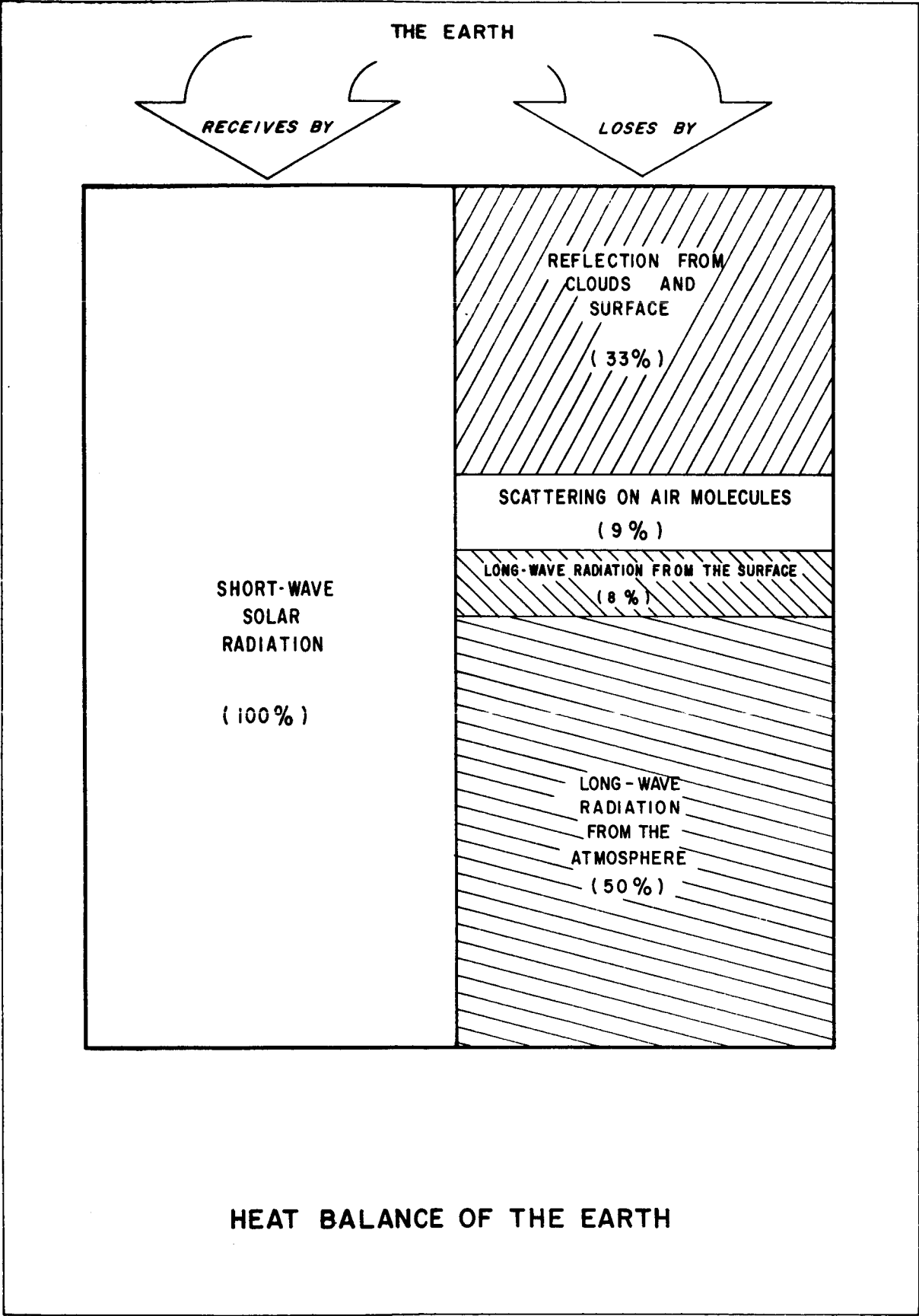


Figure 29

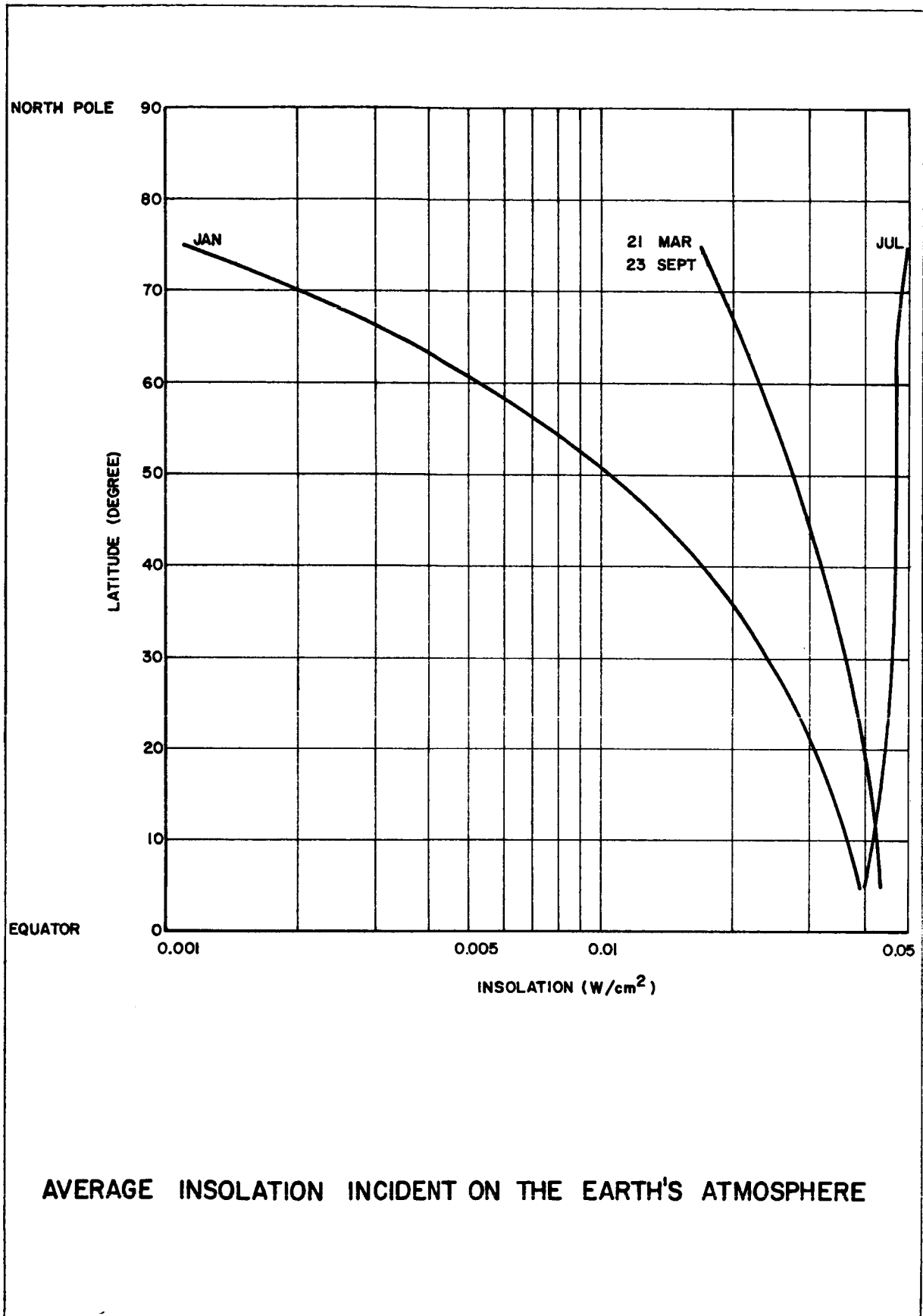


Figure 30

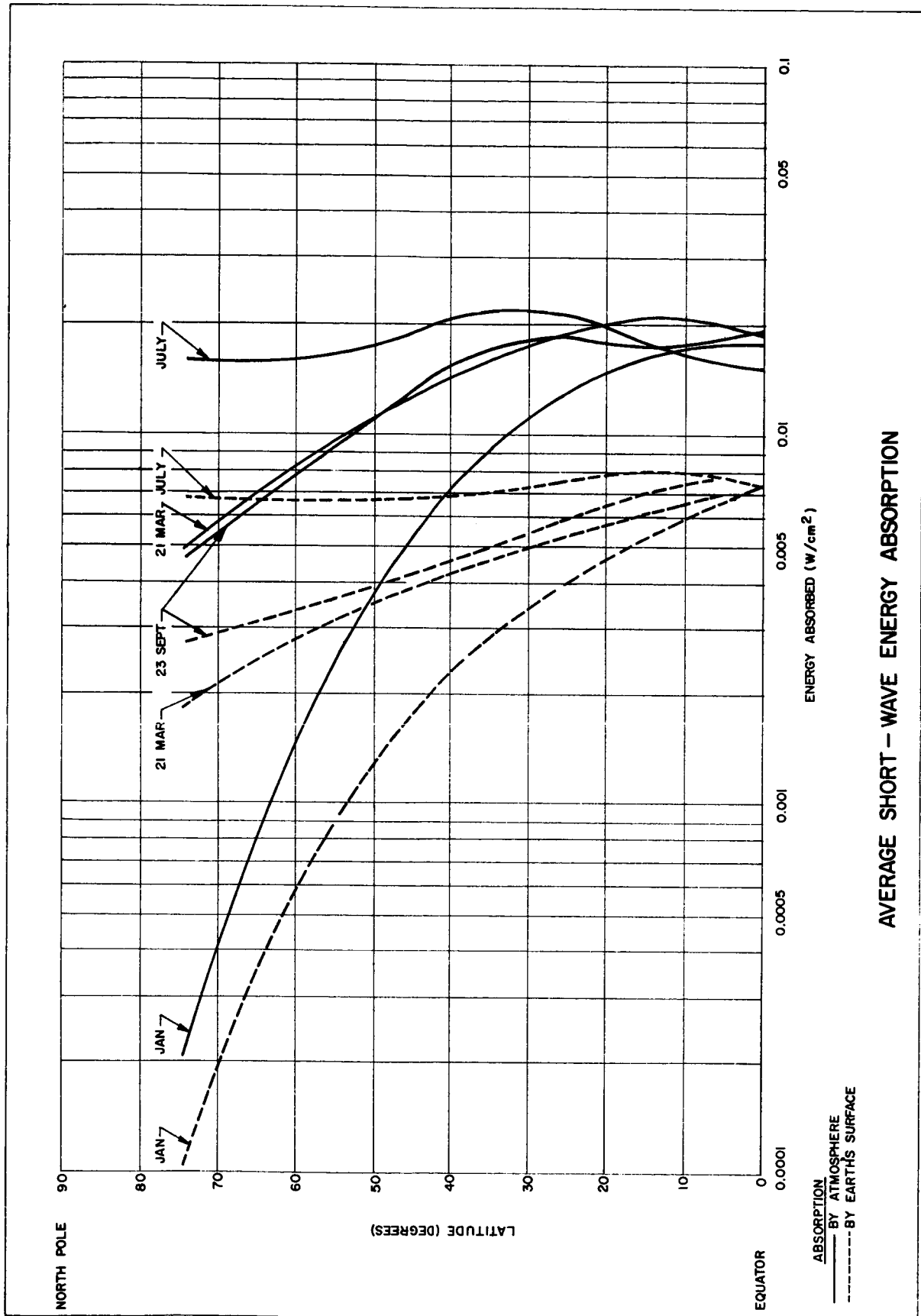


Figure 31

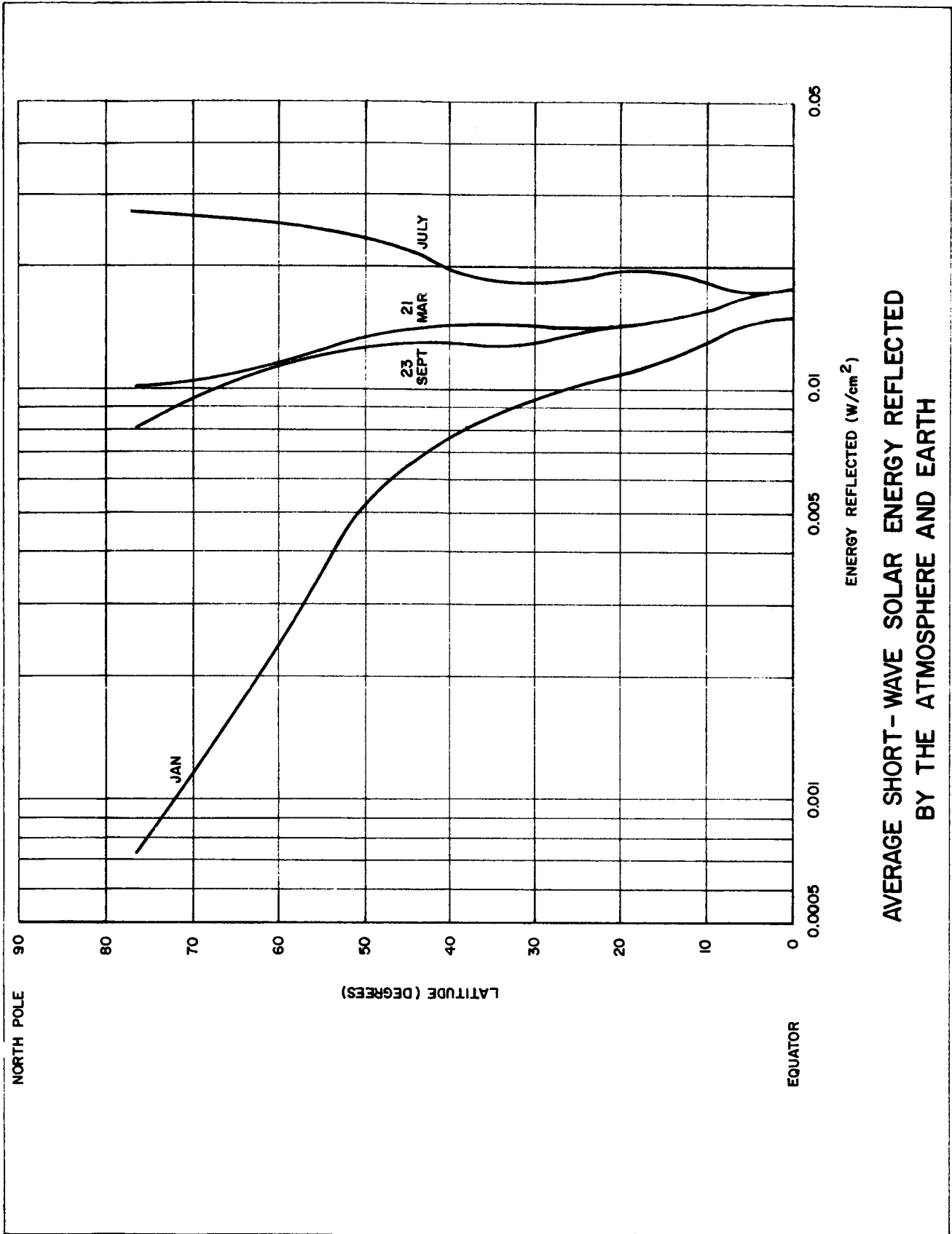
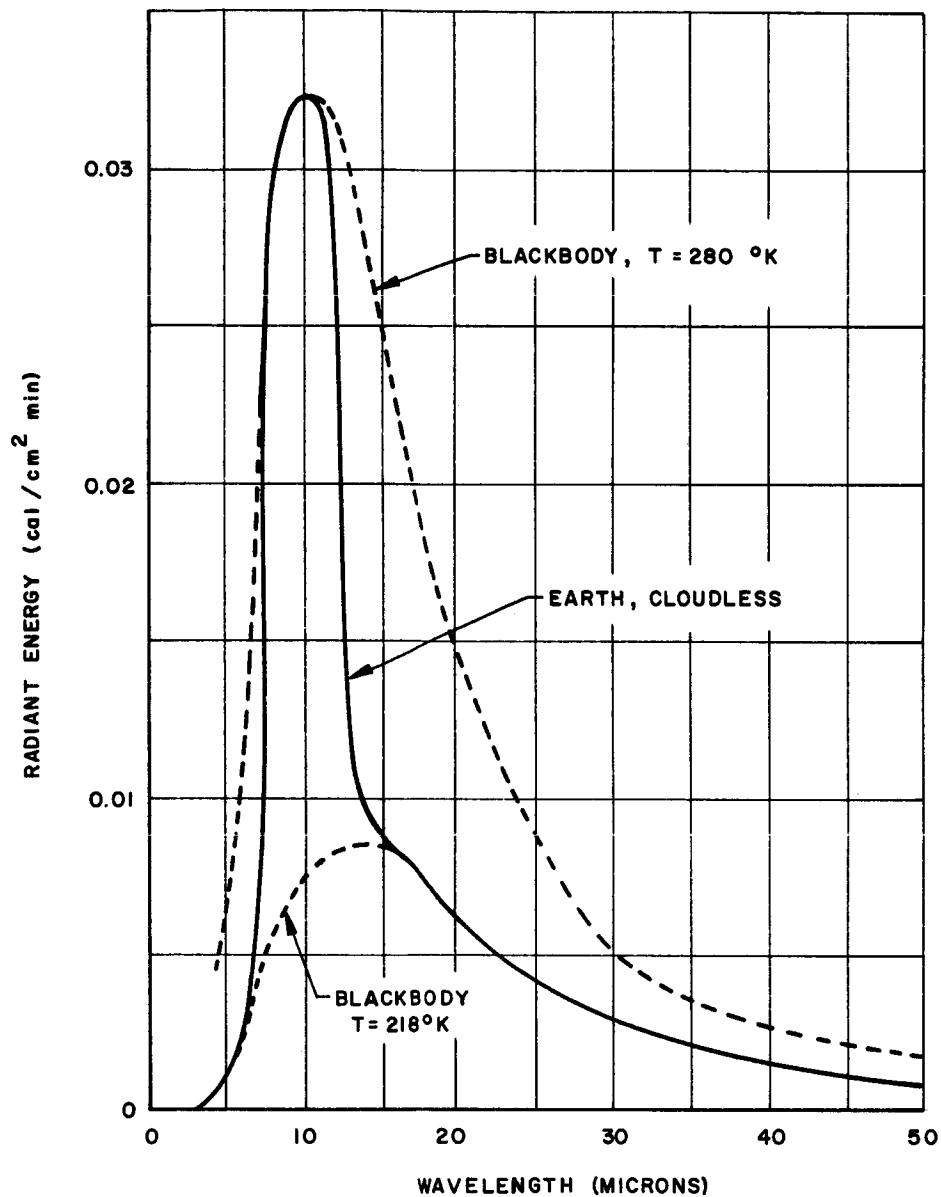


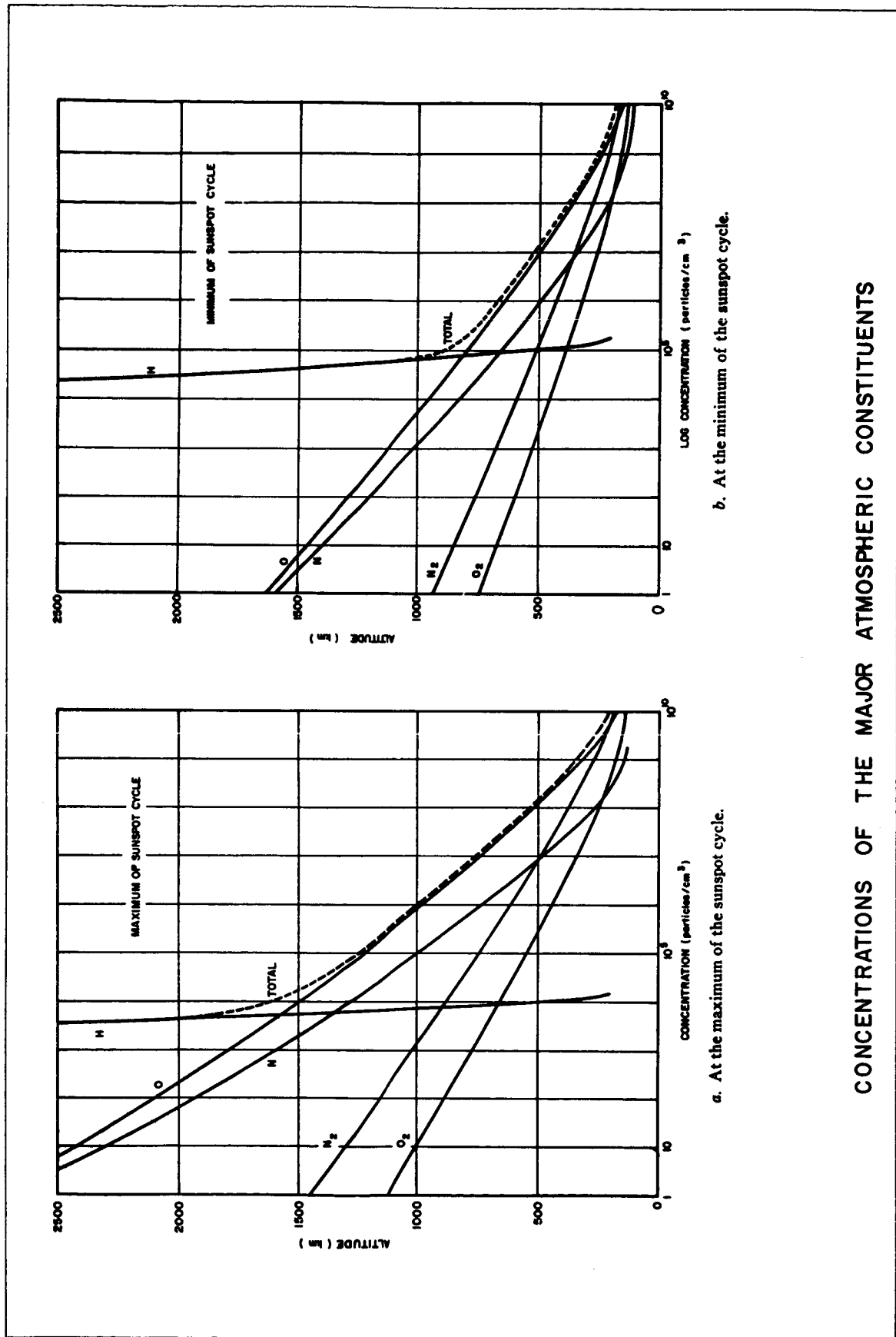
Figure 32



THERMAL EMISSION SPECTRUM OF THE EARTH



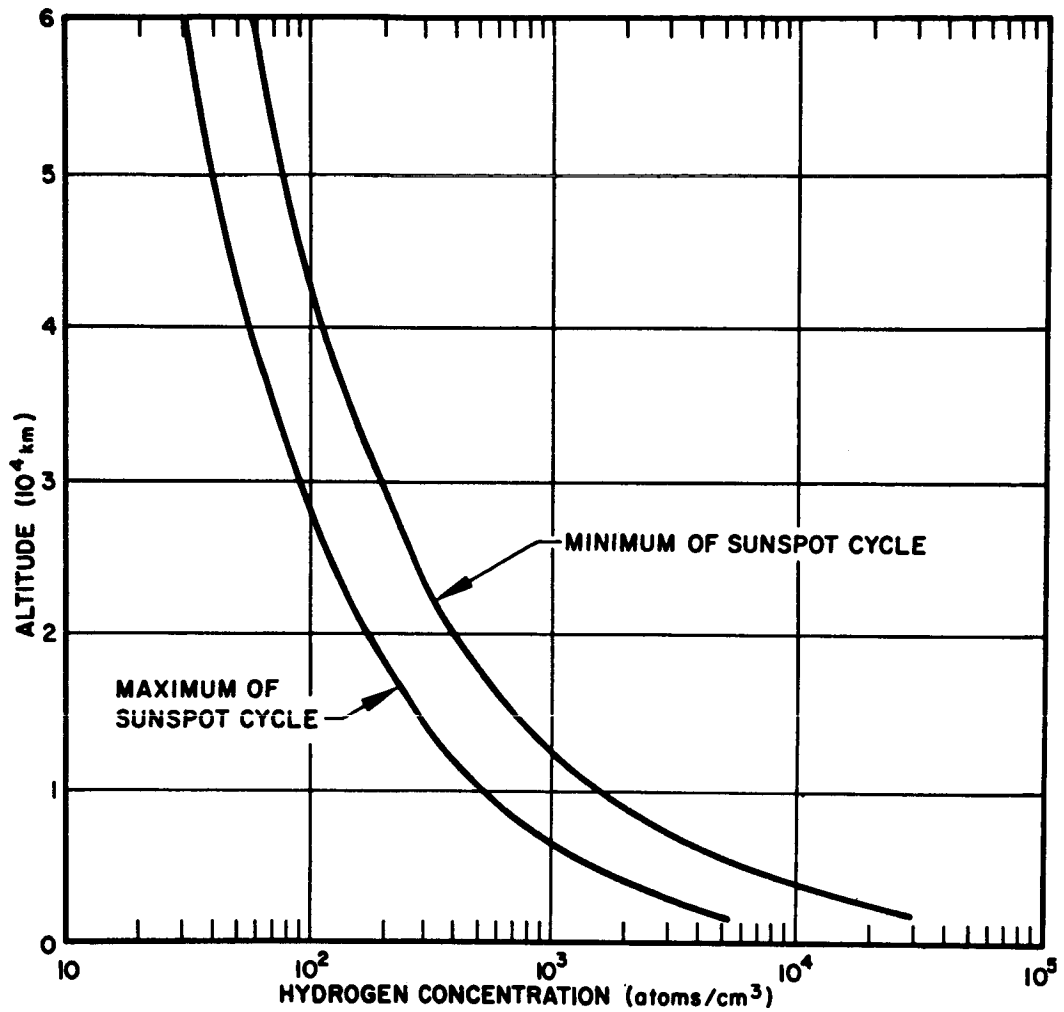
Reproduced by permission of the Stanford University Press from Satellite Environment Handbook, ed. Francis S. Johnson, copyright 1961 by Lockheed Aircraft Corp.



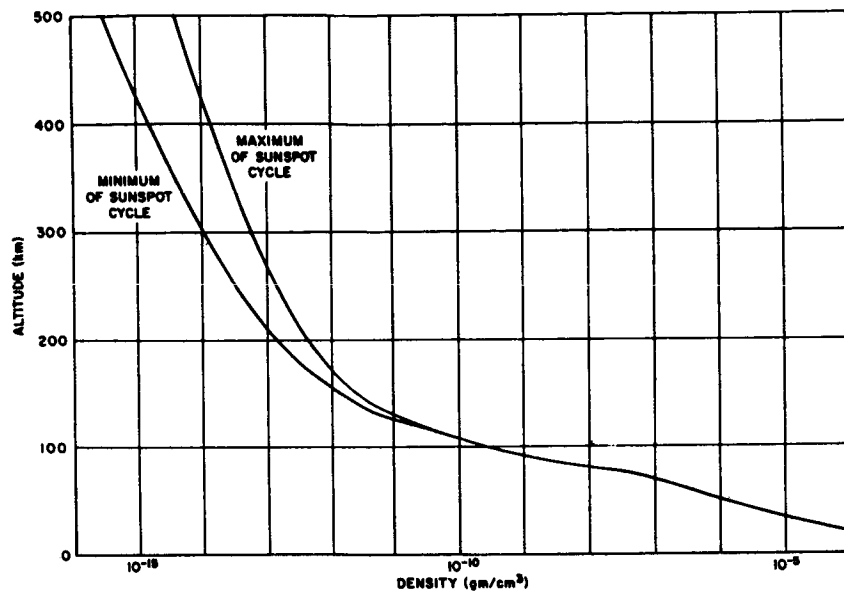
CONCENTRATIONS OF THE MAJOR ATMOSPHERIC CONSTITUENTS



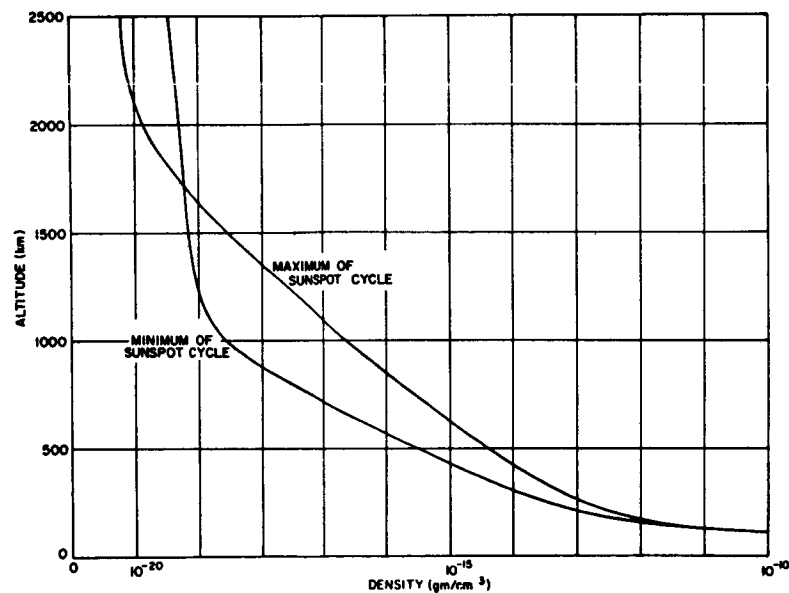
Reproduced by permission of the Stanford University Press from Satellite Environment Handbook, ed. Francis S. Johnson, copyright 1961 by Lockheed Aircraft Corp.



DISTRIBUTION OF ATOMIC HYDROGEN OUT TO 60,000 km FROM  
THE EARTH AT THE EXTREMES OF THE SUNSPOT CYCLE



a. 0 to 500 km.



b. 0 to 2500 km.

# AVERAGE DAYTIME ATMOSPHERIC DENSITIES AT THE EXTREMES OF THE SUNSPOT CYCLE

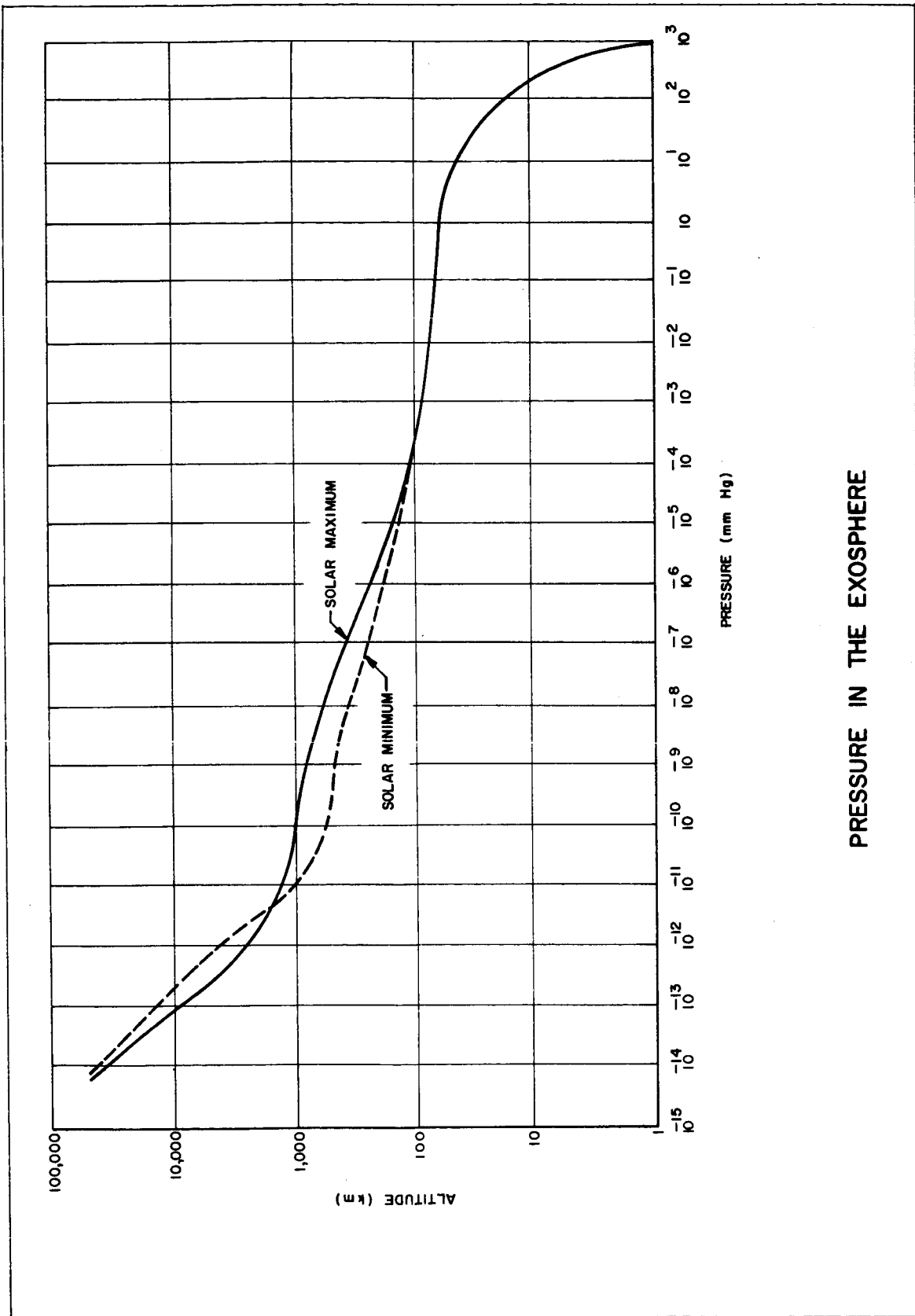
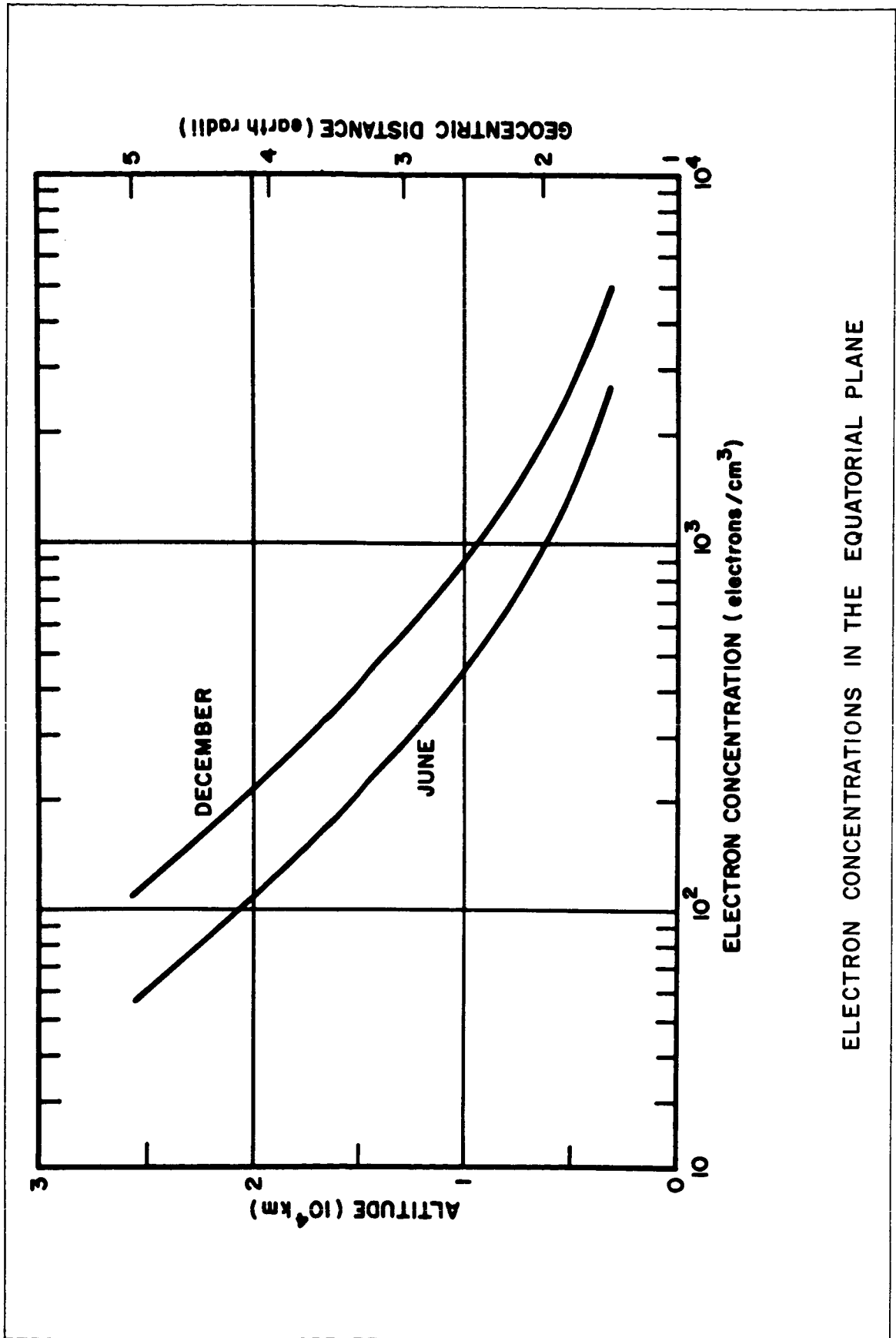
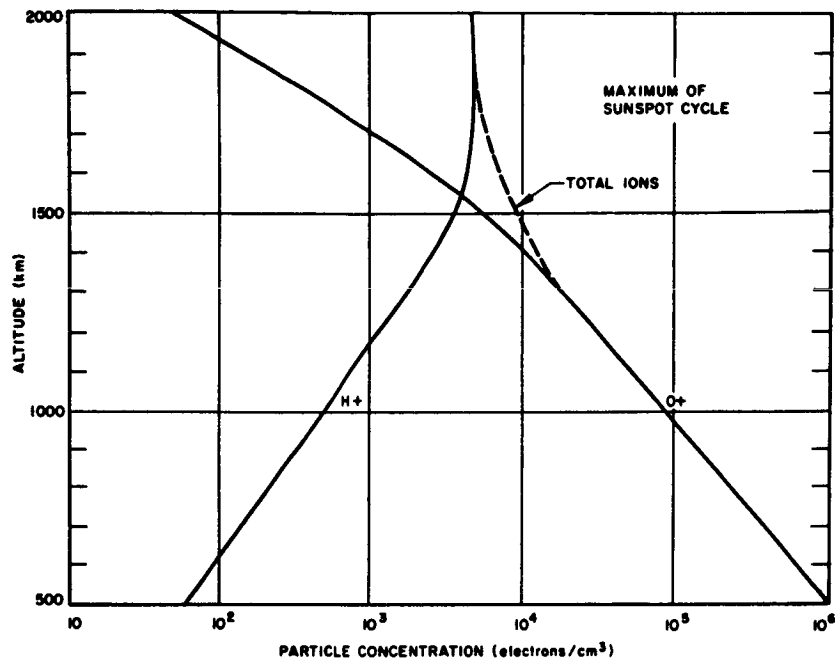


Figure 38

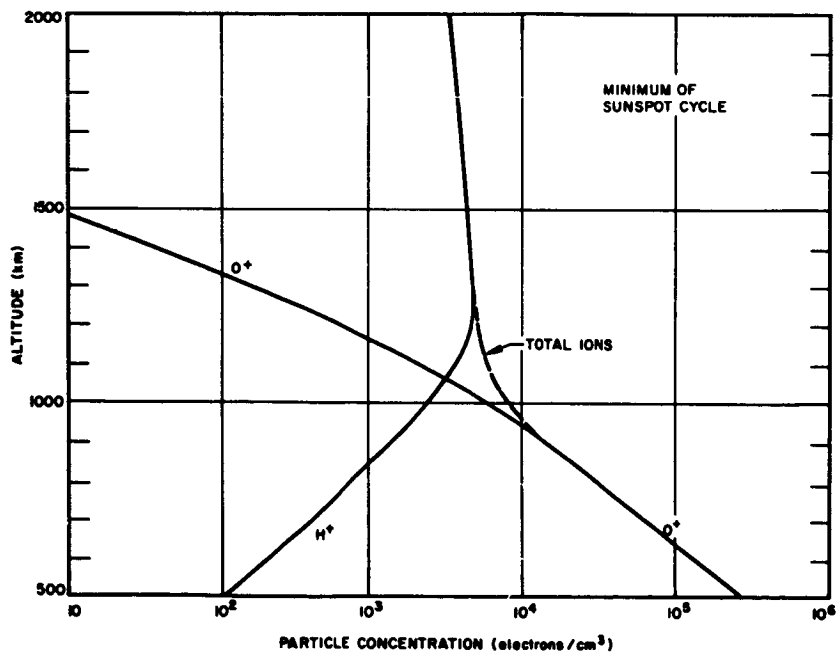
Reproduced by permission of the Stanford University Press from Satellite Environment Handbook, ed. Francis S. Johnson, copyright 1961 by Lockheed Aircraft Corp.



ELECTRON CONCENTRATIONS IN THE EQUATORIAL PLANE

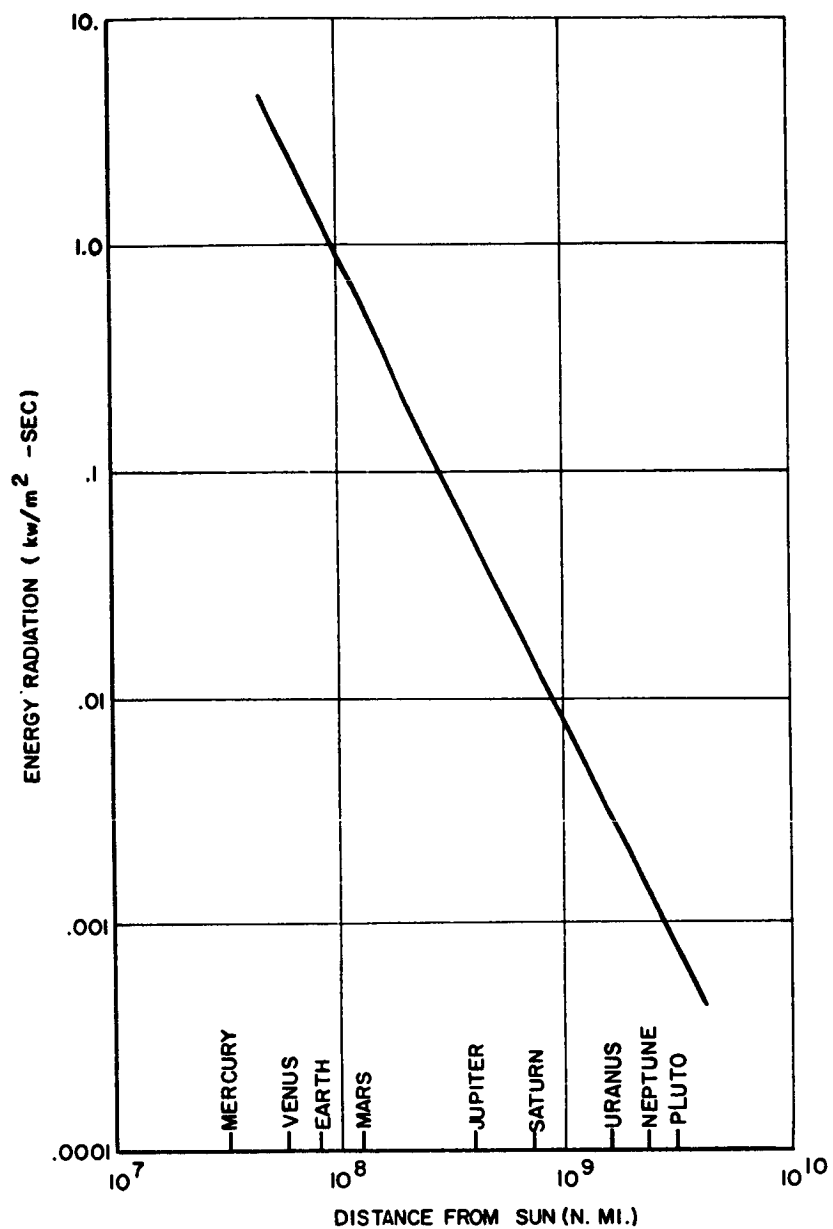


a. Near the maximum of the sunspot cycle.

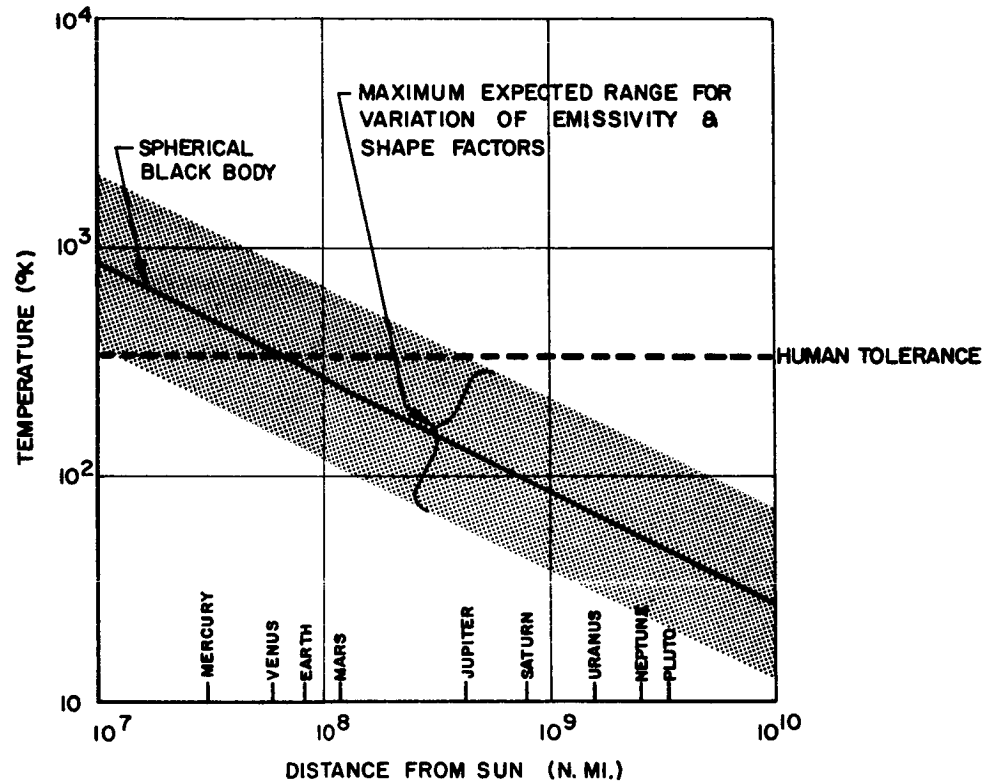


b. Near the minimum of the sunspot cycle.

ION CONCENTRATIONS IN THE TRANSITION REGION BETWEEN  
THE NORMAL IONOSPHERE AND THE PROTONOSPHERE

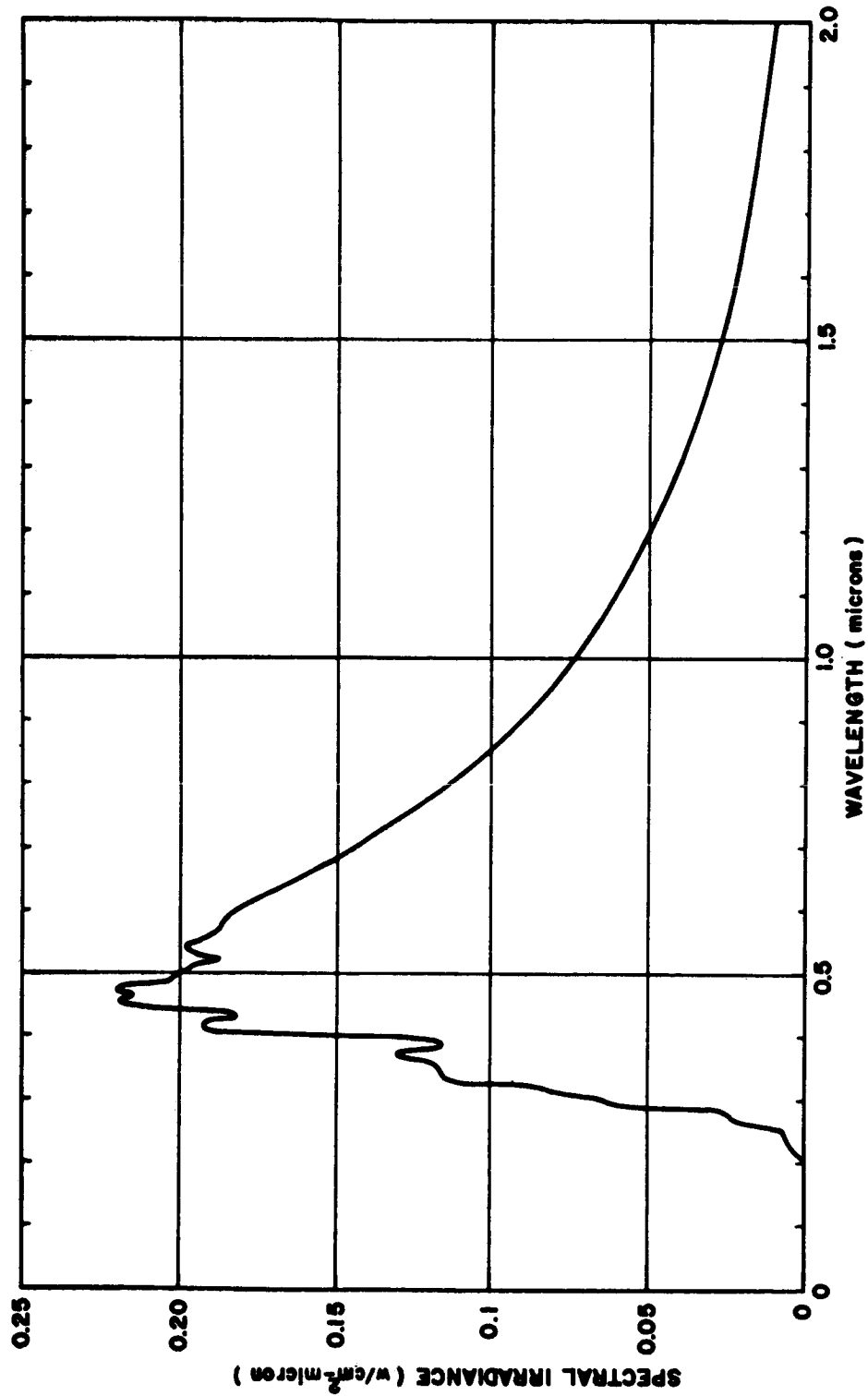


RADIATION ENERGY FIELD OF THE SUN



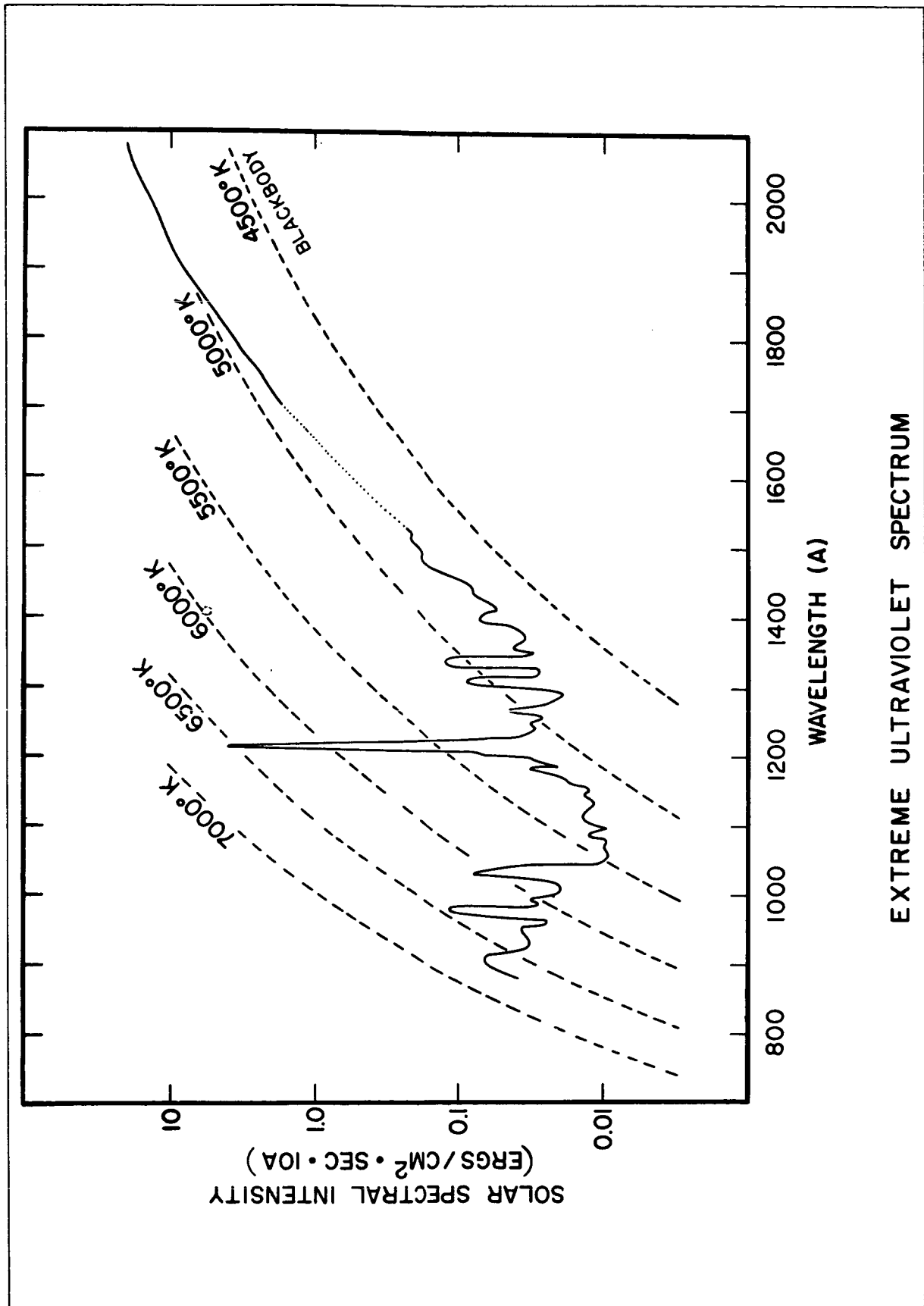
RADIATION EQUILIBRIUM TEMPERATURES FOR A  
SPHERICAL BLACK BODY IN SPACE

Reproduced by permission of the Stanford University Press from Satellite Environment Handbook, ed. Francis S. Johnson, copyright 1961 by Lockheed Aircraft Corp.

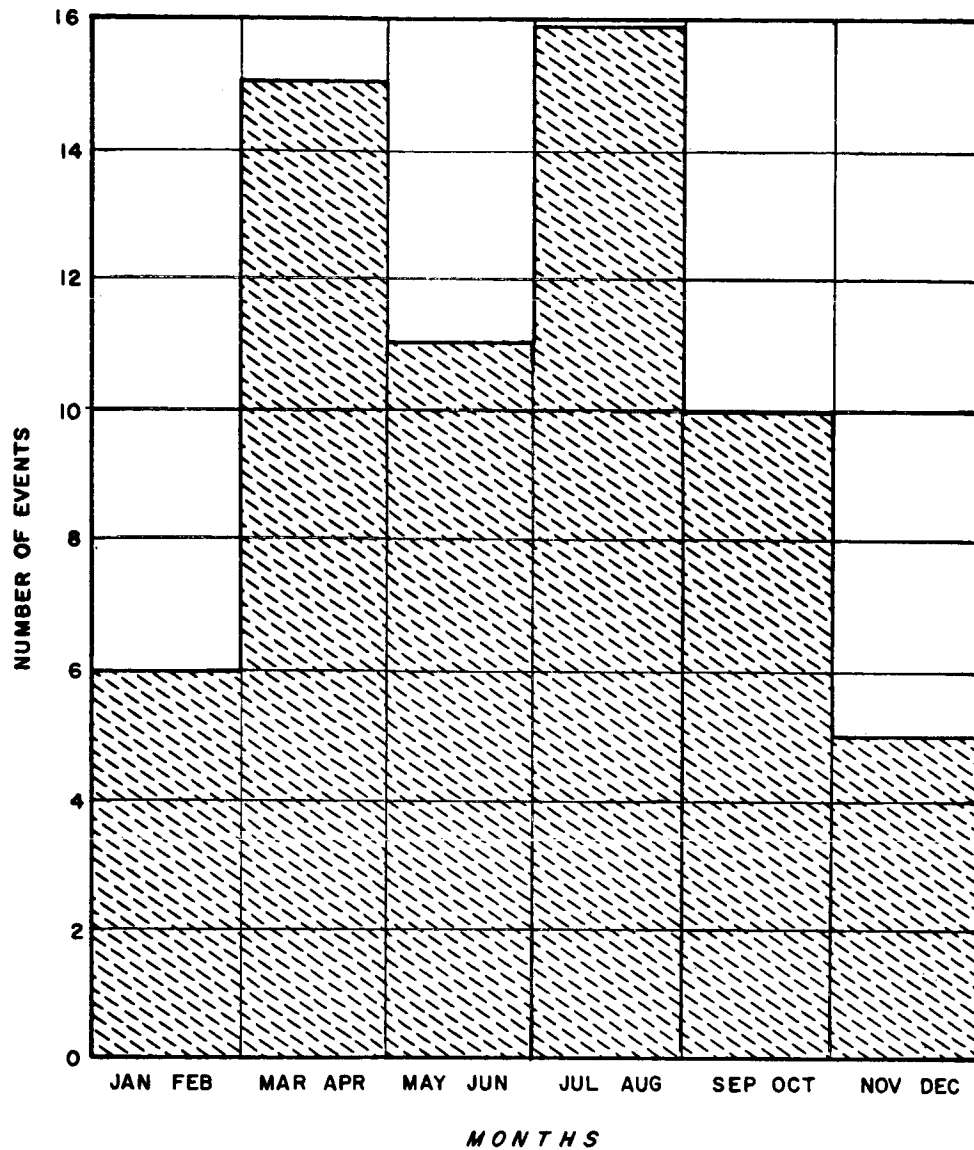


SOLAR SPECTRAL IRRADIANCE ABOVE THE EARTH'S ATMOSPHERE AT THE EARTH'S MEAN DISTANCE FROM THE SUN



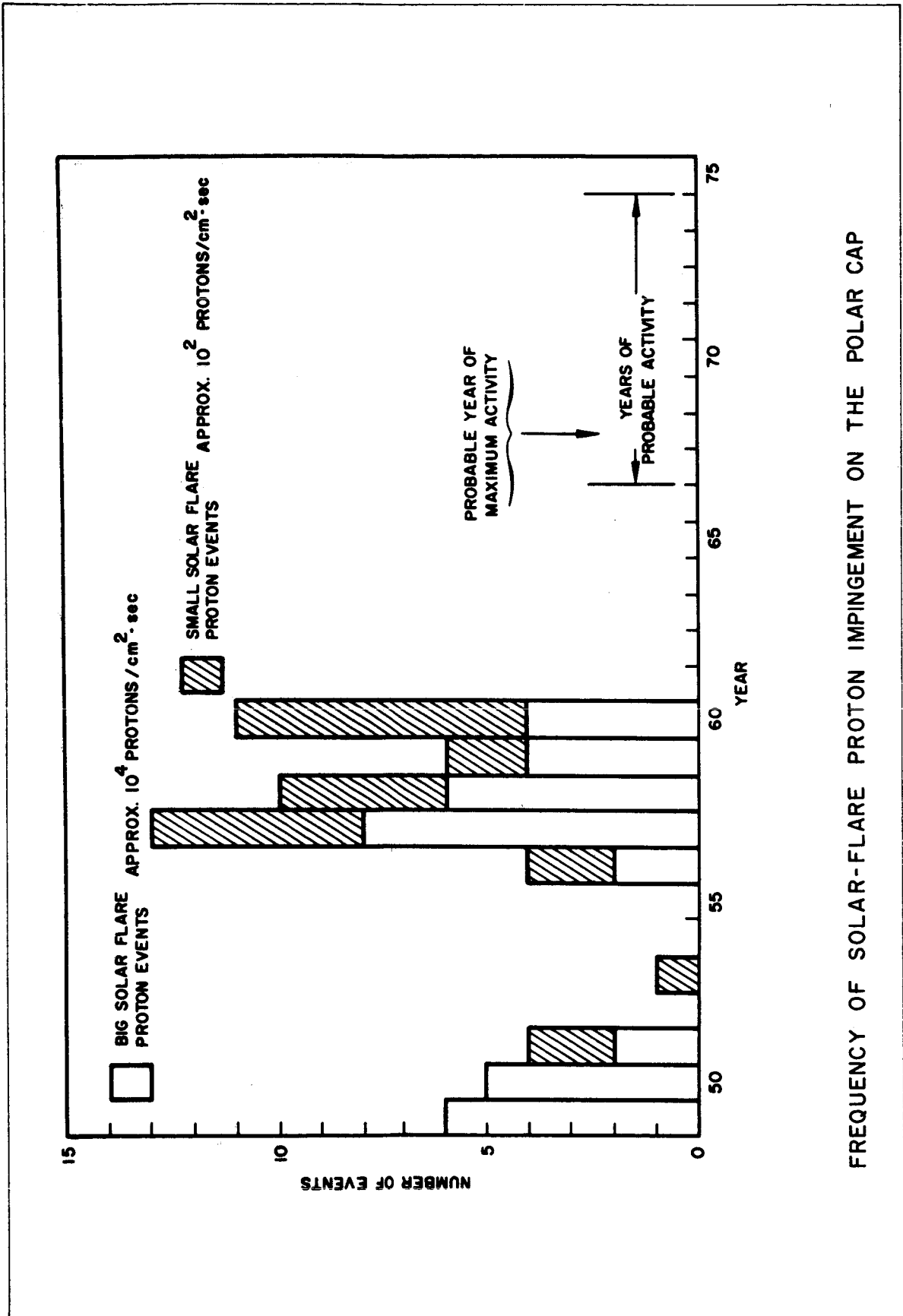


EXTREME ULTRAVIOLET SPECTRUM

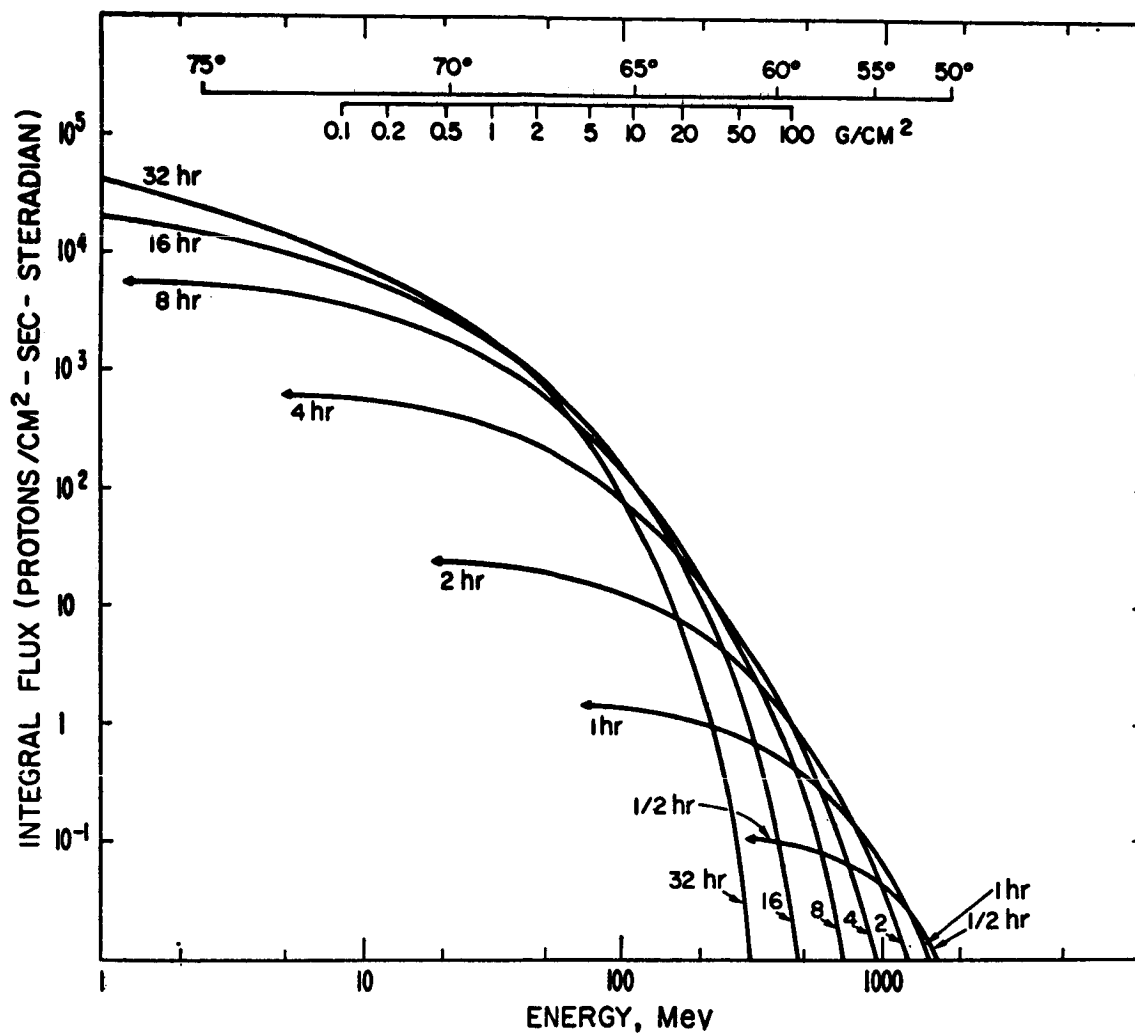


**B1 - MONTHLY DISTRIBUTION OF POLAR CAP ABSORPTION EVENTS  
FOR THE PERIOD 1949 TO 1960**

Reproduced by permission of the Stanford University Press from Satellite Environment Handbook, ed. Francis S. Johnson, copyright 1961 by Lockheed Aircraft Corp.



FREQUENCY OF SOLAR-FLARE PROTON IMPINGEMENT ON THE POLAR CAP



SPECTRA OF PARTICLES ARRIVING AT THE EARTH  
AT VARIOUS TIMES FOLLOWING A SOLAR FLARE

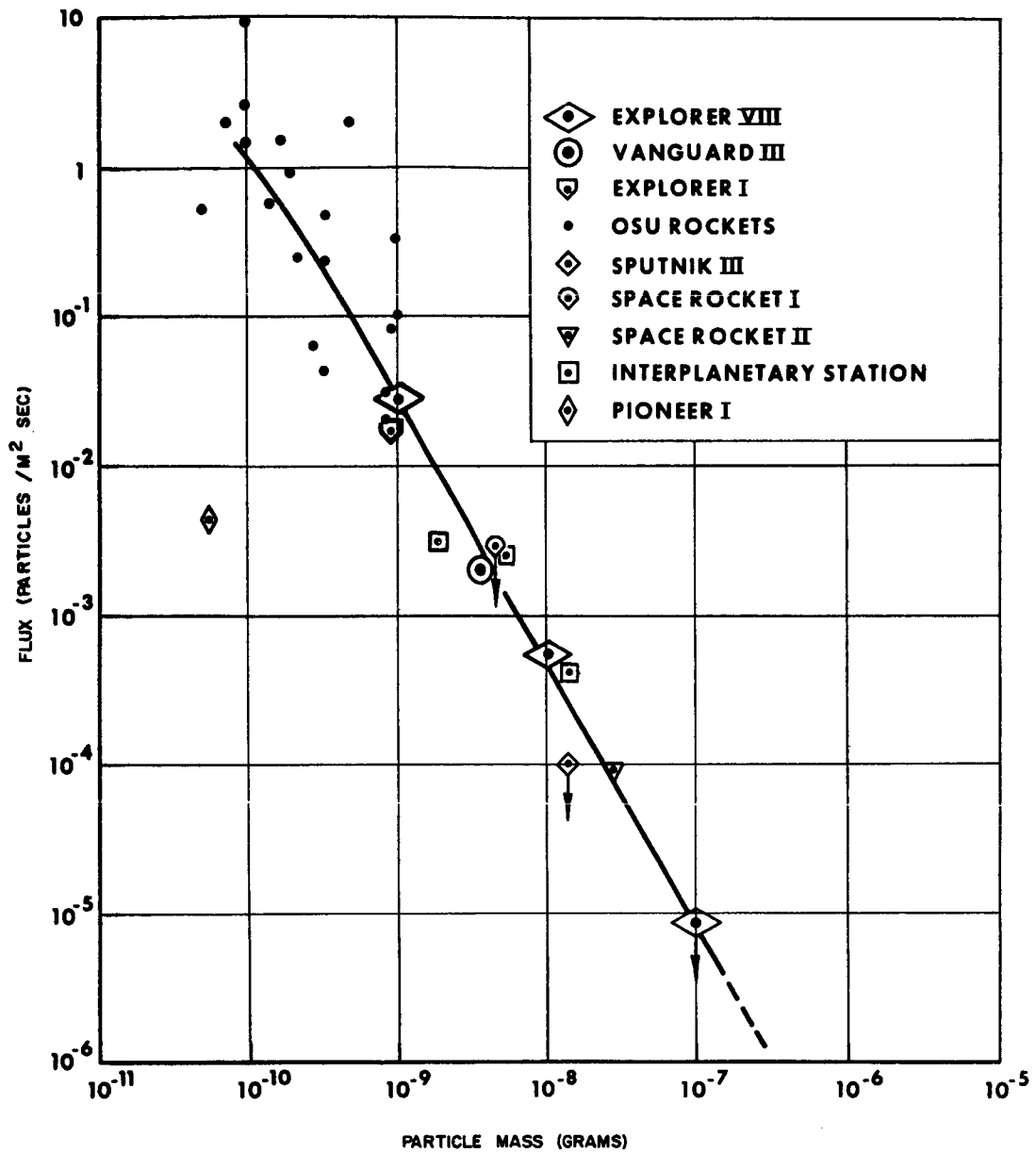


Figure 48

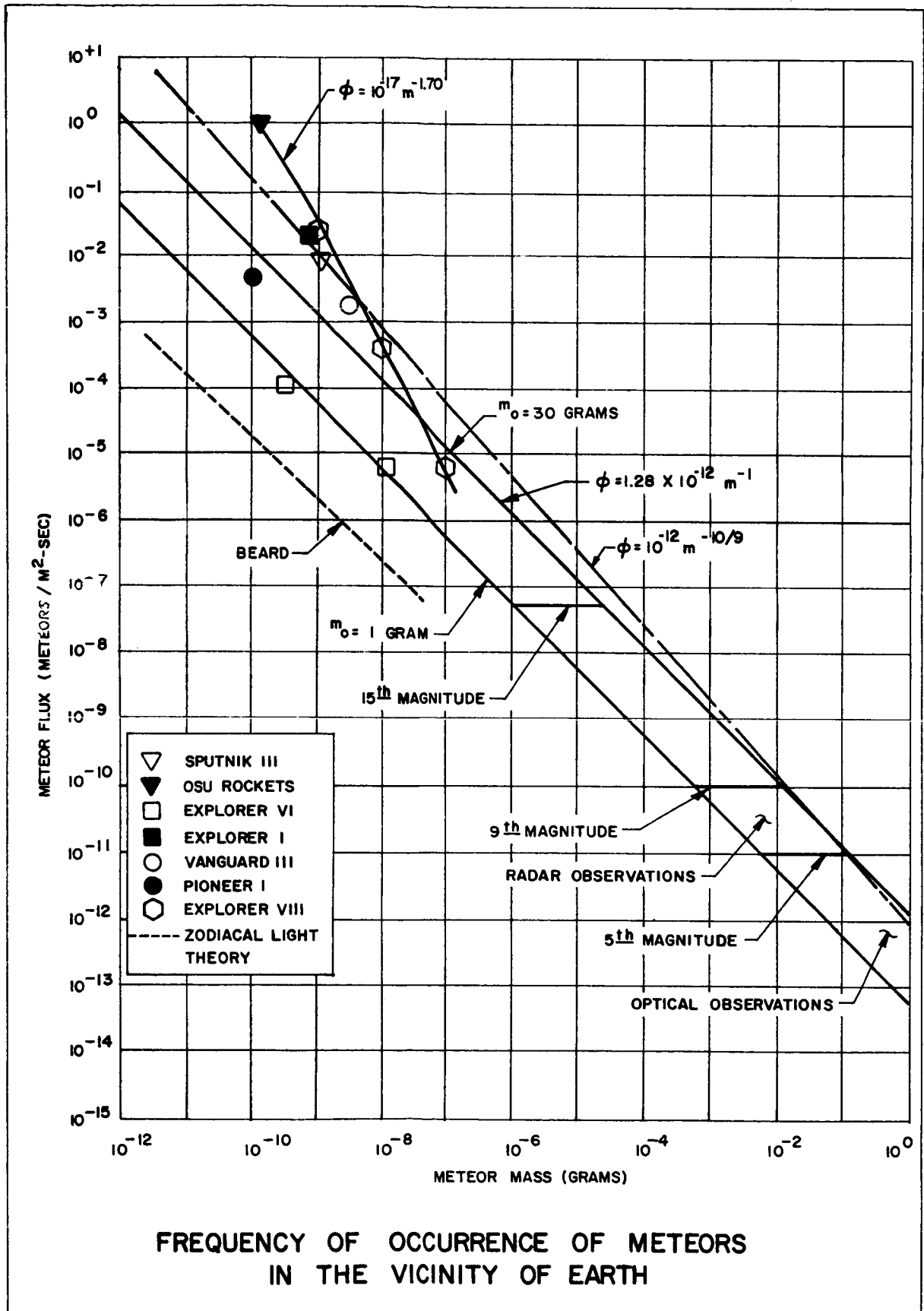
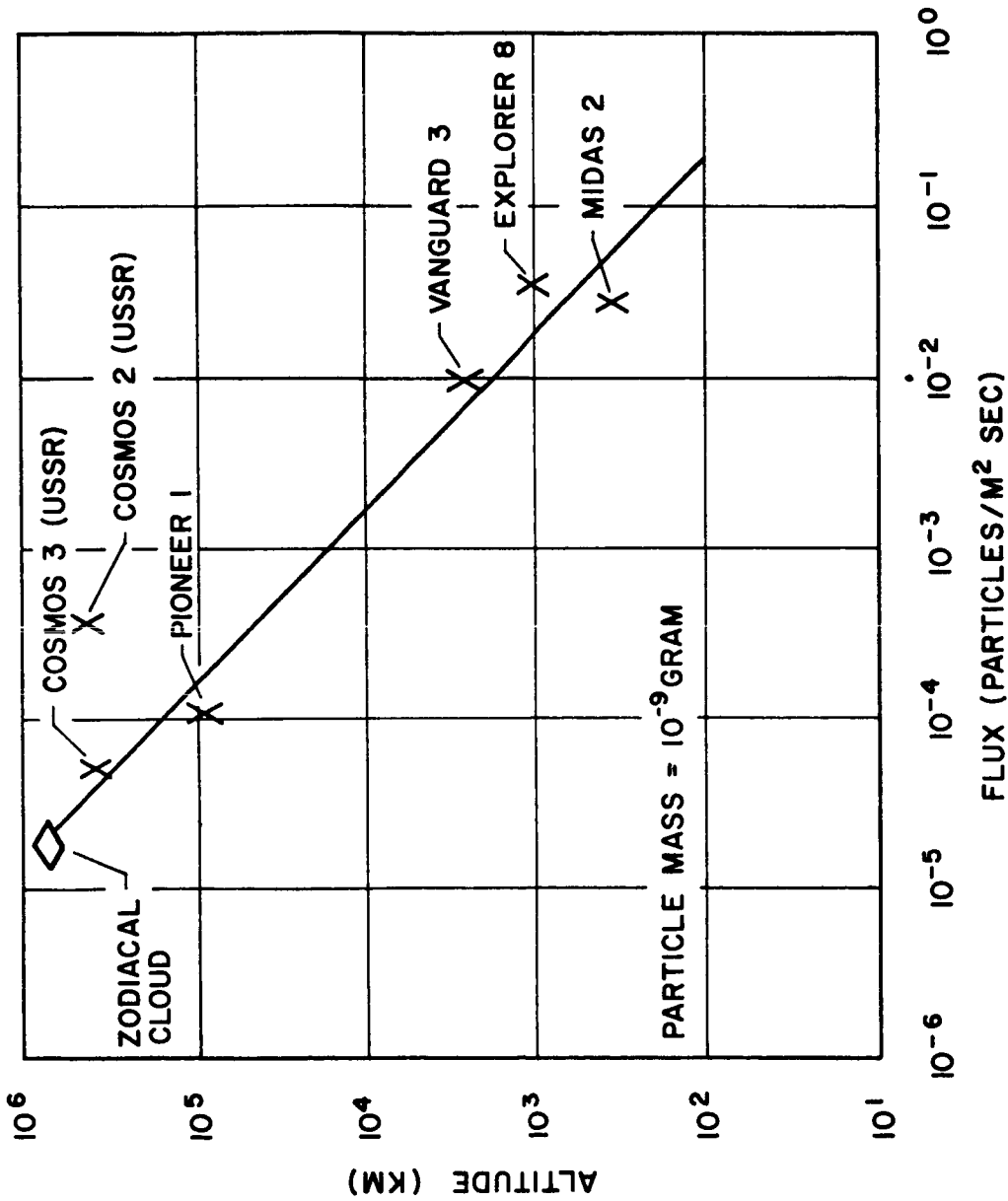
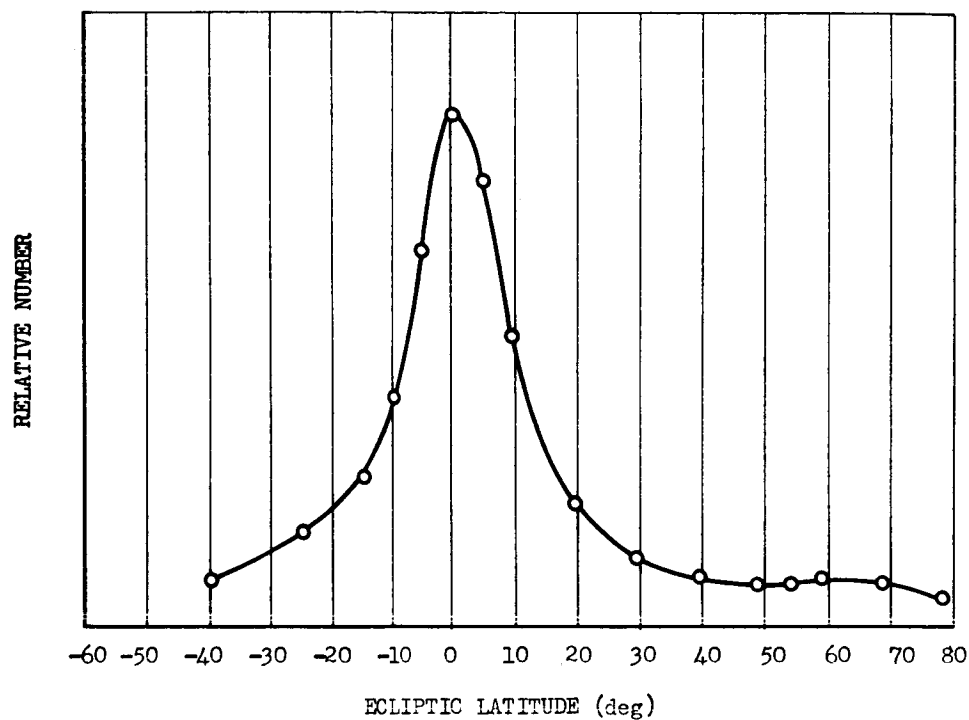


Figure 49



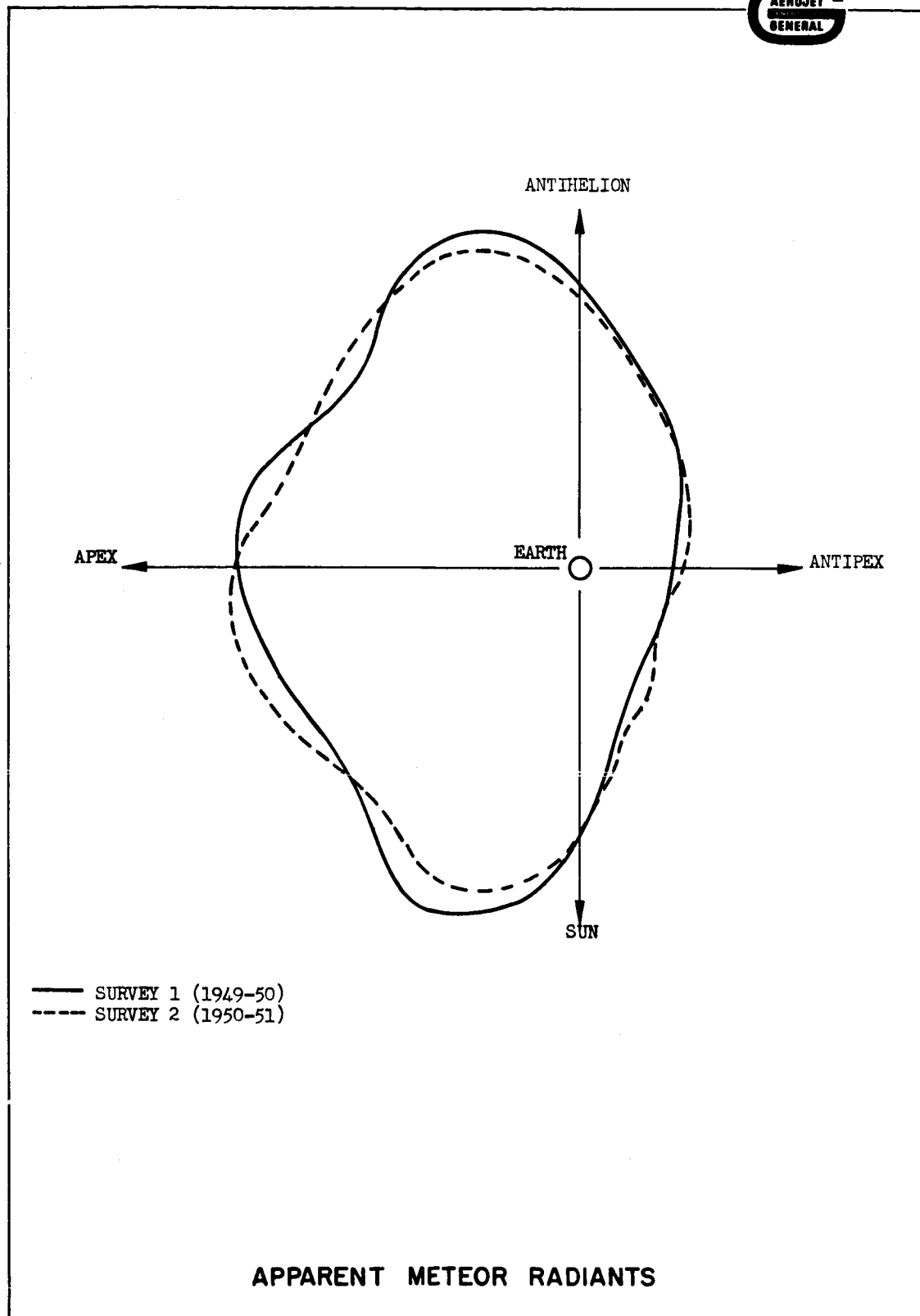
ALTITUDE - DEPENDENCE OF MICROMETEOROID FLUX



DISTRIBUTION OF VISUAL RADIANTS  
OF SPORADIC METEORS IN THE ECLIPTIC LATITUDE

10-087-118





10-007-110

Figure 52

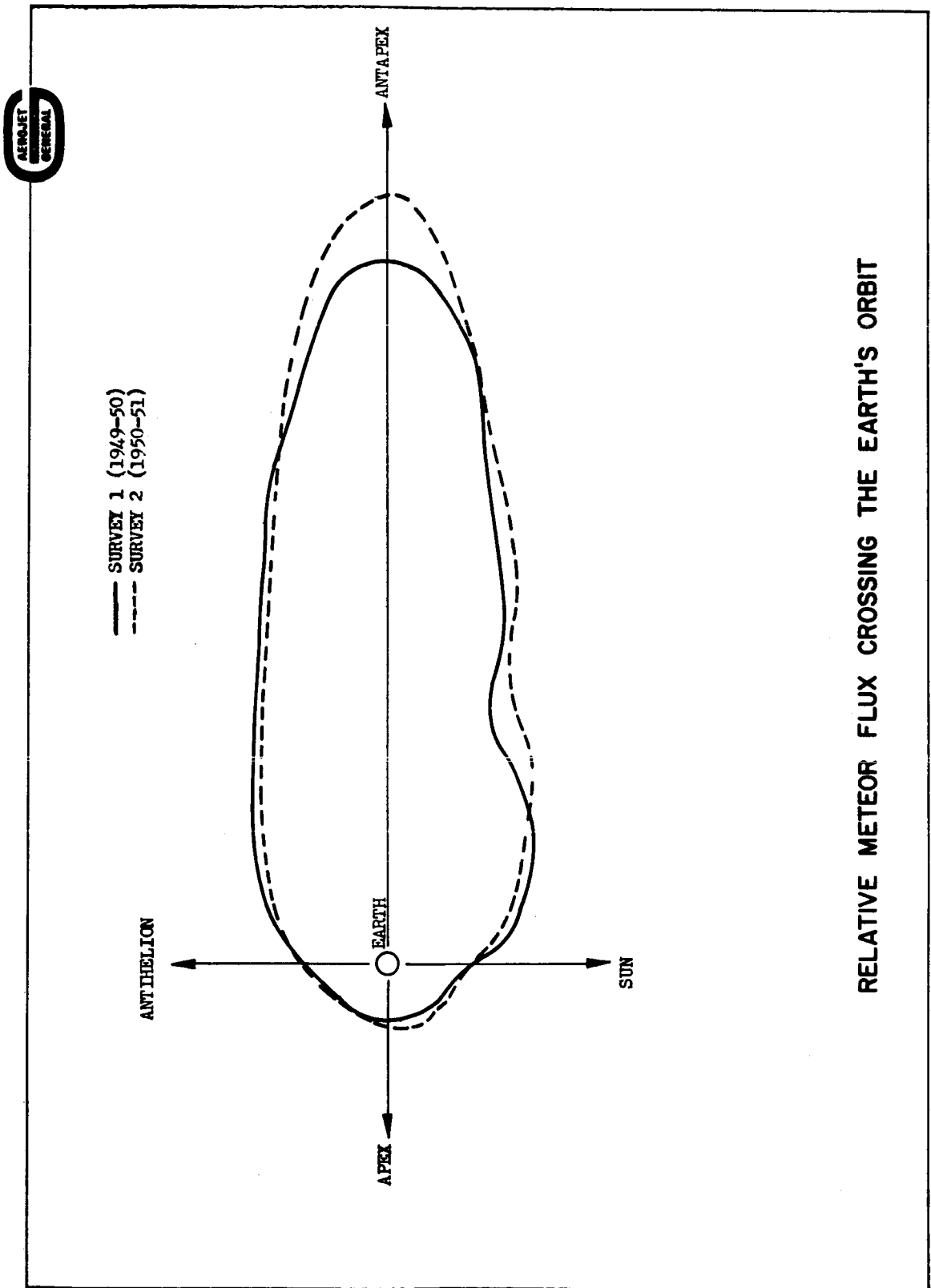
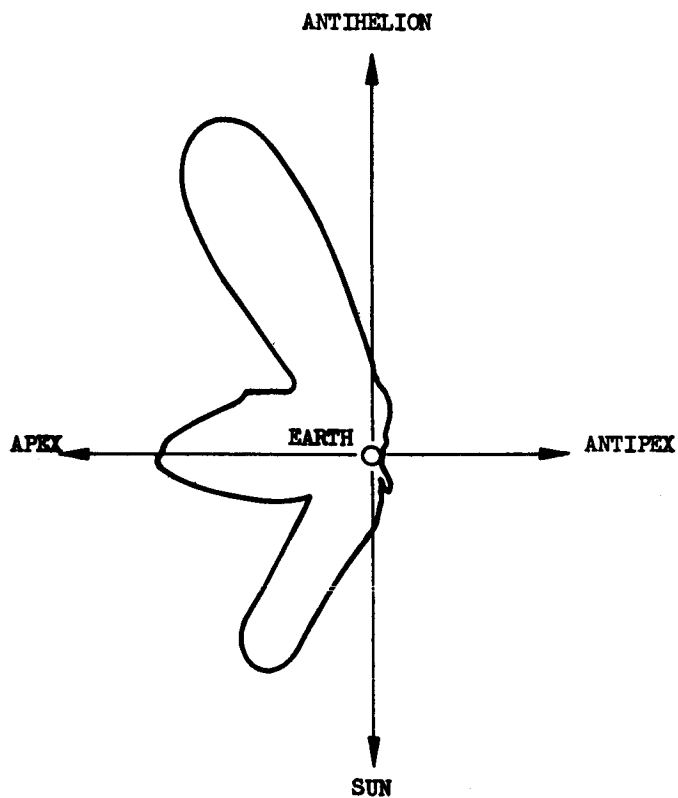
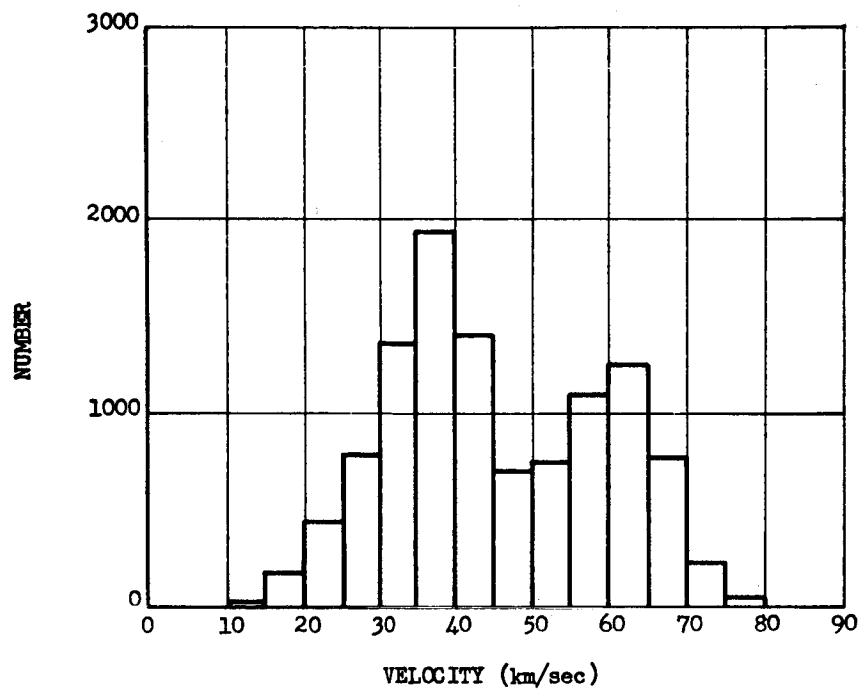


Figure 53



OBSERVED RADIANTS OF METEORIDS IMPACTING THE EARTH

10-007-110



VELOCITY DISTRIBUTION OF 10,933 SPORADIC METEORITES

10-007-118

DISTRIBUTION

	<u>No. of Copies</u>
NASA Western Operations Office 150 Pico Boulevard Santa Monica, California 90406	
Office of Technical Information	1
Contracts Management Division	1
General Counsel for Patent Matters	1
 NASA HEADQUARTERS Washington, D.C. 20546	
Mr. Henry Burlage, Jr. Chief, Liquid Propulsion Technology, RPL	4
 Mr. Vernon E. Jaramillo Advanced Manned Mission, MTA	1
 Scientific and Technical Information Facility NASA Representative, Code CRT P. O. Box 5700 Bethesda, Maryland 20014	25
 TECHNICAL MANAGER Mr. Louis Toth Jet Propulsion Laboratory 4800 Oak Grove Drive Pasadena, California 91103	1
 Ames Research Center Moffett Field, California 94035	2
 Goddard Space Flight Center Greenbelt, Maryland 20771	2
 Jet Propulsion Laboratory California Institute of Technology 4800 Oak Grove Drive Pasadena, California 91103	2
 Langley Research Center Langley Station Hampton, Virginia 23365	2

DISTRIBUTION (Cont.)

	<u>No. of Copies</u>
Lewis Research Center 21000 Brookpark Road Cleveland, Ohio 44135	2
Marshall Space Flight Center Huntsville, Alabama 35812	2
Manned Spacecraft Center Houston, Texas 77001	2
Western Operations Office 150 Pico Boulevard Santa Monica, California 90406	2
Advanced Research Projects Agency Washington 25, D.C.	1
Aeronautical Systems Division Air Force Systems Command Wright-Patterson Air Force Base Dayton, Ohio	1
Air Force Missile Development Center Holloman Air Force Base, New Mexico	1
Air Force Missile Test Center Patrick Air Force Base, Florida	1
Air Force Systems Command, Dyna-Soar Air Force Unit Post Office Los Angeles 45, California	1
Arnold Engineering Development Center Arnold Air Force Station Tullahoma, Tennessee	1
Bureau of Naval Weapons Department of the Navy Washington 25, D.C.	1

DISTRIBUTION (Cont.)

	<u>No. of Copies</u>
Defense Documentation Center Headquarters Cameron Station, Building 5 5010 Duke Street Alexandria, Virginia 22314 Attn: TISIA	1
Headquarters, U.S. Air Force Washington 25, D.C.	1
Picatinny Arsenal Dover, New Jersey 07801	1
Rocket Research Laboratories Edwards Air Force Base Edwards, California 93523	1
U.S. Atomic Energy Commission Technical Information Services Box 62 Oak Ridge, Tennessee	1
U.S. Army Missile Command Redstone Arsenal, Alabama 35809	1
U.S. Naval Ordnance Test Station China Lake, California 93557	1
Chemical Propulsion Information Agency (CPIA) Johns Hopkins University Applied Physics Laboratory 8621 Georgia Avenue Silver Spring, Maryland	1
Aerojet-General Corporation P.O. Box 296 Azusa, California	1
Aerojet-General Corporation P.O. Box 1947 Technical Library, Bldg. 2015, Dept. 2410 Sacramento, California 95809	1

DISTRIBUTION (Cont.)

	<u>No. of Copies</u>
Aeronutronic A Division of Ford Motor Company Ford Road Newport Beach, California	1
Aerospace Corporation 2400 East El Segundo Boulevard P.O. Box 95085 Los Angeles, California 90045	1
Arthur D. Little, Inc. Acorn Park Cambridge 40, Massachusetts	1
Astropower, Inc., Subsidiary of Douglas Aircraft Company 2968 Randolph Avenue Costa Mesa, California	1
Astrosystems, Inc. 1275 Bloomfield Avenue Caldwell Township, New Jersey	1
Atlantic Research Corporation Edsall Road and Shirley Highway Alexandria, Virginia	1
Beech Aircraft Corporation Boulder Facility Box 631 Boulder, Colorado	1
Bell Aerosystems Company P.O. Box 1 Buffalo 5, New York	1
Bendix Systems Division Bendix Corporation Ann Arbor, Michigan	1



DISTRIBUTION (Cont.)

	<u>No. of Copies</u>
Boeing Company P.O. Box 3707 Seattle 24, Washington	1
Chrysler Corporation Missile Division Warren, Michigan	1
Curtiss-Wright Corporation Wright Aeronautical Division Wood-ridge, New Jersey	1
Douglas Aircraft Company, Inc. Missile and Space Systems Division 3000 Ocean Park Boulevard Santa Monica, California 90406	1
Fairchild Stratos Corporation Aircraft Missiles Division Hagerstown, Maryland	1
General Dynamics/Astronautics Library & Information Services (128-00) P.O. Box 1128 San Diego, California 92212	1
General Electric Company Missile and Space Vehicle Department 3198 Chestnut Street, Box 8555 Philadelphia, Pennsylvania 19101	1
General Electric Company Flight Propulsion Lab Department Cincinnati 15, Ohio	1
Grumman Aircraft Engineering Corp. Bethpage, Long Island, New York	1

DISTRIBUTION (Cont.)

	<u>No. of Copies</u>
Kidde Aero-Space Division Walter Kidde and Company, Inc. 675 Main Street Belleville 9, New Jersey	1
Lockheed California Company 10445 Glen Oaks Boulevard Pacoima, California	1
Lockheed Missiles and Space Company Attn: Technical Information Center P.O. Box 504 Sunnyvale, California	1
Lockheed Propulsion Company P.O. Box 111 Redlands, California	1
The Marquardt Corporation 16555 Saticoy Street Box 2013 - South Annex Van Nuys, California 91409	1
Martin Division Martin Marietta Corporation Baltimore 3, Maryland	1
Martin Denver Division Martin Marietta Corporation Denver, Colorado 80201	1
McDonnell Aircraft Corporation P.O. Box 6101 Lambert Field, Missouri	1
North American Aviation, Inc. Space & Information Systems Division Downey, California	1
Northrop Corporation 1001 East Broadway Hawthorne, California	1

DISTRIBUTION (Cont.)

	<u>No. of Copies</u>
Pratt & Whitney Aircraft Corp. Florida Research and Development Center P.O. Box 2691 West Palm Beach, Florida 33402	1
Radio Corporation of America Astro-Electronics Division Defense Electronic Products Princeton, New Jersey	1
Reaction Motors Division Thiokol Chemical Corporation Denville, New Jersey 07832	1
Republic Aviation Corporation Farmingdale, Long Island, New York	1
Rocketdyne (Library Dept. 586-306) Division of North American Aviation 6633 Canoga Avenue Canoga Park, California 91304	1
Space General Corporation 9200 Flair Avenue El Monte, California	1
Space Technology Laboratories Subsidiary of Thompson-Ramo-Wooldridge P.O. Box 95001 Los Angeles 45, California	1
Stanford Research Institute 333 Ravenswood Avenue Menlo Park, California 94025	1
TAPCO Division Thompson-Ramo-Wooldridge, Inc. 23555 Euclid Avenue Cleveland 17, Ohio	1
Thiokol Chemical Corporation Redstone Division Huntsville, Alabama	1

DISTRIBUTION (Cont.)

	<u>No. of Copies</u>
United Aircraft Corporation Research Laboratories 400 Main Street East Hartford, Connecticut 06108	1
United Technology Center 587 Methilda Avenue P.O. Box 358 Sunnyvale, California	1
Vought Astronautics Box 5907 Dallas 22, Texas	1
Battelle Memorial Institute 505 King Avenue Columbus 1, Ohio	1

CONTRACT NAS 7-98 - ENGINE OPERATING PROBLEMS IN SPACE: SUMMARY OF CONTRACT

**TASK 1: DEFINITION OF THE SPACE ENVIRONMENT**

A detailed definition of Space Environment is presented in Volume I of this report.

**TASK 2: ENVIRONMENTAL EFFECTS TEST PROGRAM**

A study to determine the effects of the space environment in general, and particularly vacuum cooldown on thrust chamber materials, is presented in Volume II of this report. The following thrust chamber materials were studied in the environments listed.

Thrust Chamber Tests	Environment (see Legend below)	TCA Operation Parameters
<b>Ablative Materials</b>		
1. Molding compound of high silica fabric with rubberized phenolic resin.	C, V, RV, SC	P <sub>c</sub> 150 psia
2. Edge-grain high silica cordage with rubberized phenolic resin.	C, V, RV	F 100 lb
3. Edge-grain high silica cordage with phenyl silane resin.	C, V, RV	L* 38.5 in
		C* 5600 (97% theo. shifting equil.)
<b>Radiation-Cooled Materials</b>		M.R. 1.6
1. Pyrolytic Graphite	C, V, SC, D, M	Injector Multi-Orifice
2. Boron Pyrolytic Graphite	C, V	Propellants N <sub>2</sub> O <sub>4</sub> /Aerozine-50
Total Number of Tests = 86		

**Legend:**

C = control tests; V = vacuum cooldown; RV = gamma radiation and vacuum cooldown;  
SC = subcooling to LN<sub>2</sub> temperatures; D = duration test; M = Simulated micrometeoroid penetration. Test durations are nominally 30 to 45 sec with at least one restart of each TCA.

**Component Tests**

The following components have been subjected to combined-environment testing:

1. Solid propellant gas generators
2. Igniters (electrical and pyrotechnic)
3. Actuators (solenoid, electric motor, pyrotechnic, pneumatic, and hydraulic)
4. Pressure transducers
5. Lubricants
6. Metals and surface finishes

**TASK 3: MICROMETEOROID PUNCTURE SELF-SEALING FEASIBILITY STUDY**

A study to determine possible methods of micrometeoroid puncture self sealing, and a feasibility demonstration was performed, and results are presented in Volume III of this report. The program consisted of two phases and three types of sealing mechanisms were studied.

**Phases**

1. Sealing-mechanism screening tests with low velocity puncture, particle 0.11 in. dia.
2. Hypervelocity testing of best methods determined on Phase 1. (Hypervelocity impact with particles at velocities up to 18,000 ft/sec)

**Sealing Mechanisms**

1. Mechanical Sealing
  - a. Teflon Spheres
  - b. Fiberglass Floc
  - c. Vistanex Gums
2. Chemical Sealing
  - a. Sebacyl Chloride and Triethylenetetramine
  - b. Silicone DC-4 and Nitrogen Tetroxide
  - c. Sebacyl Chloride and Aerozine-50
3. Combination systems with small elastomeric balls, glass fibers, etc., in the various solvents

Results: Satisfactory seal with Vistanex Gums/Aerozine-50 and N<sub>2</sub>O<sub>4</sub> for time periods up to 64 hr.

**TASK 4: SPACE MAINTENANCE**

A survey to determine the state-of-the-art in space maintenance. Components requiring space maintenance were defined and possible methods to provide maintenance suggested. Design criteria for the maintenance and service of a liquid propulsion rocket engine are presented in Volume III of this report.

**TASK 5: IMPROVED TESTING TECHNIQUES**

The state-of-the-art of environmental simulation techniques were determined and improvements recommended. The environments listed were considered both singularly and as combined environments in Volume III of this report.

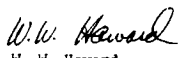
- |                      |                            |  |
|----------------------|----------------------------|--|
| 1. Vacuum            | 3. Micrometeoroid Extremes | 5. Solar Simulation  |
| 2. Nuclear Radiation | 4. Temperature Extremes    | 6. Dust, Corrosive constituents of planetary atmospheres, etc. |

**TASK 6: ABLATIVE MATERIALS WITH FLUORINATED OXIDIZERS**

A study of ablative materials for use with fluorinated oxidizers at flame temperatures as high as 8000°R was conducted and results are presented in Volume III of this report. The propellant combination selected was liquid fluorine/gaseous hydrogen. The materials tested are listed.

Chamber Material	Throat Material	Backup Materials	TCA Operation Parameters
1. High Density Graphite	High Density Graphite	Porous Carbon & Asbestos	P <sub>c</sub> 150 psia
2. High Density Graphite	Pyrolytic Graphite Disks	Porous Carbon & Asbestos	F 75 lb
3. High Density Graphite	Tungsten(92% of theo. density)	Porous Carbon & Asbestos	L* 40 in.
4. High Density Graphite	Tungsten/Silver Infiltrated	Porous Carbon & Asbestos	C* 7000 (90% theo. shifting equil.)
5. Molded Graphite/Phenolic	High Density Graphite	Molded Graphite/Phenolic	M.R. 15.0
			Injector Nonad(Eight oxidizer on one fuel)
			Propellants LF <sub>2</sub> /GH <sub>2</sub>

Period of Performance: 15 February 1962 to 15 March 1964

  
 W. W. Howard  
 Space Environment Department  
 Production Projects Division  
 AEROJET-GENERAL CORPORATION  
 Azusa, California